SIMULATION OF CLIMATE DATA FOR GEOTECHNICAL AND GEOENVIRONMENTAL DESIGN PROBLEMS

MUHAMMAD ABID NAWAZ SAHI

A THESIS SUBMITTED TO THE FACULTY OF GRADUATE STUDIES IN PARTIAL FULFILLMENT OF THE REQUIREMENTS FOR THE DEGREE OF MASTER OF APPLIED SCIENCES

GRADUATE PROGRAM IN CIVIL ENGINEERING
YORK UNIVERSITY
TORONTO, ONTARIO

August 2018

ABSTRACT

Multi year daily climate datasets are required in the design of several different geotechnical and geoenvironmental projects. The compilation of multi year daily measured climate data requires a considerable amount of time and effort. The amount of time and effort depends on the availability, completeness, and quality of the measured climate dataset. In this research, a general-purpose climate generator SIMETAW is used to generate daily climate variables of interest from readily available monthly climate normals for nine different sites across Canada. The climates at these sites range from semi-arid to pre-humid. The historical measured data for these locations were also compiled. Measured data were compared with simulated climate data based on visual presentations and numerical measures. The comparison revealed that SIMETAW is capable of simulating various climates types across Canada. Simulated climate data was used in simulations of infiltration in unsaturated soils, soil cover assessment and estimation of swelling potential of expansive soils. Adequacy of simulated climate data for use in geotechnical and geoenvironmental design problems was assessed by comparing simulations run with measured and simulated climate data. The comparison indicated that for all practical purposes, the daily climate datasets generated from monthly climate normals are quite adequate for use in geotechnical and geoenvironmental problems. It is anticipated that the work presented in this research will facilitate the future researchers and practitioners by making the climate data more accessible.

Keywords: Climate data, *SIMETAW*, monthly climate normals, infiltration assessment, soil-atmosphere models, soil cover design, expansive soils.

Dedication

To our beloved Prophet Muhammed (*PBUH*) and our creator Allah …

Acknowledgements

I would like to acknowledge and express my gratitude for the funding provided by the Office of Graduate Studies for the pursuit of my education at York University. I would like to thank my supervisors Dr. Bashir and Dr. Sharma for all the guidance and scientific support that I received since I embarked on this academic program. I would also like to thank my committee: Dr. Beddoe for being an excellent mentor and all her continued support during the development of this research. Special thanks to Dr. Czekanski for all the valuable help and assistance with the completion of this document. I would also like to thank my supervisors for the opportunity granted to have been accepted as a student at the Civil Engineering Department.

Special thanks to all my family members for their countless support during my studies. Many thanks to my classmate Eric Pastora for his invaluable scientific and technical support during the academic program. Finally, I want to express my great gratitude to my wife Samrah Ashraf for the moral support throughout my academic years.

TABLE OF CONTENTS

List of Tables

List of Figures

Chapter 1

Introduction

1.1 Background

Multi-year climate data is used in design of several different geotechnical and geoenvironmental projects. These projects include (but are not limited to): design of soil cover systems for waste management, heaving and settlement predictions for expansive soils, and slope stability assessments. The top boundary in these projects is the ground surface, which is exposed to the atmosphere. The amount of water that enters or leaves the top boundary is a critical design parameter. In order to determine the magnitude and direction of water fluxes and associated water balance at the ground surface, Actual Evaporation (*AE*) needs to be estimated (Fredlund et al. 2011, 2012). Actual evaporation from a soil surface can be significantly less than potential evaporation and is a function of local climatic conditions and transient water content of the soil (Fredlund et al. 2011, 2012).

Soil-atmosphere models can be used to estimate the actual evaporation from a soil surface. A soil-atmosphere model simulates the movement of moisture (water & vapor) and heat across the soil-atmosphere interface and estimates *AE* (Wilson et al. 1994, Fredlund et al. 2011, 2012). The top boundary of the soil-atmosphere model comprises a multi-year climatic dataset and the surface moisture flux is estimated by coupling the soil and atmospheric processes. The climatic data set required by soil-atmosphere models include the following meteorological variables: precipitation, relative humidity, wind speed, net radiation, and temperature (Vu et al. 2007). This data is

required at least at daily resolution for 10 to 30 year period. The requirement for multi-year climatic dataset is to ensure that year-to-year variation in climate is taken into consideration (INAP, 2009).

The compilation of 10-30 years daily measured climate data requires a considerable amount of time and effort, which depends on the availability, completeness, and quality of the measured climate dataset. In many instances, the measured data is not continuous, with one or more variables missing over extended periods of time. The missing weather data may be because of instrument malfunction, break in transmission, or loss of archived dataset. Similarly, the measured weather records can have erroneous values. These erroneous values could be because of data-entry mistakes, instrument malfunction, improper calibration, transmission errors or other reasons. The replacement of missing and/or the erroneous values is termed as cleaning of weather data (Alexandridis et al. 2013).

In cases where the missing or erroneous values are for a day or two, replacement is easy. However, if the blocks of the daily data are missing, standard procedures can be adopted to fill the missing/erroneous data (Schneider, 2001). One of the approaches used is termed as meteorological approach (Alexandridis et al. 2013) or spatial interpolation. In this approach, interpolations between observations across several stations is used to replace the missing/erroneous data. The second approach is called temporal interpolation or time-series approach. In this approach, models for different variables using the climate data (excluding the erroneous data) are constructed. These models have the capability to estimate the missing/erroneous values in the data (Alexandridis et al. 2013).

The effort required in acquiring, formatting and cleaning the climate data has led to the development of weather generation procedures and tools (Tingem et al. 2007). Weather generators (*WGs*) provide means of in filling the missing weather data, or for producing long-term synthetic climate data from limited measured weather records (Wilks and Wilby, 1999). In many instances, *WGs* use monthly weather statistics (monthly climate normals) to generate daily weather data (Hong et al. 2016). Although weather generators have proven capability to generate synthetic weather data with the same statistical characteristics as the actual weather at a certain location (Richardson and Wright 1984a), the generated data needs be tested to ensure that data produced is satisfactory for the purposes for which it is to be used (Tingem et al. 2007). Keller (2015) has provided a review of existing *WGs* developed over the past decade. Although *WGs* are used extensively in water resource assessments (Hong et al. 2016), there is no evidence in the peer reviewed literature that generated climate data has ever been used for geotechnical or geoenvironmental designs.

The present research uses the climate data generator "Simulation of Evapotranspiration of Applied Water" (*SIMETAW)* (Snyder et al. 2012) in order to generate a multi-year climate datasets at a daily resolution to assess the long-term performance of geotechnical and geoenvironmental projects under the influence of local climate conditions.

1.2 Objectives

This research has following two specific objectives:

1. Assess the suitability of a general-purpose climate data generator to simulate multi-year climate dataset at daily resolution from monthly climate normals.
2. Assess the adequacy of simulated climate data for use in geotechnical and geoenvironmental design problems.

To achieve the first objective, measured daily climate data for nine different geographic locations across Canada were compiled. For the same locations, the climate data were simulated using a general-purpose climate generator *SIMETAW* using readily available climate normals.

Evidence from the literature indicates that *SIMETAW* has been used successfully for many agricultural and water resources applications (Swelam 2012, Orang et al. 2013, Mancous et al. 2013, Howes et al. 2015). However, as pointed out earlier, there is no evidence in the literature that climate data simulated by *SIMETAW* or any other climate generator has ever been used in geotechnical and/or geoenvironmental engineering design problems.

Measured data was compared with simulated climate data based on visual displays and numerical measures. Visual displays allowed for visual comparison between the similarities and differences in measured and simulated data. Numerical measures in the form of standard statistical methods were used to assess the accuracy of the simulated data in predicting the historical measured data.

The second objective was achieved by using simulated and measured climate data in soil-atmosphere modelling. Soil-atmosphere modeling and associated analyses were carried out for three different types of geotechnical/geoenvironmental design problems.

In the first set of analyses, measured and simulated climate data were used for infiltration assessment. The timing, magnitude, and intensity of infiltration influence the temporal and spatial distribution of soil moisture in the upper portion of the ground and runoff generation. Such assessments are important for following geotechnical/geoenvironmental assessments:

- ground instability or subsidence;
- slope instability or soil liquefaction;
- pollution from existing contaminant mobilization in the subsurface;
- pollution from infiltrating polluted surface water runoff;
- groundwater flooding;
- groundwater recharge; and
- deign of low impact developments (*LID*) stormwater management systems.

In the second set of analyses, measured and simulated climate data were used to predict the volume change behavior of Regina clay. Measured and simulated climate data for the City of Regina, Saskatchewan, Canada was used in soil-atmosphere models to predict the subsurface moisture content variation. Predicted moisture content variation was used to estimate the swelling potential of Regina clay.

Soil covers are an important part of domestic, industrial, and mining waste management systems. Design of these covers is highly dependent on the site climate. In

the third set of analyses, measured and simulated climate data were used for the design of a soil cover system for reactive mining waste. The design principle was to ensure a high saturation all year round to control oxygen ingress to the reactive tailings.

1.4 Thesis Organization

This thesis has been organized in six chapters. Chapter 1 presents background, defines the objectives and summary of the procedure adopted in achieving the defined objectives.

Chapter 2 provides a theoretical background and literature review of some basic concepts related to geotechnical and geoenvironmental engineering, for example unsaturated flow, soil atmosphere modelling and climate data variables etc.

Chapter 3 presents the details about compilation of climate data for nine selected regions across Canada. It also presents the climate data variables in detail for two different types of climate conditions (semi-arid and humid). Compiled climate variables included: maximum and minimum temperature (°*C*), mean relative humidity (*%*), total precipitation (*mm*), wind speed (*km/h*), and total solar net radiation ($MJ/m^2 – day$).

Chapter 4 presents the procedure of climate data simulation. Literature review of *SIMETAW* is presented followed by the methodology to simulate the climate data. In this chapter simulated data is also compared with the measured data. This comparison is based on both visual and statistical analyses.

Chapter 5 presents the assessment of adequacy of This chapter is divided into three subsections. The first section presents the modelling results obtained from simulations of water dynamics for which measured and simulated climate data were used. In the second section the results for calculated swelling potential for Regina Clay are presented. The third and final section presents an example of soil cover system design.

Chapter 6 provides a summary of the thesis followed by the specific conclusions drawn from the work presented in this thesis. Contributions of this research to generation knowledge are also mentioned. The chapter concludes with recommendations for the future research.

Chapter 2

Theoretical Background

2.1 Water flow in unsaturated soils

The moisture dynamics analysis in unsaturated soils is an essential requirement for many geotechnical and geoenvironmental design problems (Fredlund et al. 2012). In the unsaturated zone pores are partially filled with water, i.e. pores contains water and air. The flow of water occurs within the connected pores of the soil, which are either partially or fully filled with water.

Moisture movement in unsaturated soils in vicinity of ground surface is subjected to prevailing climatic condition and soil hydraulic properties. For example, in arid climatic conditions any amount of water available at the ground surface will tend to evaporate before it can infiltrate into the deeper soil layers. Contrary, in wetter climatic conditions the excess of available water will move downwards to reach ground water table.

The unsaturated flow can be represented by the Richards equation (Richards, 1931):

$$\frac{\partial \theta}{\partial t} = -\frac{\partial q}{\partial z} - S = \frac{\partial}{\partial z}\left[K(h)\left(\frac{\partial h}{\partial z} + 1\right)\right] - S \qquad \text{Eq. (2.1)}$$

where θ is the volumetric water content (L^3/L^3), t is time (T), and S is the sink term (L^3/L^3T) that accounts, for example, for root water uptake (transpiration), q is the flux density or volumetric water flux flowing through a unit surface area per unit time (L^3/L^2T),

K(h) is the unsaturated hydraulic conductivity (*L/T*) and is the function of the soil water pressure head (*h*), and *z* is the elevation head or height above a reference level (*L*)

The solution of Richards equation requires input of two set of hydraulic properties, namely soil water characteristic curve (*SWCC*) and the unsaturated hydraulic conductivity function (*K(h)*) relationship (Bashir et al. 2015). The *SWCC* defines the relationship between soil water content (θ) and soil water pressure (*h*). van Genuchten, (1980) proposed the following equation to represent *SWCCs* based on Mualem, (1976) theory:

$$\theta = \frac{(\theta_s - \theta_r)}{[1+(|\alpha h|)^n]^m} + \theta_r \qquad \text{Eq. (2.2)}$$

where θ_s is the saturated water content (L^3/L^3), θ_r is the residual water content (L^3/L^3) and α ($1/L$), n (-), and m (-) are curve fitting parameters. The m parameter is assumed to be equal to 1-1/n. The n parameter is related to the pore size distribution index. The parameter α can be related to the inverse of air entry value (Fredlund and Rahardjo, 1993).

van Genuchten, (1980) formulated the following equation for unsaturated hydraulic conductivity function:

$$\mathrm{K(h)} = \mathrm{K_s S_e^{\ell}}\left[1 - \left(1 - \mathrm{S_e^{1/m}}\right)^{\mathrm{m}}\right]^2 \qquad \text{Eq. (2.3)}$$

Where *l* is commonly assumed to be 0.5 and the effective saturation, S_e, is computed as shown below:

$$S_e = \frac{\theta - \theta_r}{\theta_s - \theta_r} \qquad \text{Eq. (2.4)}$$

The unsaturated hydraulic properties can be measured in the laboratory or in the field. However, these measurements are very time consuming and expensive (Saxton and Rawls, 2006). A number of pedotransfer functions to estimate unsaturated hydraulic properties from easily measured soil properties, such as texture, bulk density, and particle size distribution have been proposed over the years. A recent review of pedotransfer functions is presented by Patil and Singh, (2016). Additionally a catalogue of soil hydraulic properties corresponding to the *12* soil textural classes of the *USDA* textural triangle has been compiled based on the work of Carsel and Parrish, (1988). The hydraulic properties reported in the catalogue are averages of large number of measured values reported in the literature.

Figure 2.1 shows the *USDA* textural triangle as defined by US Department of Agriculture (USDA, 1987) (Garc a-Gaines and Frankenstein, 2015). The soil textural classification is based in the percentage of three main soil types consisting of sand, silt and clay. Based on the fraction of soil particle sizes, soils can be classified into 12 major textures as shown in the Figure 2.1. Figure 2.2 shows the *SWCC* for various soil texture classes. This figure has been plotted with data from Carsel and Parrish, (1988). This figure shows that the hydraulic properties vary widely between the different textural classes. For example, for coarse grained soils most of the water can be drained from soils at relatively small suction values. This contrasts with fine grained soils where some water can still remain in the pores even at higher suctions.

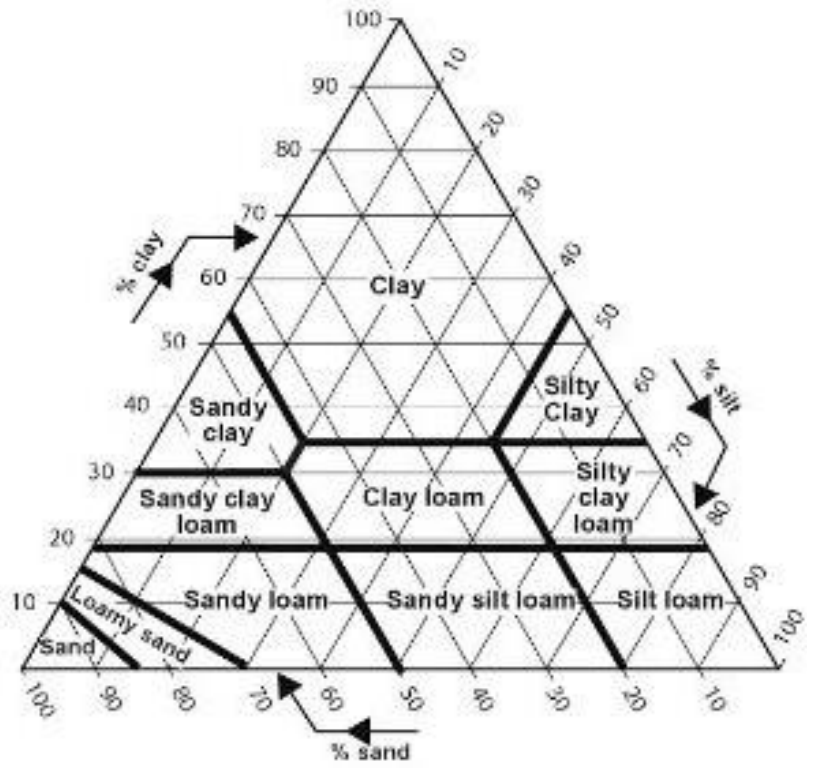

Figure 2.1: USDA soil texture classification. Modified from Friske et al. 2010

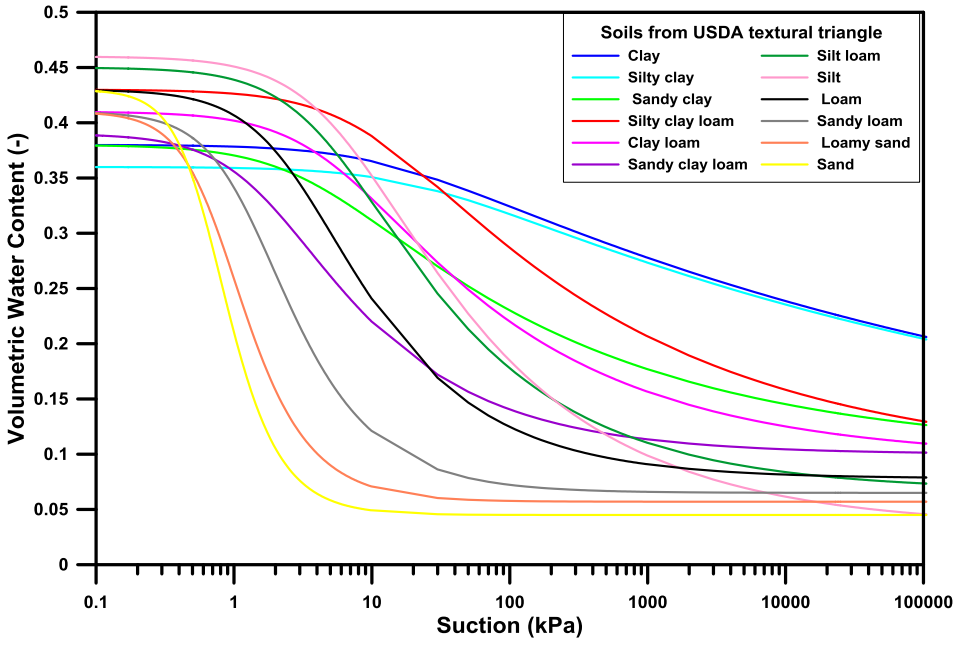

Figure 2.2: SWCC for different USDA soil texture classes (Data from Carsel and Parrish, 1988)

2.2 Estimation of water balance at the soil-atmosphere interface

Water from precipitation (*P*) available at the ground surface can infiltrate into the soil, run over the surface as runoff (*RO*) or can be evaporated back into the atmosphere. (Figure 2.3). Potential evaporation (*PE*) refers to the maximum amount of evaporation from a surface based on atmospheric condition provided that a limitless source of water is available at the surface. Actual evaporation (*AE*) refers to the actual amount of water evaporated in cases where the evaporative demand exceeds the water availability at the surface. The *AE* at soil surface is a function of *PE* and soil moisture availability at the soil surface.

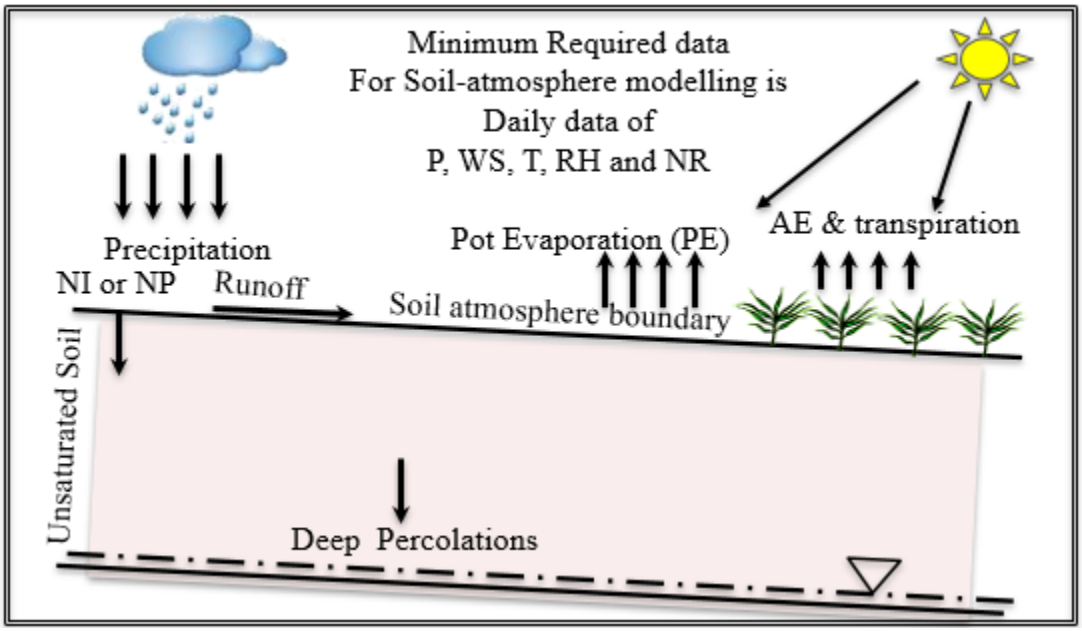

Figure 2.3: Schematic drawing of soil-atmosphere model

Net infiltration (*NI*) refers to the quantity of the meteoritic water that enters the soil surface evading evaporation. Mathematically it can be represented as:

$$NI = P - AE - RO \qquad \text{Eq. (2.5)}$$

where *P* is the precipitation (*L*), *AE* is the actual evaporation (*L*), and *RO* is the runoff (*L*).

Eq. 2.5 indicates that the estimation of two climatic variables, namely *P* and *AE,* are required for water balance assessments at the ground surface. Actual evaporation can be estimated from *PE* and transient soil moisture conditions. *PE* itself is a function of climatic variables, such as temperature, wind speed, relative humidity, and net radiation. These variables are measured at most weather stations. The following sections provide a brief description of climatic variables, followed by methods to estimate *PE* and *AE*.

2.3 Climate variables

2.3.1 Precipitation

Precipitation refers to the condensation of atmospheric water vapor and includes drizzle, rain, sleet, snow, graupel and hail. Precipitation can be measured using rain and snow gauges. Historically, rain gauges have been classified as recording or non-recording types. A non-recording rain gauge requires the measurement to be performed manually by an observer. The two most common types of recording gauges are siphon rain gauges or tipping bucket rain gauges. Siphon rain gauges typically have a built-in recorder but require an observer to physically visit the site to obtain data. Tipping bucket rain gauges generate an electrical signal for each unit of precipitation collected and allows automatic or remote observation. Environment Canada uses standard Canadian Type B rain gauge for manual measurement of rain. Nipher Shielded Snow Gauge System is the standard instrument used for measuring fresh snowfall water equivalent at many weather stations in Canada (Environment Canada, 2018d). However, at many weather stations

snowfall precipitation is measured from ruler measurements of the depth of freshly fallen snow and by assuming the density of fresh snow to be 100 kg/m^3 (i.e., ratio 10 to 1) (Metcalfe et al. 1997).

Environment Canada has ordinary stations and principal weather stations. At ordinary stations, precipitation measurements are measurements are taken twice daily. However, at some stations, only daily measurement is made. At principal weather stations measurements are taken at 6-hour intervals. Environment Canada also operates a supplementary network where large-capacity recording precipitation gauges for the measurement of precipitation amount at 15-min intervals are installed (Metcalfe et al. 1997).

2.3.2 Temperature

Environment Canada measures the air temperature on Celsius scale, which have 100 division between freezing and boiling point of water. The temperature is normally measured on hourly basis. The equipment normally used for the measurement of air temperature consist of a Stevenson Screen including stand, a maximum thermometer, and a minimum thermometer (Environment Canada, 2018d).

2.3.3 Relative humidity

The ratio of water vapour quantity in air compared with maximum amount the air can hold at that particular temperature is called relative humidity (Environment Canada,

2018d). Environment Canada records the relative humidity on an hourly basis in percentage (%). Relative humidity is not recorded at all weather stations whereas dew point (temperature at which dew forms) is recorded on almost all locations. The relative humidity can also be calculated if the dew point temperature value is available. The August-Roche-Magnus equation was originally developed to calculate the dew point temperature, where relative humidity and dry bulb temperature were known. The same equation can be rearranged to calculate the relative humidity when the dew point temperature is known and the following conditions are met (Fredlund et al. 2012).

$$0^o C < T < 60^o C$$

$$1\ \% < h_r < 100\ \% \qquad \text{Eq. (2.6)}$$

$$0^o C < t_d < 50^o C$$

The rearranged August-Roche-Magnus equation to calculate the relative humidity can be written as follows (Fredlund et al. 2012).

$$h_r = 100 \exp\left[\frac{ab\,(T_d - T)}{(b + T)(T_d + b)}\right] \qquad \text{Eq. (2.7)}$$

where h_r correspond to relative humidity (%), T is the dry bulb temperature (^oC), t_d is dew point temperature (^oC), a is constant with value 17.271 and b represent 237.7 ^{o}C.

2.3.4 Solar radiation

Solar radiation is the electromagnetic energy emitted by the sun. Global and diffuse solar radiation can be measured using thermoelectric pyrometers. A pyrometer consists of a thin blackened surface which is supported from inside by a massive well-polished case. The temperature of the surface rises when the solar radiation hits the surface. The temperature keeps on rising until an equilibrium is achieved when the rate of loss of heart by all the cases is equal to the rate of gain of heat by the radiation. The rise in temperature sets up a thermal electromotive force which is recorded by the millivoltmeters or recorder (Pandey and Katiyar, 2013). Pyrheliometer is an instrument used for direct solar radiation measurement. The sensor in pyrheliometer is fixed at the lower end of a tube attached to the diaphragm to receive only direct radiation from sun. The sensor surface is aligned normal to the line from the sun to the receiver. In this case only the radiation from sun is received by the sensor (Pandey and Katiyar, 2013). The measurement by Environment Canada is conducted at a high frequency (30-100 Hz or up to one reading every 10 ms) to allow for recording of high ramp-rate events. The recording is carried out using wirelessly-controlled, automatic recording irradiance sensors (Environment Canada, 2018d).

2.3.5 Net radiation

There are only few locations across Canada where the net radiation is recorded (Environment Canada, 2018d). Net radiation (Q_n) is the difference between all upward and downward fluxes of radiation, which are the measure of energy available at ground

surface (Irmak et al. 2003). Radiation values are recorded hourly in local apparent time. The unit of measurement is *MJ/m²*. Q_n is normally positive during the day and negative during the night time, whereas the total daily amount is normally positive except for the higher altitude areas (Allen et al. 1998). The widely-used procedure for estimating Net radiation (Q_n), presented by Allen et al. (1998), can be written as:

$$Q_n = Q_{ns} - Q_{nl} \quad \text{Eq. (2.8)}$$

where Q_n is the net radiation (*MJ/m²/d*), Q_{ns} is incoming net shortwave radiation (*MJ/m²/d*) and Q_{nl} is outgoing net longwave radiation (*MJ/m²/d*).

The incoming net shortwave radiation is imputed to the balance between incoming and reflecting solar radiation and can be formulated as:

$$Q_{ns} = (1 - \alpha)Q_s \quad \text{Eq. (2.9)}$$

where α is albedo or canopy reflection coefficient and Q_s is total incoming solar radiation (*MJ/m²/d*).

The longwave energy emission rate correspond to the absolute temperature of the surface raised to the fourth power, the quantitively expressed relation is as follows (Allen et al. 1998):

$$Q_{nl} = \sigma \left[\frac{T_{max,K}^4 + T_{min,K}^4}{2}\right] \left(0.34 - 0.14\sqrt{e_a}\right) \left(1.35\frac{Q_s}{Q_{so}} - 0.35\right) \quad \text{Eq. (2.10)}$$

where σ is Stefan-Boltzmann constant ($4.903x10^{-9}$ $MJ/K^4/m^2/d$), $T_{max,K}$ is the maximum absolute temperature ($^oC+273.16$), $T_{min,K}$ is the minimum absolute temperature ($^oC+273.16$), e_a is the actual vapor pressure (kPa) and Q_{so} is the calculated clear sky solar radiation ($MJ/m^2/d$).

The actual vapor pressure can be calculated using following equation:

$$e_a = 0.6108\, exp\left[\frac{17.27\, T_d}{T_d + 237.3}\right] \quad \text{Eq. (2.11)}$$

where T_d is the dew point temperature (^oC).

The daily value of clear sky solar radiation (Q_{so}) can be calculated using relation presented by Doorenbos and Pruitt, (1977). It is the function of station elevation (z) in m and extraterrestrial radiation Q_a ($MJ/m^2/d$), and can be written as:

$$Q_{so} = (0.75 + 2 \times 10^{-5} z) Q_a \quad \text{Eq. (2.12)}$$

The extraterrestrial radiation Q_a can be calculated on daily basis as a function of day of the year, solar constant, solar declination, and latitude by:

$$Q_a = \frac{1{,}440}{\pi} G_{sc} d_r \left(\omega_s sin(\varphi) sin(\delta) + cos(\varphi) cos(\delta) sin(\omega_s)\right) \quad \text{Eq. (2.13)}$$

where G_{sc} is the solar constant (0.0820 $MJ/m^2/min$), d_r is the inverse relative distance from earth to sun, ω is the sunset hour angle (rad), ϕ is latitude (rad), and δ is

the solar declination. Following equations can determine the values of variables ϕ, d_r, δ and ω, to calculate the extraterrestrial radiation Q_a, the equations are:

$$\varphi\ (rad) = \frac{\pi}{180}[decimal\ degrees] \quad \text{Eq. (2.14)}$$

$$d_r\ = 1 + 0.033\cos\left(\frac{2\pi}{365}JD\right) \quad \text{Eq. (2.15)}$$

$$\delta\ = 0.409\sin\left(\frac{2\pi}{365}JD - 1.39\right) \quad \text{Eq. (2.16)}$$

$$\omega_s\ = \arccos[-\tan(\varphi)\tan(\delta)] \quad \text{Eq. (2.17)}$$

where *JD* is the day of the year.

2.3.6 Wind speed

The movement of air from high pressure to low pressure generate wind speed. This movement is normally controlled by change in temperature. There are number of factors affecting the wind speed which include: pressure gradient, Rossby waves (wind in the upper troposphere), and local weather conditions. Pressure gradient is a physical quantity which describes the direction and the rate at which the pressure changes abruptly around particular location. The pressure gradient has a direct influence on the wind speed. The higher the pressure gradient, the faster the wind blows to balance the pressure difference. Environment Canada measures the speed of moving air in either *km/h* or *knot*, usually at an elevation of 10 m from the ground surface. Reported speed is

normally the average speed during two-minute observation period (Environment Canada, 2018d).

2.4 Potential evaporation

Potential Evaporation (*PE*) or potential evapotranspiration (*PET*) is defined as the maximum amount of water, which can evaporate from the ground surface, in response to the atmospheric demand and where unlimited water source is available (Thornthwaite 1948, Penman 1948, Fredlund et al. 2012). Thornthwaite, (1948) used the term potential evaporation for the climate classification, later this was used by Penman, (1948) while struggling to find an absolute relation between elements of weather and evaporation of water from an open source, and a relation among losses from the soil and the open source in the same climate. Penman, (1948) provides the relationship for estimating evaporation from natural surface, by linking evaporation rate to the net flux of radiation energy and the effective ventilation by the air in motion (Thom and Oliver, 1977). Penman equation for the estimation of the *PE* can be written as follows (Fredlund et al. 2012):

$$\mathrm{PE} = \frac{\Gamma Q_n + \eta E_a}{\Gamma + \eta} \qquad \text{Eq. (2.18)}$$

Where *PE* is the potential evaporation (*mm/day*), Γ is the slope of saturation vapor pressure versus temperature curve (*kPa/^{o}C*), Q_n is the net radiation at the water surface (*mm/day*), η is the psychrometric constant (*kPa/^{o}C*), E_a can be referred as aerodynamics term and can be obtained from the following relation:

$$E_a = 2.625\,(1 + 0.146W_w)\,(u_{v0}^{air} - u_v^{air}) \quad \text{Eq. (2.19)}$$

where W_w is the wind speed (*km/h*), u_{v0}^{air} is the saturated vapor pressure at the mean air temperature (*kPa*) and u_v^{air} is the vapor pressure in the air above water surface or saturated ground (*kPa*).

The saturated vapor pressure (u_{v0}^{air}) can be calculated using equation presented by Tetens, (1930). He demonstrated that the saturation vapor pressure is a function of temperature and the equation can be written as:

$$u_{v0}^{air} = 0.6108\,exp\left(\frac{17.27T_a}{T_a + 237.3}\right) \quad \text{Eq. (2.20)}$$

where T_a is the air temperature (^oC). Tetens, (1930) also presented the equation for the slope of the saturation vapor pressure against temperature curve and can be expressed as follows:

$$\Gamma = \frac{4098u_{v0}^{air}}{(T_a + 237.3)^2} \quad \text{Eq. (2.21)}$$

where all the parameters are as defined earlier. The psychrometric constant η can be calculated using the following relation (Fredlund et al. 2012):

$$\eta = \frac{C_a\bar{u}_a}{\varepsilon L_v} \quad \text{Eq. (2.22)}$$

where C_a is the specific heat of moist air equal to *1.013 kJ/(kg^{o}C)*, $\bar{u}_a$ is the absolute atmospheric pressure equal to (u_{atm}+u_a) here u_{atm} is the standard pressure at sea level i.e. *101.3 kPa*, ε is the ratio of molecular weight of water vapor to dry air equal to *0.622* and L_v is the latent heat vaporization (*MJ/kg*).

The latent heat of vaporization alters with the temperature with respect to the following equation by Harrison, (1963):

$$L_V = 2.501 - 0.002361T_a \qquad \text{Eq. (2.23)}$$

where all the parameters are as defined earlier. The absolute atmospheric pressure ($\bar{u}_a$) fluctuates with respect to elevation and temperature in conformity to the following equation presented by Burman, (1987):

$$\bar{u}_a = u_{atm}\left[\frac{T_{K0} - \alpha_1(z - z_0)}{T_{K0}}\right]^{\frac{g}{(R\alpha_1)}} \qquad \text{Eq. (2.24)}$$

where z is elevation (*m*), z_o is the reference elevation (*m*), g is gravitational acceleration (*9.81 m/s^2*), R is specific gas constant (*287 J/(kg K)*, α_1 is the constant lapse rate for moist air (*0.0065 K/m*), T_{ko} is the reference temperature, *K*, at reference elevation i.e., T_{ko} = *273.16*+T_a, here T_a is the mean air temperature for the time period (*^{0}C*).

2.5 Actual evaporation

Actual evaporation is the absolute amount of water escape from the soil surface. The amount of actual evaporation depends upon the available water, its pressure in the soil and climate condition of the area. Quantification of actual evaporation helps to establish a better water balance condition at the ground surface. Only in the case of fully saturated soils the rate of actual evaporation may be equal to potential evaporation. As the soil starts desaturating actual evaporation also starts decreasing. There are several methods proposed for the calculation of actual evaporation. A recent review of the *AE* methods has been carried out by Tran, (2013). In the following sections two different methods to estimate *AE* are presented.

2.5.1 Modified Wilson-Penman equation for computing actual evaporation

Wilson, (1990) proposed an equation for determining the actual evaporation by extending the Penman, (1948) approach for predicting the *PE* from wetter or saturated soil surface. In Wilson's modified approach, the difference in temperature and relative humidity between soil surface and the air above it was taken into consideration. Therefore, atmospheric coupling was achieved in this modified equation. The Penman-Wilson equation can be written as follows (Wilson et al. 1994):

$$\mathrm{AE} = \frac{\Gamma Q_n + \eta E_a}{\Gamma + {}^{\eta}/_{h_s}} \qquad \text{Eq. (2.25)}$$

where: *AE* is actual evaporation (*mm/d*), *Γ* is the slope of saturation vapor pressure versus temperature curve (*kPa/°C*), Q_n correspond to net radiation at the water surface (*mm/d*), *η* is psychrometric constant equal to *0.06733kPa/°C*. E_a in the above equation is the flux associated with "mixing" in (*mm/d*) and can be written as

$$E_a = f(u)p_a\left({}^{1}/_{h_r} - {}^{1}/_{h_s}\right) \qquad \text{Eq. (2.26)}$$

where *f(u)* is the function dependent on wind speed, P_a is the vapor pressure in the air above the evaporating surface (*kPa*), h_r is the relative humidity in the air above ground (*i.e.*, u_v^{air} / u_{v0}^{air}), h_s is the relative humidity at the soil surface (i.e., u_v^{soil} / u_{v0}^{soil}), u_v^{air} is the water vapor pressure in the air above ground surface (*kPa*), u_{v0}^{air} is the saturated vapor pressure in the air above ground surface (*kPa*) and u_{v0}^{soil} is the saturated vapor pressure in the soil at ground surface (*kPa*).

For the calculation of evaporation from an unsaturated soil surface Wilson-Penman equation takes into consideration net radiation, wind speed and relative humidity for both air and soil surface, whereas in the case of fully saturated soil the conventional Penman, (1948) method can be used. This Wilson-Penman approach for estimating *AE* is available in commercial soil-atmosphere modeling software *VADOSE/W* (GEO-SLOPE International Ltd. 2012)

2.5.2 System-dependent boundary condition at soil-atmosphere interface

The calculation of actual evaporation in unsaturated flow and transport software *Hydrus-1D* is implemented as a system dependent boundary condition (Simunek et al. 1998). The direction and magnitude of the surface flux depends on the climatic conditions and the prevailing soil moisture condition near surface; therefore, it cannot be defined or estimated prior. In *system-dependent boundary condition*, the surface boundary condition can change from prescribed flux to prescribed head and vice-versa. The solution can be obtained by fulfilling following two conditions (Neuman et al. 1974):

$$\left|-K\frac{\partial h}{\partial x}-K\right| \leq E \quad \text{at x = L} \qquad \text{Eq. (2.27)}$$

$$h_A \leq h \leq h_S \quad \text{at x = L} \qquad \text{Eq. (2.28)}$$

where E is the maximum rate of infiltration or evaporation in the current atmospheric conditions [LT^{-1}], h_A and h_S are minimum and maximum pressure head, respectively, at the soil surface. The minimum allowed pressure head at the soil surface under prevailing climate conditions can be calculated from the air humidity and can be written as (Simunek et al. 1998):

$$H_r = exp\left[\frac{h_A\, Mg}{RT}\right] \qquad \text{Eq. (2.29)}$$

$$h_A = \frac{RT}{Mg}\, ln(H_r) \qquad \text{Eq. (2.30)}$$

where M is the molecular weight of water [$Mmol^{-1}$], g is the gravitational acceleration [LT^{-2}] and R is the gas constant [$Jmol^{-1}K^{-1}$].

2.6 Climate classification

Climate classification methods are used to identify different climate types. These methods are essential in understanding spatial and seasonal climate variability. Climate classification at a particular site is also very important for the quantification of water balance at the ground surface. It has been recommended that the average climatic conditions along with its variation should be understood by conducting climate classification before any numerical modelling for subsurface moisture movement is conducted (Fredlund et al. 2011). The Thornthwaite climate classification system (Thornthwaite 1948; Thornthwaite and Hare 1955) was developed in the United States and has been used for evaluating the climate for engineering purposes (Bashir et al. 2016, Fredlund et al. 2012). The Thornthwaite climate classification relies on the estimate of annual moisture index (I_m) as follows:

$$I_m = 100\left(\frac{P}{PE} - 1\right) \qquad \text{Eq. (2.31)}$$

where P is total annual precipitation and PE is the annual potential evaporation. Precipitation is usually measured at all weather stations and potential evaporation can be estimated by several different methods including the Penman, (1948) method. The annual moisture index may vary from positive values indicating moist/humid climates to negative

values indicating dry climates. The climate categories based on estimated annual moisture index is presented in Figure 2.4. It can be observed that the Thornthwaite climate classification system divides the climate in six different regions ranging from arid to pre-humid. It should be noted that in terms of water availability at the ground surface a positive value of I_m indicates that there is potential for net water availability at the ground surface. An I_m value of zero signifies that the annual precipitation and potential evaporation are equal and net neutral water conditions can be expected. Similarly, a negative value of I_m is indicative of expected net water loss conditions at the ground surface. Figure 2.4 shows the corresponding climate classification related to calculated moisture.

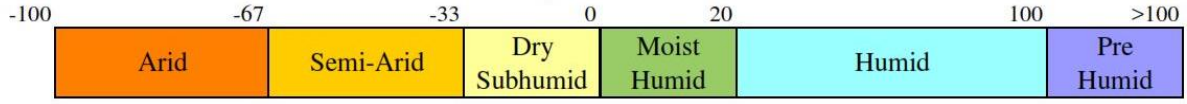

Figure 2.4: Climate classification criteria (moisture index (I_m) range -100 to >100)

2.7 Seasonal consideration

Frozen ground condition can be expected in most areas in Canada during the winter season. For the assessment of water balance at the ground surface, a calendar year can be divided into active and inactive periods. A schematic of the partitioning of a calendar year in active and inactive periods is shown in Figure 2.5. The inactive period starts when the precipitation starts to accumulate at the ground surface in the form of snow. This is the period when the ground surface becomes frozen and moisture flow into the ground surface is negligible. The first date of freezing (i.e., start of inactive period) can be identified by reviewing air and ground surface temperature records.

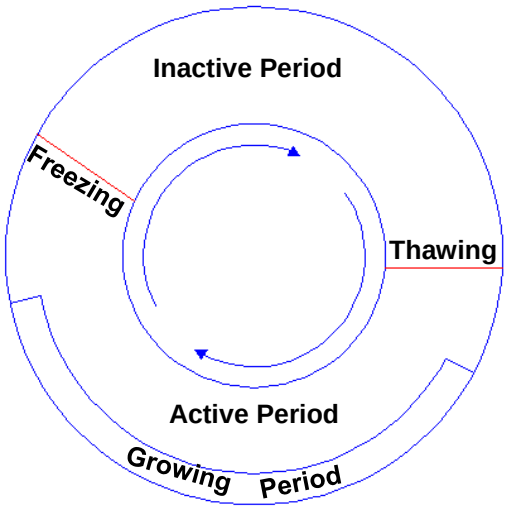

Figure: 2.5: Active and Inactive partition of a calendar year (modified from Fredlund et al. 2012)

Spring-like conditions mark the end of inactive period and start of the active period. At the start of the active period the snow accumulated over inactive period starts melting and the ground starts to thaw. This period is normally the start of the spring freshet and can result in significant availability of water at the ground surface. Significant water movement across the soil-atmosphere interface can also take place during this period. The start of the spring-like conditions can also be identified by reviewing air and ground surface temperature records. Summer-like conditions are considered to prevail over the rest of the active period when there is considerable activity in terms of heat and moisture movement across the soil atmosphere. A growing season for vegetation is also included in the active period.

Chapter 3

Measured Climate Data Compilation and Classification

This chapter presents the methodology related to the compilation and processing of climate data from different locations across Canada. There were two specific objectives for the climate data compilation. First, to have measured data sets against which the performance of climate generator can be assessed. Second, to use the data in geotechnical analysis and design involving soil-atmosphere boundary and comparing them with similar analyses using generated data.

3.1 Climate data compilation, processing, and classification

Daily continuous multi-year climate datasets were compiled from nine different locations across Canada. Figure 3.1 shows the geographical distribution of the weather stations selected for this study based on different climate types, including: St. John's (*NL*), Halifax (*NS*), Toronto and Timmins (*ON*), Regina (*SK*), Calgary and Whitecourt (*AB*) and Vancouver and Barriere (*BC*). Based on the climate classification by Thornthwaite and Hare, (1955), the climate variability of the selected locations ranges from semi arid to humid conditions.

The datasets consisted of daily values of precipitation, maximum and minimum temperature, relative humidity, wind speed and net radiation. Climate datasets for Toronto, Timmins, Regina, Calgary and Barriere were acquired from Bashir, (2014). The climate datasets for the remaining locations: St. John's, Halifax, Whitecourt, and Vancouver were compiled from measured historical weather data from Environment

Canada. Precipitation, maximum and minimum temperature, relative humidity and wind speed data was downloaded from Environment Canada website for historical data (Environment Canada, 2018a). Solar radiation data were obtained from Canadian Weather Energy and Engineering Dataset (*CWEEDS*) (Environment Canada, 2018b). Information on the Environment Canada weather stations associated with all locations is presented in Table 3.1 below.

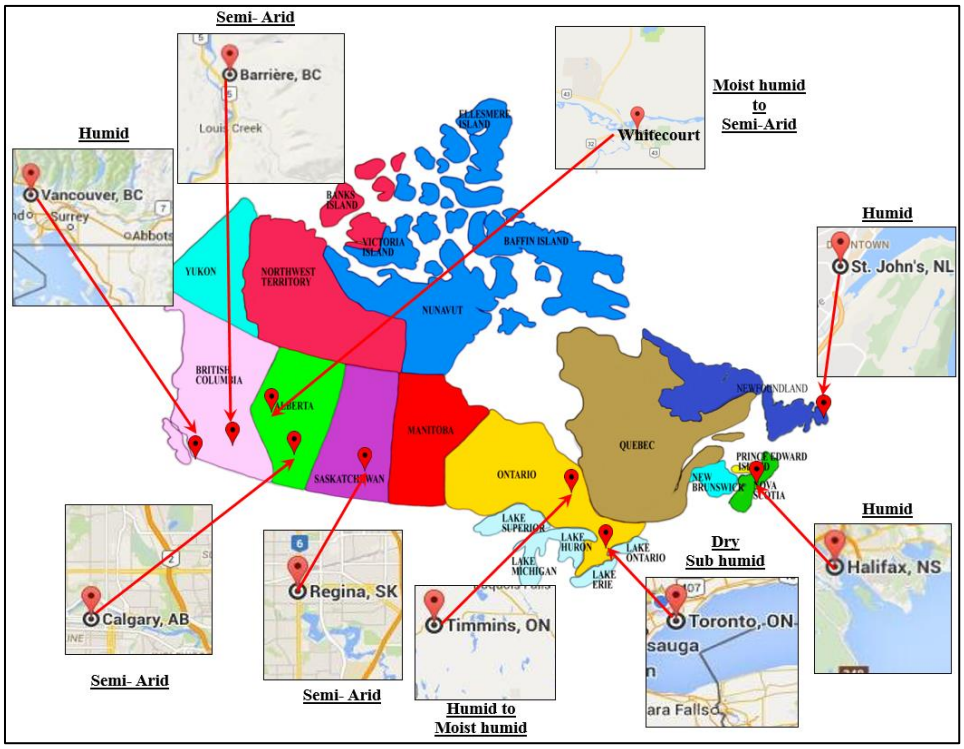

Figure 3.1: Location Map for Selected Weather Stations across Canada

The available historical climate data for each location were reviewed for completeness, and quality. Missing or erroneous values were infilled or replaced using the spatial (Alexandridis et al. 2013) or temporal interpolation (Alexandridis et al. 2013) methods. The compiled sets of data were analyzed to identify the relevant and significant features of the various climate variables. For the sake of brevity, the detailed analysis of the

compiled datasets for only Calgary and Halifax is presented in the following sections. The summary of all the datasets is presented in Table 3.2 at the end of this chapter and relevant plots are presented in Appendix-A.

Table 3-1: Weather station details

Location	***Weather Station***	***Latitude***	***Longitude***	***Compiled data # of years***
St. John's	St. John's Intl Airport	47°37'07''	52°45'09''	30
Halifax	Halifax Stanfield Intl A	44°52'48''	63°30'00''	32
Toronto	Toronto Intl Airport	43°40'36''	79°37'50''	30
Timmins	Timmins Victor Power A	48°34'11''	81°22'36''	30
Regina	Regina Intl Airport	50°26'00''	104°40'00''	16
Calgary	Calgary Intl Airport	51°06'50''	114°01'13''	10
Whitecourt	Whitecourt Airport	54°08'38''	115°47'12''	10
Vancouver	Vancouver Intl Airport	49°11'42''	123°10'55''	16
Barriere	Barriere	51°11'00''	120°07'00''	14

3.2 Semi-arid climate condition – Calgary

The city of Calgary is situated at the confluence of the Bow and Elbow river in the south of the province of Alberta. Calgary experiences semi arid climate according to the climate classification by Thornthwaite and Hare, (1955). The average daily temperature ranges from 16.5 °C in July to -6.8 °C in December. The minimum temperature in winter can dip below -20 °C, whereas in summer the temperature can exceed 30 °C. Average annual precipitation of 418.8 mm is recorded at Calgary international airport located northeastern section of city (Environment Canada, 2018a).

A 10-year climate dataset for Calgary from January 2005 to December 2014 was compiled. Daily precipitation records for this period are shown in Figure 3.2. The cumulative and the average annual precipitation values are also shown in the same

figure. The average annual precipitation for this compiled dataset was *428* mm, which correlates well with the reported station normal value of *418* mm for period 1981-2010 (Environment Canada, 2018c). Review of the precipitation data indicates that over the 10-year period there was only a single storm of 70 mm or more occurring on June 5th, 2007.The data also reveals that over this period there were only 1% precipitation events for which the total amount of precipitation exceeded 20 mm. It can also be observed that for more then 95% events the total amount of precipitation was less than 7 mm/day.

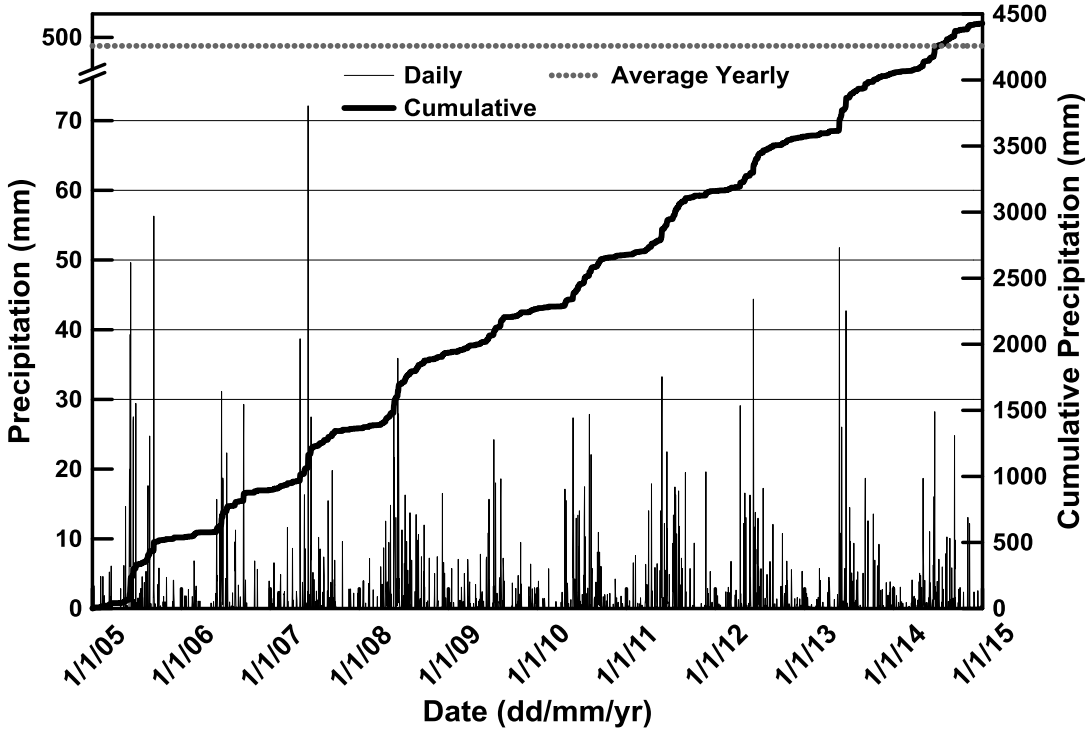

Figure 3.2: Precipitation data for Calgary (2005-2014)

The daily maximum and minimum temperature for Calgary is shown in Figure 3.3. The maximum temperature of 33.9 ^{o}C was recorded on August 18th, 2008, the minimum temperature on the same day was 13.68 ^{o}C. The temperature greater then 30 ^{o}C was

normally observed in the months of July and August. The minimum recorded temperature in ten years compiled data was -35.23 ^{o}C. This temperature was observed on January 13th, 2005. The average maximum temperature in ten years was 10.46 ^{o}C, whereas the average minimum temperature was -1.56 ^{o}C. Based on the detailed review of the temperature data November 19th was estimated to be date when freezing condition were expected to develop. A similar review of the data led to the identification of April 9th to be start of the thawing period. Based on these days, it was concluded that on average the active period lasts from April 9th to November 18th, comprising 224 days in a calendar year.

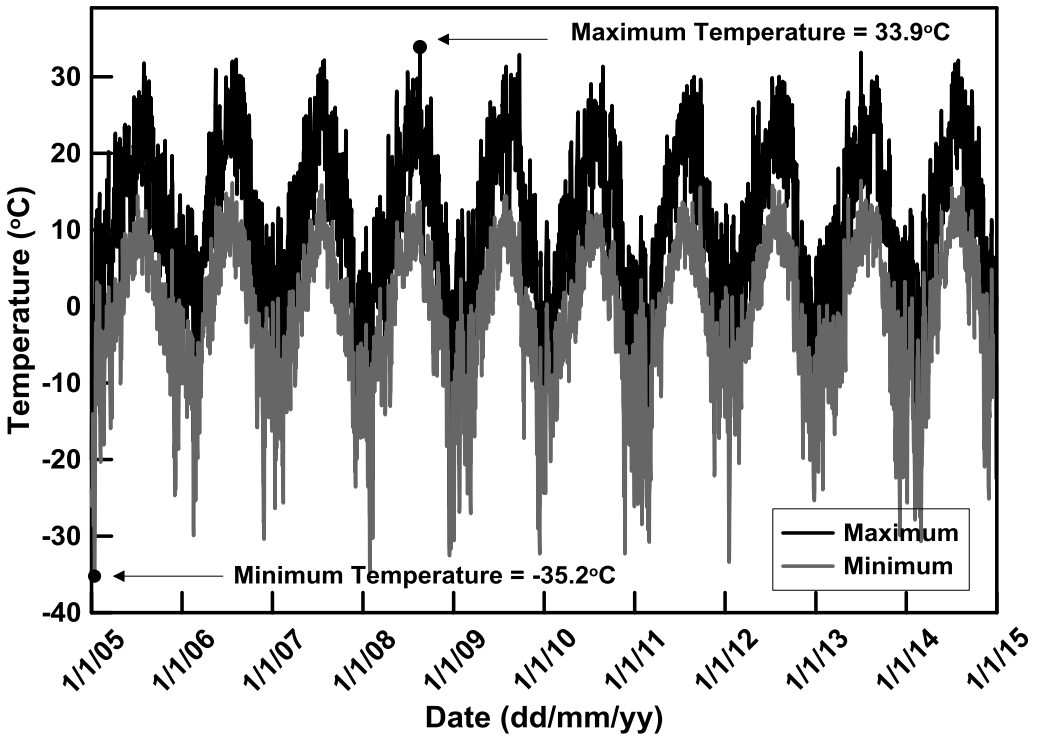

Figure 3.3: Temperature data for Calgary (2005-2014)

The daily minimum and maximum values of relative humidity for Calgary from 2005 to 2014 are shown in Figure 3.4. The average values with standard deviation are also shown in the same figure. It was observed from the compiled data that relative humidity less then 70% was observed for more than sixty percent of the days over the ten years period. Also, values greater than 80% were observed for only 18% of days. The relative humidity greater than 90% was recorded only for 189 days which makes only 5% of total recorded data. The compiled dataset values correlated well with the yearly average reported values of relative humidity 71.7% and 48.3% at 0600 and 1500 hrs respectively (Environment Canada, 2018c).

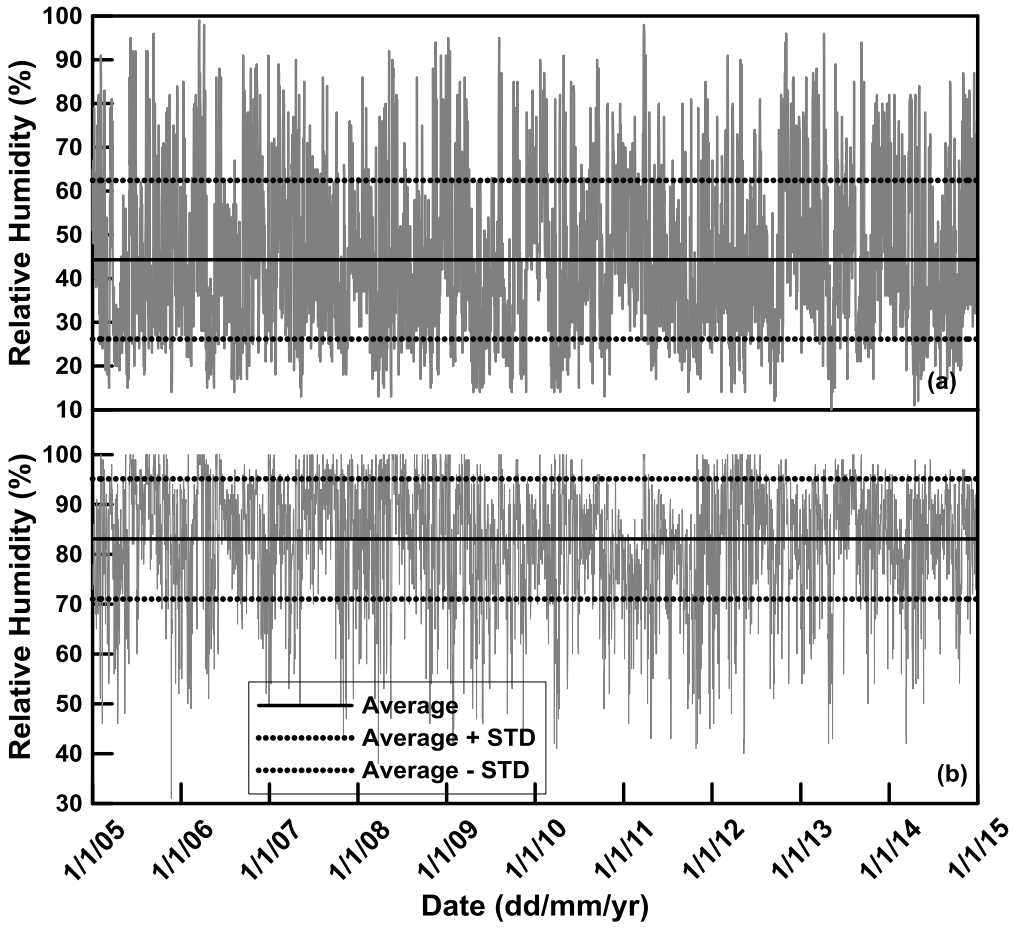

Figure 3.4: Relative humidity data for Calgary (2005-2014). (a) minimum (b) maximum

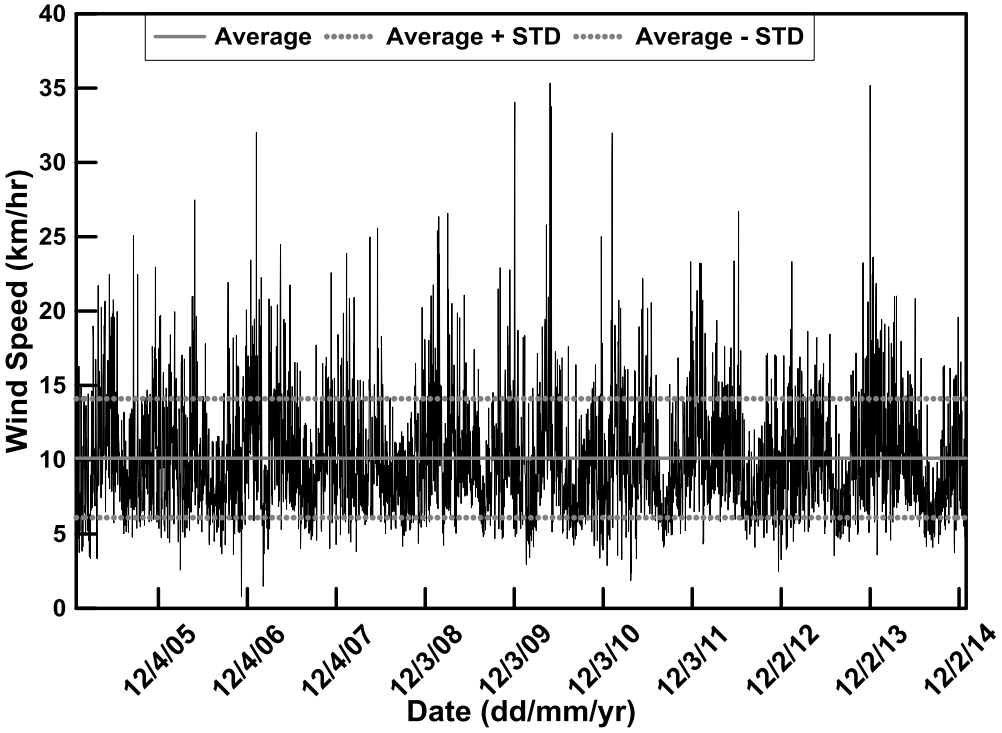

Figure 3.5: Average daily wind speed data for Calgary (2005-2014)

The measured daily solar radiation and calculated net radiation data for Calgary for the year 2005-2014 are shown in Figure 3.6. Net radiation was estimated based on equations formulated in terms of total solar radiation, relative humidity, and temperature (Allen et al. 1998, Irmak et al. 2003).The maximum, minimum and average estimated values for net radiation for the compiled dataset were 30.24 MJ/m^2/d, 1.40 MJ/m^2/d and 13.19 MJ/m^2/d respectively.

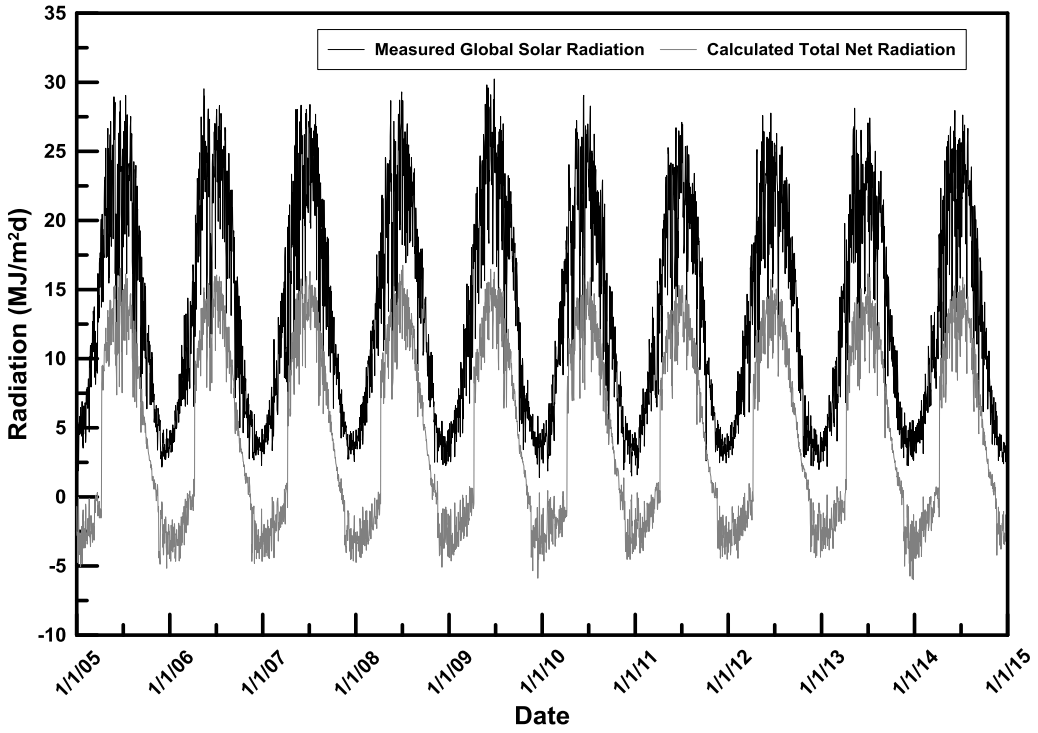

Figure 3.6: Average daily solar and net radiation data for Calgary (2005-2014)

Potential evaporation for Calgary was estimated using the compiled climate dataset employing the Penman, (1948) method. The climate for Calgary was classified by computing the annual moisture index (Thornthwaite, 1948; Thornthwaite and Hare, 1955) using the measured precipitation and estimated potential evaporation. The climate classification is shown in Figure 3.7.

It can be observed that the climate can be classified as being “semi arid” with an average moisture index of -54.1. It can also be observed that there is no significant variation between the years for which the climate data was compiled as standard deviation for moisture index was estimated to be only 7.

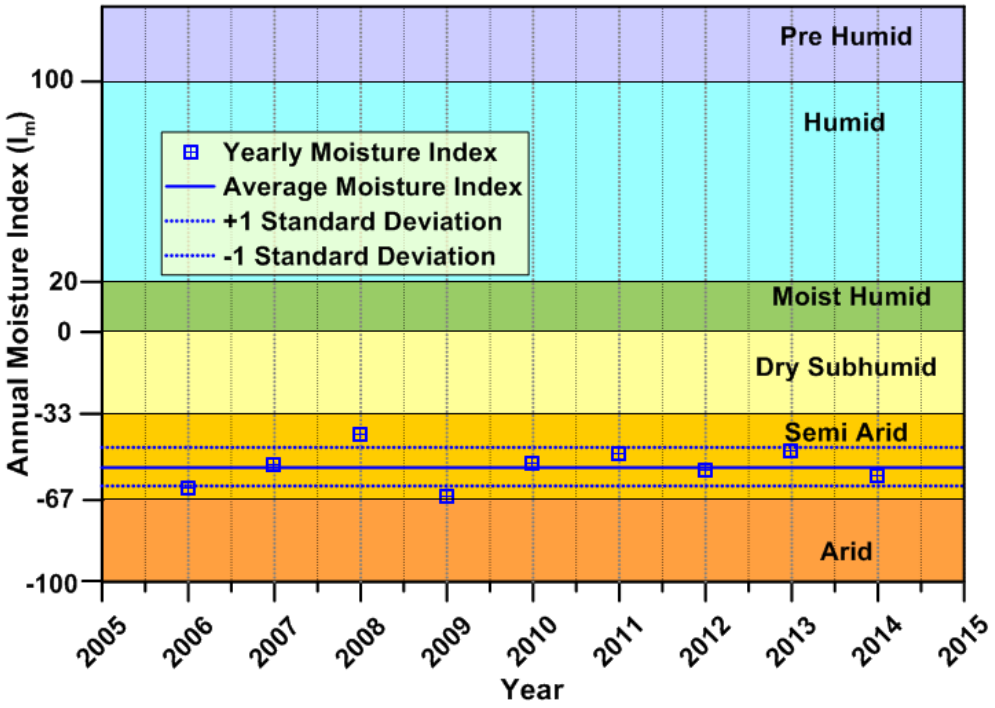

Figure 3.7: Climate classification for Calgary

3.3 Humid climate condition – Halifax

Halifax, legally knows as the Halifax Regional Municipality (HRM), an Atlantic Ocean Port in eastern Canada, is the capital of the province of Nova Scotia. HRM occupies an area of 5,577 km^2 which is about 10% of the total land area of Nova Scotia. HRM has Humid climate according to the climate classification by Thornthwaite and Hare, (1955). The average daily temperature ranges from -5.9 ^oC in January which is the coldest month to 18.8 ^oC in July the warmest month. The minimum temperature in winter can dip below -28.5 ^oC, whereas in summer the temperature can go up to 35 ^oC. Average annual precipitation of 1396.2 mm recorded at Halifax Stanfield international airport, which is located almost at the center of HRM (Environment Canada, 2018a).

A 32-year climate dataset for Halifax from January 1974 to December 2005 was compiled. Daily precipitation records for this period are shown in Figure 3.8. The cumulative and average annual precipitation values are also shown in the same figure. The average annual precipitation for this compiled dataset was 1398 mm, which correlates well with the reported station normal value of 1396.2 mm for the 1981-2010 period (Environment Canada, 2018c). Review of the precipitation data indicates that over the 32-year period there were seventeen (17) precipitation events of 70 mm or more. The maximum precipitation recorded in a single day was 100.1 mm occurring on January 14th, 1978.The data also reveals that over this period there were only about 6% precipitation events for which the total amount of precipitation exceeded 20 mm.

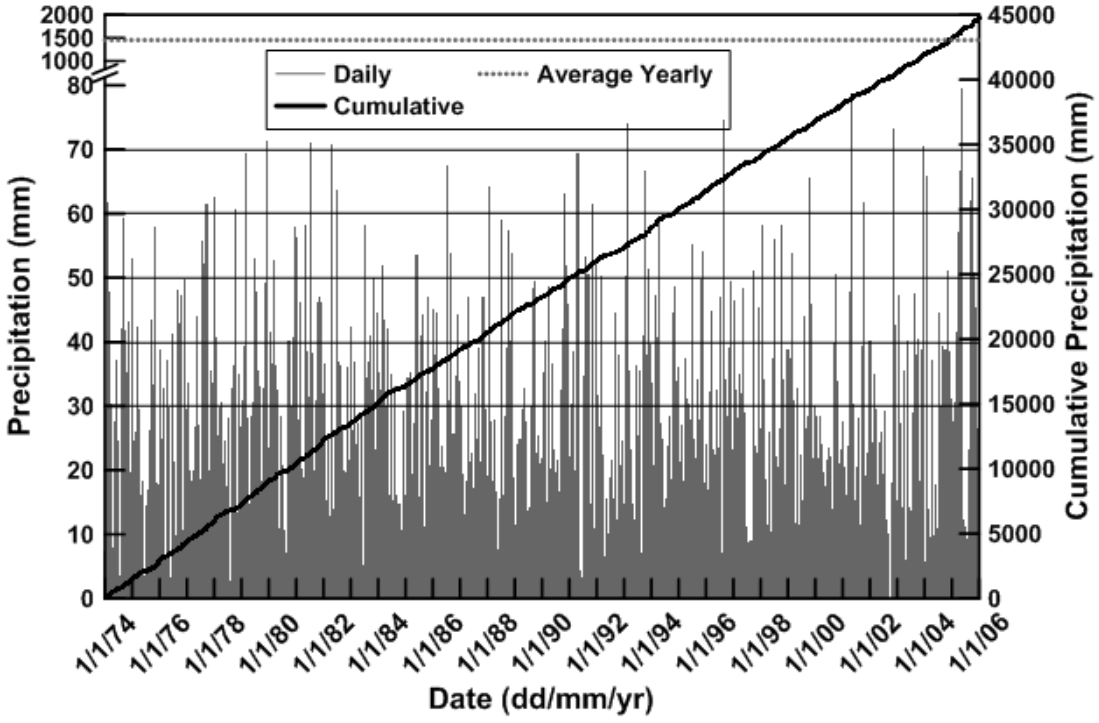

Figure 3.8: Precipitation data for Halifax (1974-2005)

It can also be observed that for more than 80 % events the total amount of precipitation was less than 7 mm/day.

The daily maximum and minimum temperature for Halifax are shown in Figure 3.9. The maximum temperature of 35 ^{o}C was recorded on August 1st, 1995, the minimum temperature on the same day was 16.4 ^{o}C. The temperature greater than 30 ^{o}C was normally observed in June to August, whereas in 1977 and 1992 the temperature exceeded 30 ^{o}C at the end of May. The minimum recorded temperature in thirty-two years compiled data was -28.5 ^{o}C. This temperature was observed on January 31st, 1993 and January 26th,1994. The average maximum temperature in thirty-two years was 11.09 ^{o}C whereas the average minimum temperature was 1.75 ^{o}C.

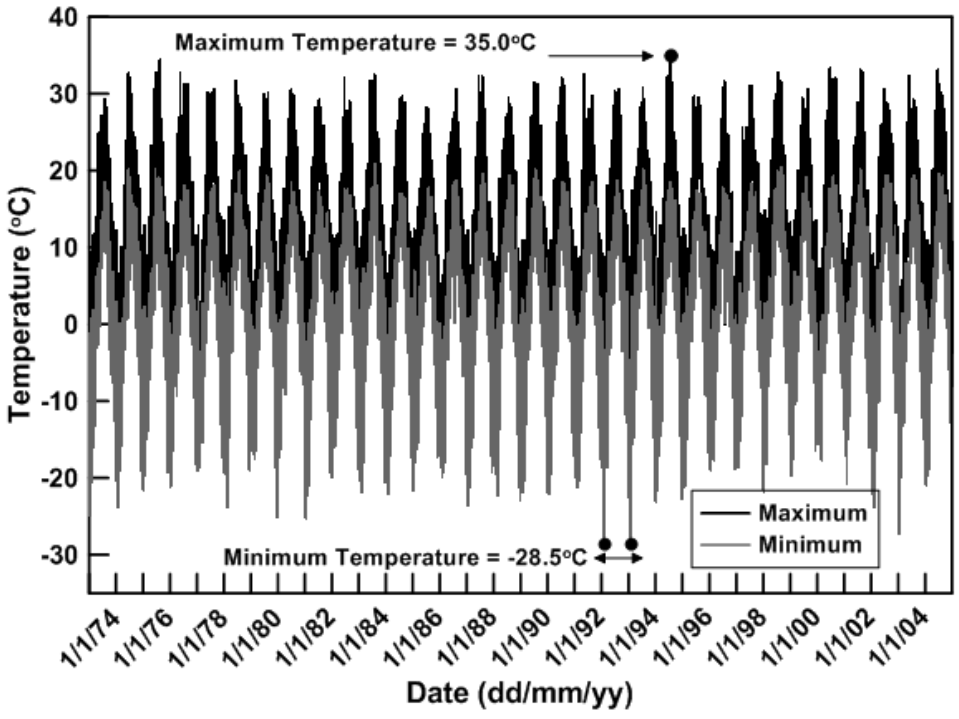

Figure 3.9: Temperature data for Halifax (1974-2005)

Based on the detailed review of the temperature data November 26th was estimated to be date when freezing condition were expected to develop. A similar review of the data led to the identification of April 14th to be start of the thawing period. Based on these days, it was concluded that on average the active period lasts from April 14th to November 25th, comprising 226 days in a calendar year.

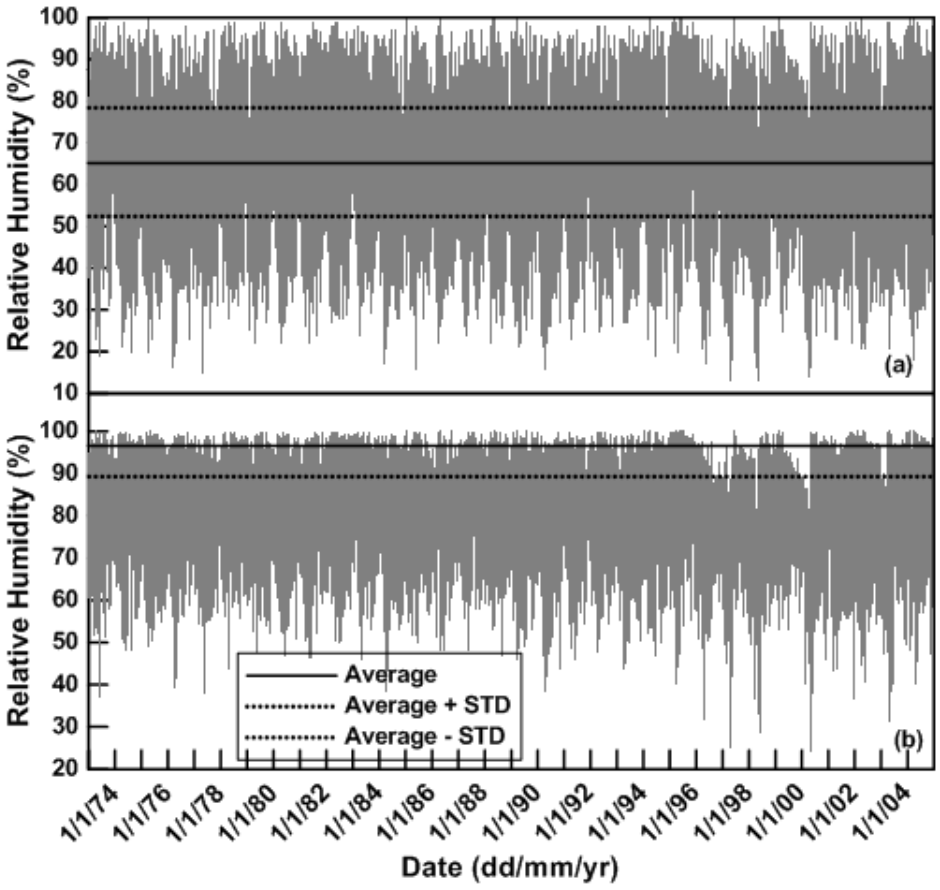

Figure 3.10: Relative humidity data for Halifax (1974-2005). (a) minimum (b) maximum

The daily minimum and maximum values of relative humidity for Halifax from 1974 to 2005 are shown in Figure 3.10. The average values with standard deviation are also shown in the same figure. It was observed from the compiled data that relative humidity

greater than 70% was observed for more then seventy percent of the days over the thirty-two years period. Also, values greater than 80% was recorded for more than 50% of total recorded data. The relative humidity values less than 50% was observed for only 153 days which makes only 1.31% of total recorded data. The compiled dataset values correlated well with the yearly average reported *RH* values of 87.1% and 66.5% at 0600 and 1500 hrs, respectively (Environment Canada, 2018c).

The average daily wind speed data for the compiled dataset for Halifax is shown in Figure 3.11. The yearly average and standard deviation values are also shown in the same figure. The maximum and minimum recoded wind speed was 52.83 km/hr and 0.29 km/hr respectively. The average wind speed value was 16.6 km/hr and correlates well with the reported average value of 16.5 km/hr (Environment Canada, 2018c).

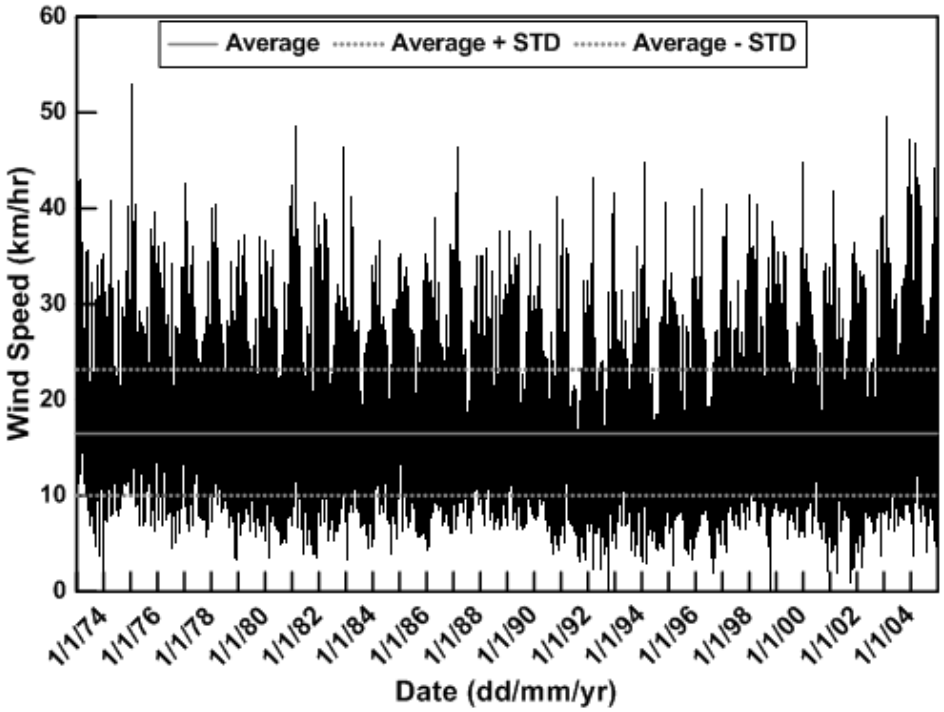

Figure 3.11: Average daily wind speed data for Halifax (1974-2005)

The measured daily solar radiation and calculated net radiation data for the city of Halifax for the year 1974-2005 is shown in Figure 3.12. Net radiation was estimated based on equations formulated in terms of total solar radiation, relative humidity, and temperature (Allen et al. 1998; Irmak et al. 2003). The maximum, minimum and average estimated values for net radiation are 33.43 MJ/m^2/day, 0.60 MJ/m^2/day and 12.27 MJ/m^2/day, respectively.

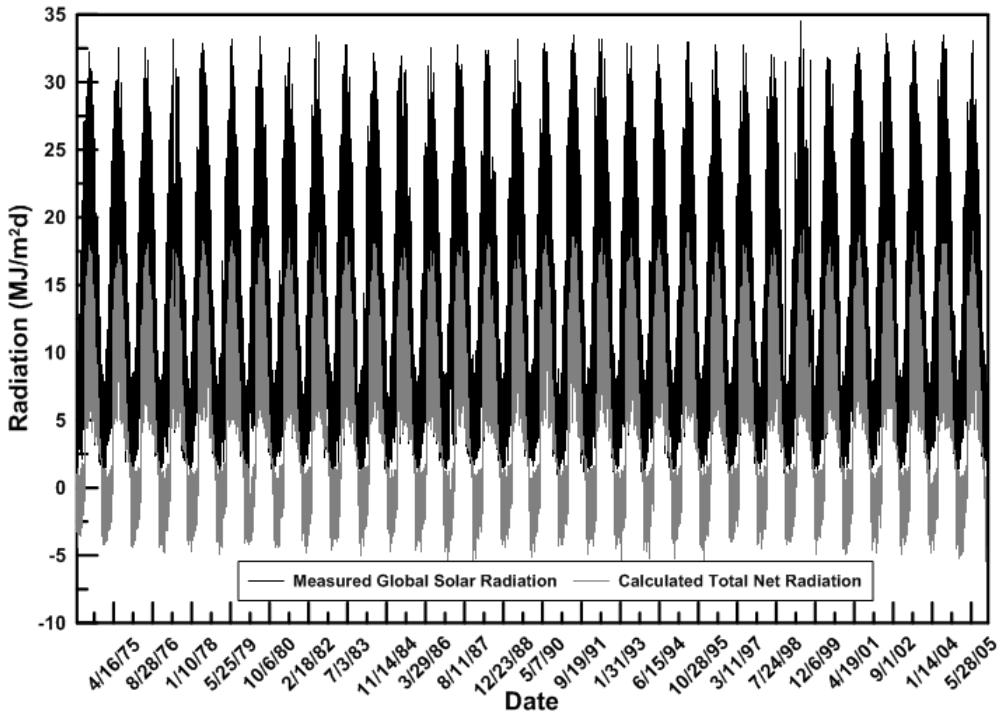

Figure 3.12: Average daily solar and net radiation data Halifax (1974-2005)

Potential evaporation for Halifax was estimated using the compiled climate dataset employing Penman, (1948) method. The climate for Halifax was classified by computing the annual moisture index (Thornthwaite, 1948; Thornthwaite and Hare, 1955) using the measured precipitation and estimated potential evaporation. The climate classification is shown in Figure 3.13. It can be observed that the climate can be classified as being

"Humid" with an average moisture index of 69.12. It can also be observed that the years for which the climate data were compiled the standard deviation for moisture index was estimated to be 25. The figure also shows that in comparison to Calgary, there is a lot of variation in year to year climatic conditions for Halifax.

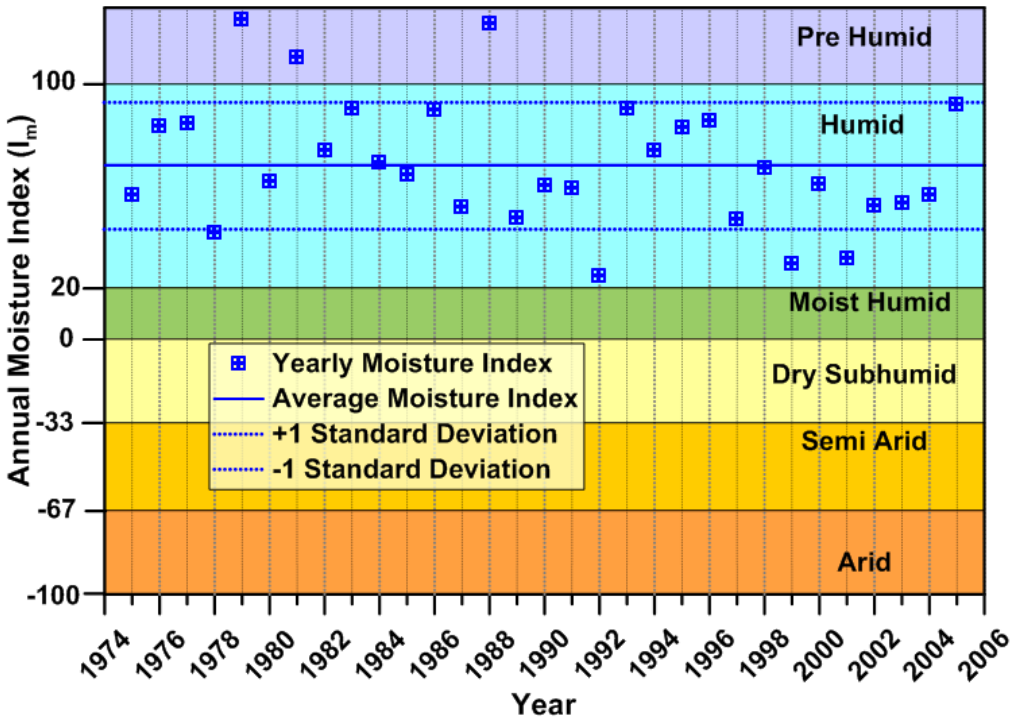

Figure 3.13: Climate classification for Halifax

3.4 Climate data summary

Pertinent summary for yearly average conditions for all sites are provided in Table 3.2.

Table 3.2: Climate data summary for all sites

Location	Precipitation (mm)		Temperature (^{0}C)		Relative Humidity (%)		Wind Speed (km/h)		Net Radiation (MJ/m^2/d)	
	Min	Max	Min	Max	Min	Max	Min	Max	Min	Max
Toronto	0	118.5	37.9	-31.3	100	10	54.21	0.96	34.39	0.79
Vancouver	0	91.6	34.4	-15.2	100	15.5	41	0.87	89.99	0.43
Halifax	0	100.1	35	-28.5	100	13	52.83	0.29	99.99	0.6
Timmins	0	87.6	38.9	-44.2	100	7	58	0.2	32.8	0.33
Calgary	0	72.1	33.9	-35.2	100	19.4	44.47	1.01	30.24	1.4
Whitecourt	0	56.2	34.7	-42.7	100	3.89	31.76	0.21	32.95	0.58
Barriere	0	48.8	40	-38	100	12	35.71	0.08	31.77	0.02
Regina	0	76	37.5	-41.9	100	14	67	0.83	31.37	0.01
St. John	0	99.4	31.5	-23.8	100	33.6	72.81	1.77	74.04	0.5

The plots of all the dataset are shown in Appendix A. The climate classification based on Thornthwaite and Hare, (1955) for all the sites is presented in Figure 3.14.

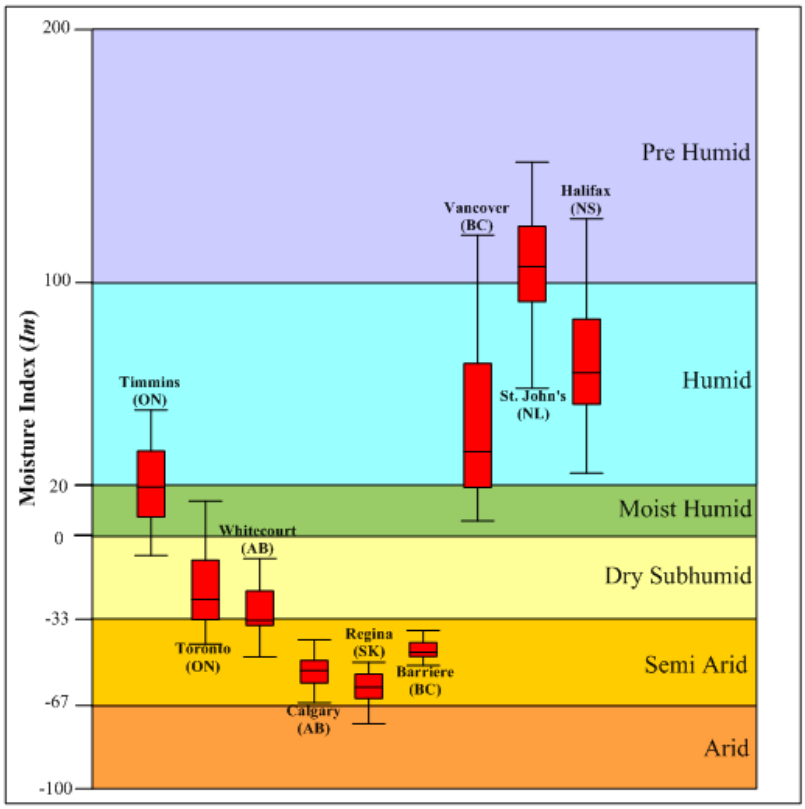

Figure 3.14: Climate classification summary for all sites

In this figure, it can be observed that Vancouver and Halifax belong to humid climate condition. Regina and Barriere have semi-arid climate condition, Toronto and Whitecourt have dry sub-humid, Timmins belong to moist humid and St. John's to pre-humid climate condition. This figure also indicates that the compiled dataset coves most of the climate types in the climate classification system.

Chapter 4

Climate Data Simulation

This chapter is divided into three sections. The first section provides detail of general purpose weather generator namely: *SIMETAW* (Snyder et al. 2012). The second section presents the methodology used for the simulation of multiyear daily climate dataset for nine different geographical regions across Canada. In the third section comparison between the measured and simulated climate data is presented. The comparison is presented for dry and wet climates, corresponding to Calgary and Halifax. The comparison for other seven locations is presented in Appendix B. The measured and simulated climate data is compared visually and statistically.

4.1 Simulation of evapotranspiration of applied water - *SIMETAW*

The rapid land reduction associated with salinity, alkalinity and waterlogging problems, is result of poor water resource management and climatic effects (Alexandrina et al. 2010). This has encouraged the researchers to look for better procedures to estimate evapotranspiration of applied water (Alexandrina et al. 2010). *SIMETAW* has helped water resource planners, engineers, and researchers around the globe to determine actual evapotranspiration, and evapotranspiration of applied water. The State of California is currently using *SIMETAW* to estimate the demand for irrigation water in order to improve the water resources management (Alexandrina et al. 2010).

Developed by the University of California Davis, and the California Department of Water Resources, *SIMETAW* aims to provide the best possible information on agricultural water demand, and can also be used in other water resource planning activities (Orang and Snyder, 2004). *SIMETAW* not only estimates crop coefficient (K_c) and reference evapotranspiration (ET_o) but also has the capability to simulate daily climate data from monthly climate normals. The monthly climate normals are three-decade averages of various climate variables. The climate normals used by *SIMETAW* are solar radiation (MJ/m^2), maximum temperature (^oC), minimum temperature (^oC), wind speed (m/sec), dew point temperature (^oC), precipitation (mm), number of rainy days (#), elevation (m) and latitude (^{o}). The program estimates the evapotranspiration of applied water (ET_{aw}) for specific soil, crop, and climate conditions. The program can also compute crop evapotranspiration (ET_c) and daily water balance with effective rainfall. The data simulated by *SIMETAW* can also be used to fill in the missing measured data both spatially and temporally. In this research the daily climate data simulated by *SIMETAW* from monthly climate normals is evaluated for its adequacy to be used in geotechnical and geoenvironmental analysis and design.

SIMETAW simplifies the parameter estimation procedure of Richardson and Wright, (1984), requiring only the monthly means as inputs. The software establishes the climate condition of a region either based on the input of historically measured daily climate data or widely available climate normals. *SIMETAW* follows the procedure of identifying the wet or dry day condition first, and then simulates the other variables.

SIMETAW's estimated ET_o is based on Penman-Monteith equation (Walter et al. 2001). The programme can also be used for the quantification of the effect of variations

in temperature and precipitation on evapotranspiration patterns (Richard et al. 2004, Orang and Snyder, 2004, Snyder et al. 2012, Ebrahimpour et al. 2014). Crop coefficient (K_c) and ET_c for the field crops cultivated under different irrigation strategies can be updated based on the variation in temperature and precipitation (Alexandrina et al. 2010).

Rainfall pattern method is used by *SIMETAW* to simulate daily rainfall data from thirty-year average monthly data (*Climate normals*). This method is based on the recognition of two main facts. Firstly, rainfall patterns are normally skewed to the right towards extreme heavy amount. The second is that the rain status of the previous day tends to affect the present-day conditions. *SIMETAW* uses Gamma distribution and Markov chain modelling approach to define the rainfall patterns (Orang and Snyder, 2004).The monthly average precipitation along with the number of rainy days in a particular month are used to obtain the rest of variables in *SIMETAW* model (Orang and Snyder, 2004).

SIMETAW simulates the wind speed using gamma distribution function. The gamma distribution normally gives good estimates of the extreme values but has a tendency to estimate few unrealistically high values. To overcome this problem *SIMETAW* developers have set an upper limit for simulated wind speed at twice the mean wind speed (Orang and Snyder, 2004).

Temperature and solar radiation data is simulated by *SIMETAW* using a Fourier series distribution model. This model can be expressed mathematically as follows:

$$X_{ki} = \mu_{ki}(1 + \delta_{ki}C_{ki}) \qquad \text{Eq. (4.1)}$$

Where *X* is either temperature or solar radiation based on the input of *k = 1,2* and *3* (*k=1 represents maximum temperature; k=2 represents minimum temperature; and k=3 represents solar radiation*), μ_{ki} is the estimated daily mean, and C_{ki} is the estimated daily coefficient of variation of the i^{th} day, *i=1, 2, …., 365* and for the k^{th} variable.

Table 4.1 lists the relevant inputs required to simulate multi year daily climate data from monthly climate normals. The output variables from *SIMETAW* are also identified in the same table. Please note that crop/soil data is used in estimation of ET_0 and is required for the program to run. However, this information has no implications on simulated climate data

Table 4.1: *SIMETAW* climate data input and output

Input	Output
1- Climate Normals of solar radiation, Precipitation, temperature, wind speed, number of rainy days, elevation and latitude. 2- Crop / Soil data i. Study area # ii. Crop information iii. Soil type iv. Covered area 3- Site information i. Filename ii. Latitude iii. Elevation	Daily simulated climate data values of i. Solar radiation (MJ/m^2) ii. Max temperature (^0C) iii. Min temperature (^0C) iv. Wind speed (m/sec) v. Dewpoint temperature (^0C) vi. Precipitation (mm/day) vii. Reference evapotranspiration (mm/day)

For detail please refer to the programme's user guide in Appendix C (California Department of Water Resources, 2018).

4.1.1 *SIMETAW* previous work

Anderson et al. (2008) used *SIMETAW* to estimate the effect of climate change on evapotranspiration rate and its impact on future water demand for agriculture. They

recommended the use of their findings for planning, mitigation, and adaptation strategies for the changing climate.

HUANG et al. (2012) used *SIMETAW* to calculate the average crop water requirements and effective rainfall for several different crops. The study was carried out to quantify how the modern cropping pattern have altered the water resources in the greater Beijing metropolitan area, an expanding megacity which also includes rural counties. The results of their study indicated that the change in cropping pattern have a considerable impact on the water resources. Recommendation on the need of policy development for adjusting the use of water between agriculture and industry was made.

Swelam, (2012) used *SIMETAW* to help the Egyptian water policy planners to develop a methodology to maximize irrigation water productivity in agricultural cropping system. The study calibrated *SIMETAW* using continuous ten (*10*) years of measured data for Zanklon location of the Nile Delta region. The actual K_c for two different crops namely wheat and maize were evaluated by using *SIMETAW*. The study also explains the procedure of determining the ET_{aw}. The study concludes that *SIMETAW* can be used efficiently to estimate the water balance and evaluate different irrigation strategies.

Orang et al. (2013) used *SIMETAW* to calculate ET_{aw} for water resource planning in the state of California. Their study discuses the *SIMETAW* model in detail and perform the daily soil water balance to estimate ET_c, ET_{aw} and applied water (*AW*) to be used for the main objective of resource planning.

Yang et al. (2013) calculated ET_c and ET_{aw} using *SIMETAW* for summer maize crop in the Huang-Huai-Hai (*HHH*) region of China. The purpose of their study was to

demonstrate the importance of ET_c in water resource planning. For their study they used fifty years daily weather data from 1960-2009 to estimate ET_c and ET_{aw}. The temporal and spatial distribution of ET_c and ET_{aw} was interpreted by applying inverse distance weighted interpolation (*IDW*) method. It was observed that in the *HHH* farming region, the ET_c of the summer maize in the growing season has shown a downward trend. A decrease in the value from 335.6 mm/decade to 311.4 mm/decade was recorded for average ET_c over the period of 1960-1969 and 2000-2009 respectively. However, there was no reduction noted in ET_{aw} because of yearly fluctuation of effective rainfall (R_{eff}) in growing season and improvement in irrigation procedures. It was also observed that the average ET_c value is higher in the eastern region and lower in western region, which were inversely proportional to the observed ET_{aw} values. This was as a result of employing different irrigation system in different regions and the impact of climate change in the region. For example, because of reduction in solar radiation a lower value of ET_c was observed and a higher value of ET_c was recorded because of lower precipitation and relative humidity.

Ebrahimpour et al. (2014) investigated the effects of climate change on ET_o using *SIMETAW*. In their study, daily climate data was simulated for four different locations in Iran. Their study highlights the consideration of effect of climate change on ET_o for formulating reasonable policy for future water supply. The data simulated by *SIMETAW* was used in the climate change study. The calculated ET_o values were compared with the simulated values by *SIMETAW.* It was observed that except for the daily wind speed *SIMETAW* accurately simulate all other variables very well.

Shah, (2014) assessed the feasibility of reusing the wastewater in the carbon sequestration forest in Davis, CA. The main objective of the study was to choose a crop based on the amount of carbon it can sequester per year considering the climate and water quality requirements. The ET_{aw} was simulated for several trees, for example, Douglas Fir, Ponderosa Pine and Redwood. These were identified as potential species that have the capability for maximum long-term carbon sequestration. Finally, Redwood trees were recommended species, which may be cultivated on about 570 acres of the city-owned land based on the results that showed that they can capture greatest mass of carbon/acre/year.

Huang et al. (2015) carried out a case study in the Beijing region for reducing the agricultural water footprints of wheat and maize crops. In this study, both irrigation water and nitrogen application rate were reduced by 33% during a season compared to the current practice. The reductions did not cause a significant decline in the yield. Furthermore, it reduced the water eutrophication footprint from 52.3% to 27.5%. The water consumption to produce crop was determined using ET_c and accessible R_{eff} using *SIMETAW*. In the case study the irrigation and nitrogen reduction were conducted separately during typical rainfall conditions. The authors recommended further studies to quantify the coupled effects of water-fertilizer option on crop yield.

Yin et al. (2016) studied the effect of climate variation on maize, rice, soybean, and spring wheat crop yield in the Northeast Farming Region of China (*NFR*) for the period ranging from 1961-2010. The study was carried out for three main growth phases which were; pre-flowering, flowering, and post-flowering. The climate variables calculated for each growth phase were; mean minimum temperature, thermal time, average daily solar

radiation, accumulated precipitation, aridity index and heat degree-day index (*HDD*). The aridity was calculated using estimated ET_o by *SIMETAW* model. The results of study indicated that projected future climate change may affect crop yield in different growth phases through different climate variables. The adaptation measures were suggested for better agricultural water management.

SIMETAW's previous work indicate that it has mainly been used in the water resource studies related to agriculture in many different parts of the world. There are no documented studies on *SIMETAW's* use in geotechnical and geoenvironmental analysis and design from a water balance or climate data simulation perspective.

4.1.2 Simulation of climate data

Climate data were simulated for nine regions across Canada. Thirty-year historical Climate normals were used as input data. Climate normals were acquired from the database of climate normals (Environment Canada, 2018c) and *NASA* (NASA, 2018). The geographical locations considered in this study were Toronto and Timmins (*ON*), Halifax (*NS*), St.John's (*NL*), Regina (*SK*), Calgary and Whitecourt (*AB*), Berriere and Vancouver (*BC*). Other details of these locations have already been described previously in Chapter 3. As mentioned earlier these locations represent different climate types across Canada. The climate data was simulated for the same number of years as the compiled daily measured data.

SIMTEAW simulates daily values of maximum and minimum temperature, dew point temperature, wind speed, and solar radiation. *SIMETAW* does not simulate relative

humidly (*RH*) values as model output. Relative humidity values are required for estimation of potential evaporation (*PE*) by Penman, (1948) method and estimation of actual evaporation (*AE)* by Wilson, (1994) method. Therefore, daily data for *RH* was calculated from simulated dew point temperatures using Eq. 2.7 presented in Chapter 2. The estimated *RH* data were also compared to measured *RH* data. In addition to the comparison of measured climate variables, comparison between estimates of *PE* and moisture indices (I_m) from measured and simulated climate data were also carried out. *Potential evaporation* was estimated using the Penman, (1948) method and I_m was estimated using the measured and simulated annual precipitation and *PE* values.

Review of the simulated climate data indicated that *SIMETAW* in some instances simulates erroneous values for daily wind speed. It was found that for some locations *SIMETAW* simulated either negative values or unusually high values for wind speed. However, these values were less than 2.4% of the total simulated data. The negative wind speed values were modified by replacing them with a zero value. Similarly, wind speed values greater than the maximum hourly speed were replaced with the maximum hourly speed for the respective month. It should be noted that maximum hourly speed data is also reported as part of the climate normals for a site.

4.1.3 Comparison of measured and simulated climate data

The comparison between simulated and measured climate data, and associated quantities was carried out for all nine locations. However, for the sake of brevity the comparison here is only presented for Calgary and Halifax. These locations were selected

for two reasons. First Calgary has arid climatic conditions, while Halifax has humid climate. Therefore, such a comparison would quantify the ability of *SIMETAW* to simulate climate data for range of climatic conditions. Secondly the compiled dataset for Calgary only comprised of a 10-year record, while the compiled dataset for Halifax was for 32 years. It is anticipated that this comparison would highlight issues, if any, related to shorter climate datasets.

The climate data simulated from *SIMETAW* were compared to the compiled measured data by two different methods namely, visual presentation methods and numerical measures. Both methods provide important, non-overlapping information. Visual presentation methods allow for visual comparison of similarities and differences between the simulated and measured climate data. Visual displays are useful for a rough estimate of the agreement between the simulated and measured data and indicate where the predictions are most problematic. Numerical measures using statistical methods provide summary measures of overall accuracy of the predictions. They indicate if the trend relative magnitudes are captured, and how much is the deviation from the exact data locations. A brief review of the statistical methods used for comparison is provided in the following section. Comparison of different climate variables and associated estimated quantities required slightly different strategies. This is explained in the respective comparison section for these variables.

4.2 Comparison Statistics

Two types of numerical measures were made in order to evaluate the goodness-of-fit between simulated and measured data. The first type indicates the accuracy of how

well the trend of relative magnitudes is captured. The second measure indicates the deviation from the exact location of data. This analysis is in line with the recommendation by Schunn and Wallach, (2005), who recommended that at least one measure of each type should be used for a proper statistical comparison.

4.2.1 Coefficient of Determination (R^2)

Coefficient of determination (R^2) can be used to evaluate how well the trend relative magnitudes are captured. It determines the discrepancy between the compared data as ratio of variation explained by the regression to the total variation. The regression indicates the relation between mean values of both datasets. For the measured and simulated data, the coefficient of determination (R^2) is computed according to the expression given by Fasshauer et al. (2007):

$$R^2 = \frac{[n\sum_{i=0}^{n}(m_i)(s_i) - (\sum_{i=0}^{n} m_i)(\sum_{i=0}^{n} s_i)]^2}{\left[n\sum_{i=0}^{n} s_i^2 - \left(\sum_{i=0}^{n} s_i\right)^2\right]\left[n\sum_{i=0}^{n} m_i^2 - \left(\sum_{i=0}^{n} m_i\right)^2\right]} \qquad \text{Eq. (4.2)}$$

where *m* and *s* refer to measured and simulated data respectively and *n* is the number of data points used for comparison. The resultant value of coefficient of determination ranged between *0* and *1*. The value of *1* indicates that the regression equation has interpreted *100%* variation, with a well captured trend relative magnitude. Conversely, a value of *0* indicates that the regression equation has failed to interpret any variation and, no trend relative magnitude is captured.

4.2.2 Root Mean Squared Deviation (*RMSD*)

Root Mean Squared Deviation (*RMSD*) is used to evaluate goodness-of-fit with respect to the exact location (Schunn and Wallach, 2005). In the context of comparing exact location, *RMSD* has been used in several climate and environmental research studies to demonstrate the goodness-of-fit of simulated values (Willmott and Matsuura, 2005). *RMSD* represents the simple standard deviation of the differences between simulated value and measured value. *RMSD* is the square root of mean squared deviation and can be written as:

$$RMSD = \sqrt{\frac{\sum_{i=0}^{n}(s_i - m_i)^2}{n}} \qquad \text{Eq. (4.3)}$$

One noticeable advantage of *RMSD* is that avoids the use of absolute value, which is inadmissible in a number of mathematical calculations (Chai and Draxler, 2014). The reason of squaring the deviations is to concentrate on the values which does not fit well than the one which fit well. This means that if the simulated value is two units off the data generates a penalty of four times as greater as a value that is one unit off (Schunn and Wallach, 2005).

4.2.3 Mean Absolute Deviation (*MAD*)

Mean Absolute Deviation (*MAD*) is the sum of all the magnitudes (absolute values) of deviations (total deviation) divided by the total number of data points (*n*). Mean absolute deviation places equal weighting on all the deviations. For example, the calculated *MAD*

of *1.25* means that the simulated values were off from the measured values on an average of *1.25* (Schunn and Wallach, 2005). *MAD* can be expressed as:

$$MAD = \frac{\sum_{i=0}^{n} |s_i - m_i|}{n} \qquad \text{Eq. (4.4)}$$

where all the parameters are as described earlier.

4.3 Comparison for maximum and minimum temperature, dew point, *RH*, wind speed and radiation

Maximum and minimum temperature, dew point temperature, wind speed, solar radiation, and relative humidity were compared by calculating average daily values. The comparisons for Calgary and Halifax are shown in Figures 4.1 and 4.2, respectively. The comparisons of other seven locations are presented in Appendix B. Figures 4.1 and 4.2 indicate that the *SIMETAW* does a good job in simulating the average daily values for both semi arid and humid climate conditions. It can also be observed that *RH* values, which were estimated from simulated dew point temperatures, correlate well with measured data.

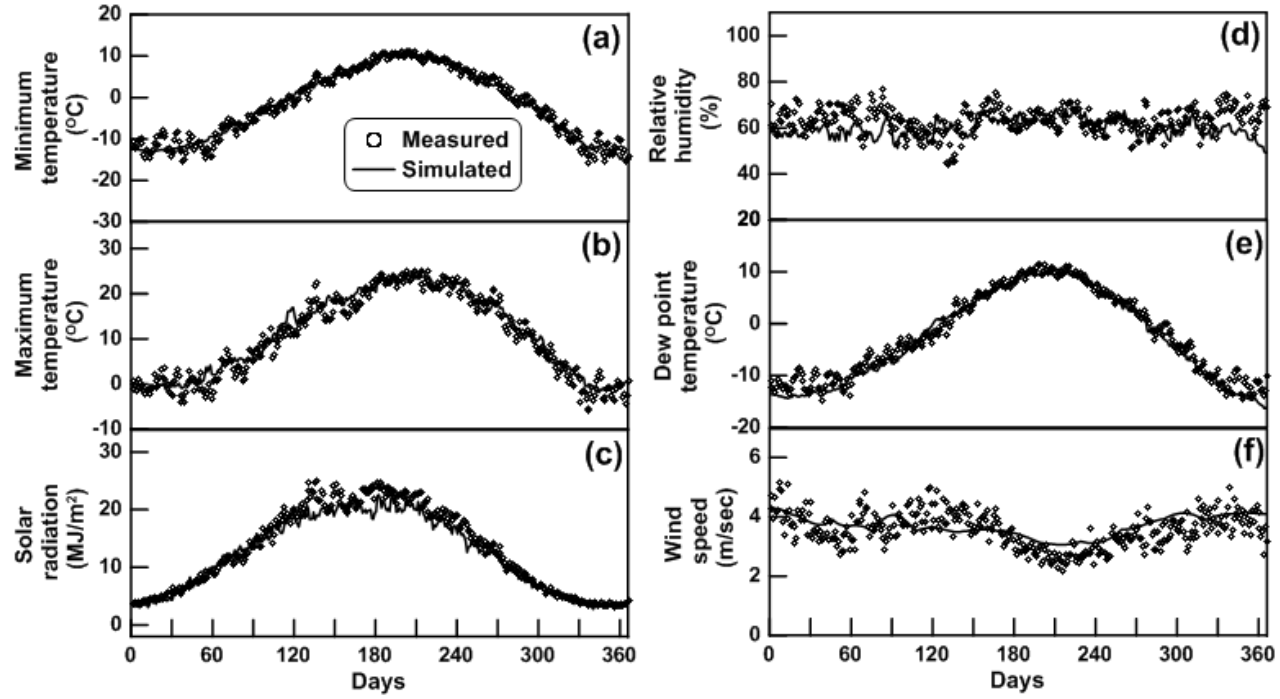

Figure 4.1: Comparison of measured and simulated climate data for Calgary.

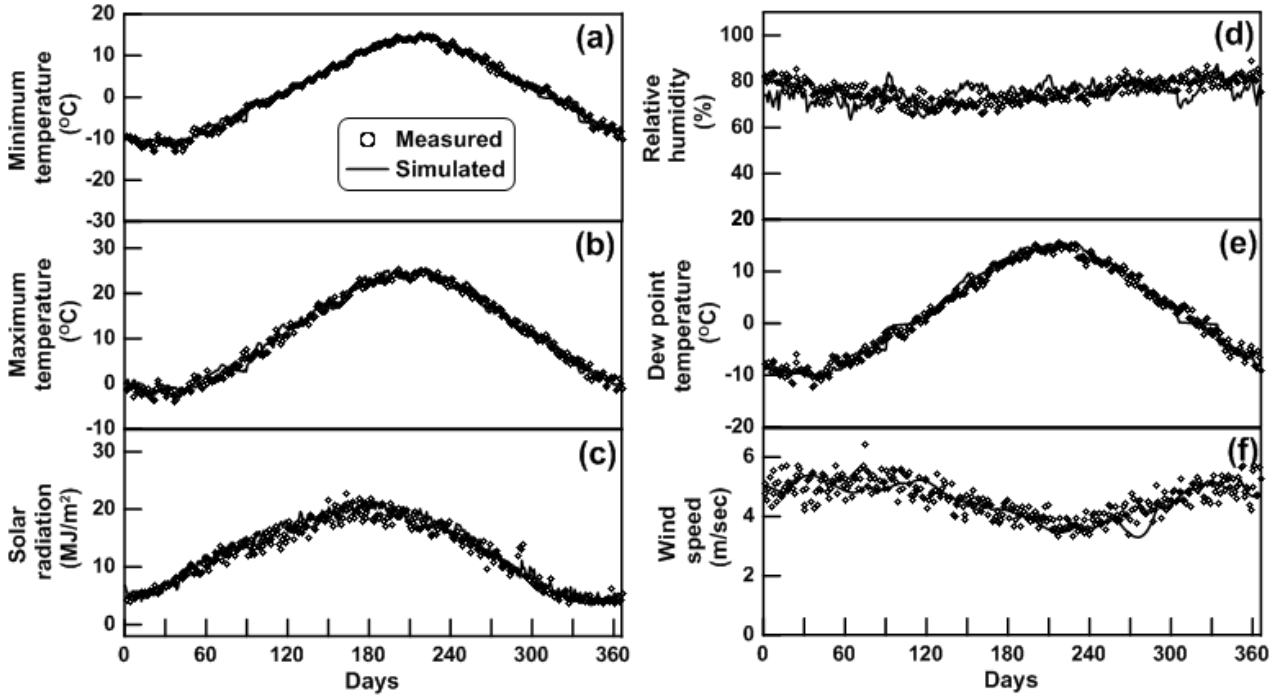

Figure 4.2: Comparison of measured and simulated climate data for Halifax.

Table 4.2 summarize the comparison statistics for the measured and simulated values for Calgary and Halifax. The trend of relative magnitudes for simulated data correlated well with the measured data for solar radiation, maximum and minimum temperature, and dew point temperature. However, wind speed and relative humidity data did not show good trend relative magnitudes. The reason for poor trend relative magnitudes for wind speed and relative humidity is as follows. Both wind speed and relative humidity are measured on hourly basis. The relative humidity follows a diurnal cycle and is associated with variation of temperature during the day. For example, in summers the relative humidity can potentially be higher in the morning than in the afternoon. This is because the cooler morning air is closer to saturation than the hot afternoon air, even with the same amount of water vapor. Estimating daily average *RH* results in values that vary over a narrow range as can be seen in Figures 4.1 and 4.2. Additionally, the day-to-day variation in *RH* does not show any consistent trend as it also dependent on the availability of energy and moisture in a day. This can also be observed in the measured data in Figures 4.1 and 4.2. Therefore, comparison of relative trends between the measured and simulated data is not a good quantitative measure for comparison. It should be noted that visual comparison between the measured and simulated *RH* values in Figures 4.1 and 4.2 indicates that deviation between the measured and simulated values for *RH* is quite small. Relevant statistics for deviation are presented in the following section. Review of the measured average daily data for wind speed also indicates no consistent trend and therefore it can also be argued that comparison of relative trends between the measured and simulated data is not a good quantitative measure for comparison. Once again, visual comparison in Figures 4.1 and

4.2 indicate that deviation between the measured and simulated values for wind speed is quite minimal.

Table 4.2: Comparison statistics for measured and simulated data for Calgary and Halifax

Variable	R^2		RMSD		MAD	
	Calgary	Halifax	Calgary	Halifax	Calgary	Halifax
Solar Radiation	0.97	0.94	1.67	1.41	1.18	1.10
Maximum Temperature	0.95	0.98	2.16	1.28	1.68	1.03
Minimum Temperature	0.97	0.99	1.53	1.02	1.18	0.80
Wind Speed	0.31	0.61	0.52	0.41	0.43	0.31
Dew Point Temperature	0.97	0.98	1.67	1.23	1.24	0.99
Relative Humidity	0.01	0.04	7.30	5.66	5.64	4.66

The data in Table 4.2 provides the quantitative measure of the deviation of the simulated data from the measured data. It can be observed that for most of the variables the *RMSD* and *MAD* values are smaller. A smaller value is indicative of a better correlation between the measured and simulated data. For *RH*, larger values for *RMSD* and *MAD* can be observed for both locations. However, this needs to be considered within the context of numerical values for *RH*. For example, for Calgary the *MAD* value is *5.64%*. This implies that simulated *RH* data is off from the measured data by this much. Considering that the values of *RH* varies from *55%* to *75%* this value is acceptable.

4.4 Comparison for measured and simulated precipitation

The comparison between the measured and simulated precipitation data was done by three different approaches. First the measured and simulated precipitation data is presented in side-by-side graphs. This technique has limited application as comparison can only be done at the qualitative level (Schunn and Wallach, 2005). In the second

approach the data sets were assessed for differences in cumulative and average precipitation values. Comparison related to the difference in extreme precipitation events was also part of this approach. The third approach involved comparison of number of precipitation occurrences for specific precipitation intervals. This approach can highlight how comparable the number of events are for a certain precipitation intensity between the measured and simulated climate data.

The measured and simulated climate data for the cities of Calgary is shown in Figure 4.3. This figure indicates that for both datasets most of the precipitation events are of intensities less than 15 mm/d. From a visual perspective it can also be observed that measured dataset appears to have higher number of higher intensity events. The cumulative precipitation and average yearly values of precipitation are also shown in Figure 4.3.

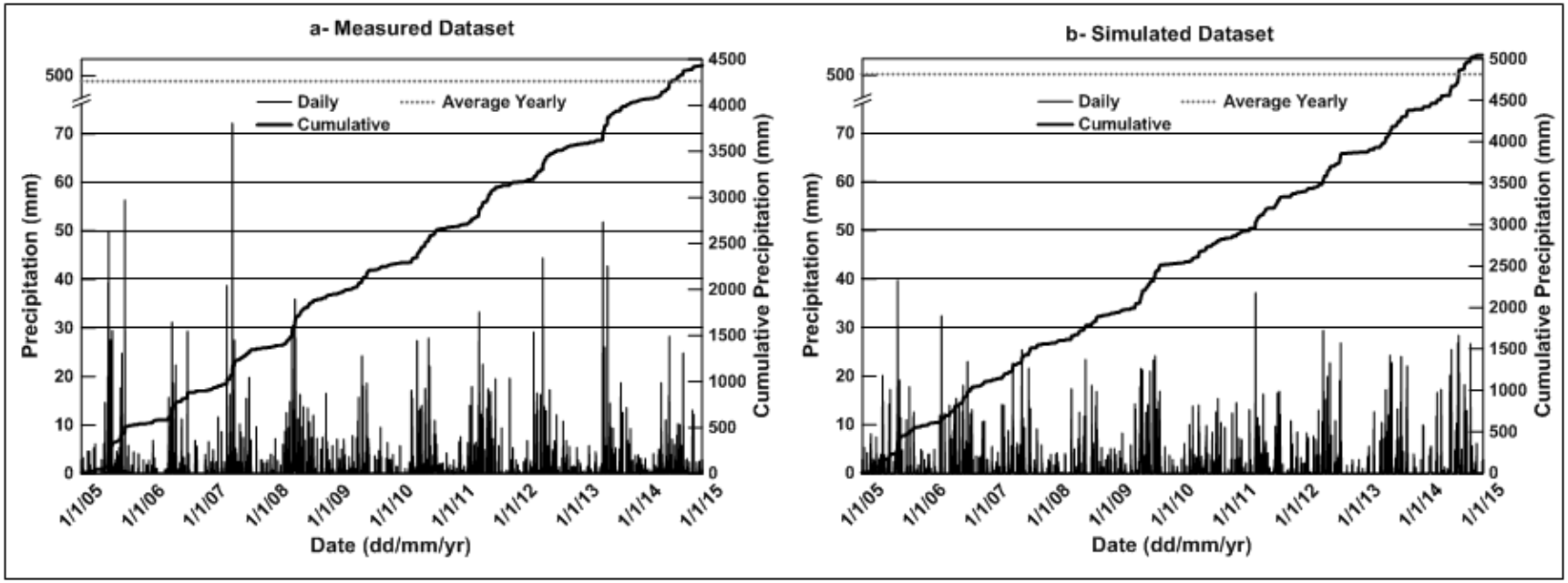

Figure. 4.3: Comparison of measured and simulated daily Precipitation data for Calgary.

Figure 4.3 shows that for Calgary the cumulative precipitation value from measured dataset is 4,427 mm; while for simulated dataset it is 5,041 mm. This implies that simulated data resulted in additional 614 mm of precipitation over the 10-year period. This difference would constitute an additional yearly water availability of 61.4 mm for the simulated data. Figure 4.3 also shows that the average annual precipitation from measured daily data was 442 mm, while for simulate data it was 504 mm.

Review of measured precipitation data also indicates that over the 10-year period there were twelve precipitation events of 30 mm or more in the measured climate data and only three precipitation events of similar intensity in the simulated climate data. Review of measured data indicates a maximum precipitation event of 72 mm occurred on June 5th, 2007. Simulated data shows a maximum precipitation event of 40 mm occurring on July 31st, 2005.

The occurrence of specific precipitation intensities was estimated for measured and simulated data and is presented in Figure 4.4. Review of the measured data and simulated data indicated that either there was little or no precipitation during approximately 2,500 days. This constitutes approximately 70% of the total number of days. Figure 4.4 shows that for most of the precipitation intensity intervals there is a close match between the number of events between measured and simulated climate datasets. The largest difference was observed for events that are greater than or equal to 6 mm/d but less than 7 mm/d. For this interval the simulated dataset has 240 more events than the measured dataset.

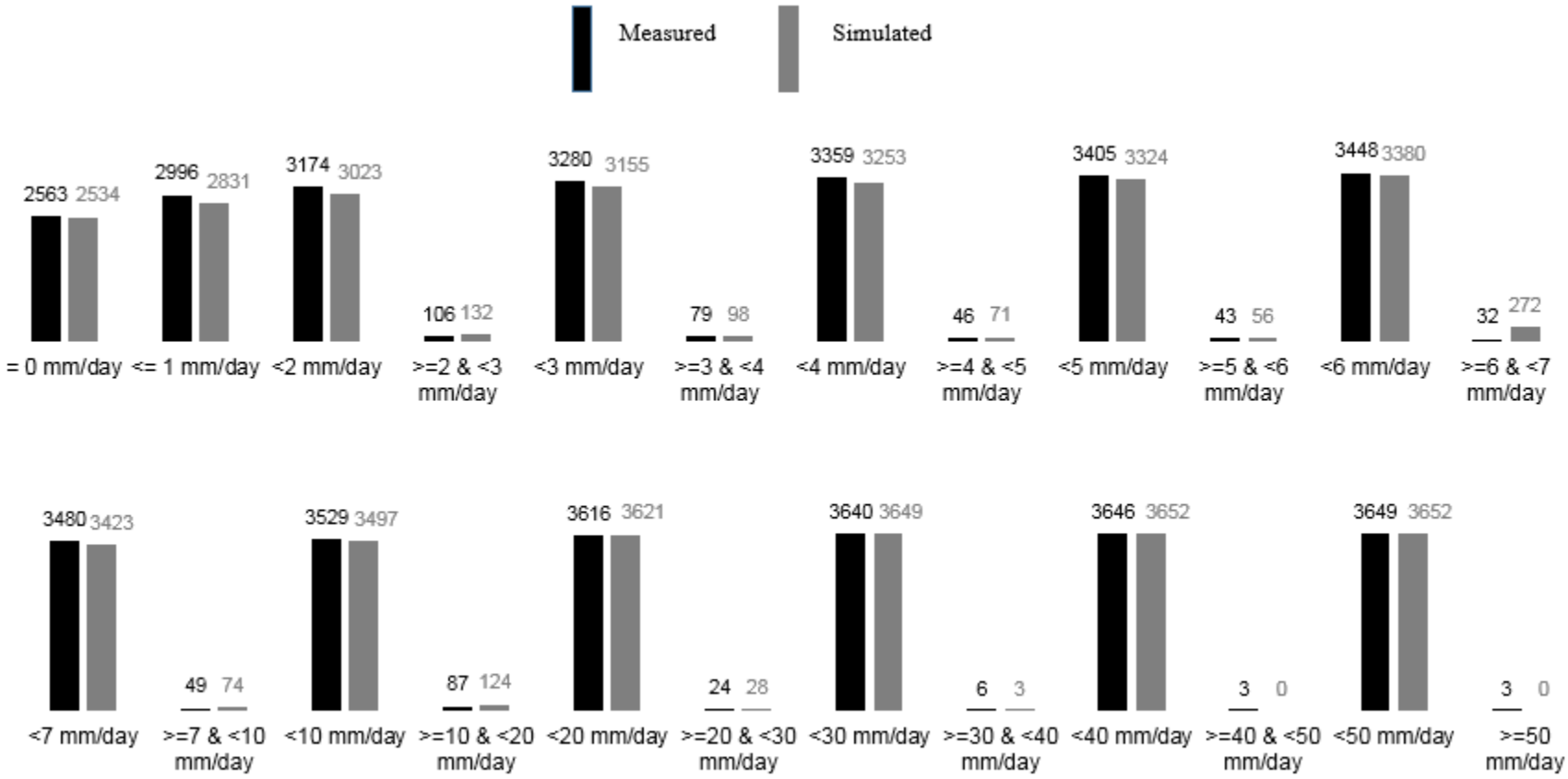

Figure. 4.4: Comparison of precipitation occurrences for measured and simulated data for Calgary.

Based on the above observations it can be concluded that *SIMETAW* over-predicts the yearly precipitation for Calgary by approximately 61 mm/year on average. It also under-predicts the extreme precipitation events. However, the number of days with no or trace amount of precipitation are predicted very well. Similarly, *SIMETAW* also does a good job in predicting the occurrence of specific precipitation intensities. This leads one to conclude that on average *SIMETAW* simulated an acceptable daily precipitation record for the city of Calgary only using 12 monthly average precipitation values.

The measured and simulated climate data for Halifax is shown in Figure 4.5. This figure indicates that for both datasets most of the precipitation events are of intensities less than 30 mm/d. However, in comparison to the climate data for Calgary there are far more events with intensities 30mm/d or higher. Figure 4.5 also shows that both dataset appear to have almost similar intensity events, at least from a qualitative comparison. The cumulative precipitation and average yearly values of precipitation are also shown in Figure 4.5. It can be observed that for Halifax the cumulative precipitation is 44,747 mm and 45,241 mm for measured and simulated climate datasets, respectively. This translates to a difference of less than 500 mm over 32 years and an average yearly difference of only 15 mm. Considering that average annual precipitation for measured daily data is 1,398 mm and simulated data is 1,413 mm, a yearly difference of approximately 1% is quite acceptable. These observations lead one to conclude that *SIMETAW* simulated the cumulative and yearly average values of precipitation for Halifax quite well.

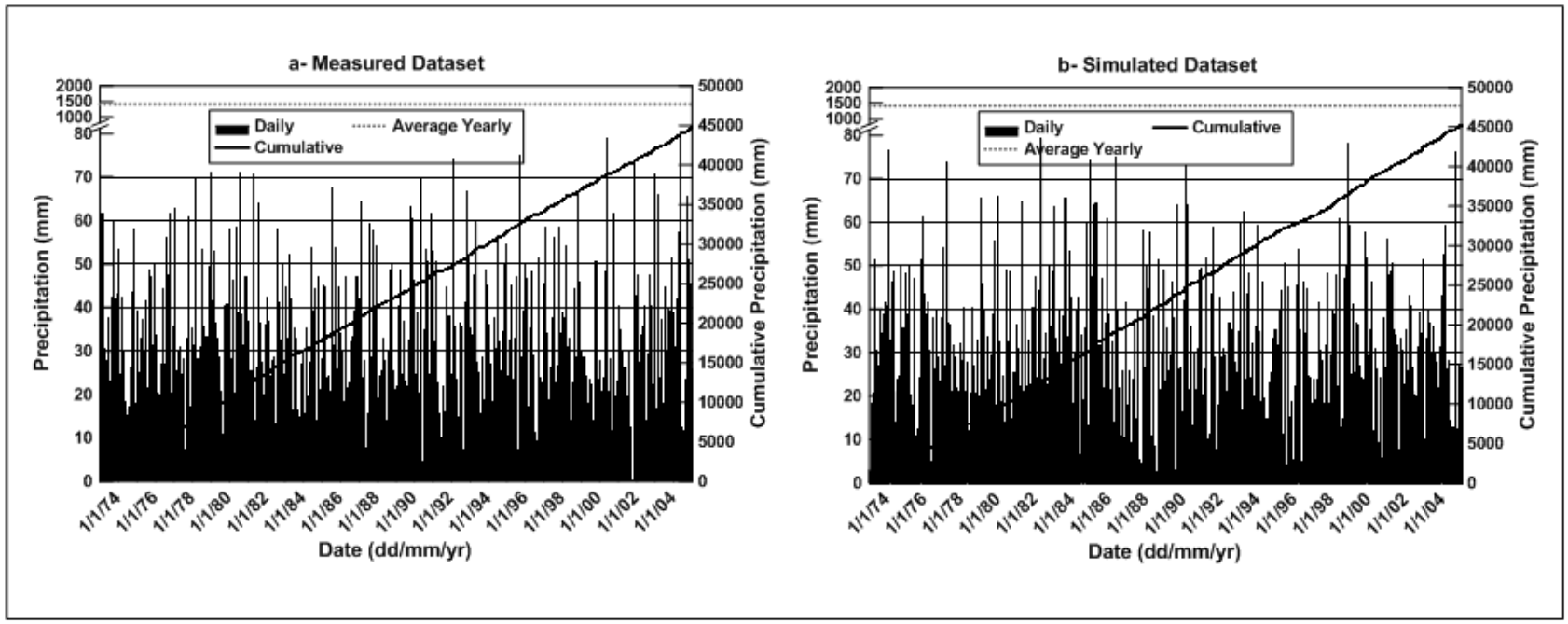

Figure. 4.5: Comparison of measured and simulated daily Precipitation data for Halifax.

Review of measured precipitation data indicates, that over the 32-year period there were 312 events of 30 mm/day or more in the measured climate data. A similar review for simulated data indicated 294 events of similar intensity in the simulated climate data. It was also estimated that in both instances, this corresponded to approximately 2.5% of the total precipitation event. These observations lead to the conclusion that both datasets have very similar higher intensity precipitation events.

The occurrence of specific precipitation intensities was estimated for measured and simulated data and is presented in Figure 4.6. Review of the measured data and simulated data indicated that either there was little or no precipitation during 6,366 days for measured data and 6,832 days for simulated data. It was also estimated that these translate to instances approximately 55% and 58% of the days were with no or trace amount of precipitation for the measured and simulated climate datasets, respectively. Figure 4.6 shows that for most of the precipitation intensity intervals there is a close match between the number of events between measured and simulated climate datasets. Review of measured data indicates a maximum precipitation event of 100 mm occurred on January 1st,1978. Simulated data shows a maximum precipitation event of 125 mm occurring on December 25th,1994. The number of days with little or no precipitation are predicted with minor difference of 3% of the total number of days in the dataset. Similarly, *SIMETAW* also does a good job in predicting the occurrence of specific precipitation intensities. This leads one to conclude that on average *SIMETAW* simulated good daily precipitation record for Halifax by only using 12 monthly average values.

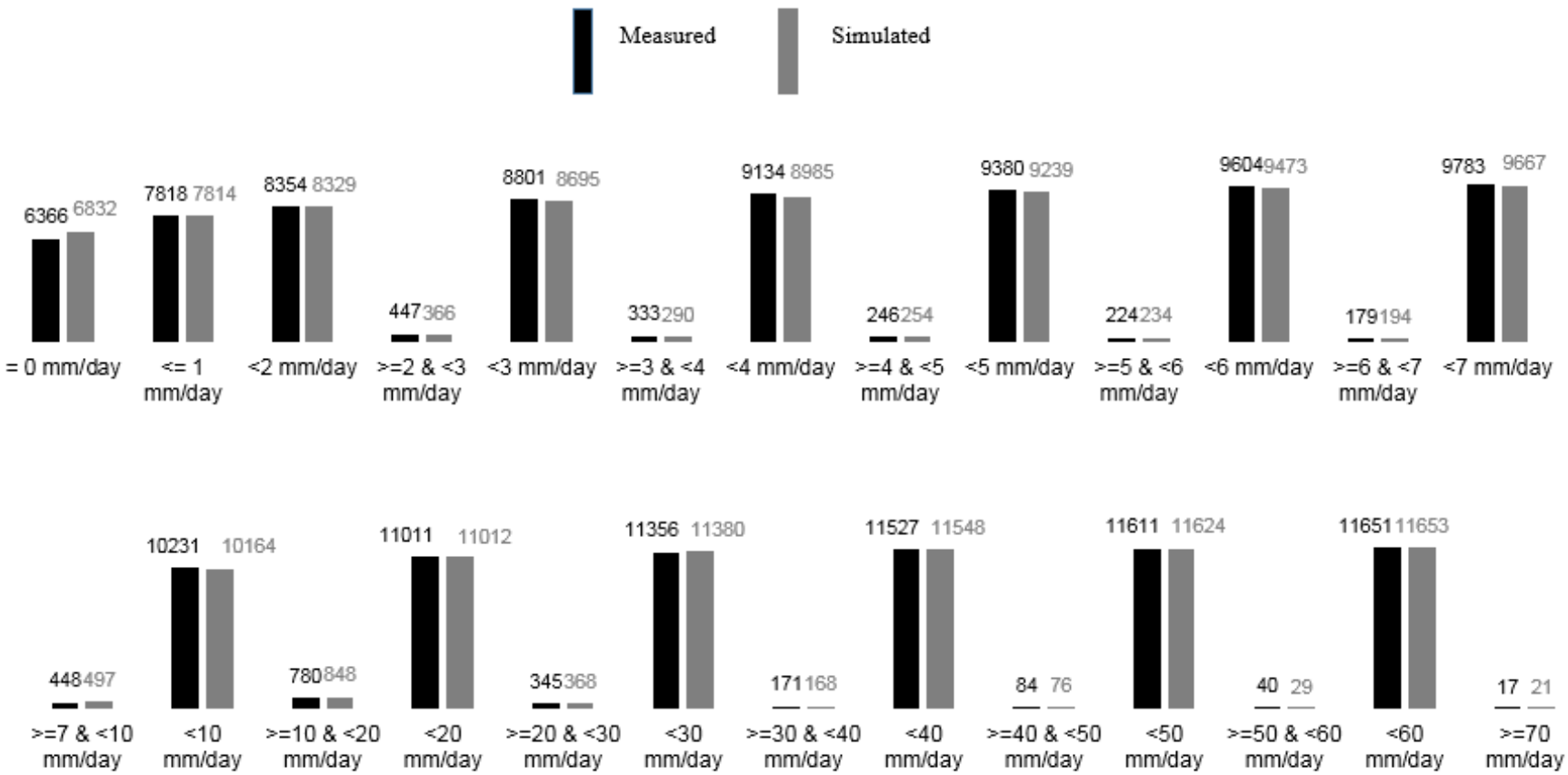

Figure. 4.6: Comparison of precipitation occurrences for measured and simulated data for Halifax.

4.5 Comparison for potential evaporation

Potential evaporation (*PE*) was estimated using the Penman (1948) method for measured and simulated datasets. The daily average values are presented in the form of box and whisker plots for Calgary and Halifax in Figures 4.7 and 4.8 respectively. Box and whisker plots present the data in the form of five-point summary. The summary consists of: the most extreme values in the data set (the maximum and minimum values), the lower and upper quartiles, and the median value. The presentation of the data in this manner provides a good descriptive analysis of the data.

Comparison of potential evaporation values estimated from measured and simulated climate data for city of Calgary is shown in Figure 4.7. The results show similar values of *PE* estimated from measured and simulated climate data. For example, the upper quartiles for measured and simulated data are 4.1 mm/d and 4.3 mm/d, respectively. Similarly, the lower quartiles were 0.98 mm/d and 1.1 mm/d for measured and simulated climate data respectively. It can also be observed that median and upper limit of the PE values for the two datasets are also very similar. The biggest difference between the two datasets can be observed for the minimum value of *PE* where difference of 0.26 mm/d can be noted. Based on these observations it can be concluded that the *PE* estimates from the measured and simulated climate data for Calgary are very similar.

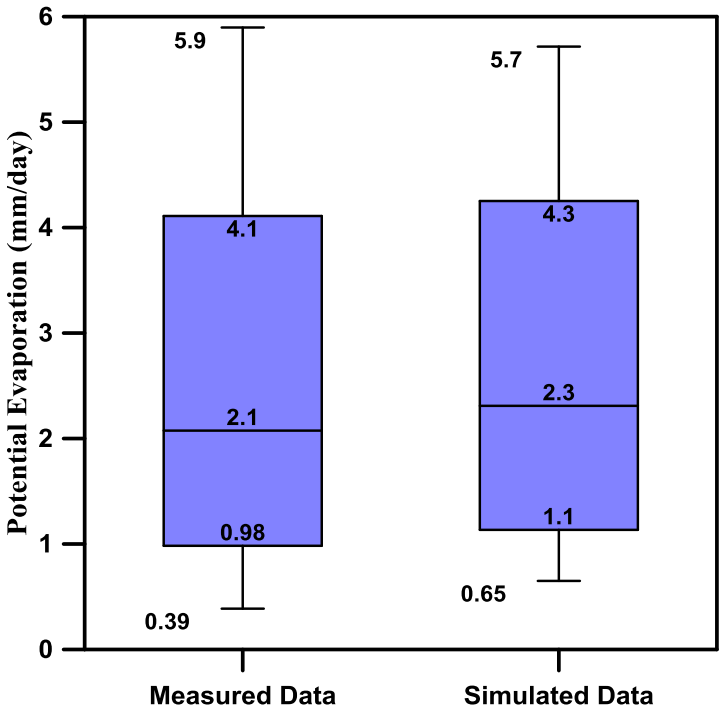

Figure 4.7: Comparison of box and whisker plots for measured and simulated potential evaporation for Calgary.

Figure 4.8 shows a comparison of potential evaporation values estimated from measured and simulated climate data for Halifax. Review of this figure indicates that maximum and upper quartile values from the measured and simulated climate data are very similar with a difference of only 0.2 mm/d. It can also be observed that the median, lower quartile and lowest value show a little difference between the measured and simulated climate data. However, the overall center and spread of the data are very similar. Therefore, it can be concluded that the *PE* estimates from simulated data are quite similar to those from measured climate dataset.

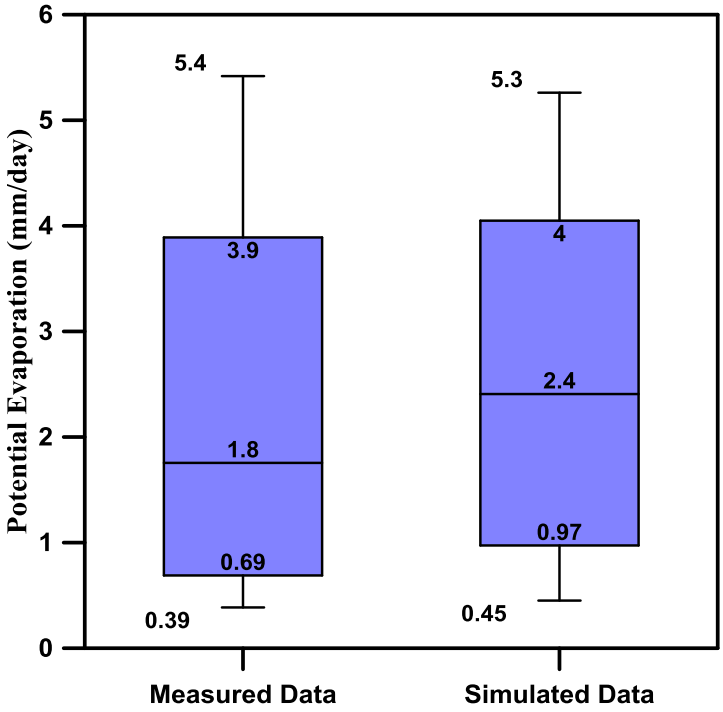

Figure 4.8: Comparison of potential evaporation using box and whisker plots for measured and simulated data for Halifax.

4.6 Comparison for Climate Classification

The climate classification for the measured and simulated climate data for Calgary and Halifax was carried out by computing the annual moisture indices according to the procedure described by (Thornthwaite and Hare 1955). The comparison of climate classification is presented in Figure 4.9 for Calgary and in Figure 4.10 for Halifax. The average moisture index and standard deviation results are also shown in these two figures. It should be noted that in both figures the moisture indices were also rearranged in a manner to quantify, for how many years the measured and simulated moisture indices are identical.

Review of the climate classification for measured and simulated climate data for Calgary indicates that the climate can be classified as semi-arid with an average moisture index of -54 for measured data and -50 for the simulated data. It can be observed that both data sets show very little year-to-year variation in climatic conditions. It can also be observed that apart from one year the moisture indices for measured and simulated climate data are in close agreement to each other. Therefore, it can be concluded that climate classification using simulated climate data is very similar to one carried out using measured climate date.

Figure 4.10 shows that for Halifax, climate can be classified as humid with an average moisture index of 69 for measured data and 55 for the simulated data. Review of the figure indicates that there is a lot of variation in climatic conditions over the years for both measured and simulated climate datasets. It can be observed that, on average, measured climate has a lot more wetter years than the simulated dataset. For example, for simulated dataset there is only one year when the climactic conditions are representative of pre-humid climatic conditions. In comparison measured climate dataset has three years for which climate can be classified as pre-humid. Similarly, for drier climates it can be observed that simulated climate datasets have two years when the climate can be classified as moist humid and one year when the climate can be classified as dry sub humid. This is in contrast with the measured climate data where none of the years have these drier climates. However, it should be noted that for most years the climate can be classified as humid for measured and simulated climate data. Therefore, it can be concluded that the climate classification using simulated data is reasonably similar to the classification using measured climate data.

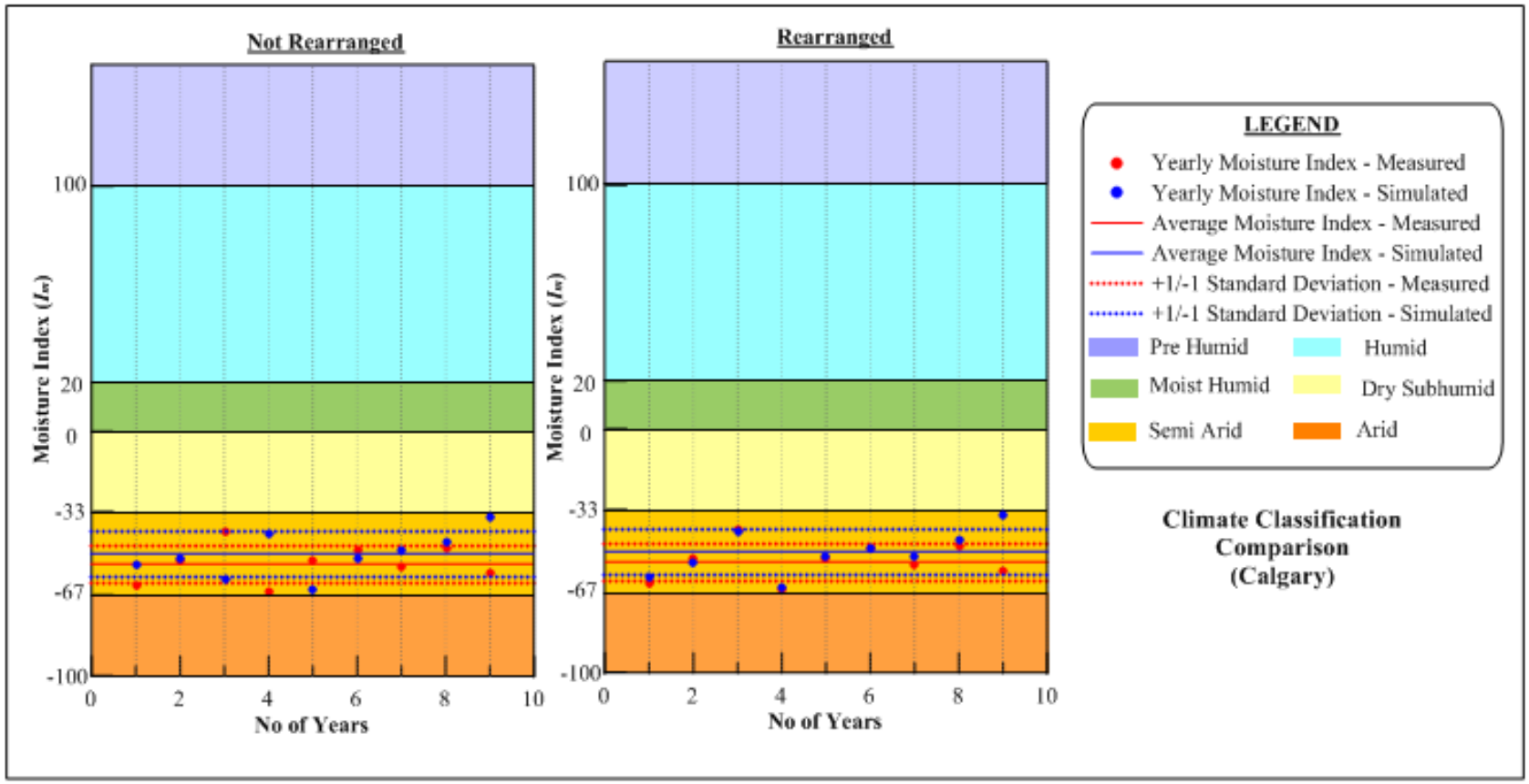

Figure 4.9: Comparison of climate classification for measured and simulated data for Calgary.

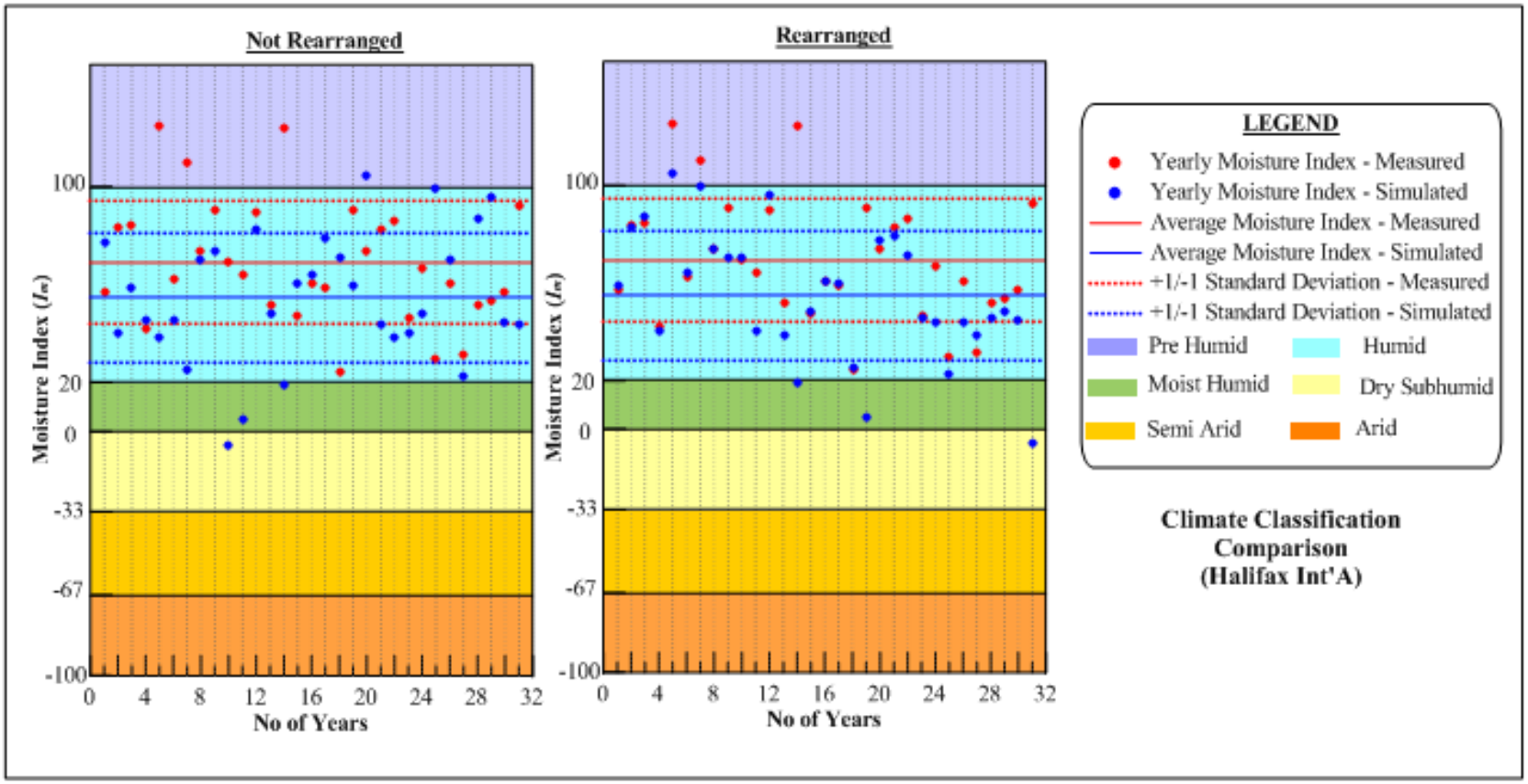

Figure 4.10: Comparison of climate classification for measured and simulated data for Halifax.

Chapter 5

Modeling of geotechnical and geoenvironmental problems using measured and simulated climate data

This chapter presents the application of measured and simulated meteorological input data in modeling practical geotechnical and geoenvironmental problems. Simulations were run for three different types of analyses to assess the feasibility of using *SIMETAW* generated climate data at a daily resolution.

- The first set of simulations focused on infiltration assessment in variably saturated soils. The simulations were run using Hydrus-1D (Simunek et al. 1998) software for three different soil types, i.e. clay, sand, and silt.
- The second set of simulations were intended to quantify the swelling potential of expansive soil (Regina clay). These simulations were carried using VADOSE/W software (GEO-SLOPE International Ltd. 2012).
- The third set of simulations were performed to assess the performance of a soil cover to limit oxygen and water ingress to reactive tailings. These simulations were also carried out using VADOSE/W software.

For all three simulation scenarios, measured and simulated climate data were used as the top boundary to evaluate its further usability in designing the solution for practical civil engineering problems.

5.1 Infiltration assessment

Measured and simulated climate data from Barriere region in the province of British Colombia was used as an input to estimate the effect of soil type on the water flux at the ground surface in variably saturated soils. For this analysis, simulations were run using precipitation (*P*) and potential evaporation (*PE*) data at a daily resolution. Simulations were carried out using *Hydrus-1D* (*version 4.16.0110*) (Simunek et al. 1998) for three different soil types.

5.1.1 Model Details

The models consisted of a one-dimensional (*1D*) soil column of 100 cm depth. The initial condition of the models was assumed to be a uniform pressure head of -100 cm. In all simulations an atmospheric boundary condition with surface runoff was imposed at the top of the column. The top boundary comprised 15-year continuous dataset that corresponds to 3,416 days (244 active water days for both measured and simulated climate data). Zero-gradient water flow boundary condition was set at the bottom to simulate free drainage. Three different soil types (sand, silt, and clay) were used in the analysis. The soil hydraulic properties used were similar to those available in the Hydrus soil catalogue for *USDA* soil textural classes for sand, silt and clay. The soil water characteristic curves and unsaturated hydraulic conductivity functions for the three soil types are shown in Figures 5.1 and 5.2, respectively. van Genuten (1980) parameters for the soil hydraulic functions are provided in Table 5.1.

Table 5.1: Hydraulic soil properties used in the simulations

Material	θ_r (-)	θ_s (-)	Alpha (1/mm)	n (-)	K_s (m/s)	l (-)
Clay	0.068	0.38	0.0008	1.3	1.33×10^{-5}	0.5
Sand	0.045	0.43	0.0145	2.68	1.98×10^{-3}	0.5
Silt	0.034	0.46	0.0016	1.37	1.67×10^{-5}	0.5

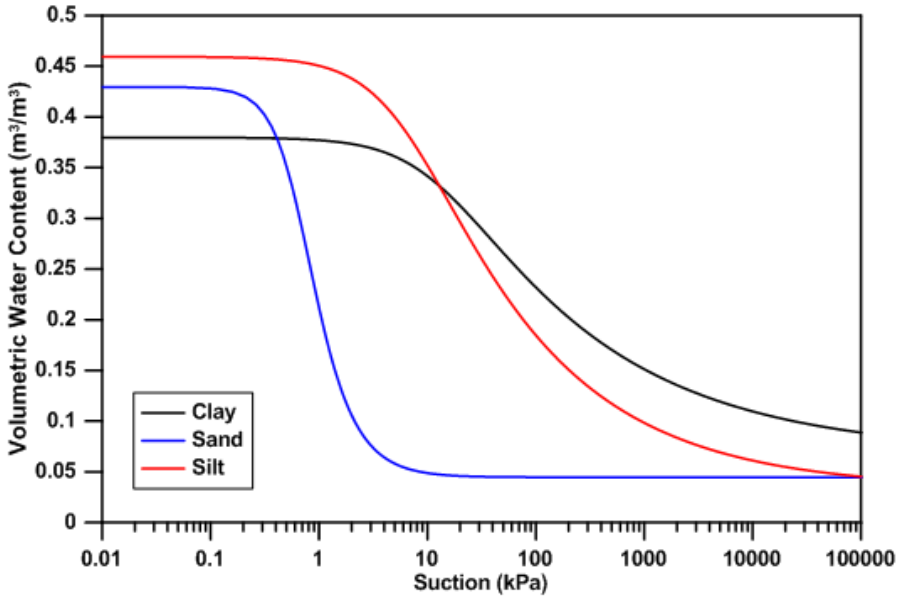

Figure 5.1: SWCC for clay, sand and silt used in infiltration assessment

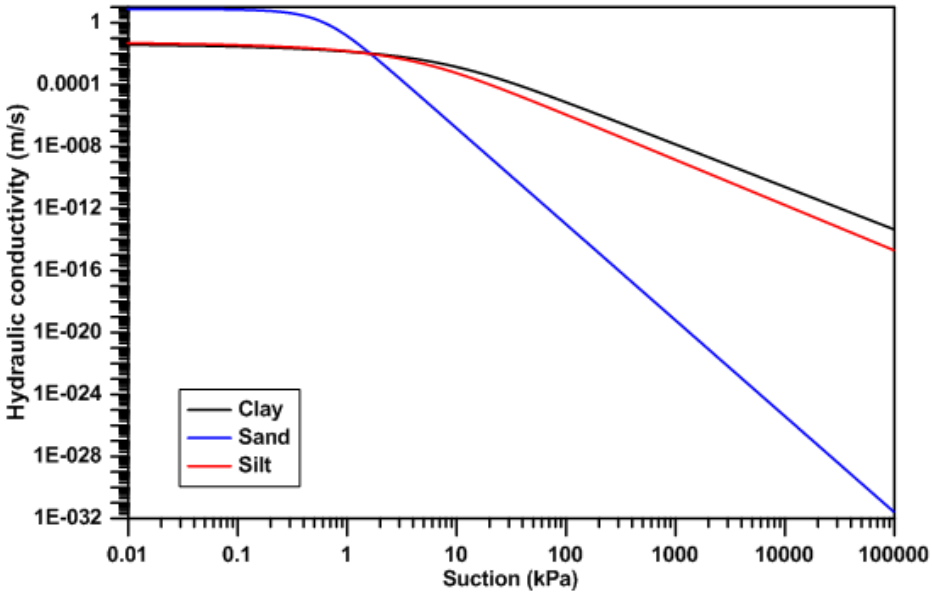

Figure 5.2: Unsaturated hydraulic conductivity functions for clay, sand and silt used in infiltration assessment

5.1.2 Water balance comparison

Figure 5.3 shows the cumulative water balance at the ground surface for the simulations run for the three different soil types using measured and simulated climate data. The results are cumulative over the 14-year active period. It should be noted that in Figure 5.3 the water fluxes entering the soil domain are reported as positive values while fluxes leaving the system are reported as negative values. By this analogy, a positive value of net infiltration (*NI*) implies a water gain to the soil domain while a negative value will be representative of water loss conditions at the ground surface.

Comparison of water balance between the three different soil types indicated that at the ground surface water balance for sand is very different from that for silt and clay. It can be observed that *NI* value for sand is significantly higher than the values predicted for silt and clay. This implies that for sand a significant quantity of water will make its way into soil domain, while for silt and clay very small quantities of water will enter the system. This difference can be attributed to the low retention and high conductivity of the sand when compared to silt and clay. Higher retention and low conductivity of the silt and clay tends to keep water in near surface soil layers for longer period of times resulting in higher actual evaporation and lower NI values.

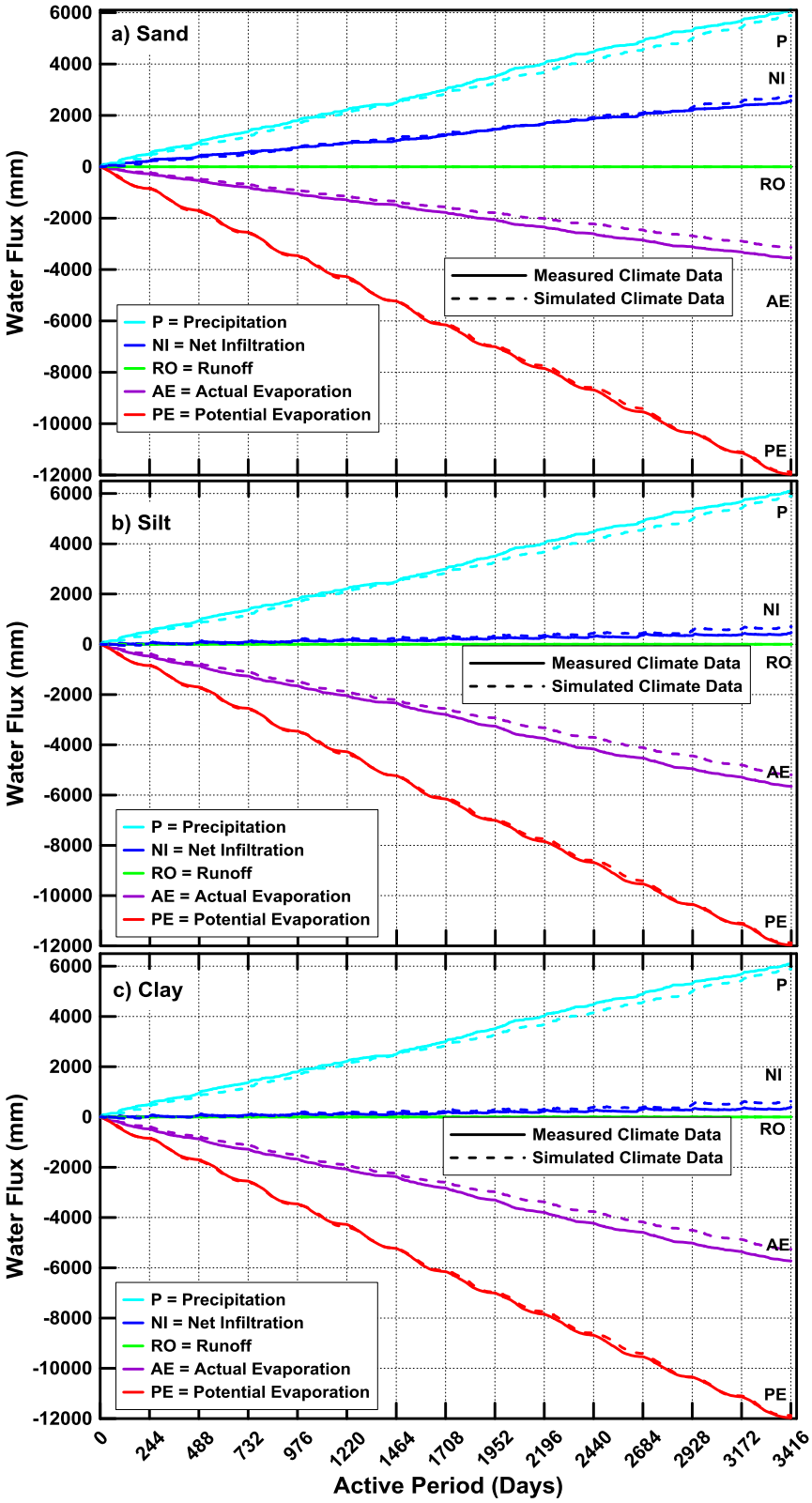

Figure.5.3: Water balance at the ground surface. a) sand b) silt c) clay

Review of the Figure 5.3 also indicates that the *NI* values for the simulations run with measured and simulated climate data are quite similar. Review of the results indicated that on average the difference in *NI* values from measured and simulated climate data were less than 16 mm/year. The simulations run with simulated climate data slightly over predicted the *NI* values.

The over prediction of the *NI* from simulated data can be explained in the following manner. The cumulative measured precipitation value (6100 mm) was 200 mm higher than the cumulative simulated value (5900 mm) over a 14-year period. Similarly, the cumulative potential evaporation estimated from measured climatic data was 90 mm higher than the cumulative potential evaporation from simulated climate over the same period. These observation leads one to conclude that for measured climate data the water availability is 110 mm higher than for simulated climate data. This conclusion would imply that one should expect higher *NI* values, when measured climate data is used for infiltration assessment. However, as mentioned above the results indicate that this is not the case, and assessments using simulated climate data tend to predict higher *NI* values. The reason for this discrepancy is that although for measured climate data the cumulative water availability is higher, the quantity of water that makes it way into the soil domain also depends on the availability of meteoric water and evaporative demand on a daily basis. For example, estimates of daily potential surface flux, which is the difference in daily precipitation and potential evaporation values indicate that the cumulative potential flux for simulated climate is 137 mm higher than that for measured climate data. It should also be noted that in addition to the quantity of potential surface flux, the distribution of precipitation events also influences the *NI* quantities. For example, for two different

climate datasets the cumulative potential surface flux values might be similar; however, if in one of the datasets the days of precipitation occurrences are more closely spaced, they can potentially result in increased *NI* due to wetter soil conditions. In general, it can be concluded that the data simulated using *SIMETAW* shows a very little difference over the extended period of analysis in terms of water balance at the ground surface and can be used for infiltration assessments.

5.2 Modeling of expansive soil behavior

Expansive soils also known as shrink-swell soils, are common in many arid and semi arid regions of the world. Expansive soils undergo volume changes in response to moisture content changes. Increase in moisture content results in soil expansion, while the reduction in moisture content results in soil shrinkage.

In this study, the main objective was to investigate the effect of moisture dynamics and swelling potential calculations using continuous multiyear measured and simulated climate data at a daily resolution. The swelling and shrinkage behaviour of expansive soils is due to the presence of expansive clay minerals, such as montmorillonite (Mitchell and Soga 2005). Lightly loaded structures such as residential buildings are more prone to damage from expansive soils. Similarly, water and gas pipelines embedded in expansive soils can undergo severe differential movement caused by shrink/swell behaviour of expansive soils (Kodikara et al. 2013). Such movements can eventually lead to pipe failures.

Regina clay is a highly plastic, unsaturated expansive clay that undergoes large volume change as the soil water content changes (Vu et al. 2007). Regina clay's origin was a proglacial lake basin that existed where the city of Regina is now located (Donahue et al. 2011). Regina clay is mainly composed of clay minerals such as smectite, illite, kaolinite and vermiculite (Ito and Azam 2010, Donahue et al. 2011). Frendlund (1975) has defined the Regina clay as a highly plastic, inorganic calcium montmorillonitic clay with very high swelling potential.

An estimation of moisture flow across the soil-atmosphere boundary is required for the prediction of volume change in expansive soils (Wilson et al. 1994). In the previous two decades, several studies have utilized soil-atmosphere modeling approach to predict moisture dynamics and associated volume change in the Regina clay (Vu et al. 2007, Ito and Hu 2011, Azam and Ito 2012, Adem and Vanapalli 2014). In this study, the main objective was to investigate if the simulated climate data can be used effectively to predict moisture dynamics and swelling potential of Regina clay.

5.2.1 Previous work

A one-dimensional soil-atmosphere model was developed by Vu et al. (2007) to study the seasonal variation of moisture content in Regina clay. One of the objectives of the study was to estimate expansive soil movement based on the moisture distribution predicted from the soil-atmosphere modeling. The modeling was carried out for a site in south central Regina, Saskatchewan, with a history of frequent incidents of water main breakage owing to the presence of expansive soil. The study concluded that the infiltration

at the ground surface and associated suction profiles in the expansive soils are strongly dependent on the climatic parameters such as solar radiation, precipitation and wind speed.

Ito and Hu (2011) carried out a study to predict the displacement behavior of Regina clay. They employed a two-dimensional soil-atmosphere model with one year of climate data for Regina from May 1, 2009 to April 30, 2010. The matric suction profiles obtained form the soil-atmosphere modeling were used in a soil-displacement model to estimate the vertical displacement in the soil. The results of the study suggest that soil suction and water content vary widely near the ground surface, and variation decreases with depth. The variation in suction leads to large soil displacements near the ground surface. In addition to climate variables, such as solar radiation, wind speed and precipitation, irrigation of the park was also found to affect the moisture distribution and its variation with depth.

Azam and Ito (2012) carried out coupled soil-atmospheric modeling for Regina Clay to estimate the soil-atmosphere interaction. Their model used measured and estimated soil hydraulic properties and one year of measured climate data for the city of Regina. The model was able to predict the degree of saturation as a function of time and depth and was validated using measured soil saturation data. The swelling potential of the expansive soil was calculated using the following relationship:

$$SP = \frac{(e_{max} - e_0)}{(1 + e_0)} \qquad \text{Eq. (5.1)}$$

where *SP* is the swelling potential, e_o is the initial field void ratio, and e_{max} is the maximum void ratio. Results indicate that Regina Clay has the capability of high water absorption and retention because of its soil properties and the climate condition of the area. The top 2.5 m layer of clay was identified as the active zone for the soil-atmosphere interaction. The highest swelling potential of 37% was predicted for the late summer period.

Adem and Vanapalli (2014) used a soil-atmosphere model to estimate the suction variations in Regina Clay over a period from May 2009 to May 2010. The site under their consideration was the same as Ito and Hu (2011). The suction variations predicted by the soil atmosphere model were used to assess suitability of a modulus of elasticity–based method (*MEBM*) to predict expansive soil movement. The results suggested that *MEMB* can be used as the simple approach for calculating the swell-shrink behavior of Regina clay.

5.2.2 Numerical modeling

Numerical simulations were carried out using *VADOSE/W* (GEO-SLOPE International Ltd. 2012). to simulate the temporal and spatial distribution of moisture content/suction in Regina Clay. *VADOSE/W* is capable of analyzing the flow from the environment, across the soil-atmosphere interface, through the unsaturated zone and into the local groundwater regime. *VADOSE/W* also has the ability to simulate surface vegetation and can use measured climate data including temperature, relative humidity,

wind speed, precipitation, and net radiation. The software is also capable of carrying out a rigorous water and energy balance at the soil-atmosphere interface.

A one-dimensional variably saturated flow model with soil-atmospheric boundary condition was used for the simulations. The model was capable of estimating the water balance at the ground surface and soil moisture distribution with depth. The model also estimated the actual evaporation (*AE*) based on prevailing climate conditions and transient soil moisture conditions. The model was run with multi-year measured and simulated daily climate data for the city of Regina.

The geometry of the model comprised a 10 m soil column. The top 4 m of the soil column was assumed to consist of fissured clay layer whereas bottom 6 m was assumed to be non-fissured. This geometry is consistent with the previous study by Vu et al. (2007). It is also well known that the top few meters of the Regina clay could be highly fractured (Schwartz et al. 1982); therefore, an order of magnitude higher value of hydraulic conductivity was assumed for the top 4 m. The saturated hydraulic conductivity for the fissured clay was set at 2.25×10^{-8} m/s, whereas 2.17×10^{-9} m/s was assigned to non-fissured clay (Vu et al. 2007).

Soil hydraulic properties namely soil water characteristic curve (*SWCC*) and unsaturated hydraulic conductivity function are required for soil-atmosphere analysis. Figure 5.4 shows the *SWCC* and hydraulic conductivity function for Regina Clay. The *SWCC* is based on the measurements by Vu et al (2007). Unsaturated hydraulic conductivity function was estimated by the *SWCC* and saturated hydraulic conductivity value based on the procedure described by van Genuchten (1980).

In addition to soil hydraulic properties, initial and boundary conditions are also required to perform the soil-atmosphere analysis. For the initial condition, a constant suction of 1600 kPa was used for the top 4 m of clay and 600 kPa for the bottom 6 m in a preliminary model. This model was then run with the complete climate dataset. Consequent models were run with initial condition representative of the moisture content distribution over the domain at the end of the previous models. The models were run several times to remove the effect of initial conditions.

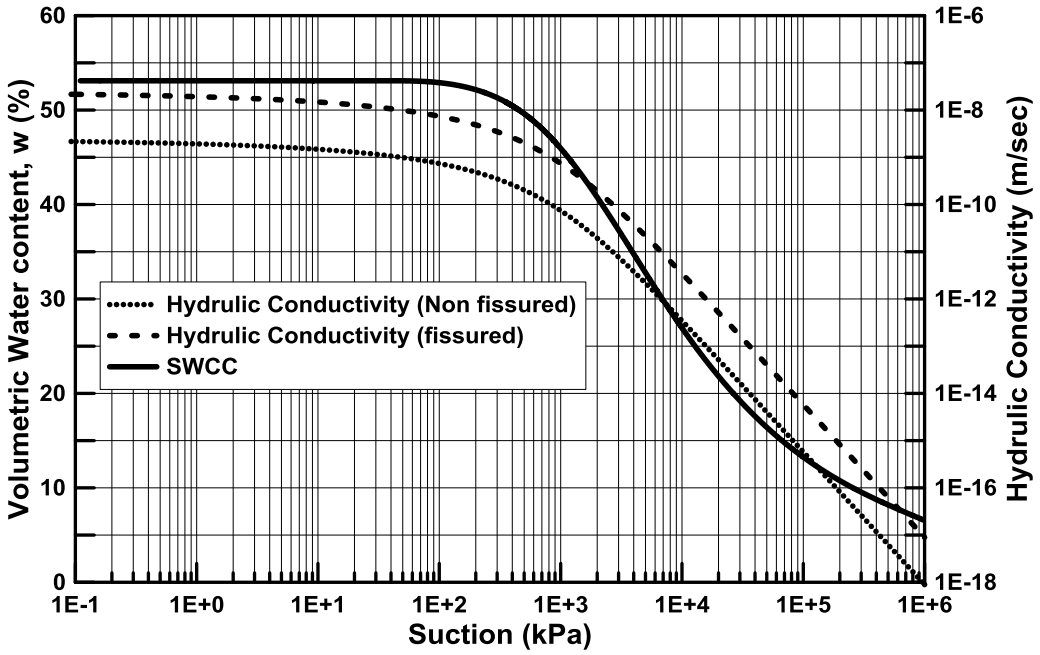

Figure 5.4: Soil water characteristic curve and unsaturated hydraulic conductivity function for Regina clay used in simulations (data from Vu et al. 2007)

In all simulations, an atmospheric boundary condition with surface runoff was imposed at the top of the soil column. The top boundary comprised the measured and simulated daily climate records. A zero-gradient water flow boundary condition was set at the bottom of the column to simulate free drainage. This is representative of deep

groundwater table conditions and represents the groundwater conditions in the city of Regina.

Multi-year climate dataset is very helpful in estimating the water availability at the ground surface. It is essential to carry out a statistical analysis of the past several years of weather conditions to establish the weather fingerprint for a particular location (Fredlund et al. 2012). The climate classification was carried out for both measured and simulated data using Thornthwaite climate classification system (Thornthwaite and Hare 1955). The climate classification using measured and simulated climate data is shown in Figure 5.5. Graphical results indicate that on average the climate of Regina can be classified as semi-arid. It can also be observed that the climate classification using measured and simulated data are quite similar.

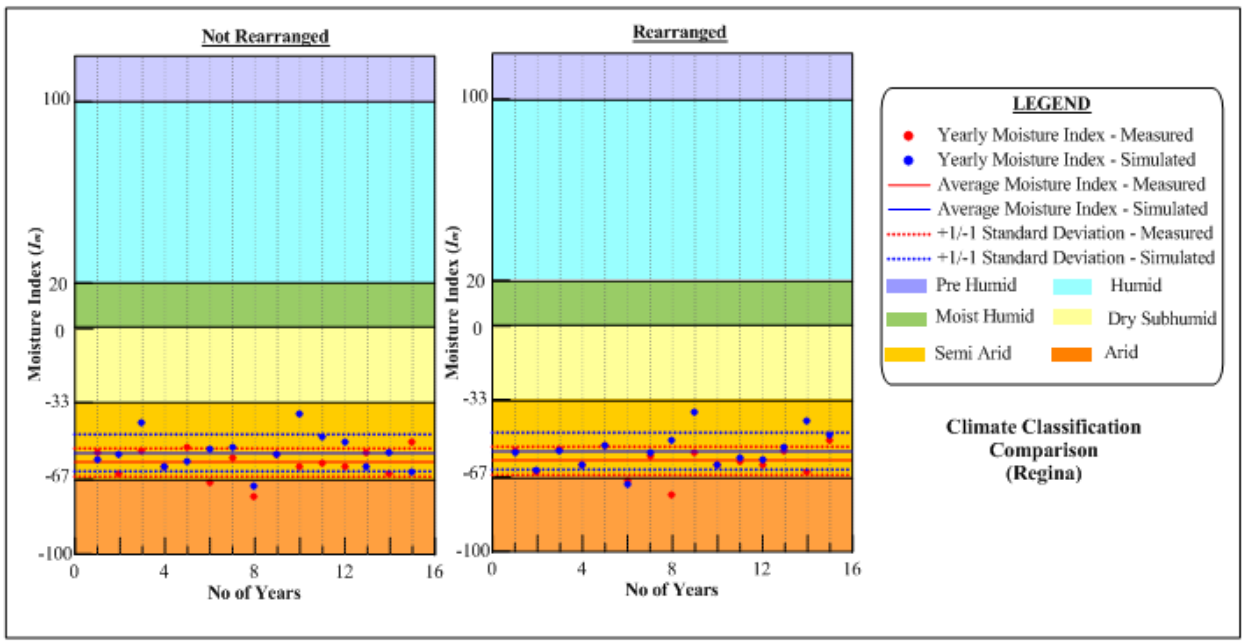

Figure 5.5: Measured and simulated data moisture index for Regina region

Each year of the simulation can be divided into active and inactive time periods. The active period represents thawed ground conditions when precipitation can either make its way into the ground as infiltration or can flow away as runoff. The inactive period represents the period when the ground is frozen, and precipitation accumulates on the ground surface as snow. The first date of freezing (i.e., start of winter) was selected to be November 10th based on the air temperatures from the climatic data. Spring-like conditions consists of a period where the precipitation that accumulates over the winter is applied as a major infiltration event. The first date of spring was selected to be April 9th (i.e., a date where the soil column could be expected to be thawed). The spring infiltration event was assumed to continue for two weeks ending on April 23rd of each year. Summer-like conditions consists of a period when there is considerable activity in terms of heat and moisture movement. Detailed soil-atmosphere modelling was conducted through the 214-day active period when the majority of moisture can flow through the soil domain (i.e., spring and summer). A schematic of the active and inactive periods is shown in Figure 5.6. The moisture flow through the ground shuts down during the winter when the soil at the surface freezes. Soil-atmospheric modelling was not continued through the winter months. It should be noted that freeze and thaw dates from both measured and estimated climate data were similar.

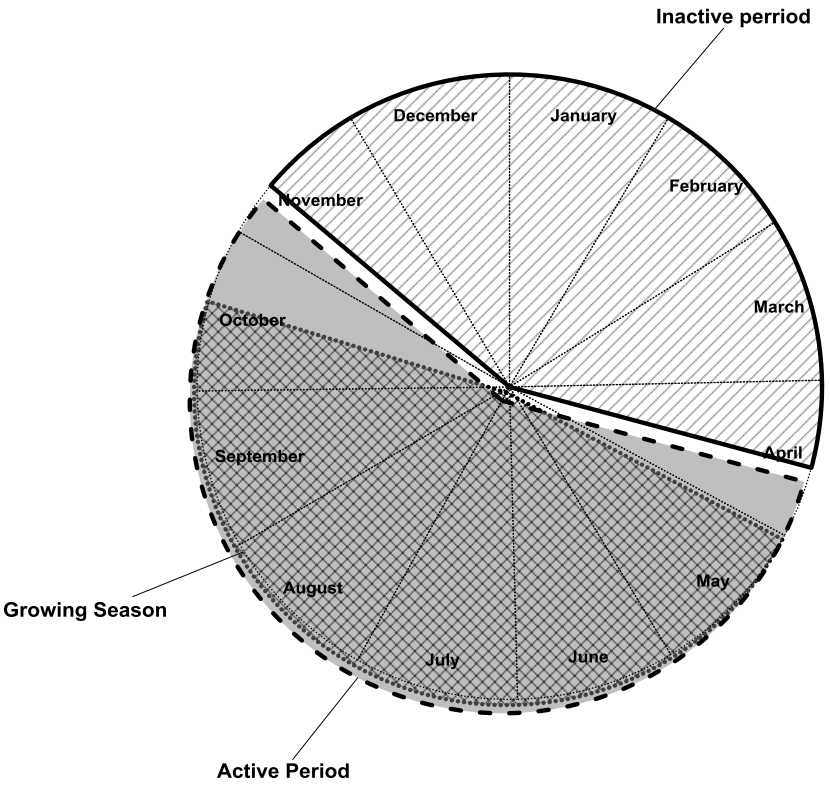

Figure 5.6: Schematic of the active and inactive periods for the city of Regina

5.2.3 Modeling results

The results from the soil-atmosphere analysis can be presented in many different ways, such as water balance at the ground surface and temporal and spatial distribution of moisture content and suction with depth. Figure 5.7 shows the water balance at the ground surface for simulations run with measured and simulated climate data. These results are cumulative values for 15 years average, and wet, dry and average year climates. The wet, dry and average years for measured and simulated climate data were identified by reviewing the yearly moisture indices presented in Figure 5.5. It should be noted that presenting the results in this manner provides an opportunity to compare the year-to-year water balance differences. For example, it can be observed that for dry year

climate, net moisture loss conditions can be observed throughout the active period. This observation is consistent for the simulations run with measured and simulated climate data. It can also be observed that this is in contrast to the results for wet year where moisture gain conditions can be observed during many days in the active period.

In general, the water balance results from simulations using measured and simulated climate data are quite similar. Some of the difference between measured and simulated water balance results can be attributed to the selection of dry, wet and average years. The selection was based on a good match between the yearly average moisture index values. This selection criterion implies that the ratio of the total yearly precipitation and potential evaporation are similar. The water balance at the ground surface on the other hand not only depends on the total quantity of precipitation and potential evaporation but also on the sequence of the precipitation events. However, in spite of some variation between the results from measured and simulated climate data, on average the results are very similar.

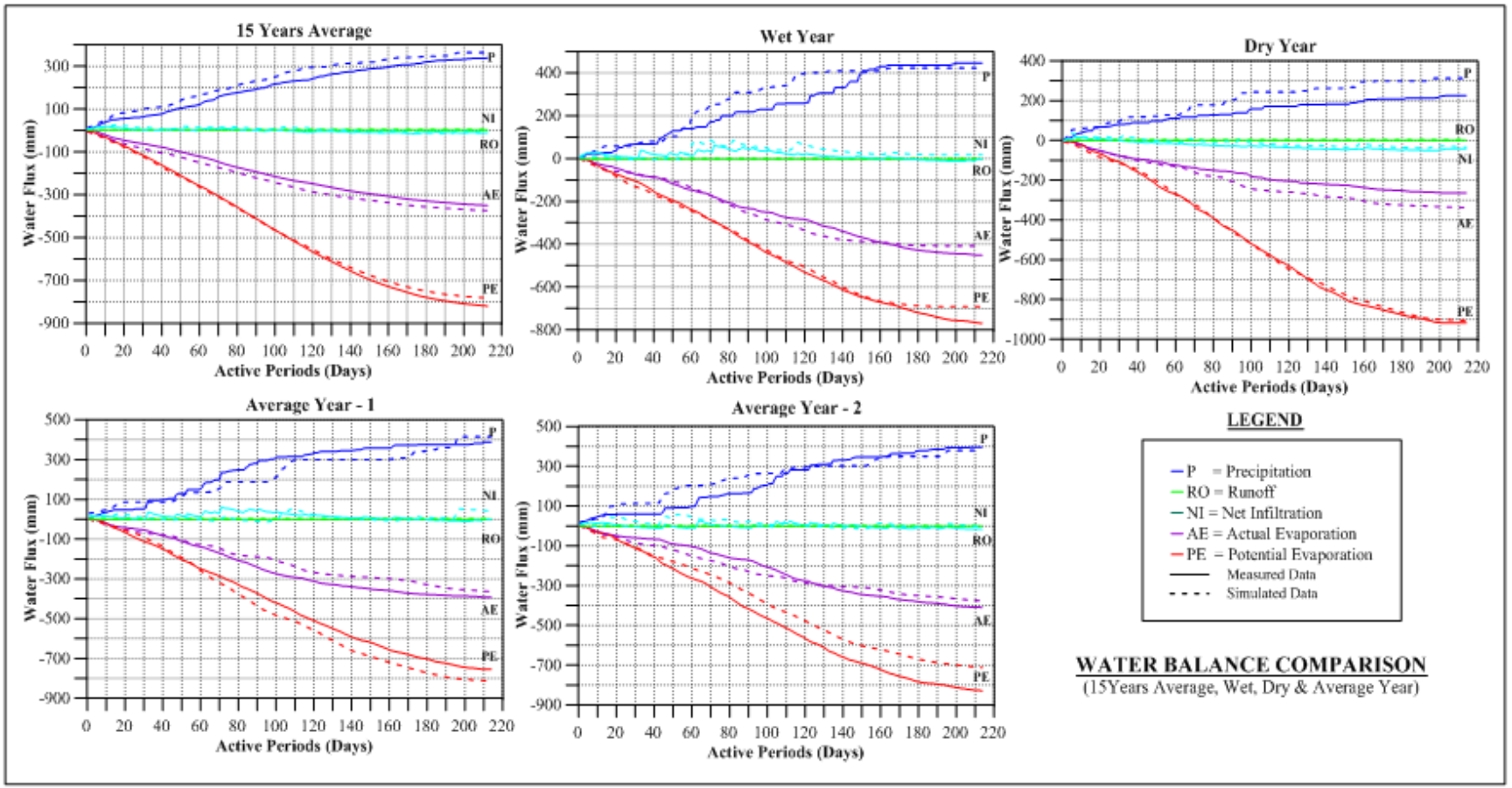

Figure 5.7: Water balance for measured and simulated data for Regina

Temporal and spatial distribution of swelling potential of Regina clay was estimated using Eq. (5.1). The use of Eq. (5.1) requires that the shrinkage curve for the soil as a function of gravimetric water content is known. Figure 5.8 shows the shrinkage data for Regina clay from a number of sources from the literature (Shuai 1996, Hung 2002, Azam et al. 2013, Fredlund and Houston 2013) . Fredlund et al. (2002) have proposed a hyperbolic mathematical equation for shrinkage curve as follows:

$$e(w) = a_{sh}\left[\frac{w^{c_{sh}}}{b_{sh}^{c_{sh}}} + 1\right]^{1/c_{sh}} \qquad \text{Eq. (5.2)}$$

Where $e(w)$ is the void ratio as a function of gravimetric water content, $a_{sh}$is the minimum void ratio ($e$min), b_{sh} is the slope of the line of tangency, c_{sh} is the curvature of the shrinkage curve, and w is the gravimetric water content. The hyperbolic function was fitted to the compiled dataset using curving fitting tool box of MATLAB (The Mathworks 2009). The fit to the data and with fitted parameters are also shown in Figure 5.8. The predicted volumetric moisture contents from soil-atmosphere modeling were used to compute the gravimetric water content in order to estimate the swelling potential as a function of time and depth. The initial void ratio was estimated using the predicted moisture content values employing Eq. (5.2). Figure 5.9 shows the estimated swelling potential time history with respect to the depth for Regina Clay using the measured and simulated climate data. The results are shown for the 15 year continuous period and indicate that the swelling potential generation is highest at and near the ground surface and gradually decreases with the depth.

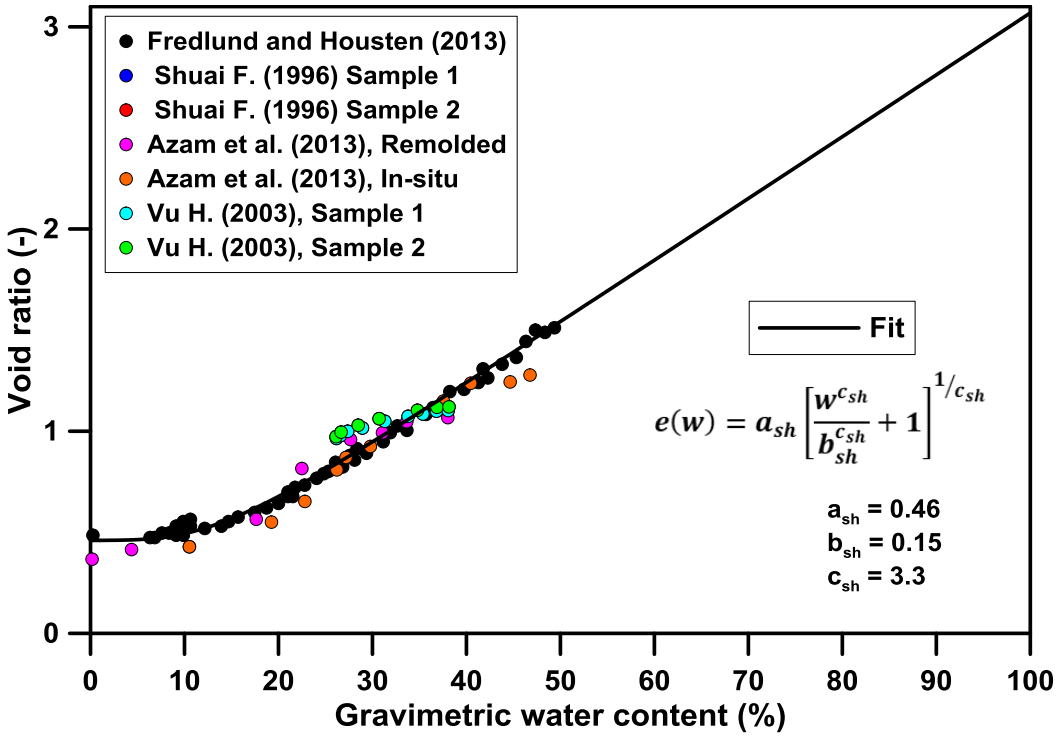

Figure 5.8: Experimental relationship between gravimetric water content and void ratio for Regina Clay

This leads one to conclude that the soil volume change will be higher near or at the ground surface resulting in differential settlement and heaving. Figure 5.9 also indicates that the predicted values for swelling potential from measured and simulation climate data are quite similar. The predictions from measured data showed slightly higher swelling potentials with depth. It can be observed that for some years the swelling potential of 30% was predicted at a depth of 2 m from the ground surface. For the same time periods the model using simulated climate data predicted swelling potential of 29% which constitutes a difference of only 3%. In general, it can be concluded that models run with simulated climate data show similar performance to those run with measured climate data.

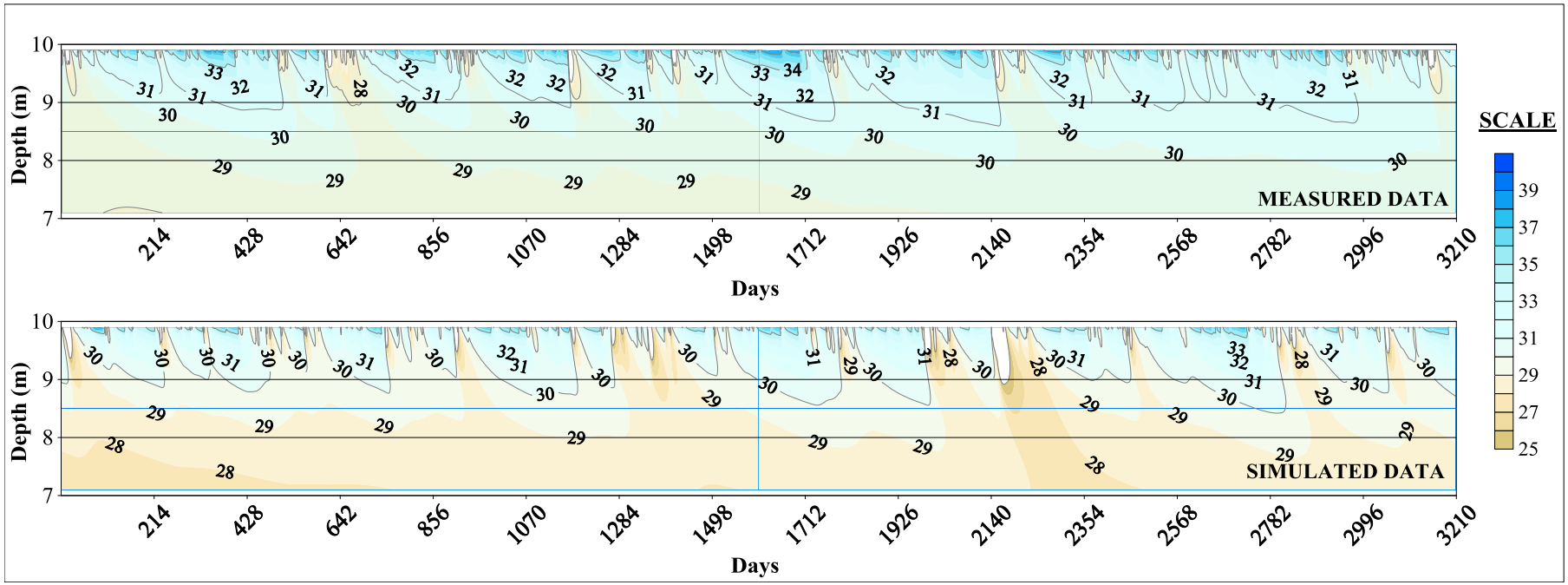

Figure 5.9: Fifteen years continuous comparison of swelling potential for Regina Clay calculated using measured and simulated data.

5.3 Soil cover system design

Cover systems are commonly placed over waste rock, tailings, or landfills to separate the waste from direct interaction with the atmosphere. A cover has a variety of potential functions including to limit infiltration, control air entry, limit thermal influences, block radiation, or resist erosion by wind and water. It is expected that a cover would remain stable both statically and seismically over a defined period of time. The design of soil cover systems constitutes one of the most challenging soil mechanics analysis faced by geotechnical engineers (Fredlund et al. 2012).

Soil covers can be classified into many different categories depending upon the role of the cover system, for example, the primary role for a store and release percolation barrier is to minimize moisture flux by maximizing near surface storage of moisture with the subsequent release by evapotranspiration. Cover classification based on the primary role is presented in Table 5.2 (O'Kane et al. 2002).

Table 5.2: Cover Classification (Modified from O'Kane et al. 2002)

Cover classification	Primary role of cover
Oxygen transport barriers	Retain moisture and provide a low diffusion barrier to atmospheric oxygen.
Oxygen consumption barriers	Act as an oxygen consuming sink to provide low oxygen concentrations at the tailings interface.
Reaction inhibiting barriers	Act to inhibits reactions, neutralizes pH.
Store and release percolation barriers	Act to minimize moisture flux by maximizing near surface storage of moisture with subsequent release by evapotranspiration.
Low permeability barriers	Act to minimize moisture flux by generating ponding in the surface of the barrier due to its low hydraulic conductivity. Water can be then released in the form of runoff or evapotranspiration.

Soil cover systems can range in complexity from a single layer of soil to multiple layers comprised of different materials as shown in Figure 5.10. The first designed cover systems generally consisted of compacted clays, to provide hydraulic resistance to meteoric water in reaching underlying waste. However, with time, new concepts and materials have evolved in soil cover design. Alternative covers, also known as evapo-transpiration (*ET*) covers, water balance covers, or store-and-release covers, are constructed on the principle of balancing the storage capacity of well-graded cover soils with the water removal capabilities of evaporation and transpiration. Similarly, materials other than clays and native soils have been used for soil cover construction. These materials range from non-reactive tailings and/or waste rock, to geosynthetic materials, and oxygen consuming organic materials.

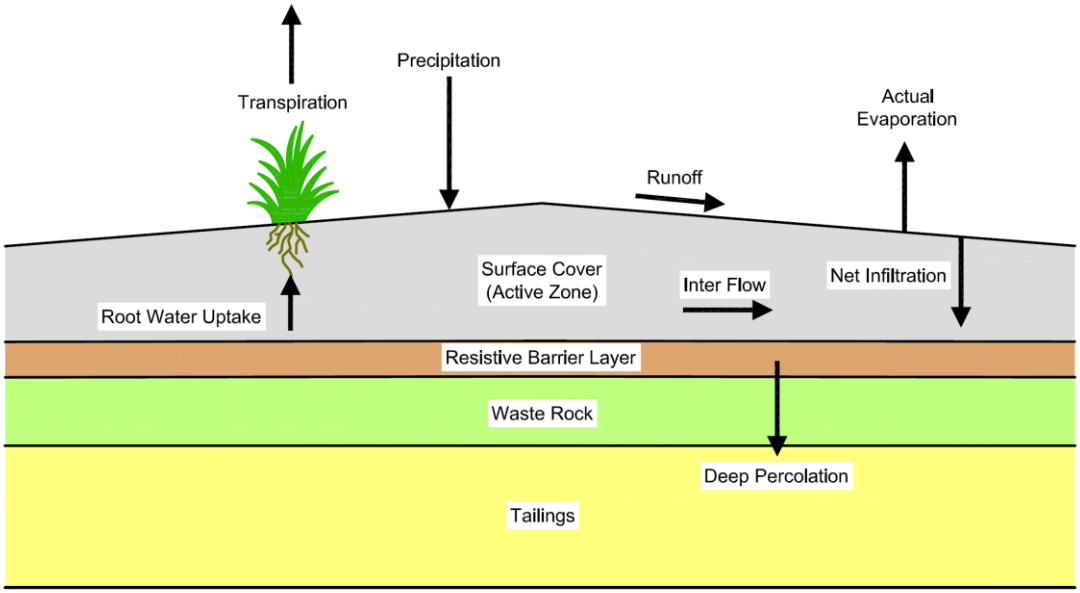

Figure 5.10: Hydrological processes within a multilayer cover system

5.3.1 Climate considerations and initial screening of soil covers

The climate data for site is one of the most important input variables for soil cover design. Climate classification using historic climate data for the site, spanning over a number of years, provides an overall picture of the climatic conditions at the site and can be used as a soil cover screening tool. Soil cover screening helps to identify the types of soil cover systems that are well suited to function in the given climate conditions depending on a particular design objective.

The annual precipitation and total potential evapotranspiration can be determined from multiyear climate dataset for the site and can be used to conduct preliminary screening of soil cover options. One of the procedures is based on the Holdridge life zone classification and uses a tri-linear plot of Annual Precipitation, Potential Evaporation Ratio, and Climate Classification as shown in Figure 5.11 (INAP, 2009). The Potential Evapotranspiration Ratio is computed as the total annual potential evapotranspiration divided by the total annual precipitation. The Potential Evapotranspiration Ratio together with the corresponding annual precipitation can be plotted to determine the types of soil covers that are well suited for the site climatic conditions and vegetation it can support.

The numerical simulations carried out as part of the preliminary or final design require multi-year historical climate data as direct input at a daily resolution. Historic climate data on precipitation (rainfall and snowfall), temperature (maximum and minimum), relative humidity (maximum and minimum), wind speed and net radiation forms the basis of the top boundary of the numerical model. The multiple year historic

record ensures that the simulations capture the year to year variation in climate, i.e. dry, wet and average year climates.

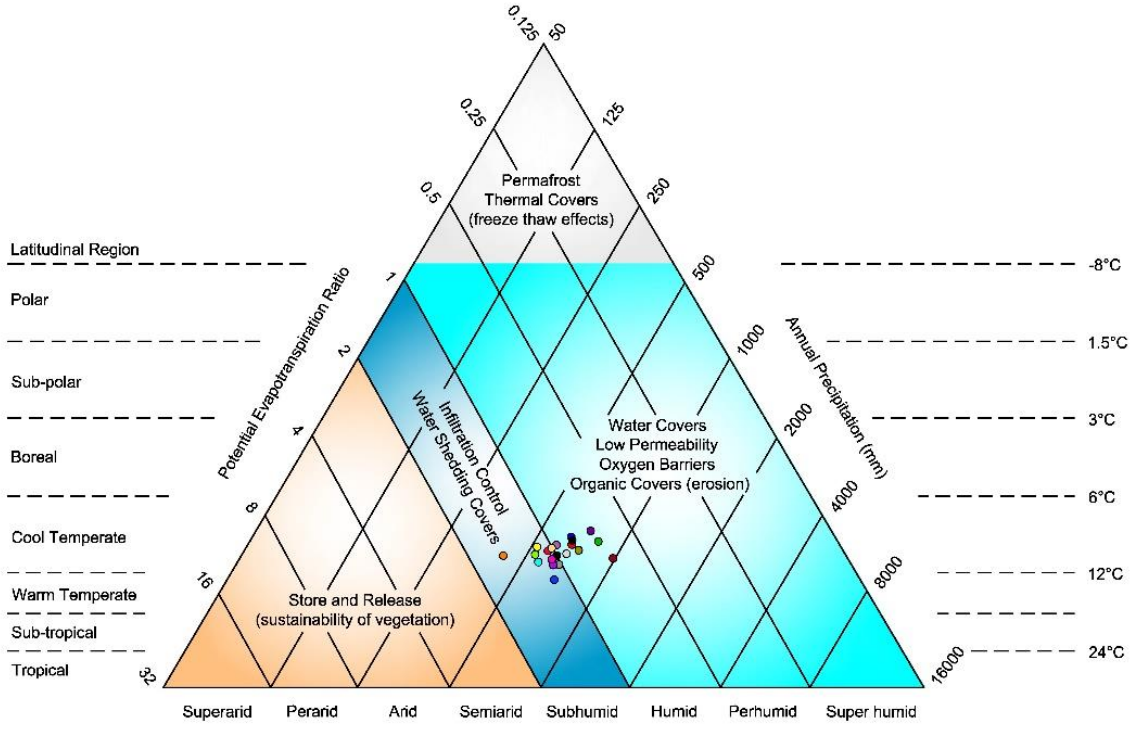

Figure 5.11: Cover screening based on climate classification

5.3.2 Covers to control acid mine drainage

Mine tailings enriched with sulphide content need be isolated from the atmosphere to control acid mine drainage (*AMD*). Acid mine drainage refers to the outflow of acidic water from sulphide-rich tailings. This is a natural phenomenon and generally depends on the amount of sulphide in the tailings and their exposure to the atmospheric oxygen. Water and oxygen are the two most important atmospheric factors that control the oxidation of the sulphide mineral in the tailings and hence the production of *AMD*. One of the strategies to control *AMD* is to install a cover which inhibits the ingress of water and oxygen to the underlying reactive tailings. Engineered soil covers with saturated fine-

grained material can be used effectively to limit the oxygen transport due to their potential to maintain high saturations. Rate of oxygen diffusion in water is four order magnitudes lower than that in air and solubility of oxygen in water is quite low (11 mg/L at 20^{o}C). Therefore, at higher soil saturation, the air in soil pores is in disassociated phase and water-filled pores act as barrier. It has been reported that the rate of oxygen diffusion through water is too slow to be of any significance to sulphide mineral oxidation (Yanful and Simms, 2005). Figure 5.12 shows the effective diffusion coefficient (D_e) of oxygen as a function of saturation predicted from different models assuming a soil porosity (n) of 0.4 and diffusion coefficients for oxygen and water as 1.8 x 10^{-5} m^2/s and 2.5 x 10^{-9} m^2/s, respectively. Measurements by Aachib et al. (2004) indicate that model by Millington and Quirk, (1961) performs the best in describing the experimental data. A review of this figure indicates that as the saturation of soil increase to 85% the diffusion coefficient is reduced by several order of magnitude.

It should be noted that at many sites, limiting oxygen ingress is not always practical, because it is difficult to keep the cover saturated, especially in arid and semi-arid climatic conditions and locations where fine-grained materials are not available. In such instances it is more feasible to reduce the net infiltration when dealing with the closure of reactive waste facilities.

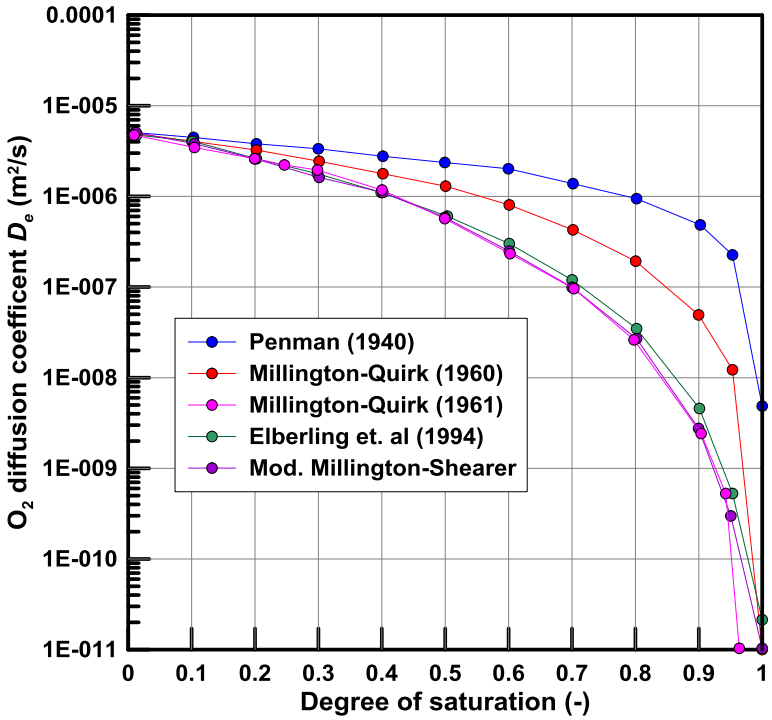

Figure 5.12: Oxygen effective diffusion coefficient as function of soil saturation estimated with different models (modified from Aachib et al. 2004)

5.3.3 Soil cover assessment

In order to assess the suitability of the simulated climate data for soil cover design, a cover system design example from *CANMET-CETEM* manual was selected (O'Kane et al. 2002). The primary function of this cover was to control the ingress of oxygen and water to the underlying reactive waste rock. The general arrangement of the cover system is 800 mm of till materials in three different sublayers as shown in Figure 5.13. The first layer comprises 300 mm of non-compacted till overlying 250 mm of compacted till. The top non-compacted clay layer would eventually function as a growth medium. Underlying the top two till layers is a 250 mm thick bentonite amended till layer placed directly on the waste rock material (O'Kane et al. 2002). The bentonite amended till was produced by mixing 8% bentonite on mass basis with native till.

Figure 5.13: Soil cover profile. (modified from O'Kane et al. 2002)**.**

The soil cover modelling was carried out with finite element soil atmosphere modelling program *VADOSE/W* Version 8.12.3.7901 (GEO-SLOPE International Ltd. 2012). *VADOSE/W* is capable of solving the governing partial differential equations for vapour, water and heat transport and estimates actual evaporation based on the formulation described by Wilson et al. (1994). A transient coupled analysis was carried out using *VADOSE/W*. The geometry of the model comprised a 3.8 m of the soil column. The upper part (0.8 m) of the soil column consisted of three layers representing the soil cover, whereas, underlying 3 m represented the waste rock.

The soil hydraulic properties used in the cover simulation were as per the *CANMET-CETEM* manual wherein it is reported that the cover material is sandy, non-plastic silt matrix till with a trace of clay (O'Kane et al. 2002). The maximum dry density

was reported to be 2.1 gm/cm^3 for a standard Proctor compaction effort corresponding to an optimum moisture content of 10%. The waste rock was reported to be well graded angular rock with significant amount of silt material. It was also reported that presence of silty material in the rock is a result of physical, chemical, and biological weathering of the waste rock.

The hydraulic conductivity measurements for the cover materials and waste rock were carried out using a falling head apparatus during consolidation testing. The laboratory saturated hydraulic conductivity for compacted native till was reported to vary between 1x10^{-9} and 1x10^{-8} m/s. The laboratory saturated hydraulic conductivity of the waste rock samples was reported to vary between 1 x 10^{-9} cm/s and 1 x 10^{-7} cm/s. These significantly lower values of hydraulic conductivity for waste rock were attributed to the presence of significant amount of silt in upper layers of waste rock and the fact that hydraulic conductivity samples were prepared using material less than 4.75 mm (i.e. passing the No.4 sieve) (O'Kane et al. 2002).

The soil water characteristic curves for the cover materials and waste rock are shown in Figure 5.14 with data from O'Kane et al. (2002). Review of the figure indicates that addition of bentonite results in change in retention properties of the till. It can be observed that compacted tills have higher air entry values and larger variation in pore sizes than the non-compacted till. It can also be observed that addition of bentonite results in significant increase in air entry values.

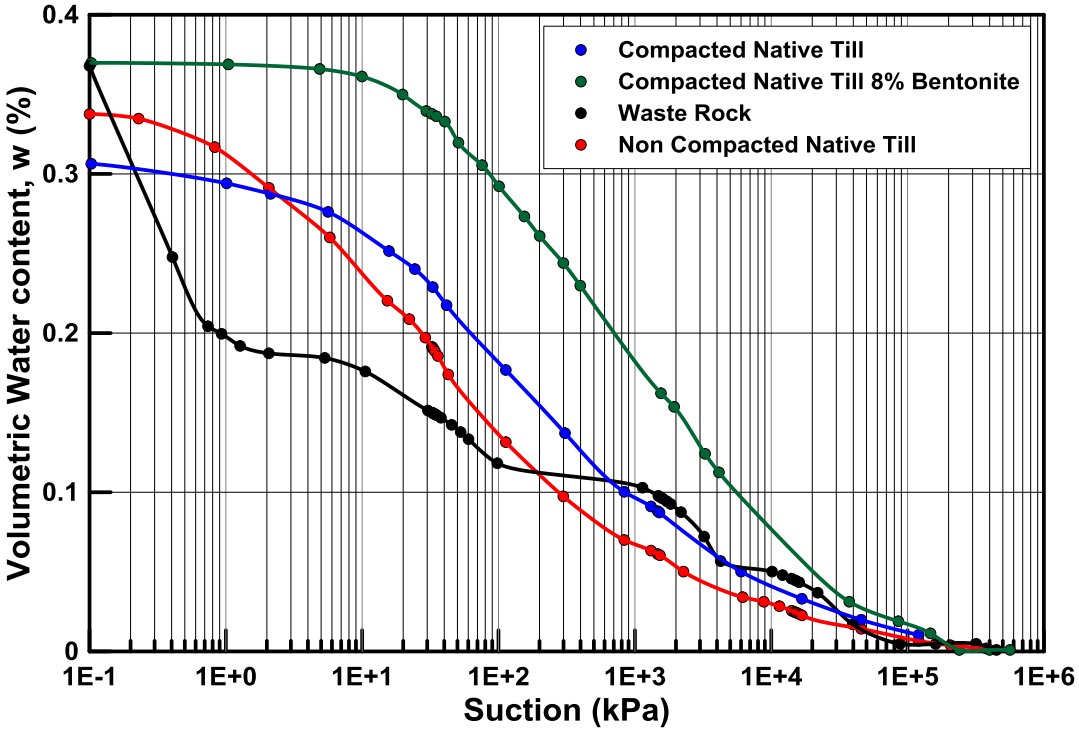

Figure 5.14: Soil water characteristic curves for cover materials and waste rock with data from O'Kane et al. 2002.

van Genuchten, (1980) functions were fitted to the experimental data for *SWCC* using RETC (van Genuchten et al. 1991). The resulting parameters are shown in Table 5.2.

Table 5.3: Parameters for van Genuchten (1980) function to experimental data

van Genuchten (1980) Parameter	Waste Rock	Non Compacted Native Till	Compacted Native Till	Compacted Native Till + 8 % bentonite
θs (-)	0.37	0.34	0.31	0.37
α (kPa^{-1})	10	0.21	0.07	0.01
n (-)	1.2	1.3	1.27	1.33
θr(-)	0	0.00023	0.0003	0.0002

Measured and simulated climate data for Timmins (*ON*) was used as the top boundary condition for soil cover analysis. The climate classification was carried out for

both measured and simulated data using Thornthwaite climate classification system (Thornthwaite and Hare 1955) as shown in Figure 5.15.

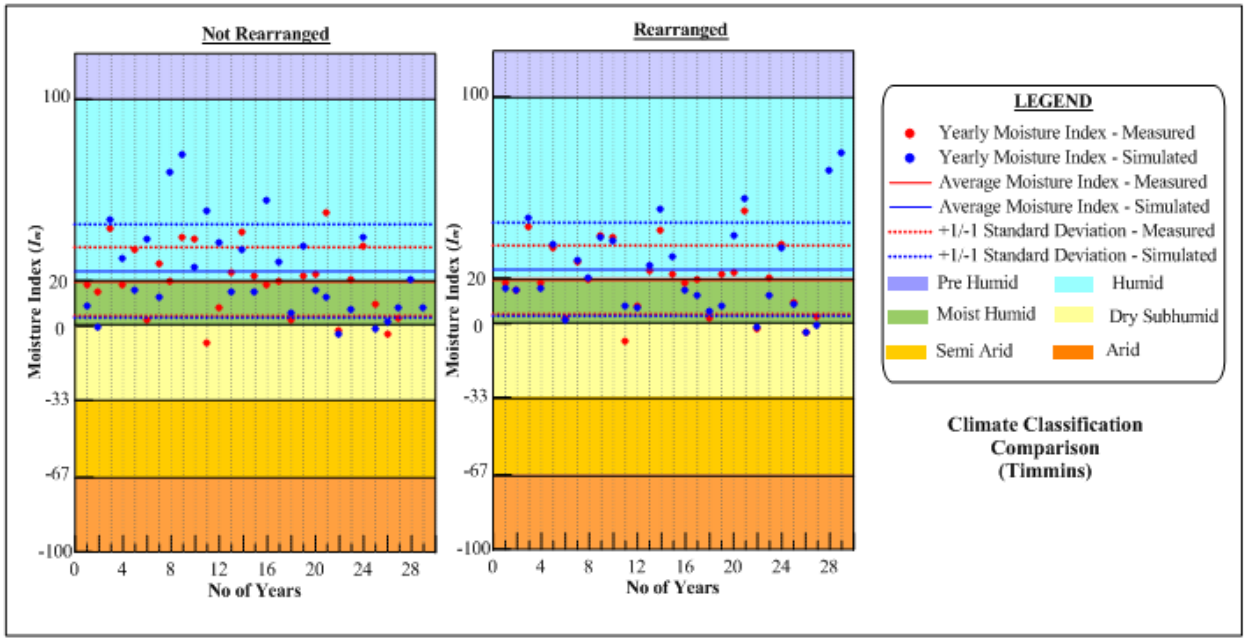

Figure 5.15: Measured and simulated data moisture index for Timmins

Review of the climate classification indicates that on average the climate of Timmins can be classified as humid to moist humid climatic conditions. The comparison of measured and simulated climate data indicates that simulated climate data appears to have a few years with higher moisture indices than the measured data. The consequence of this would be that an analysis done with simulated climate data will provide a more conservative estimate in terms of infiltration control owing to the larger availability of meteoric water at the ground surface. At the same time there is a possibility that use of simulated climate data could potentially under predict the oxygen ingress in certain years by predicting higher saturations. However, it should be noted that simulated climate data has a number of years where the moisture index is one standard deviation below the

average measured moisture index. This leads one to expect that simulation run with simulated climate data should be able to identify any design issues related to oxygen ingress. Figure 5.16 shows a comparison of 15-year average measured and simulated climate data for Timmins. The range of maximum and minimum values from the measured and simulated data are presented in Table 5.4. Review of Figure 5.16 and Table 5.4 indicate that there is a good correlation between the measured and simulated climate data.

Table 5.4: Comparison of climate data variables

Value	**Temperature (^{0}C)**		**Relative Humidity (%)**	
	Measured	**Simulated**	**Measured**	**Simulated**
Maximum	38.9	35.2	92	98
Minimum	-15.1	-16.6	48	49
	Wind Speed (m/sec)		**Net Radiation (MJ/m^2/day)**	
	Measured	**Simulated**	**Measured**	**Simulated**
Average	3.2	3.1	8.66	7.15
	Precipitation Intensity (mm/day)			
	Measured		**Simulated**	
Maximum	88		47	

The model was run for 4,925 model days, in which 197 active days were used for each year. The active and inactive periods were estimated based on the thaw and freeze conditions. The active period for measured data ranges between April 18th to October 31st and the inactive period from November 1st to April 17th. Similarly, the active period for the simulated data was from April 28th to November 10th, and the inactive period range between November 11th to April 27th.

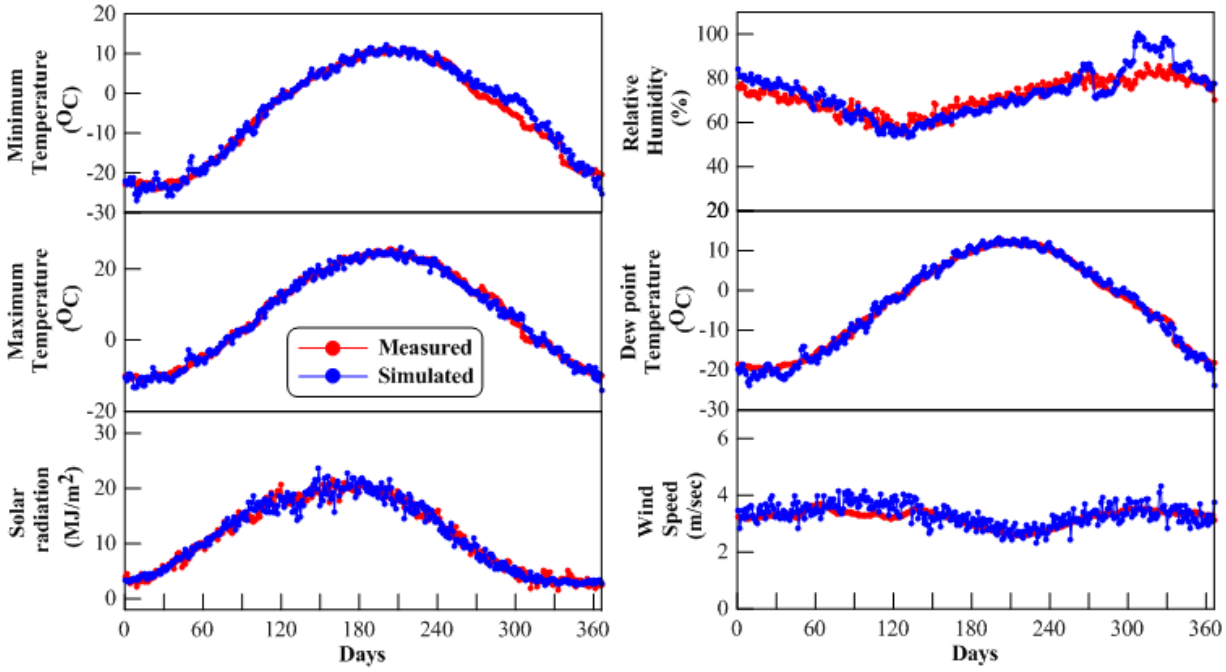

Figure 5.16: Yearly averaged measured and simulated climate data for Timmins

The results of the soil cover analysis were analyzed in terms of covers performance to limit the water and oxygen ingress to the reactive waste rock. Figure 5.17 shows the water balance at the ground surface for measured and simulated climate data. Generally, results indicate water gain conditions over an annual basis. The review of the figure indicates that predicted quantities of water getting to the soil cover (*NI*) are very similar for simulations run with measured and simulated climate data. It can also be observed that except for the *PE* values, the rest of the climate variables appear to be quite similar for both measured and simulated results. The difference between the two values is due to different years selected based on the climate classification system.

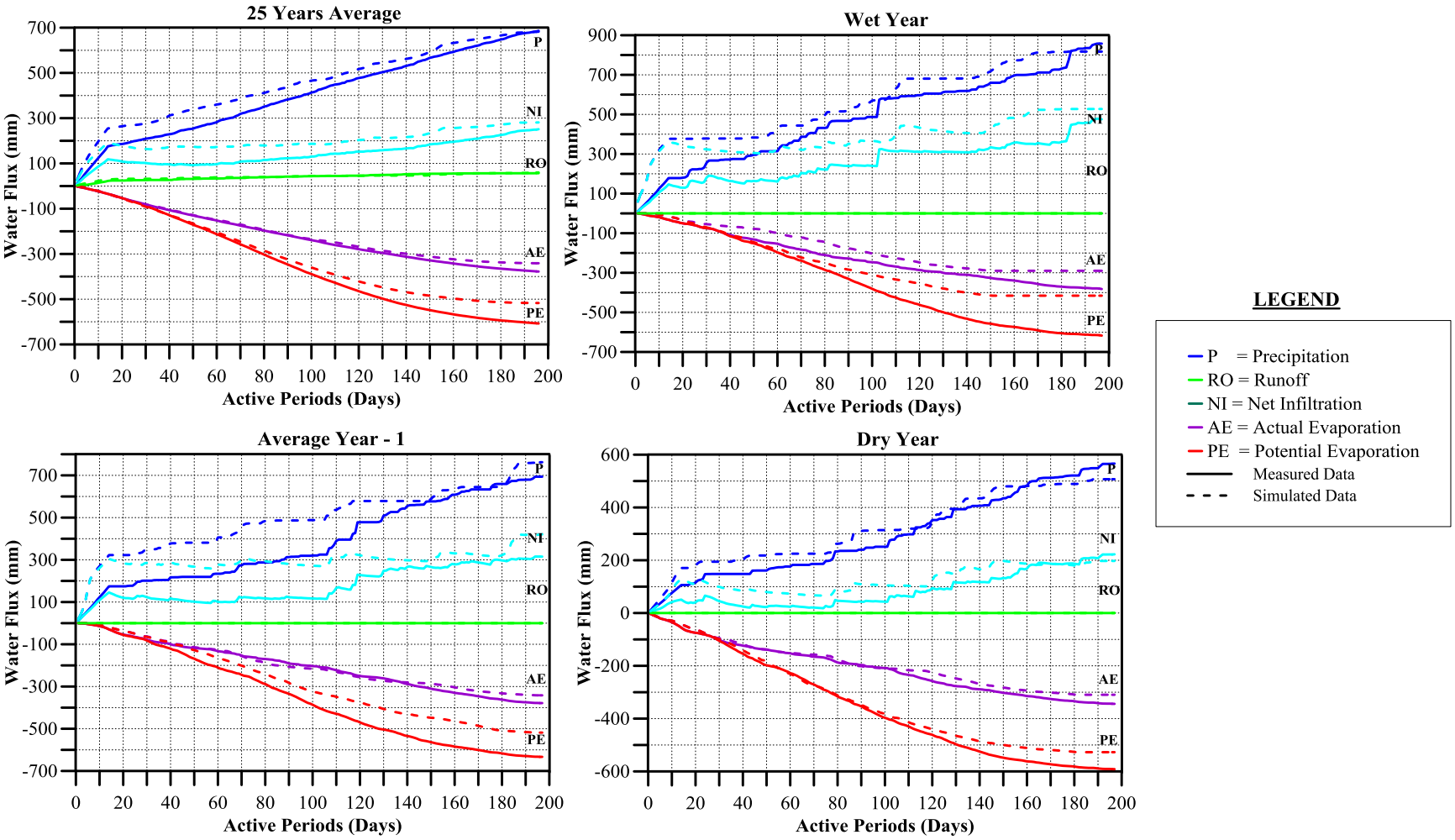

Figure 5.17: Comparison of water balance for measured and simulated data for Timmins

The ability of the cover to control oxygen ingress was analyzed by quantifying its ability to maintain higher than 85% saturation. Figure 5.18 shows the saturation distribution in the cover over the 25-year period for simulation run with measured and simulated climate data. It is shown that no significant differences are observed between the results predicted from measured and simulated climate data. In general, the results are consistent with water balance conditions presented above. It can be observed that for both set of simulations the seasonal drying region is limited to the upper portion of the compacted till and lower portion of the cover maintains a saturation of 85 %. This leads one to conclude that cover is capable of controlling oxygen ingress to the reactive waste rock. It can also be observed that more regions of higher saturation near the ground surface can be observed in the results from simulation run with simulated climate data. This is not an unexpected result as it was noticed in climate classification that the simulated climate in general had more wetter years.

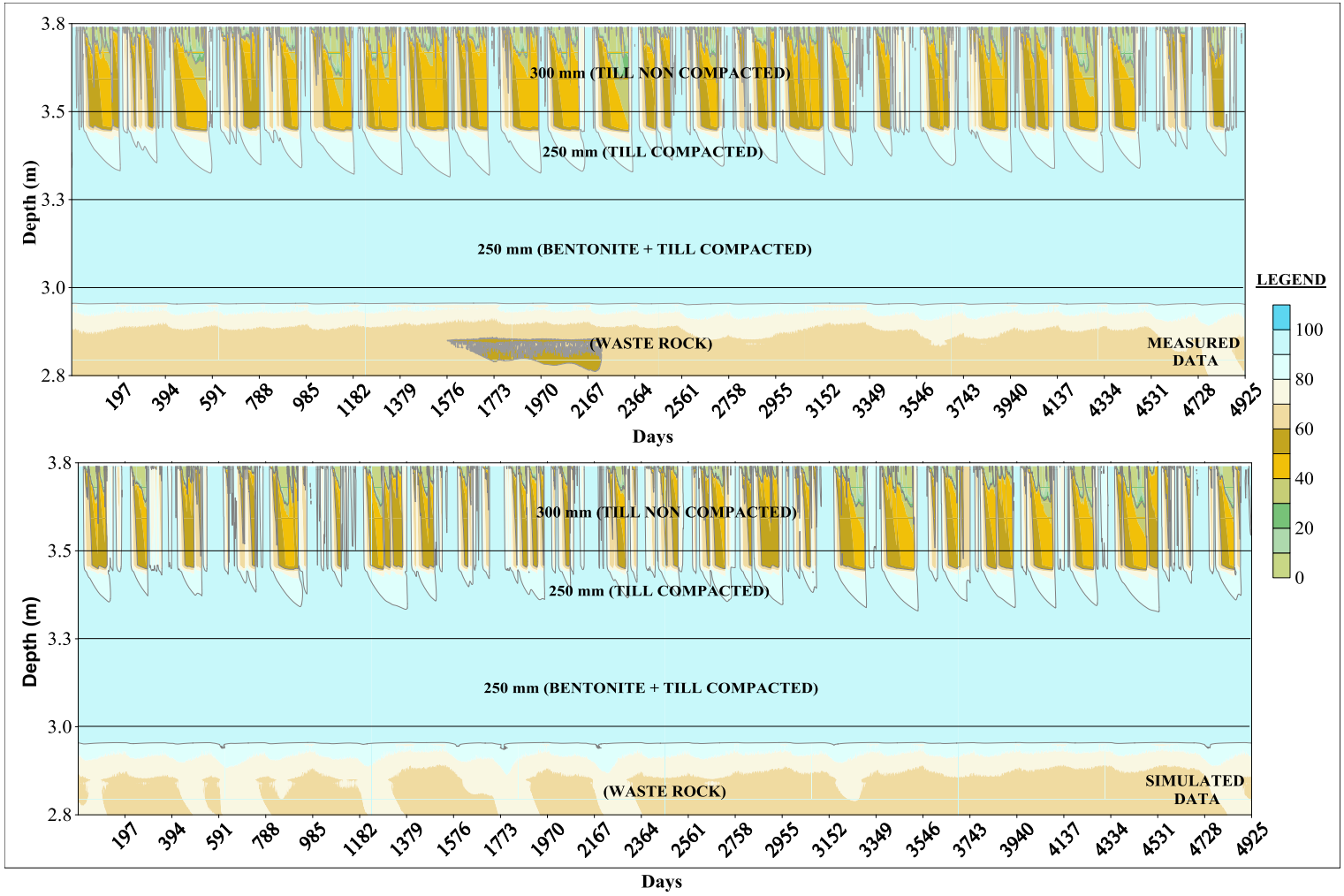

Figure 5.18: Twenty-five years comparison of saturation predicted using measured and simulated data Timmins

The performance of the cover to control the ingress of meteoric water was evaluated by estimating the quantity of water making its way into the waste rock. This quantity is termed as deep percolation. Figure 5.19 shows the deep percolation comparison for simulations run with measured and simulated climate data. It should be noted that results are not sorted over the years but are reported in the sequence that climate data was measured or simulated. This figure indicates that the cover is effective in controlling the ingress of meteoric water to underlying waste as maximum quantity of water reaching the reactive waste rock is less than 1.5% of the average yearly precipitation value. It can be observed that simulation ran with simulated data tend to predict higher deep percolation values. As pointed out earlier that this is result of the higher moisture index for the certain years in simulated climate data.

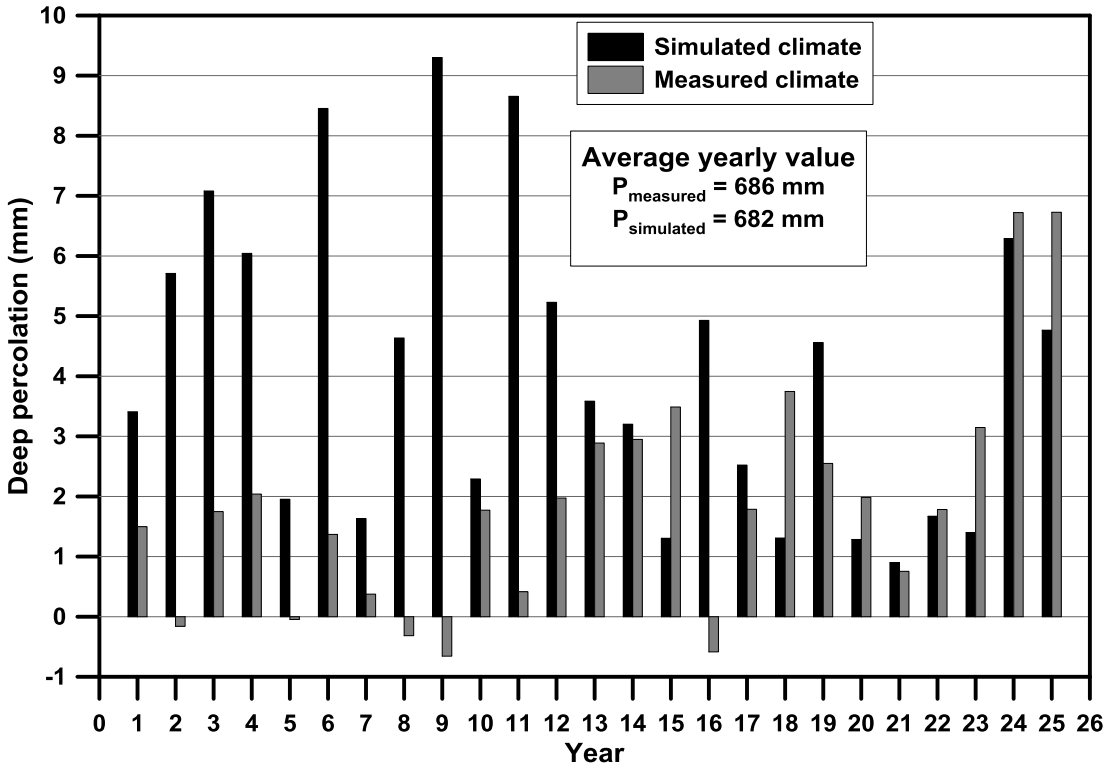

Figure 5.19: Twenty-five years comparison of deep percolation predicted using measured and simulated data

Chapter 6

Summary, Conclusions and Recommendations

6.1 Summary

This thesis had two main objectives. The first objective was to assess the suitability of a general-purpose climate data generator to simulate multi-year climate datasets at daily resolution from monthly climate normals for various location across Canada. The second objective was to assess the adequacy of the simulated climate data for use in geotechnical and geoenvironmental design problems. The research comprised three distinct phases. A brief description of each phase is provided below.

In the first phase of this research, climate data for nine different geographical locations across Canada were compiled from historical records maintained by Environment Canada. The climate datasets comprised daily records of maximum and minimum temperature, precipitation, relative humidity, wind speed, and net radiation. The historical climate data for each location were reviewed for completeness, and quality. Missing or erroneous values were infilled or replaced using the spatial or temporal interpolation methods. The compiled sets of data were also analyzed to identify the relevant and significant features of the various climate variables. The compiled climate datasets were compared with Environment-Canada-reported climate normals to ensure that the datasets are generally representative of the long-term climatic conditions of these locations. Climate classification was carried out to highlight general climate setting of the different locations and highlight the difference in water availability at the ground surface for these locations.

In the second phase of this research daily climate data was generated from monthly climate normals using a general-purpose weather generator *SIMETAW* (Snyder et al. 2012). The compiled climate normals were used in *SIMETAW* to simulate multi-year daily climate datasets. Relative humidity estimates were made from simulated dew point temperatures using August-Roche-Magnus equation as recommended by Fredlund et al. (2012). Similarly, net radiation was estimated from solar radiation using procedure described by Irmak et al. (2003). The simulated climate datasets were compared to the measured historical datasets to quantify the performance of *SIMETAW*. The comparison was carried out in two different ways. Visual presentation method was used to visually compare the similarities and differences between the simulated and measured climate data. This type of comparison provides a rough estimate of the agreement between the two datasets and clearly identifies where the predictions are most problematic. Numerical measures using statistical methods were used to provide summary measures of overall accuracy of the simulated data. These measures not only indicate whether the trend relative magnitudes are captured, but also quantify the deviation from the exact data locations. Comparison between potential evaporation and climate classification using measured and simulated climate data was also carried out.

The third phase of the research assessed the suitability of simulated climate data for geotechnical and geoenvironmental designs. Three different design problems were considered. The first design problem investigated the use of simulated climate data for the region of Barriere in the province of British Columbia for infiltration assessments. Infiltration assessments are an important part of many geotechnical and geoenvironmental designs (Bashir et al. 2016). The second design study comprised

estimation of swelling potential for Regina Clay in the city of Regina in the province of Saskatchewan. Measured and simulated climate data for the city of Regina was used in this assessment. The assessment used literature-reported values of hydraulic and geotechnical properties of Regina Clay. The third study addressed the suitability of the simulated climate data for soil cover design purposes. A case study of a soil cover to control oxygen and water ingress to reactive waste rock was selected from the literature. The performance of the soil cover was assessed using measured and simulated climate data for city of Timmins in northern Ontario. The soil hydraulic properties and cover profile used in the assessment were that same as those reported in the case study.

In the following sections, conclusion derived from each of these phases are described. Conclusions are followed by identifying some of the contributions of this research. The chapter ends with recommendations for future research.

6.2 Conclusions

6.2.1 Climate data compilation and classification

The climate data compilation for nine different geographical locations across Canada indicated that in general larger and better-quality datasets are available for large urban centres across Canada. Although the climate data available through Environment Canada web portal goes through some quality assurance and quality checking procedures, not all data on the portal is quality controlled. In many instances, the measured data might not be continuous, with one or more variables missing over extended periods of time. The missing weather data may be because of instrument malfunction, break in transmission, or loss of archived dataset. Currently, Environment

Canada does not have a mechanism to provide any estimates of data that is missing or left blank online. Similarly, the measured weather records can have erroneous values. These erroneous values could be because of data-entry mistakes, instrument malfunction, improper calibration, transmission errors or other reasons. Environment Canada recommends that in instances where questionable data is identified, an enquiry should be sent to Climate Services office within the region of the location of interest. All these observations lead one to conclude that although good quality data for many locations across Canada is available, compilation of good quality continuous climate data sets require considerable amount of time and effort. It can also be concluded that the compilation of climate data also requires some familiarity and experience of working with climate data sets to identify any questionable or erroneous data. Based on the comparison of compiled and reported climate normals it can be concluded that it a good practice to asses that the compiled dataset accurately depicts the climate of the area under consideration.

Climate classification carried out for 9 different locations across Canada indicated that for locations considered, the climate in Canada can vary from Arid to Pre-Humid. This leads one to conclude that using the Thornthwaite and Hare, 1955 annual moisture index (I_m) as the classification tool, climate in Canada covers all climate types. Climate classification also revealed that for locations considered in this research, wetter climates tend to show more year-to-year variation in climate than the locations with drier climates. The least variation in year-to-year climate was observed for the region of Barriere in the province of British Columbia and city of Regina in the province Saskatchewan. Similarly, most variation in year to year climate was observed for the city of Halifax in the province

of Nova Scotia and city of Vancouver in the province British Columbia. However, caution should be exercised with this conclusion. Although compiled datasets for Regina and Barriere showed good correlation with measured climate normals, they were approximately one half the size of datasets for Halifax and Vancouver.

6.2.2 Simulation of multi-year daily climate data from climate normals

Comparison of simulated and measured climate data indicated that in general SIMETAW does a good job in simulating multi-year daily climate datasets. Considering the fact that the climate for locations considered in this research varied from arid to pre-humid, it can be concluded that the *SIMETAW* is capable of simulating various climates types across Canada. Comparison also indicate that estimated *RH* values from simulated dew point temperatures compare well with measured *RH* values. This observation leads one to conclude that inability of *SIMETAW* to simulate *RH* should not be considered a disadvantage as reliable estimates of *RH* can be made from simulated dew point temperatures.

The strategies used for comparing measured and simulated climate data indicated that visual comparison and statistical measures both provide essential information in comparison of measured and simulated data. It can also be concluded that different strategies are required to compare different measured and simulated climate variables.

6.2.3 Suitability of simulated climate data for geotechnical and geoenvironmental designs

As mentioned above the suitability of the simulated data was assessed by using them in three different types of design problems. For infiltration assessment, the water balance comparison between simulations run with measured and simulated climate data showed similar results. Climate data simulated with *SIMETAW*, when used in infiltration assessment over predicted the net infiltration values by less than 16 mm/y for three different soil types considered in the assessment. In general, it can be concluded that climate data simulated with *SIMETAW* can be used for infiltration assessments. The results from the assessment also indicated that the water balance at the ground surface is highly dependent on the soil hydraulic properties. Coarse-grained soils have much higher net infiltration rates in comparison to fine-grained soils. This is directly related to the hydraulic properties of the soils. Fine-grained soils have higher retention and lower conductance, which tends to keep the meteoric water in near surface region for longer period of times. This results in higher actual evaporation, resulting in lower net infiltration. Conversely, coarse-grained soils have lower actual evaporation values and higher net infiltration values owing to their lower retention and higher conductance properties. This observation leads one to conclude that difference in water balance between simulations run with simulated and measured climate data should also be considered in terms of soil types. For example, similar differences in terms of net infiltration quantities for coarse and fine-grained soils can have different impact. The effect of difference in net infiltration will be due to the higher total infiltration in coarse grained soils. However, these differences might constitute higher percentage of total infiltration in fine-grained soils. The results of

the simulations also indicated that the difference between the water balance using measured and simulated climate data are not only dependent on the total quantities of precipitation and potential evaporation but their distribution as well. For example, even if the total quantity of precipitation between measured and simulated climate data is similar, the days of precipitation occurrences might be more closely spaced for one of the datasets. This can potentially result in increased net infiltration due to wetter soil conditions as more water becomes available in shorter period of time. Considering that it is not possible to replicate the days of precipitation occurrences exactly in simulated climate datasets, it can be concluded that some differences in water balance assessments will exist between the measured and simulated climate datasets.

In the second design example, the adequacy of the simulated climate data was assed for moisture dynamics and swelling potential calculations for an expansive soil in the city of Regina. Water balance assessments indicated that on average and for dry, wet and average year climates the water balance at the ground surface is similar for measured and simulated climate data. Therefore, it can be concluded that *SIMETAW* simulated a set of climate data that is quite similar to the measured dataset for the semi-arid climate of city of Regina. It can also be concluded that this dataset on average produces water balance estimates that are similar to those from measured dataset. Estimates of the temporal and spatial distribution of swelling potential for Regina Clay using measured and simulated climate data were similar. The swelling potential predictions from measured data showed slightly higher swelling potentials with depth, when compared to estimates from simulated climate data. It can be observed that for some years the swelling potential of 30% was predicted at a depth of 2 m from the ground surface. In comparison, estimates

of 29% at same depth were made using the simulated climate data. This constitutes a difference of only 3 percentage points on average. Therefore, it can be concluded that the climate data simulated with *SIMETW* can be used for assessment of moisture dynamics and swelling potential in expansive soils.

The suitability of *SIMTAW* simulated climate data was assessed for design of soil cover systems by comparing the water balance, saturation profiles and deep percolation estimates made using measured and simulated climate data for Timmins, Ontario. Water balance assessments indicated that in general estimates from simulated climate data were quite similar to those from measured climate data. These observations lead one to conclude that *SIMETAW* simulated a climate dataset that is capable of reasonably estimating the humid climatic conditions for the city of Timmins. The results also indicated that spatial and temporal distribution of saturation in the soil cover estimated using measured and simulated climate data was comparable. This translates to a similar cover performance in terms of control of oxygen ingress for measured and simulated climate data. Therefore, it can be concluded that simulated climate data can be used to assess the cover performance in terms of in terms of control of oxygen ingress. The performance of the cover to control the ingress of meteoric water was evaluated by estimating the quantity of water making its way into the waste rock using measured and simulated climate data. Based on the results it can also be concluded that use of simulated climate data results in a cover performance assessment that is comparable the one carried out using measured climate date.

6.3 Contributions of this research

The research presented in this thesis represents a pioneering study on adequacy of simulated climate data on geotechnical and geoenvironmental design problems. Considering that quantifying the effect climate change on geotechnical and geoenvironmental infrastructure is at the fore front of the research, it is anticipated that this research will make the climate data for the practitioners and researchers more accessible.

6.4 Recommendations for future research

6.4.1 Assessment of *SIMETAW* to simulate northern climates

The current study investigated climate data for nine different geographical locations across Canada. The climate at these sites ranged from arid to pre-humid, which covers all climate types according to the Thornthwaite and Hare, 1955 climate classification system. However, no geographical location in the three northern territories of Canada: Yukon, Northwest Territories and Nunavut were considered. These parts of Canada are snow and ice-covered for more than half of the year and are hotspots for climate change. Assessment of *SIMETAW* to simulate climate for these regions would be of interest to many.

6.4.2 Assessment of simulated climate data for use in other design problems

The current study looked at the three different types of design problems, namely infiltration assessment, design of soil covers and assessment of volume change behavior

of an expansive soil. The suitability of simulated climate data to be used in other geotechnical and geoenvironmental design problems should also be assessed. The two most important ones would be slope stability assessments and contaminant transport in variably saturated soils.

6.4.3 Integration of *SIMETAW* in soil-atmosphere modeling software

A recent review (Vardon, 2015) of climatic influence on geotechnical infrastructure concludes that "One of the most critical areas for climate driven processes affecting the stability of geotechnical infrastructure is the soil atmosphere boundary". This forecast has come true as soil-atmosphere boundary, once considered to be of more interest to people in soil/agriculture science has seen a renewed interest in geotechnical engineering with a number of publications on theoretical and experimental aspects in recent years (Fredlund et al. (2014), Fredlund et al. (2016), Garard et al. (2016) and Sedighi et al. (2016)). Considering that simulations with soil-atmosphere boundary require multi year climate data integration of *SIMETAW* in a soil-atmosphere modeling software should be considered. This will greatly expedite location specific analysis for many design problems.

6.4.4 Effect of climate change

There is overwhelming scientific evidence that the climate is changing and will continue to change over the foreseeable future. This research indicated that the temporal and spatial distribution of moisture in the upper soil layers is influenced by the atmospheric interactions via infiltration of meteoritic water. Similarly, in lower soil layers,

moisture distribution is controlled by change in groundwater table depth, which can also be linked to atmospheric interactions via groundwater recharge. Therefore, climate change is an important factor in many geotechnical and geoenvironmental designs. The effect of climate change can be considered by using *SIMETAW* to generate future climate data. In many instances the change in future climate is only reported as three-decade averages of various climate variables (Barrow, 2009). This information can be used to to generate daily future climate data. This approach should be further researched

References

- A. Tremblay, G., and M. Hogan, C. 2001. MEND Manual Volume 2 - Sampling and Analysis MEND 5.4.2b. 2.
- Aachib, M., Mbonimpa, M., and Aubertin, M. 2004. Measurement and prediction of the oxygen diffusion coefficient in unsaturated media, with applications to soil covers. Water, Air, and Soil Pollution, 156(1): 163–193.
- Alexandridis, K., Antonis, Z., and Achilleas, D., 2013. Weather derivatives-modeling and pricing springer. Access from http://www.springer.com/gp/book/9781461460701 (last accessed July 26, 2018).
- Alexandrina, B., Swelam, A., Snyder, R., and Orang, M. 2010. Modeling evapotranspiration of applied water in Egypt delta.
- Allen, R.G., Pereira, L.S., Raes, D., Smith, M., and others. 1998. Crop evapotranspiration-guidelines for computing crop water requirements-FAO irrigation and drainage paper 56. FAO, Rome, 300(9): D05109.
- Anderson, J., Chung, F., Anderson, M., Brekke, L., Easton, D., Ejeta, M., Peterson, R., and Snyder, R., 2008. Progress on incorporating climate change into management of California's water resources. Climatic Change, 87(S1): 91–108.
- Azam, S., and Ito, M. 2012. Coupled soil-atmosphere modeling for expansive regina clay. Journal of Environmental Informatics, 19(1): 20–29.
- Azam, S., Shah, I., Raghunandan, M.E., and Ito, M. 2013. Study on swelling properties of an expansive soil deposit in Saskatchewan, Canada. Bulletin of Engineering Geology and the Environment, 72(1): 25–35.
- Bashir, R., Sharma, J., and Stefaniak, H. 2016. Effect of hysteresis of soil-water characteristic curves on infiltration under different climatic conditions. Canadian Geotechnical Journal, 53(2): 273–284.
- Bashir, R. 2014. Personal communication. December 15, 2014.
- Barrow, E.M. 2009. Climate scenarios for Saskatchewan. Prairie Adaptation Research Collaborative (PARC) Report.
- Burman, R. D., Jensen, M. E., and Allen, R. G. 1987. Thermodynamic factors in evapotranspiration, in irrigation systems for the 21st century, in L. G. James and M. J. English (Eds.), Proceedings of a Conference Sponsored by the Irrigation and

Drainage Division of the American Society of Civil Engineers and the Oregon Section, ASCE, Portland, OR, pp. 28–30.

- Carsel, R.F., and Parrish, R.S. 1988. Developing joint probability distributions of soil water retention characteristics. Water Resources Research, 24(5): 755–769.
- California Department of Water Resources. 2018. Access from https://water.ca.gov/ (last accessed July 26, 2018).
- Chai, T., and Draxler, R.R. 2014. Root mean square error (RMSE) or mean absolute error (MAE)–arguments against avoiding RMSE in the literature. Geoscientific Model Development, 7(3): 1247–1250.
- Donahue, R., Barbour, S.C., and Headley, J. 2011. Diffusion and adsorption of benzene in Regina clay. Canadian Geotechnical Journal, 36: 430–442.
- Doorenbos, J. and Pruitt, W.O. (1977) Crop water requirements. FAO Irrigation and Drainage Papers, Rome.
- Ebrahimpour, M., Ghahreman, N., and Orang, M. 2014. Assessment of climate change impacts on reference evapotranspiration and simulation of daily weather data using SIMETAW. Journal of Irrigation and Drainage Engineering, 140(2): 04013012.
- Environment Canada, (2018a). Historical data. goo.gl/MdISJR (last accessed, July 26, 2018)
- Environment Canada, (2018b). Engineering climate datasets. goo.gl/3mRFZ6 (last accessed, July 26, 2018)
- Environment Canada, (2018c). Canadian climate normals 1981-2010 Station Data. goo.gl/KPRBdl (last accessed, July 26, 2018)
- Environment Canada, (2018d). Climate variable glossary. https://tinyurl.com/yaoudr83 (last accessed, July 26, 2018)
- Fasshauer, G., Pelsmajer, M., Nemanich, S., Lamie, E., Boubel, K., Erramilli, S., Matusiewicz, R., Palacios, E., Pnsonneault, K., Tate, J., Vasireddi, A., and Zhou, Y. 2007. Science Fair - Science fair extravaganza. Available from http://sciencefair.math.iit.edu/ (last accessed July 26, 2018).
- Feddes, R. A., Kabat, P., Van Bakel, P.J.T., Bronswijk, J. J. B., and Halbertsma, J. (1988). “Modelling soil water dynamics in the unsaturated zone—state of the art.” Journal of Hydrology, 100(1), 69–111.

- Friske, P.W.B., Ford, K.L., Kettles, I.M., McCurdy, M.W., McNeil, R.J., and Harvey, B.A. 2010. Canadian field protocols for collecting mineral soils and measuring soil gas radon and natural radioactivity. Geological Survey of Canada, Open File 6282
- Forsythe, N., Fowler, H.J., Blenkinsop, S., Burton, A., Kilsby, C.G., Archer, D.R., Harpham, C., and Hashmi, M.Z. 2014. Application of a stochastic weather generator to assess climate change impacts in a semi-arid climate: The Upper Indus Basin. Journal of Hydrology, 517: 1019–1034.
- Fredlund, D.G. 1975, October 27. Engineering properties of expansive clays.
- Fredlund, D.G., and Rahardjo, H. 1993. An overview of unsaturated soil behaviour. Geotechnical special publication,: 1–1.
- Fredlund, D.G. (2002) "Use of the soil-water characteristics curve in the implementation of unsaturated soil mechanics", UNSAT 2002, Proceeding, Third international Conference on Unsaturated Soils, Recife, Brazil, March 10-13, 3: pp.
- Fredlund, M.D., Zhang, J.M., Tran, D., and Fredlund, D.G. 2011. Coupling heat and moisture flow for the computation of actual evaporation. In Proceedings of the Canadian Geotechnical Conference and Fifth Pan-American Conference, Toronto, Ont. pp. 2–6. Access from https://tinyurl.com/y9c2mctt (last accessed July 26, 2018).
- Fredlund, D.G., Rahardjo, H., and Fredlund, M.D. 2012. Unsaturated soil mechanics in engineering practice. John Wiley & Sons. Access from https://tinyurl.com/ycbg9r26 (last accessed July 26, 2018).
- Fredlund, D.G., and Houston, S.L. 2013. Interpretation of soil-water characteristic curves when volume change occurs as soil suction is changed. Advances in unsaturated soils. CRC Press, Boca Raton, FL,: 15–31.
- Fredlund M.D., Tran D, Fredlund D.G. 2016. Methodologies for the calculation of actual evaporation in geotechnical engineering. International journal of geomechanics, vol. 16, issue 6.
- Garcia-Gaines, R.A., and Frankenstein, S. 2015. USCS and the USDA soil classification system: development of a mapping scheme. Engineer Research and Development Center Hanover NH cold Regions Research and Engineering Lab, ERCD/CRREL TR-15-4.

- Gabriel, K. R., and Neumann, J. (1962). “A Markov chain model for daily rainfall occurrence at Tel Aviv.” Quarterly Journal of the Royal Meteorological Society, 88(375), 90–95.
- Gardner, W. R. (1972). “The impact of La Richards upon the field soil water physics.” Soil Science, 113(4), 232–237.
- GEO-SLOPE International Ltd., 2012. Manual for VADOSE/W. Access from https://www.geoslope.com/ (last accessed July 26, 2018).
- Ghahreman, N., Ebrahimpour, M., and Orang, M. 2012. Application of SIMETAW model for generating daily weather data and reference evapotranspiration (ETo) in two different climates in Iran. Proc. Irrigation Australia/7th Asian Regional Con. ICID, Adelaide,: 24–29.
- Ghandour, A. 2016. Modeling evapotranspiration of applied water in the Egypt delta and Sacramento San Joaquin River delta, California, USA. International Journal of Engineering Research & Technology (IJERT), 5(10): 85–89.
- Harrison, L. P. 1965. Fundamental concepts and definitions relating to humidity, in A. Wexler and W. A. Wildhack (Eds.), humidity and moisture, fundamentals and standards, Reinhold Publishing Company, New York, Vol. 3, pp. 3–69.
- Hong, N.-M., Lee, T.-Y., and Chen, Y.-J. 2016. Daily weather generator with drought properties by copulas and standardized precipitation indices. Environmental monitoring and assessment, 188(6): 1–14.
- Howes, D.J., Fox, P., and Hutton, P.H. 2015. Evapotranspiration from natural vegetation in the central valley of California: monthly grass reference-based vegetation coefficients and the dual crop coefficient approach. Journal of Hydrologic Engineering, 20(10): 04015004.
- Huang, J., Ridoutt, B.G., Xu, C., Zhang, H., and Fu, C. 2012. Cropping pattern modifications change water resource demands in the Beijing metropolitan area. Journal of Integrative Agriculture, 11(11): 1914–1923.
- Huang, J., Xu, C., Ridoutt, B., and Chen, F. 2015. Reducing agricultural water footprints at the farm scale: A case study in the Beijing region. Water, 7(12): 7066–7077.

- INAP. 2009. Main Page - GARD guide. Access from https://tinyurl.com/y7ws99ak (last accessed July 26, 2018).
- Irmak, S., Irmak, A., Jones, J.W., Howell, T.A., Jacobs, J.M., Allen, R.G., and Hoogenboom, G. 2003. Predicting daily net radiation using minimum climatological data. Journal of Irrigation and Drainage Engineering, 129(4): 256–269.
- Ito, M., and Azam, S. 2010. Determination of swelling and shrinkage properties of undisturbed expansive soils. Geotechnical and Geological Engineering, 28(4): 413–422.
- Ito, M., and Hu, Y. 2011. Prediction of the behaviour of expansive soils. In Proceedings, 64th Canadian Geotechnical Conference and 14th Pan-American Conference on Soil Mechanics and Geotechnical Engineering. pp. 2–6. Access from https://tinyurl.com/y8p53vay (last accessed July 26, 2018).
- Jones, P. G., and Thornton, P. K. (1997). “Spatial and temporal variability of rainfall related to a third-order Markov model.” Agricultural and Forest Meteorology, 86(1), 127–138.
- Katz, R. W. (1977). “Precipitation as a chain-dependent process.” Journal of Applied Meteorology, 16(7), 671–676.
- Kim, C. P., Stricker, J. N. M., and Torfs, P. (1996). “An analytical framework for the water budget of the unsaturated zone.” Water Resources Research, 32(12), 3475–3484.
- Keller, D.E. 2015. A weather generator for current and future climate conditions. Access from https://tinyurl.com/yckwjxck(last accessed July 26, 2018).
- Khalili, M., Brissette, F., and Leconte, R. 2011. Effectiveness of multi-site weather generator for hydrological modeling. JAWRA Journal of the American Water Resources Association, 47(2): 303–314.
- Kodikara, J., Rajeev, P., Chan, D., and Gallage, C. 2013. Soil moisture monitoring at the field scale using neutron probe. Canadian Geotechnical Journal, 51(3): 332–345.
- Longley, R. W. (1953). “The length of dry and wet periods.” Quarterly Journal of the Royal Meteorological Society, 79(342), 520–527.
- Mancous, N., Mereu, S., Snyder, R.L., and Spano, D. 2013. Agricultural water use towards a sustainable irrigation. Milano.

- Maulem, Y., 1976. A new model for prediction of the hydraulic conductivity of unsaturated porous media. Water Resources Research 12(3), 513-522
- McKague, K., Rudra, R., Ogilvie, J., Ahmed, I., and Gharabaghi, B. 2005. Evaluation of weather generator ClimGen for southern Ontario. Canadian Water Resources Journal, 30(4): 315–330.
- Metcalfe, J.R., Routledge, B., and Devine, K. 1997. Rainfall measurement in Canada: changing observational methodsand archive adjustment procedures. Journal of Climate, 10(1): 92–101.
- Mitchell, J.K., and Soga, K. 2005. Fundamentals of soil behavior. Wiley, Hoboken, N.J.
- Millington, R.J., and Quirk, J.P. 1961. Permeability of porous solids. Transactions of the Faraday Society, 57: 1200–1207.
- Miller, G. R., Baldocchi, D. D., Law, B. E., and Meyers, T. (2007). “An analysis of soil moisture dynamics using multi-year data from a network of micrometeorological.” Info: Postprints, Multi-Campus.
- Milly, P. C. D. (1996). “Effects of thermal vapor diffusion on seasonal dynamics of water in the unsaturated zone.” Water Resources Research, 32(3), 509–518.
- Mualem, Y. 1976. A new model for predicting the hydraulic conductivity of unsaturated porous media. Water resources research, 12(3): 513–522.
- NASA. 2018. NASA Surface meteorology and Solar Energy: RET Screen Data. Access from https://tinyurl.com/ya656pxv (last accessed July 26, 2018).
- Neuman, S., Feddes, R.., and Bresler, E. 1974. Finite element simulation of flow in saturated-unsaturated soils considering water uptake by plants. Third Annual Report, Project No. A10-SWC-77. Hydraulic Engineering Lab., Technion, Haifa, Israel.
- Nielsen, D. R., Biggar, J. W., and van Genuchten, M.T. (1986). “Water flow and solute transport processes in the unsaturated zone.” Water Resources Research, 22(9S).
- O’Kane, M.A., Ayres, B., Christensen, D., and Meiers, G. 2002. CANMETCETEM Manual on cover system design for reactive mine waste. Report 689, 1. Access from https://tinyurl.com/yd6ooxtj (last accessed July 26, 2018).
- Orang, M.N., and Snyder, R.L. 2004. SIMETAW - A tool for water demand planning.

- Orang, M.N., Snyder, R.L., Shu, G., Hart, Q.J., Sarreshteh, S., Falk, M., Beaudette, D., Hayes, S., and Eching, S. 2013. California simulation of evapotranspiration of applied water and agricultural energy use in California. Journal of Integrative Agriculture, 12(8): 1371–1388.
- Pandey, C.K., and Katiyar, A.K. 2013. Solar radiation: models and measurement techniques. Journal of Energy, 2013: e305207.
- Patil, N.G., and Singh, S.K. 2016. Pedotransfer functions for estimating soil hydraulic properties: A Review. Pedosphere, 26(4): 417–430.
- Penman, H.L. 1948. Natural evaporation from open water, bare soil and grass. In Proceedings of the Royal Society of London A: Mathematical, Physical and Engineering Sciences. The Royal Society. pp. 120–145. Access from https://tinyurl.com/yamf7mat (last accessed July 26, 2018).
- Pham, H. Q., Fredlund, D. G., and Barbour, S. L. (2005). “A study of hysteresis models for soil-water characteristic curves.” Canadian Geotechnical Journal, 42(6), 1548–1568.
- Racsko, P., Szeidl, L., and Semenov, M. (1991). “A serial approach to local stochastic weather models.” Ecological modelling, 57(1–2), 27–41.
- Richard L., S., Morteza N., O., Shu, G., and J. Scott, M. 2004. Land and water use data collections CA. Access from https://tinyurl.com/y82w428r (last accessed 12 November 2016).
- Richards, L.A. 1931. Capillary conduction of liquids through porous mediums. Journal of Applied Physics, 1(5): 318–333.
- Richardson, C.W., and Wright, D.A. 1984. WGEN: A model for generating daily weather variables. Access from https://tinyurl.com/y9nustws (accessed 13 April 2017).
- Rykaart, M., Hockley, D., Noel, M., and Paul, M. 2006. Findings of international review of soil cover design and construction practices for mine waste closure. Journal American Society of Mining and Reclamation, 2006(2): 1804–1822.
- Saxton, K.E., and Rawls, W.J. 2006. Soil water characteristic estimates by texture and organic matter for hydrologic solutions. Soil Science Society of America Journal, 70(5): 1569.

- Schwartz, F.W., Cherry, J.A. and Roberts, J.R. 1982. A case study of a chemical spill: polychlorinated biphenyls (PCBs), 2, Hydrogeological conditions and contaminant migration. Water Resources Research,18(3): 535-545.
- Schneider, T. 2001. Analysis of incomplete climate data: Estimation of mean values and covariance matrices and imputation of missing values. Journal of Climate, 14(5): 853–871.
- Schunn, C.D., and Wallach, D. 2005. Evaluating goodness-of-fit in comparison of models to data. P Tack,: 115–154.
- Sedighi, M., Thomas, H.R., and Vardon, P.J. 2016. Reactive transport of chemicals in unsaturated soils, numerical model development and verification. In Canadian Geotechnical Journal. Vol.53, No.1.pp.162-172.
- Shah, H. 2014. Assessing the feasibility of wastewater reuse for a carbon sequestration forest in Davis, CA. Department of civil engineering, California State University, Sacramento. Access from https://tinyurl.com/y8mskser (last accessed July 26, 2018).
- Shah, N., Nachabe, M. Ross, M. 2007. Extinction depth and evapotranspiration from groundwater under selected land covers. Ground water, Vol. 45, No 3 (pages 329-338)
- Schwille, F. (1984). “Migration of organic fluids immiscible with water in the unsaturated zone.” Pollutants in porous media, Springer, 27–48.
- Shuai, F. 1996. Simulation of swelling pressure measurements on expansive soils. Department of civil engineering, University of Saskatchewan. Access from https://tinyurl.com/y9pfnlj3 (last accessed July 26, 2018).
- Simunek, J., Sejna, M., and van Genuchten, M.T. 1998. Hydrus-1D. Simulating the one-dimensional movement of water, heat, and multiple solutes in variably-saturated media, version, 2. Access from https://tinyurl.com/ybzw92ml (last accessed July 26, 2018).
- Šimunek, J. and van Genuchten, M. 2006. The handbook of groundwater engineering. Chapter 22: Contaminant transport in the unsaturated zone theory and modeling. Second Edition.CRC Press. Florida

- Singh, D., Misra, R. K., and Singh, D. (2007). “Effect of load models in distributed generation planning.” IEEE Transactions on Power Systems, 22(4), 2204–2212.
- Snyder, R.L., Geng, S., Orang, M., and Sarreshteh, S. 2012. Calculation and simulation of evapotranspiration of applied water. Journal of Integrative Agriculture, 11(3): 489–501.
- Sposito, G., and Jury, W. A. (1985). “Inspectional analysis in the theory of water flow through unsaturated soil.” Soil Science Society of America Journal, 49(4), 791–798.
- Stern, R. D., and Coe, R. (1984). “A model fitting analysis of daily rainfall data.” Journal of the Royal Statistical Society. Series A (General), 1–34.
- Swelam, A. 2012. Modeling Evapotranspiration in Nile Delta: Calibrate and validate (SIMETAW model) under Egypt’s conditions. Access from http://www.idosi.org/aerj/2(1)12/2.pdf (last accessed July 26, 2018).
- Tetens, V.O. 1930. Ubereinige meteorologische. Begriffe, Zeitschrift fur Geophysik. 6:297-309.
- The Mathworks. 2009. MATLAB. curve fitting toolbox documentation. Access from https://tinyurl.com/y74m8daj (last accessed July 26, 2018).
- Thom, A.S., and Oliver, H.R. 1977. On Penman’s equation for estimating regional evaporation. Quarterly Journal of the Royal Meteorological Society, 103(436): 345–357.
- Thom, H. C. (1958). “A note on the gamma distribution.” Monthly Weather Review, 86(4), 117–122.
- Thornthwaite, C.W. 1948. An approach toward a rational classification of climate. Geographical review, 38(1): 55–94.
- Thornthwaite, C.W. and Hare, F.K. 1955. Climatic classification in forestry. Unasylva 9(2):51-59.
- Tran D, Fredlund D.G., and Chan D.H. 2016. Improvement to the calculation of actual evaporation from bare soil surfaces. Canadian Geotechnical Journal. 53(1):118–133.
- Tingem, M., Rivington, M., Azam-Ali, S., and Colls, J. 2007. Assessment of the ClimGen stochastic weather generator at Cameroon sites. African Journal of Environmental Science and Technology, 1(4): 86–92.

- Todorovic, P., and Woolhiser, D. A. (1975). “A stochastic model of n-day precipitation.” Journal of Applied Meteorology, 14(1), 17–24.
- Tran, D.T.Q. 2013. Re-Visitation of actual evaporation theories. Ph.D. thesis, University of Alberta, Edmonton. Access from https://tinyurl.com/y7bevft8 (last accessed July 26, 2018).
- van Genuchten, M.T. 1980. A closed-form equation for predicting the hydraulic conductivity of unsaturated soils. Soil science society of America journal, 44(5): 892–898.
- van Genuchten, M.T., Leij, F.J., and Yates, S.R. 1991. The RETC code for quantifying the hydraulic functions of unsaturated soils, version 1.0. EPA report 600/2-91/1065, U.S. Salinity Laboratory, USADA, ARS, Riverside, California. Access from https://tinyurl.com/ycnu7z5k (last accessed July 26, 2018).
- Vanapalli, S., and Adem, H. 2014. Soil-environment interactions modelling for expansive soils. Article in Journal of environmental geotechnics, ICE publishing, 13.00089
- Vardon, P.J. 2015. Climatic influence on geotechnical infrastructure: a review. Environmental Geotechnics, 2(3): 166–174.
- Vu, H.Q. 2002. Uncoupled and coupled solutions of volume change problems in expansive soils. Ph.D thesis, Department of civil engineering, University of Saskatchewan. Access from https://tinyurl.com/y7sx8y34 [last accessed July 26, 2018].
- Vu, H.Q., Hu, Y., and Fredlund, D.G. 2007. Analysis of soil suction changes in expansive Regina clay. Canadian geotechnical conference, p.p 1-8. Access from https://tinyurl.com/yay45l9y (last accessed July 26, 2018).
- Walter, I.A., Allen, R.G., Elliott, R., Jensen, M.E., Itenfisu, D., Mecham, B., Howell, T.A., Snyder, R., Brown, P., Echings, S., Spofford, T., Hattendorf, M., Cuenca, R.H., Wright, J.L., and Martin, D. 2001. ASCE’s standardized reference evapotranspiration equation. American Society of Civil Engineers. pp. 1–11.
- Wilks, D.S., and Wilby, R.L. 1999. The weather generation game: a review of stochastic weather models. Progress in Physical Geography, 23(3): 329–357.

- Wilks, D. S. (1998). “Multisite generalization of a daily stochastic precipitation generation model.” Journal of Hydrology, 210(1), 178–191.
- Willmott, C.J., and Matsuura, K. 2005. Advantages of the mean absolute error (MAE) over the root mean square error (RMSE) in assessing average model performance. Climate research, 30(1): 79–82.
- Williams, C. B. (1952). “Sequences of wet and of dry days considered in relation to the logarithmic series.” Quarterly Journal of the Royal Meteorological Society, 78(335), 91–96.
- Wilson, G.W. 1990. Soil evaporative fluxes for geotechnical engineering problems. Ph.D thesis, Department of Civil engineering, University of Saskatchewan. Access from https://tinyurl.com/y8hmru74 (last accessed July 26, 2018).
- Wilson, G.W., Fredlund, D.G., and Barbour, S.L. 1994. Coupled soil-atmosphere modelling for soil evaporation. Canadian Geotechnical Journal, 31(2): 151–161.
- Yang, X., Gao, W., Shi, Q., Chen, F., and Chu, Q. 2013. Impact of climate change on the water requirement of summer maize in the Huang-Huai-Hai farming region. Agricultural Water Management, 124: 20–27.
- Yanful, E.K., and Simms, P. 1997. Review of water cover sites and research projects.Geotechnical research center, department of civil and environmental engineering. The University of Western Ontario, London, Ontario. Access from https://tinyurl.com/yao9fgct [accessed 27 July 2018].
- Yin, X.G., Olesen, J.E., Wang, M., öztürk, I., and Chen, F. 2016. Climate effects on crop yields in the Northeast Farming Region of China during 1961–2010. The Journal of Agricultural Science, 154(07): 1190–1208.

APPENDICES

Appendix A.1 – Compiled climate data – Toronto

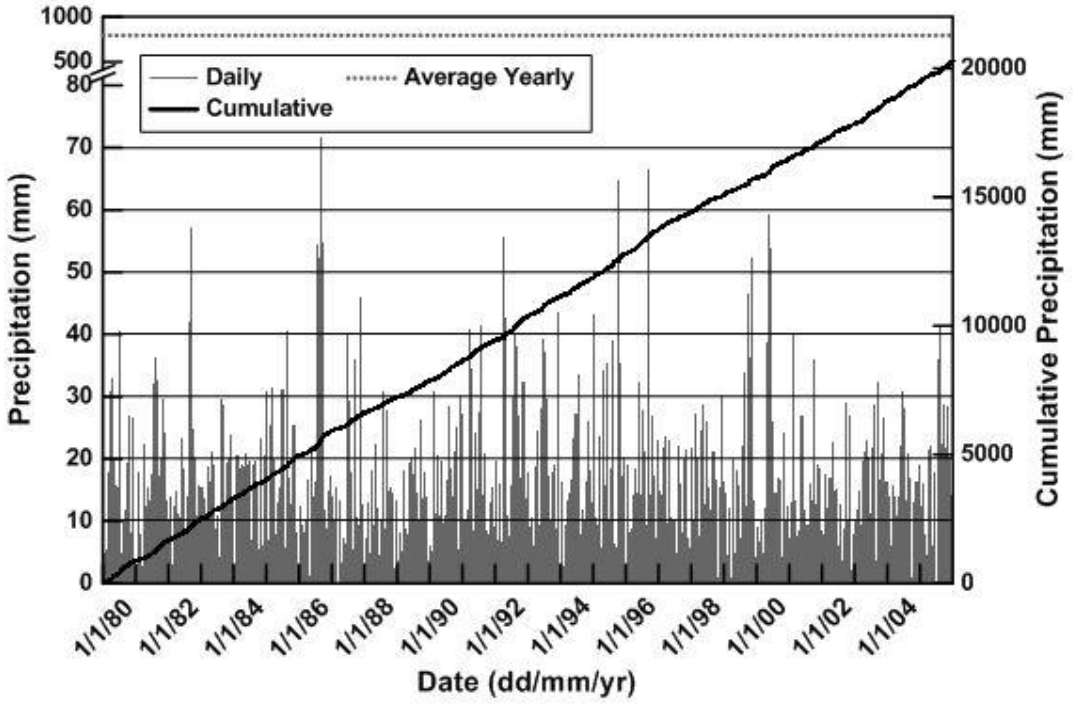

Figure. A.1.1: Precipitation data for the city of Toronto (1980-2005)

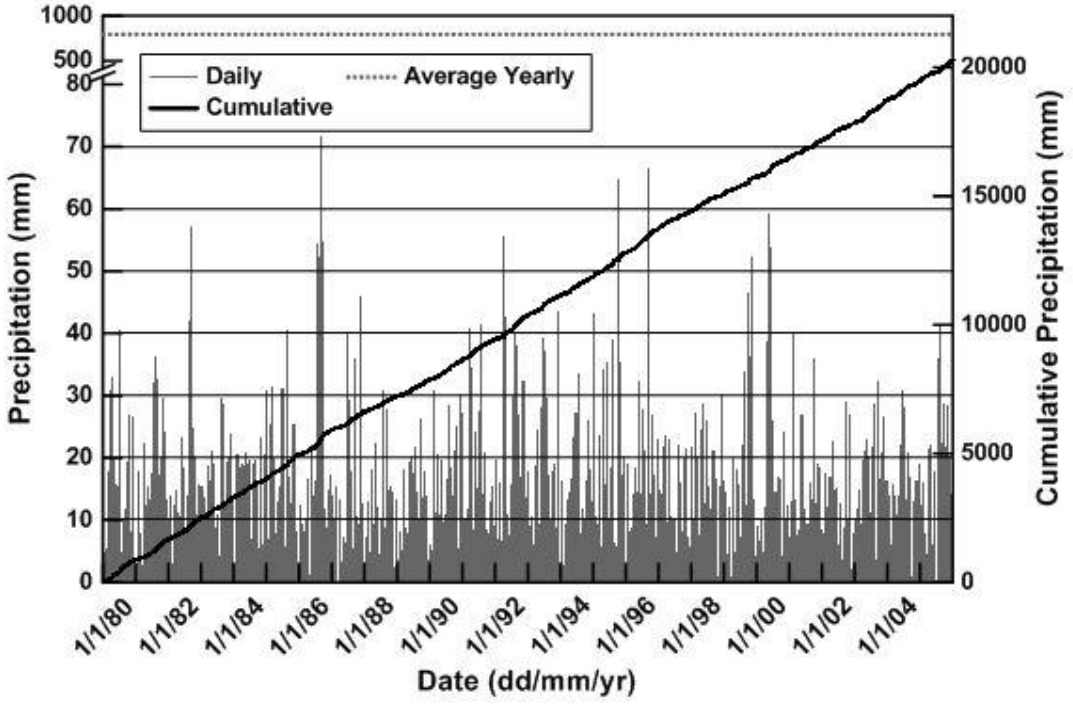

Figure. A.1.2: Temperature data for the city of Toronto (1980-2005)

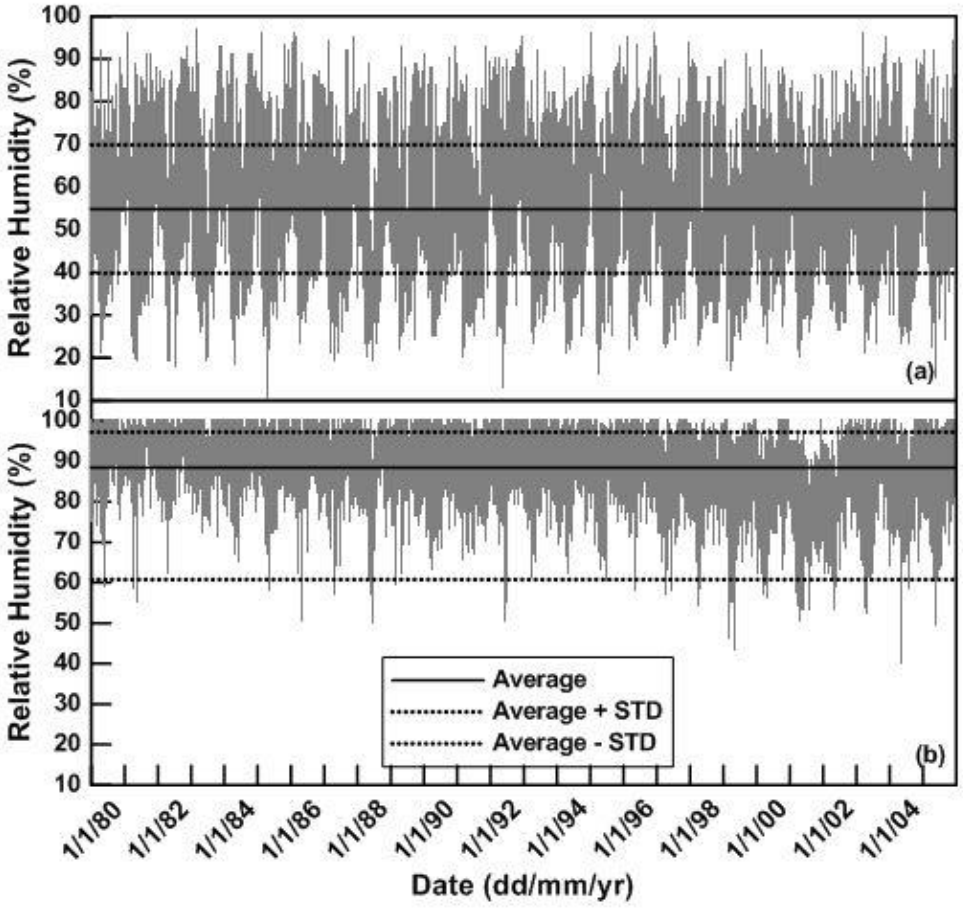

Figure. A.1.3: Relative humidity data for Toronto. (a) minimum (b) maximum

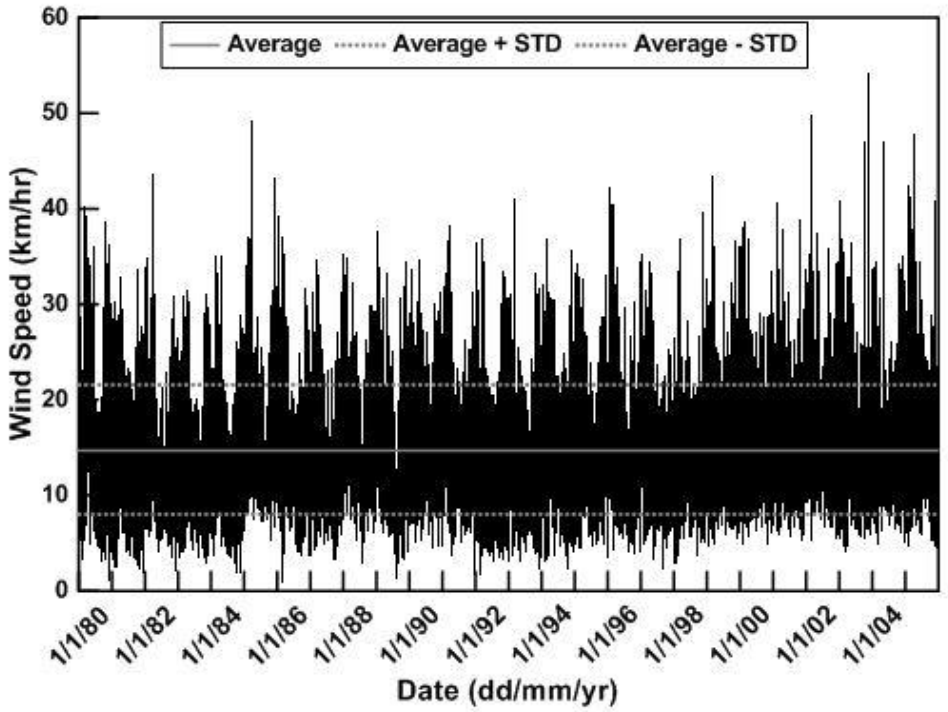

Figure. A.1.4: Average daily wind speed data city of Toronto (1980-2005)

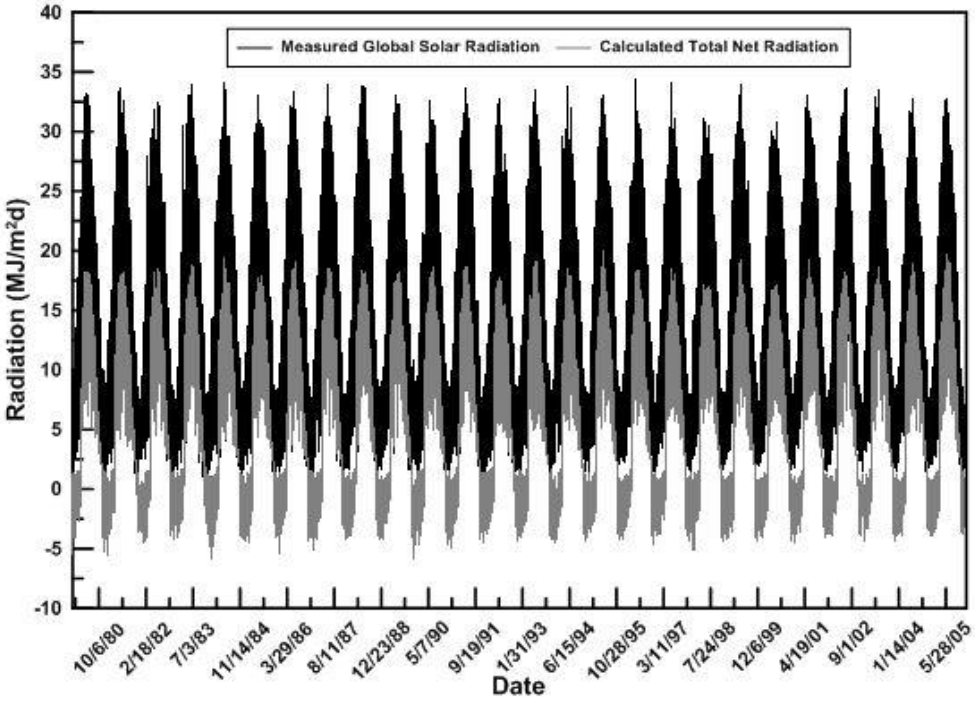

Figure. A.1.5: Average daily solar and net radiation data Toronto (1980-2005)

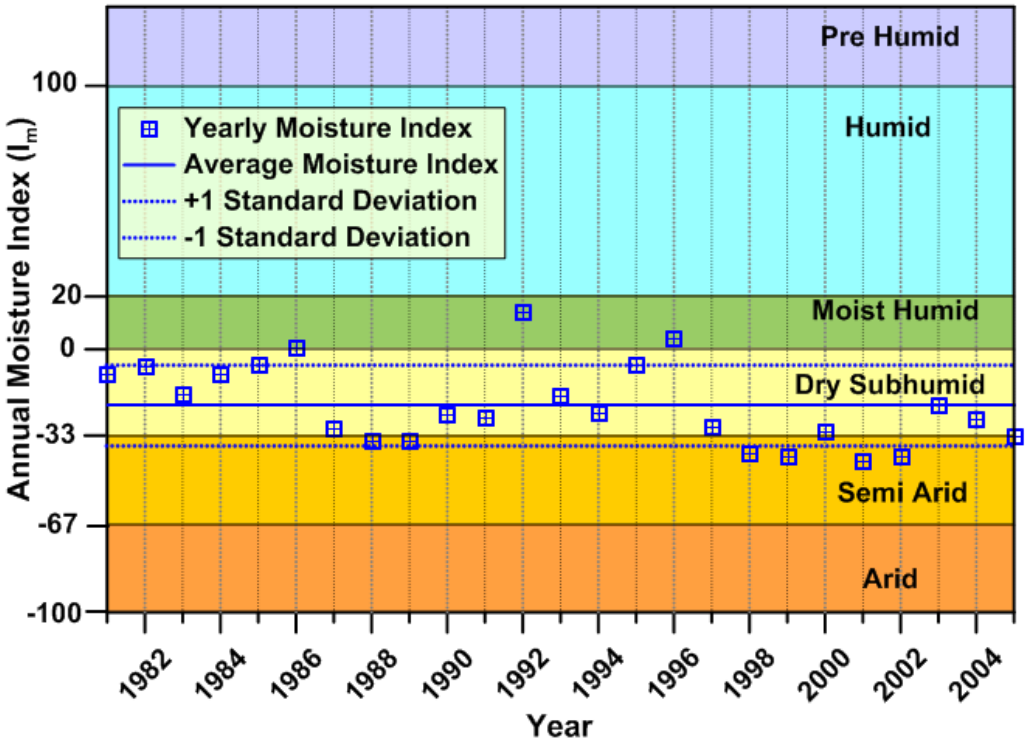

Figure. A.1.6: Climate classification city of Toronto

Appendix A.2 – Compiled climate data - Timmins

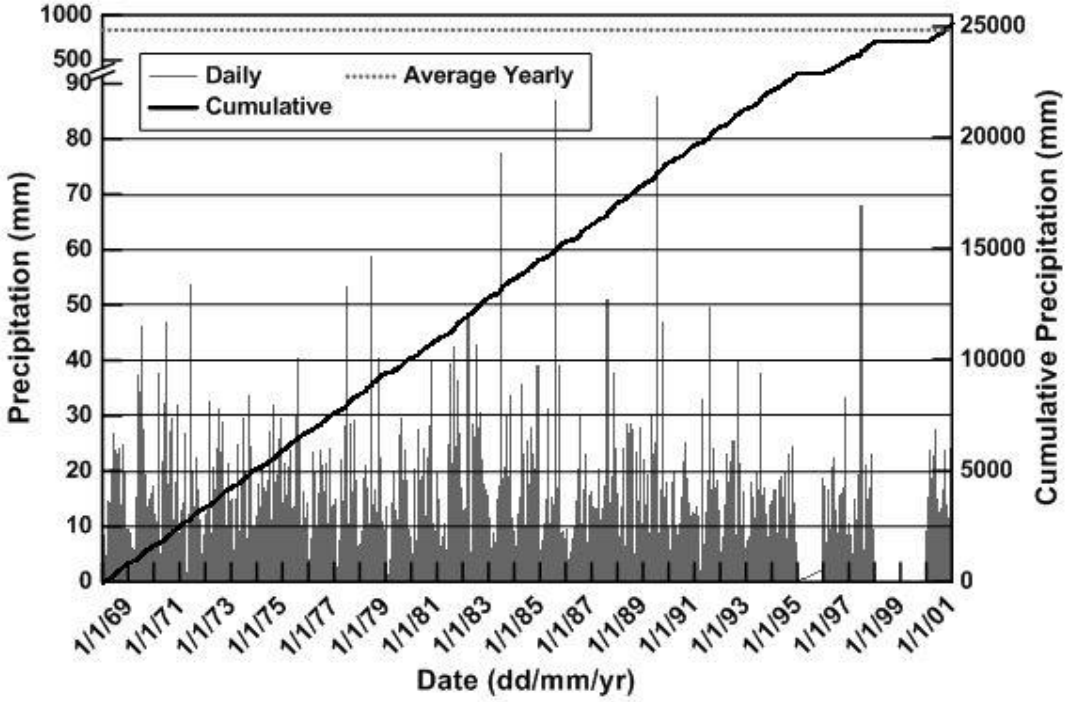

Figure. A.2.1: Precipitation data for the city of Timmins (1969-2001)

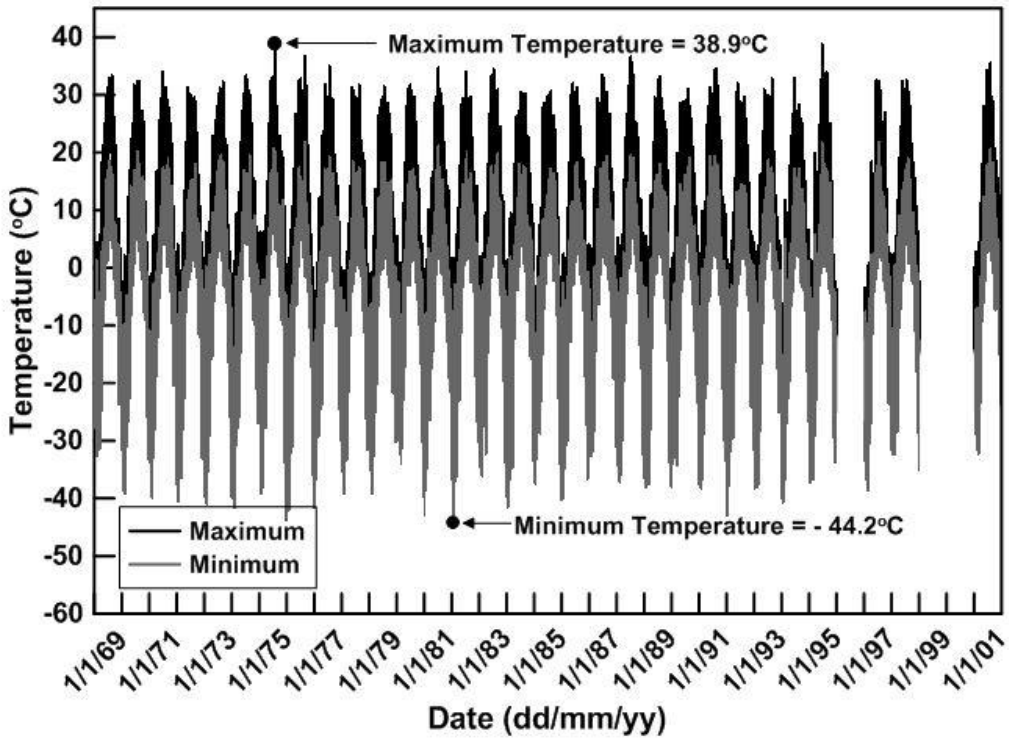

Figure. A.2.2: Temperature data for the city of Timmins (1969-2001)

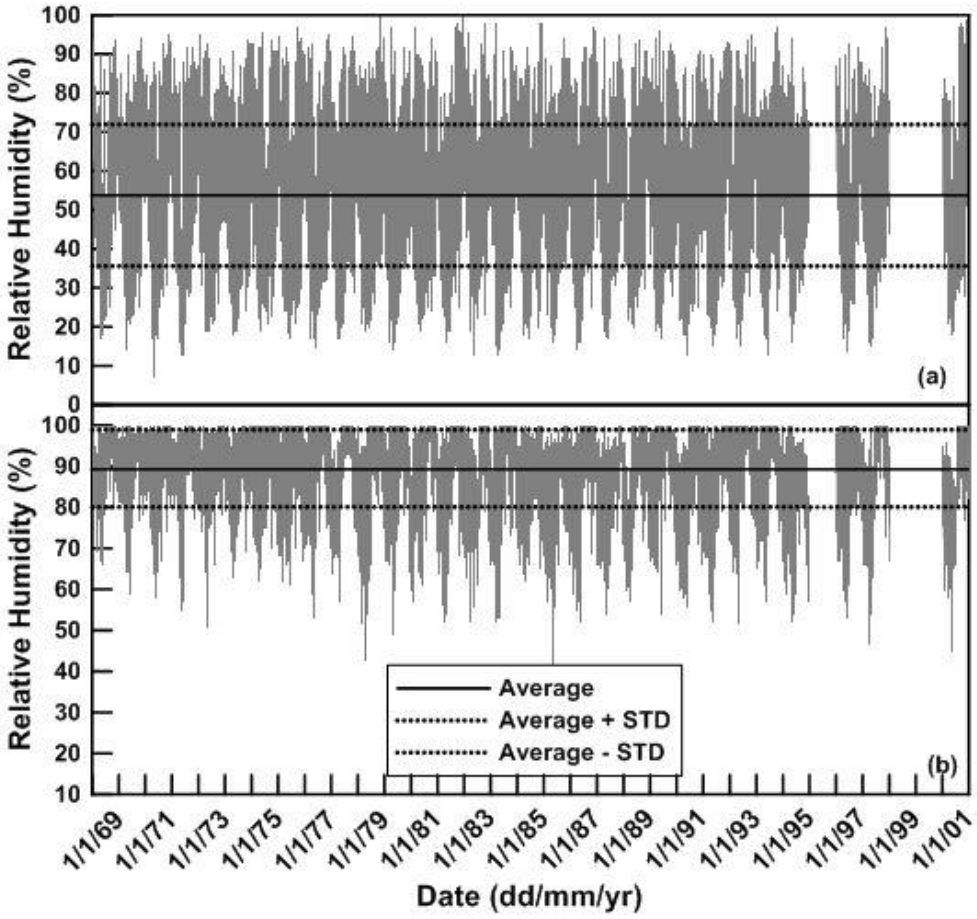

Figure. A.2.3: Relative humidity data for Timmins. (a) minimum (b) maximum

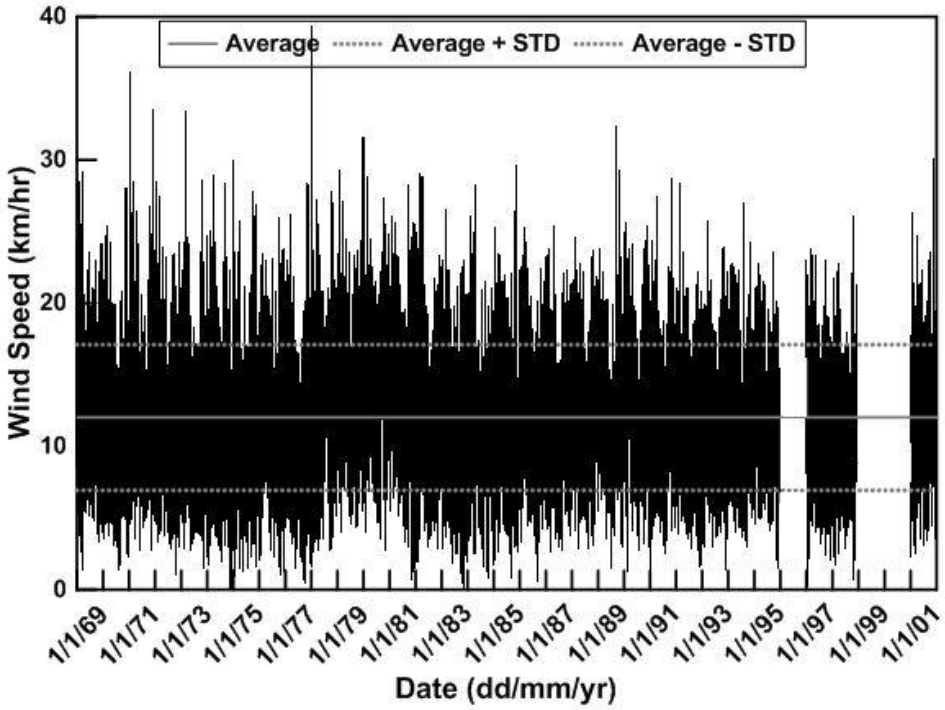

Figure. A.2.4: Average daily wind speed data city of Timmins (1969-2001)

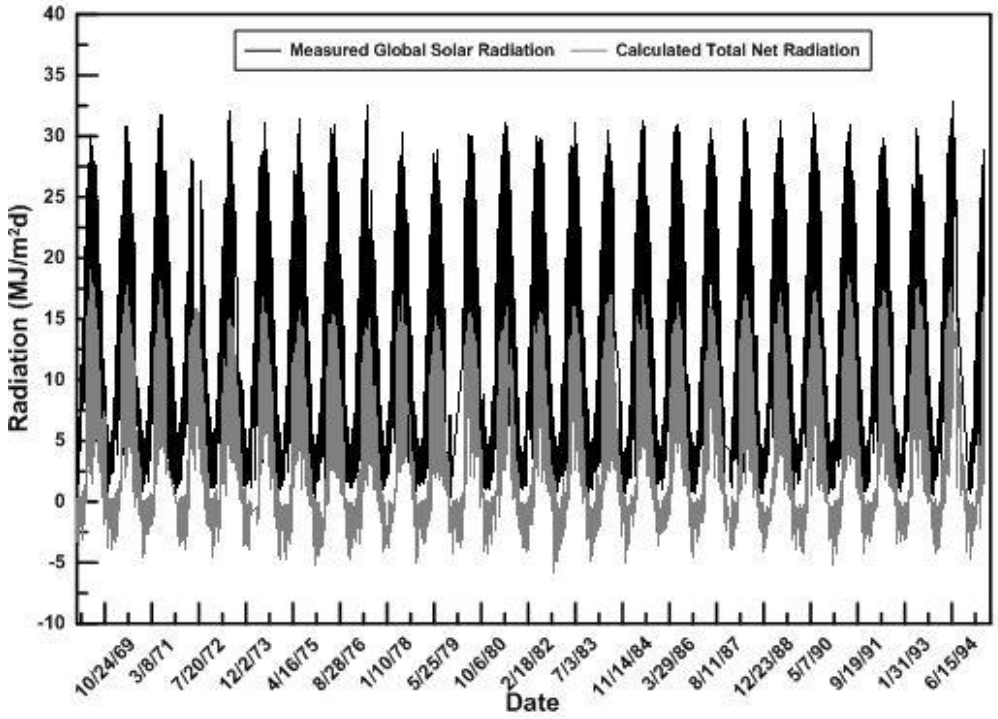

Figure. A.2.5: Average daily solar and net radiation data Timmins (1969-2001)

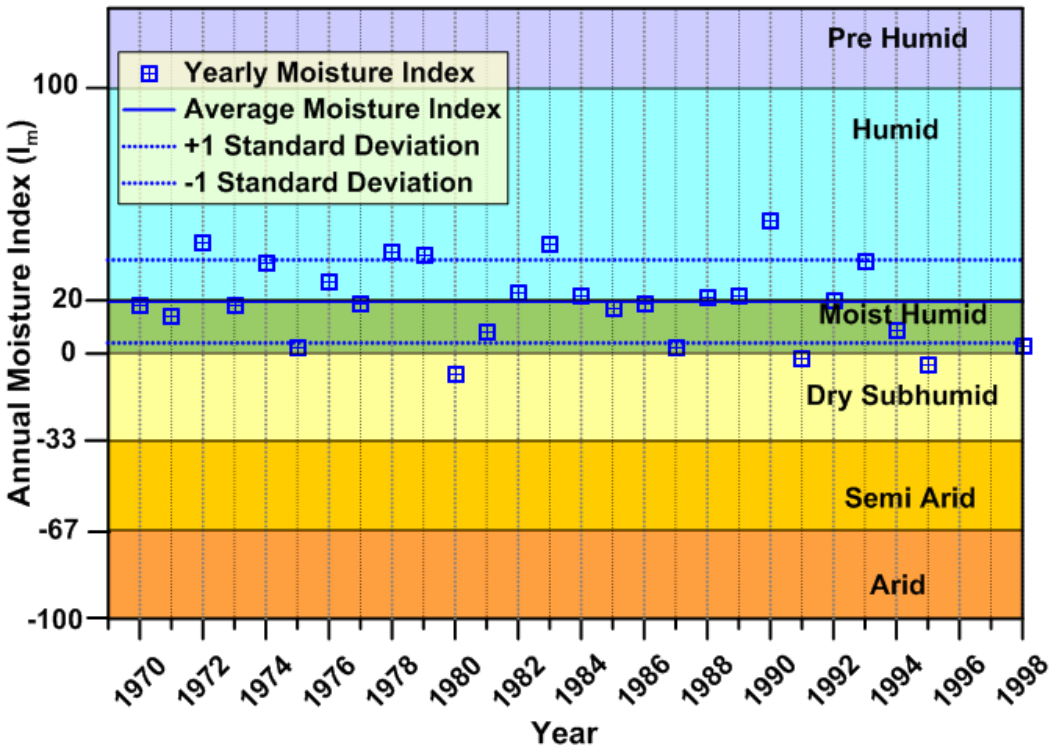

Figure. A.2.6: Climate classification city of Timmins

Appendix A.3 - Compiled climate data – Whitecourt

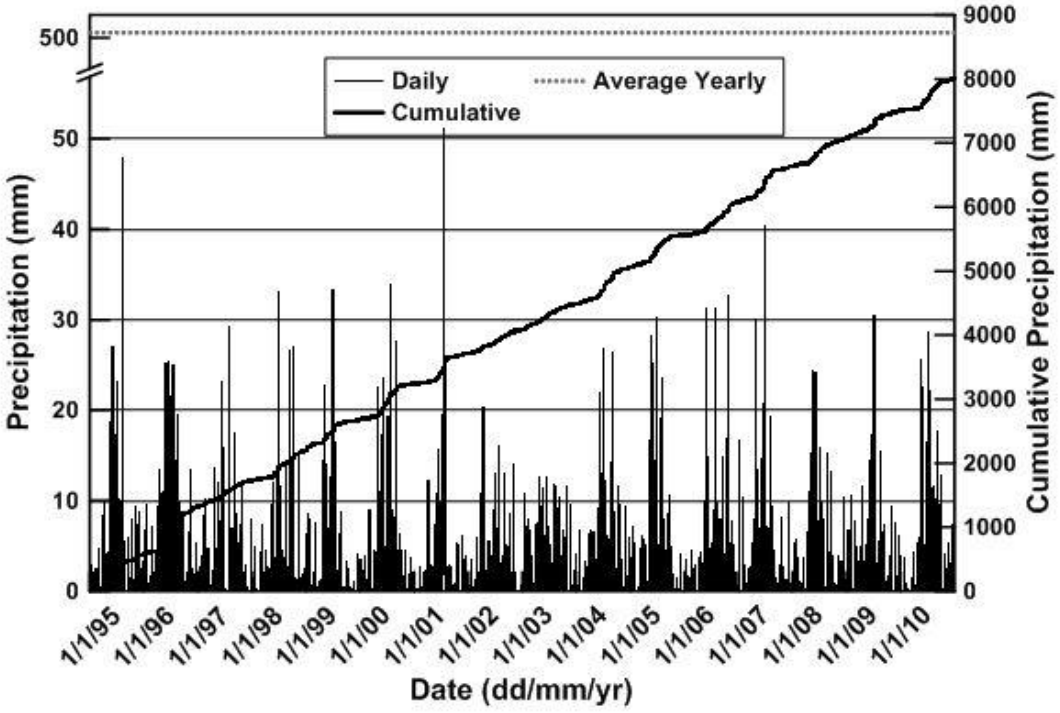

Figure. A.3.1: Precipitation data for the city of Whitecourt (1995-2010)

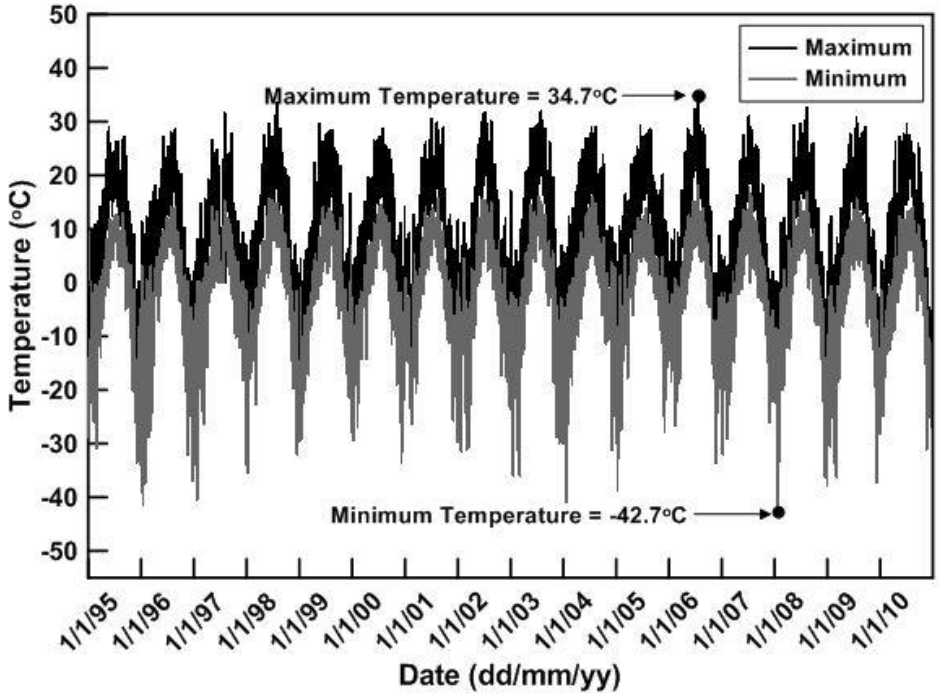

Figure. A.3.2: Temperature data for the city of Whitecourt (1995-2010)

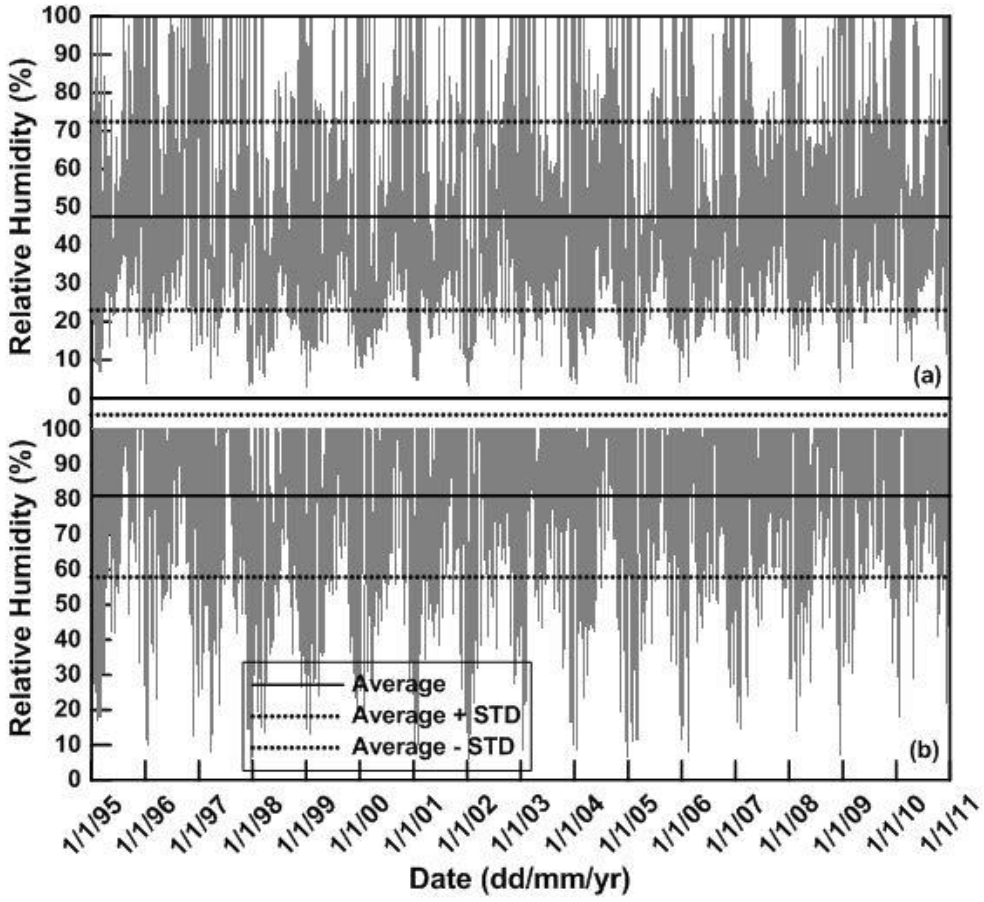

Figure. A.3.3: Relative humidity data for Whitecourt. (a) minimum (b) maximum

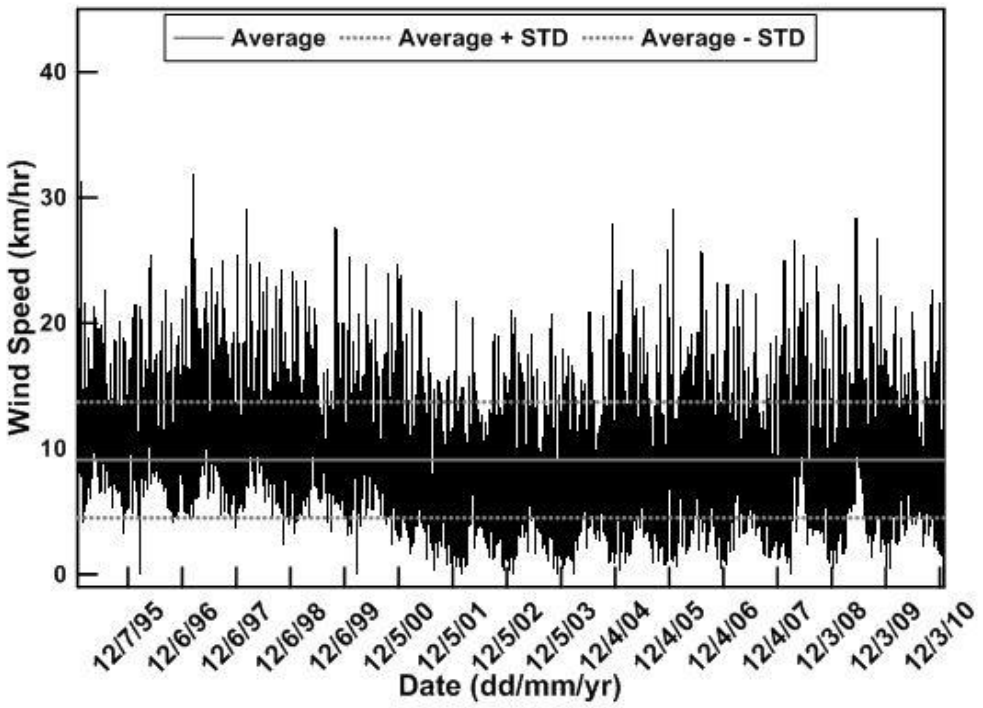

Figure. A.3.4: Average daily wind speed data city of Whitecourt (1995-2010)

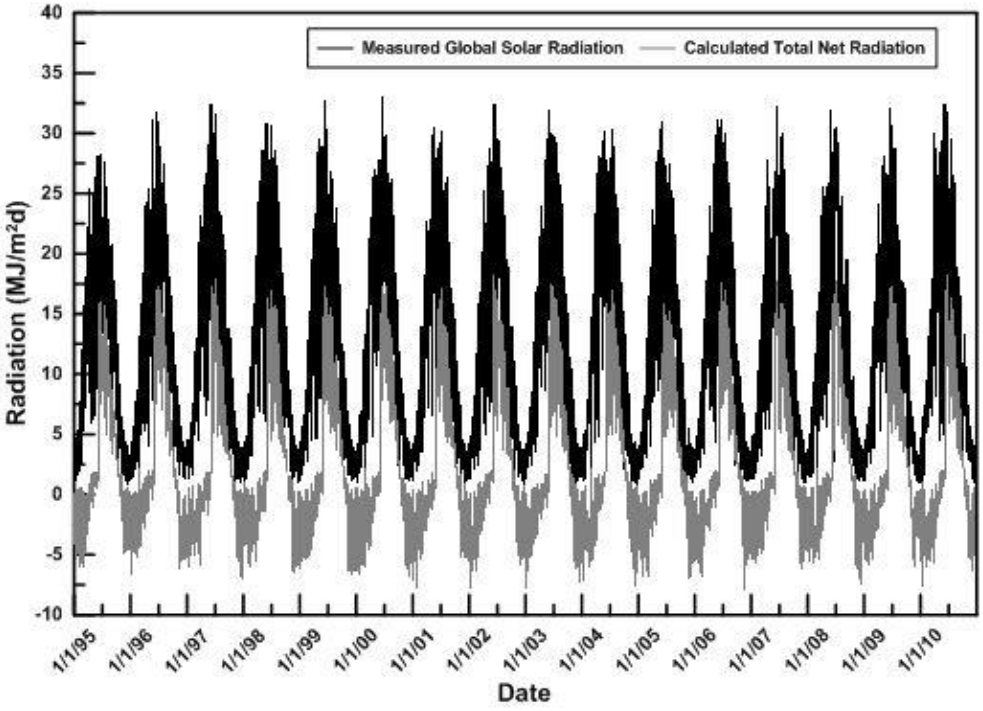

Figure. A.3.5: Average daily solar and net radiation data Whitecourt (1995-2010)

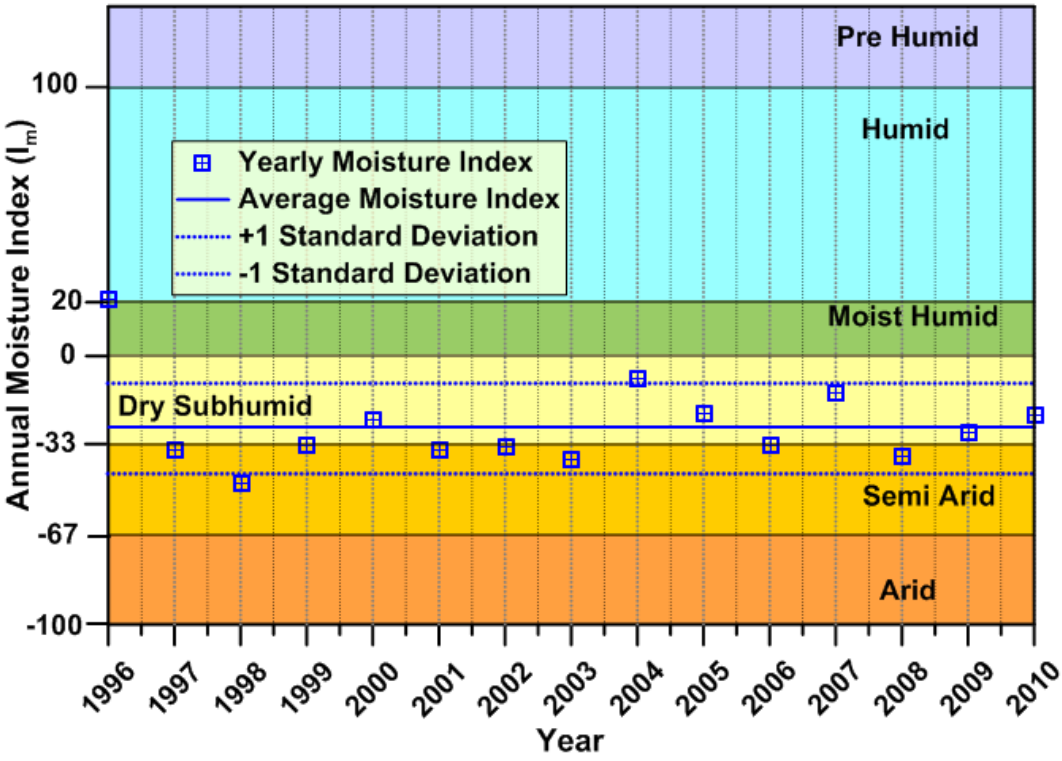

Figure. A.3.6: Climate classification city of Whitecourt

Appendix A.4 - Compiled climate data – Regina

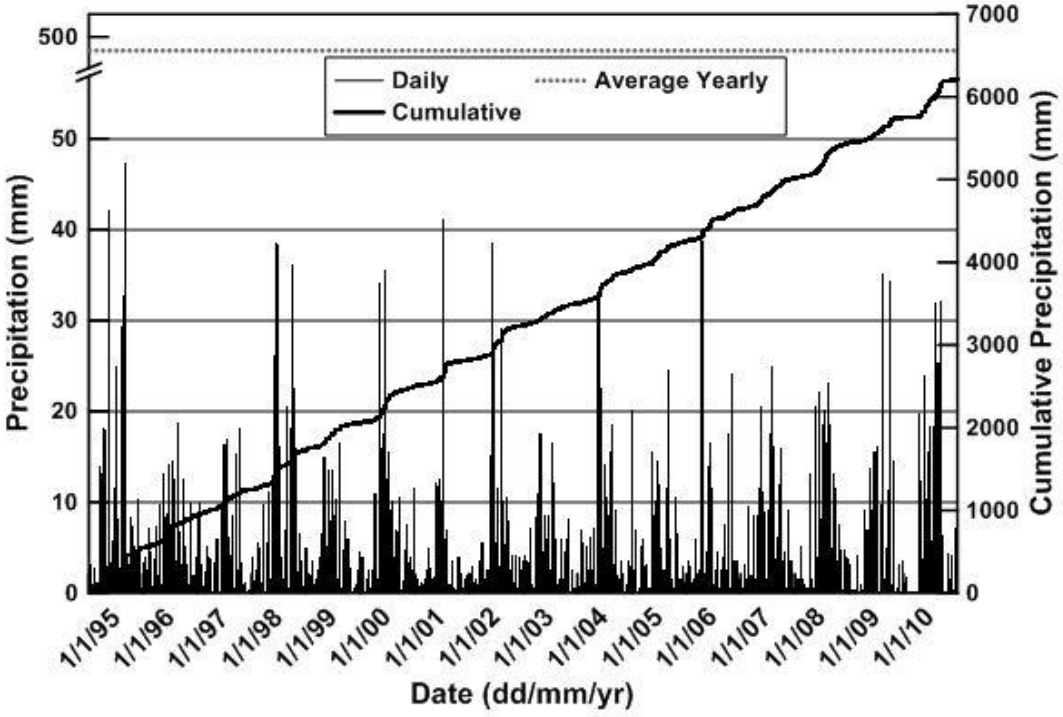

Figure. A.4.1: Precipitation data for the city of Regina (1995-2010)

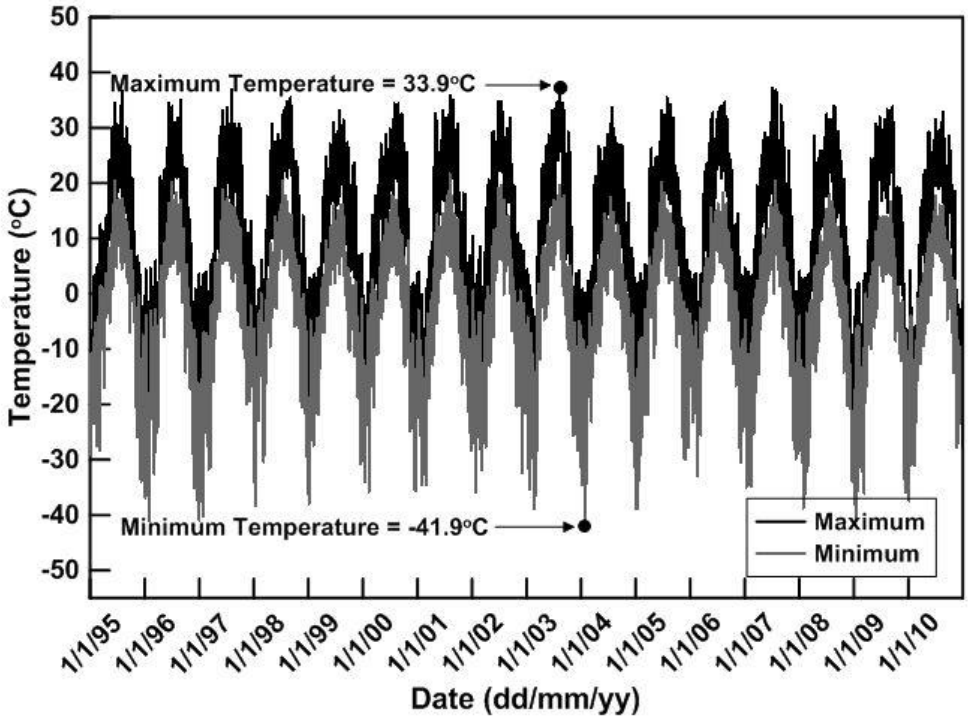

Figure. A.4.2: Temperature data for the city of Regina (1995-2010)

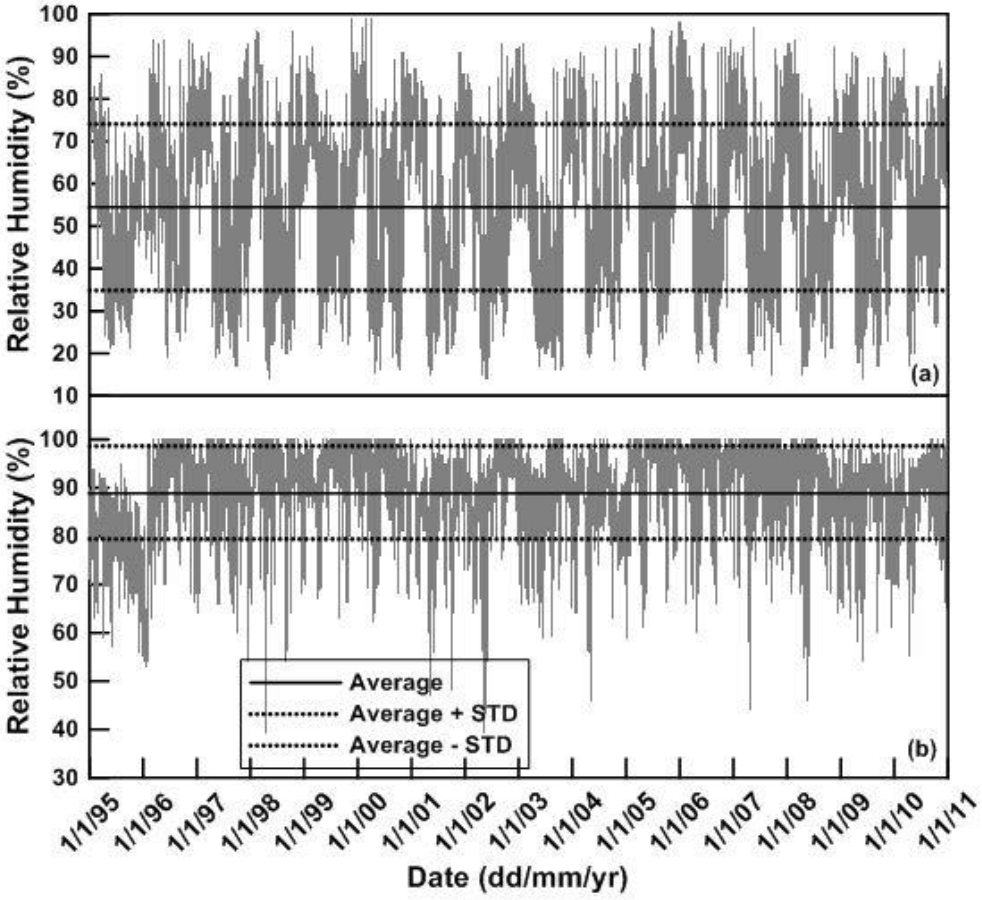

Figure. A.4.3: Relative humidity data for Regina. (a) minimum (b) maximum

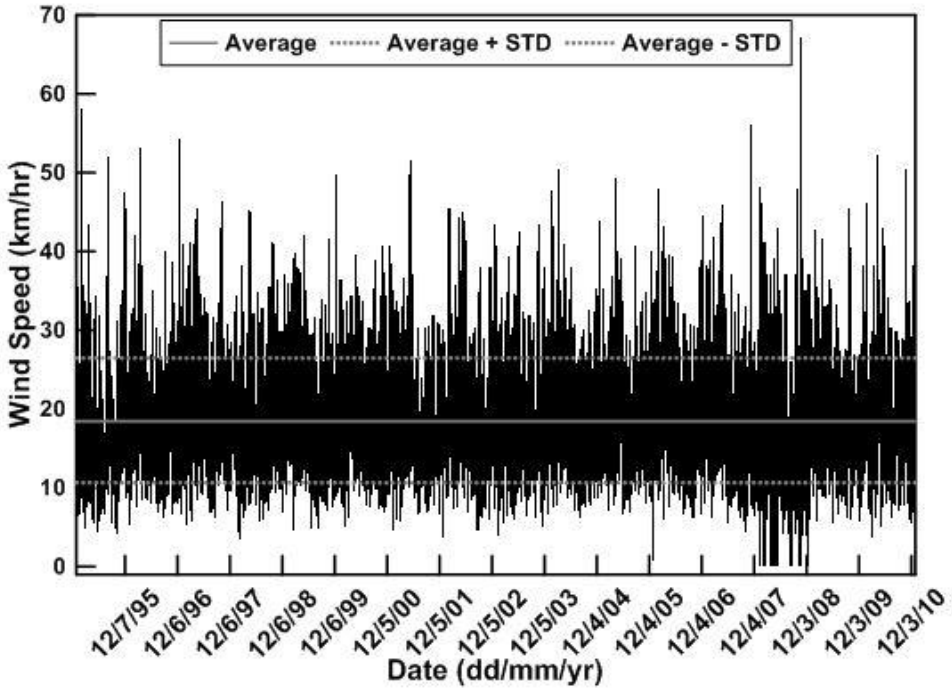

Figure. A.4.4: Average daily wind speed data city of Regina (1995-2010)

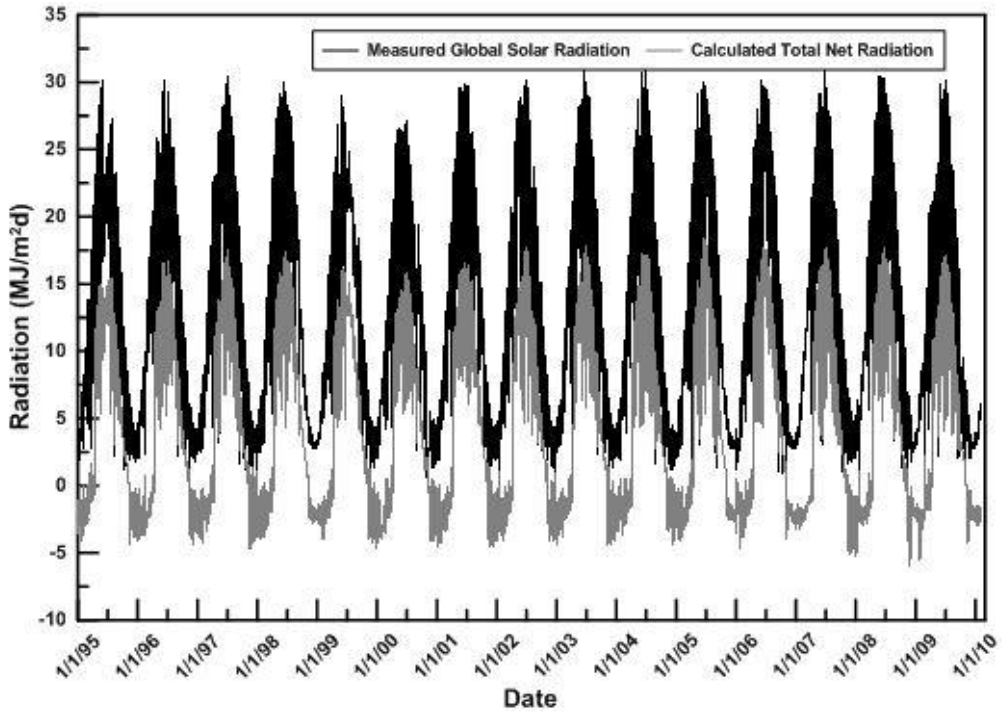

Figure. A.4.5: Average daily solar and net radiation data Regina (1995-2010)

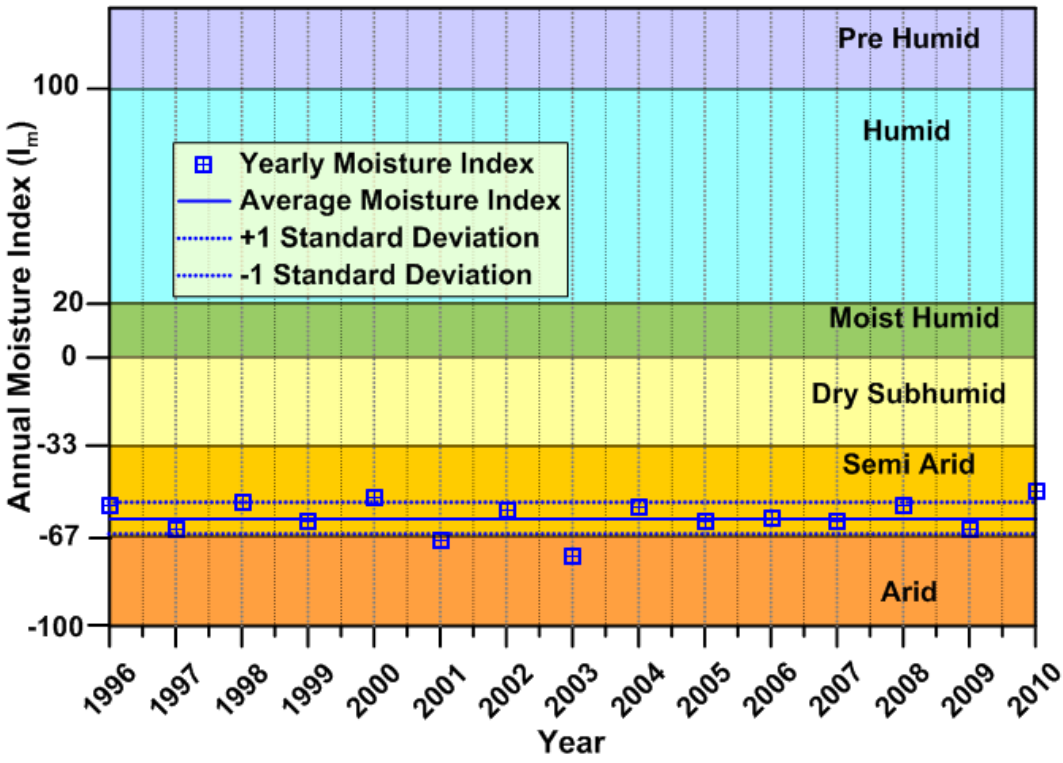

Figure. A.4.6: Climate classification city of Regina

Appendix A.5 - Compiled climate data – St. John's

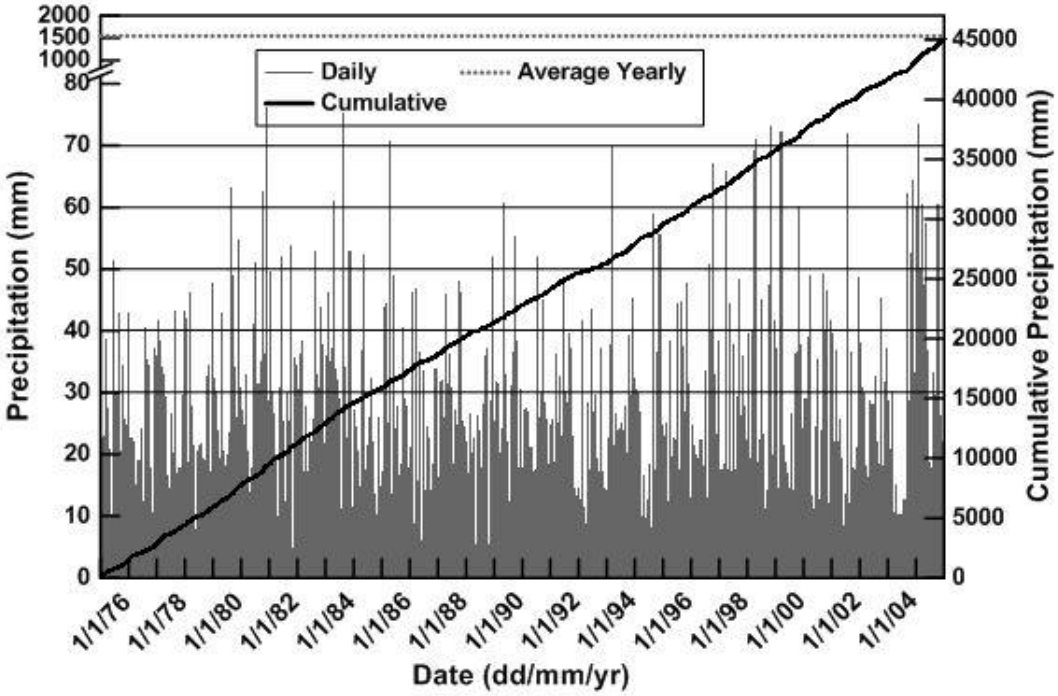

Figure. A.5.1: Precipitation data for the city of St. John's (1976-2005)

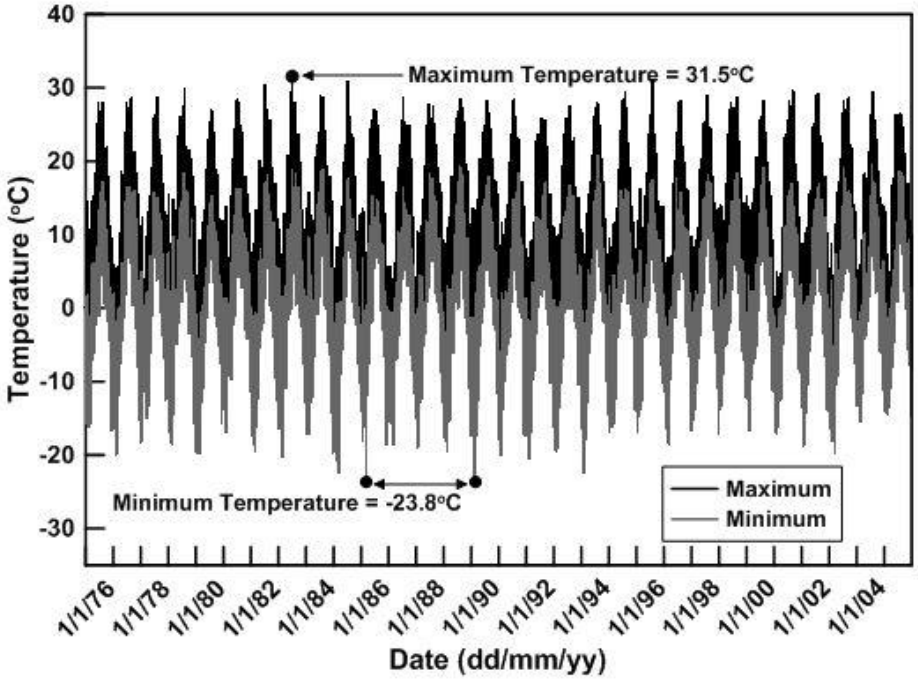

Figure. A.5.2: Temperature data for the city of St. John's (1976-2005)

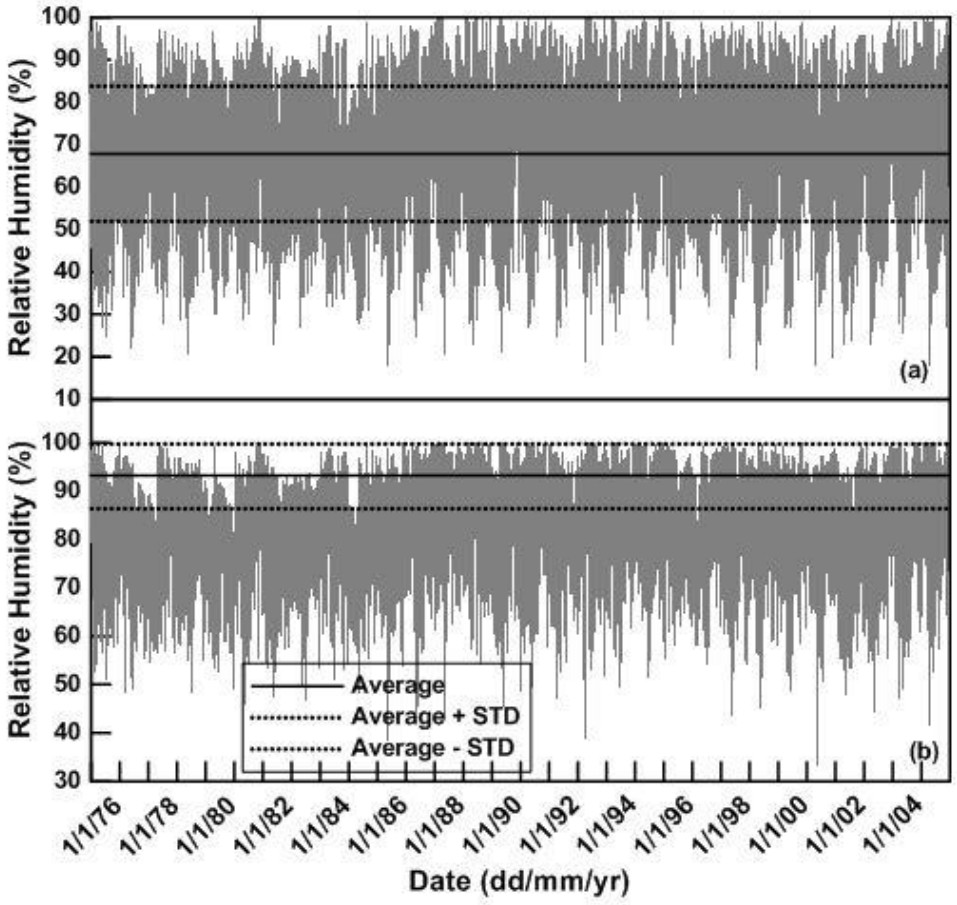

Figure. A.5.3: Relative humidity data for St. John's. (a) minimum (b) maximum

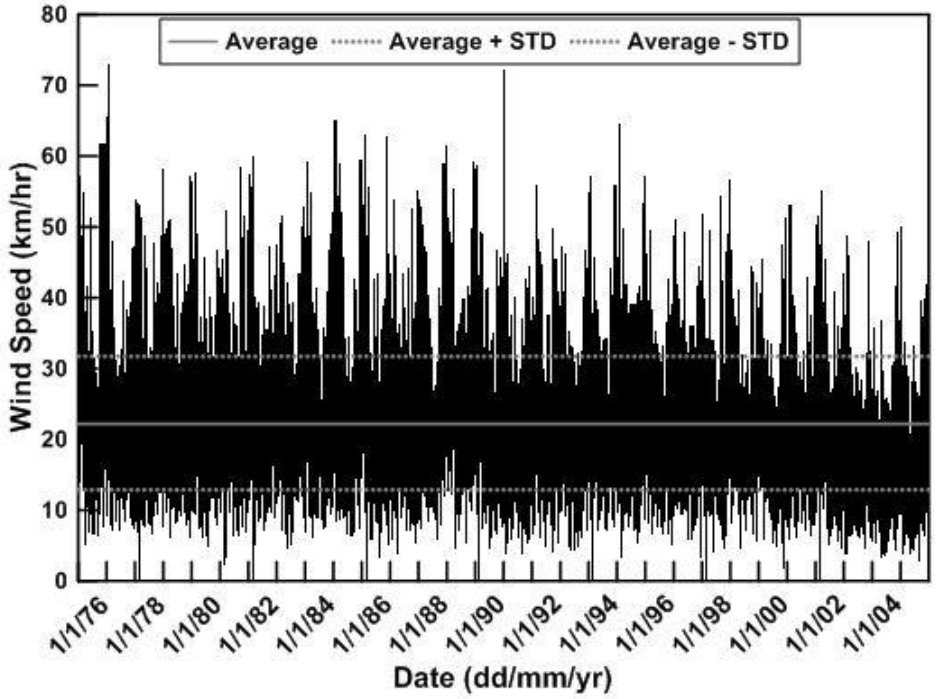

Figure. A.5.4: Average daily wind speed data city of St. John's (1976-2005)

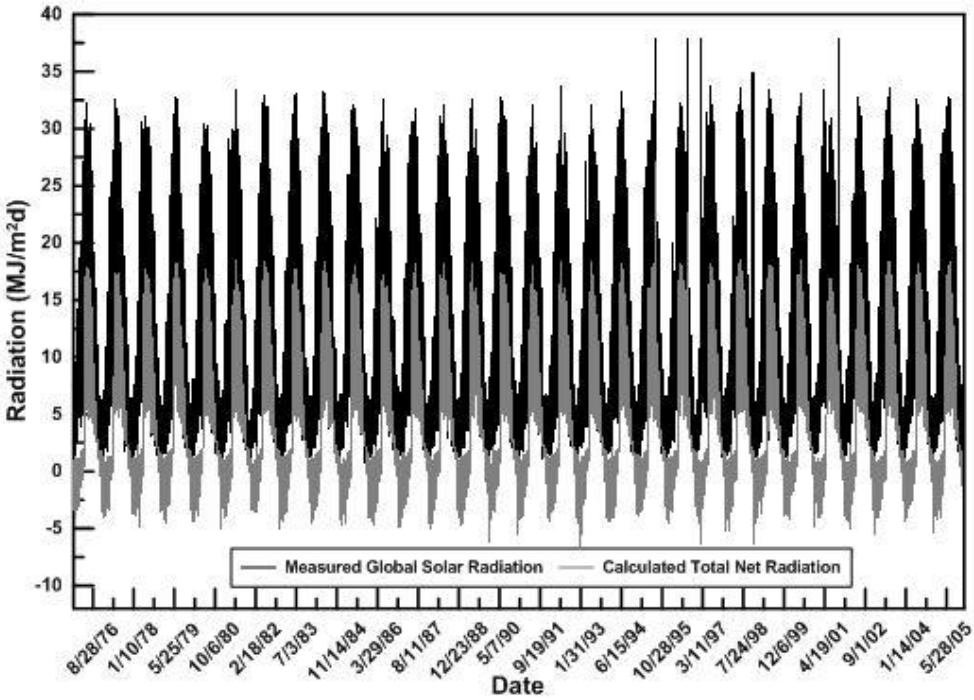

Figure. A.5.5: Average daily solar and net radiation data St. John's (1976-2005)

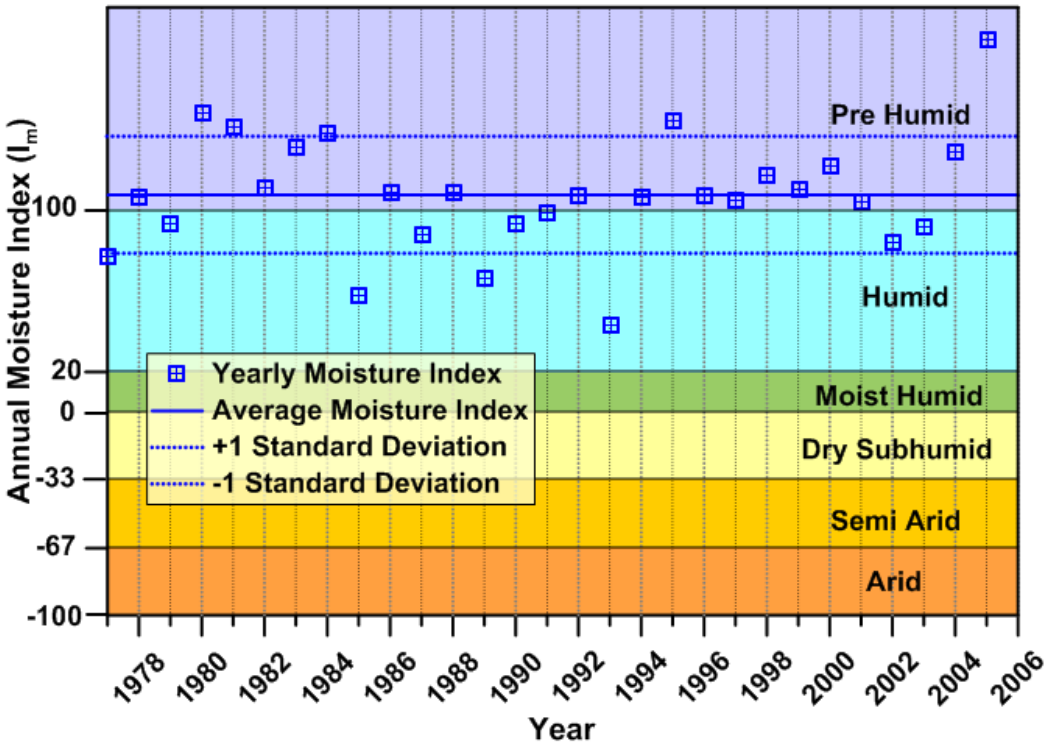

Figure. A.5.6: Climate classification city of St. John's

Appendix A.6 - Compiled climate data – Vancouver

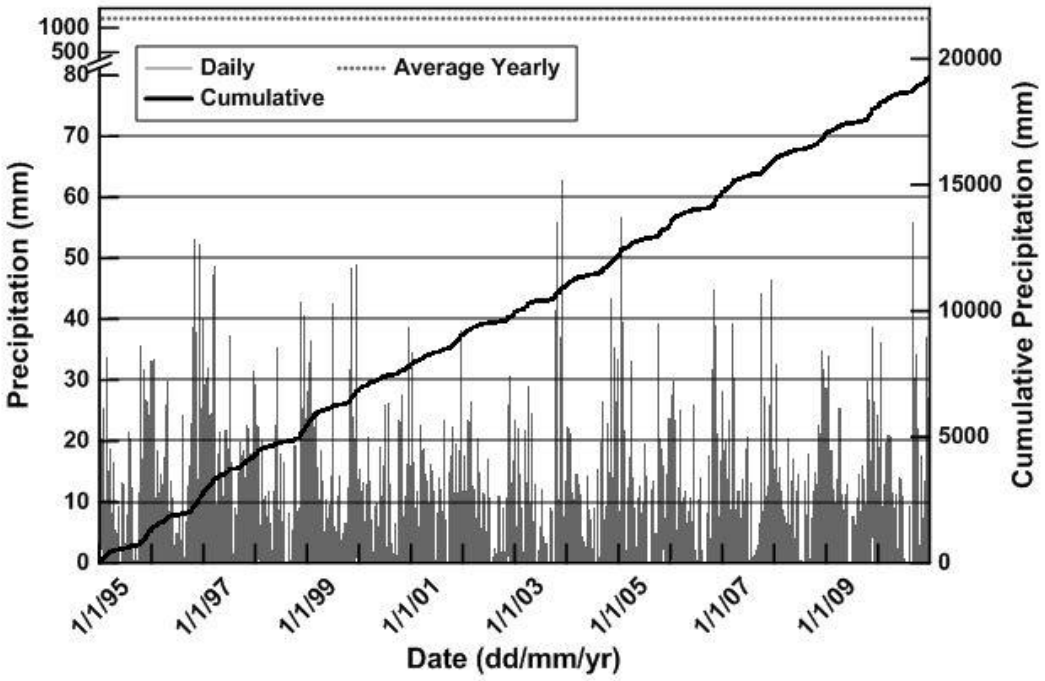

Figure. A.6.1: Precipitation data for the city of Vancouver (1995-2010)

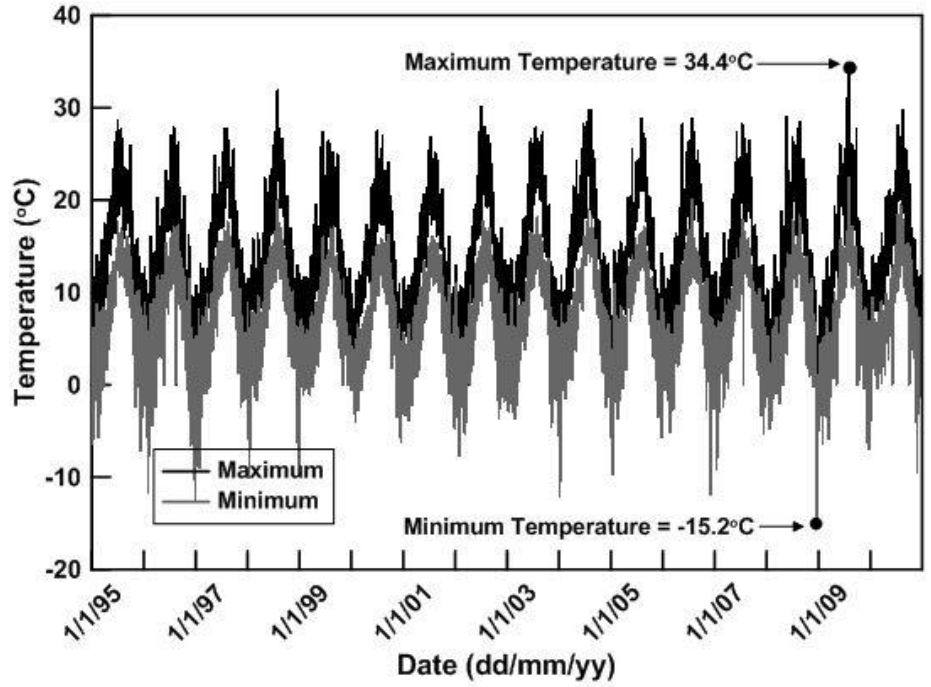

Figure. A.6.2: Temperature data for the city of Vancouver (1995-2010)

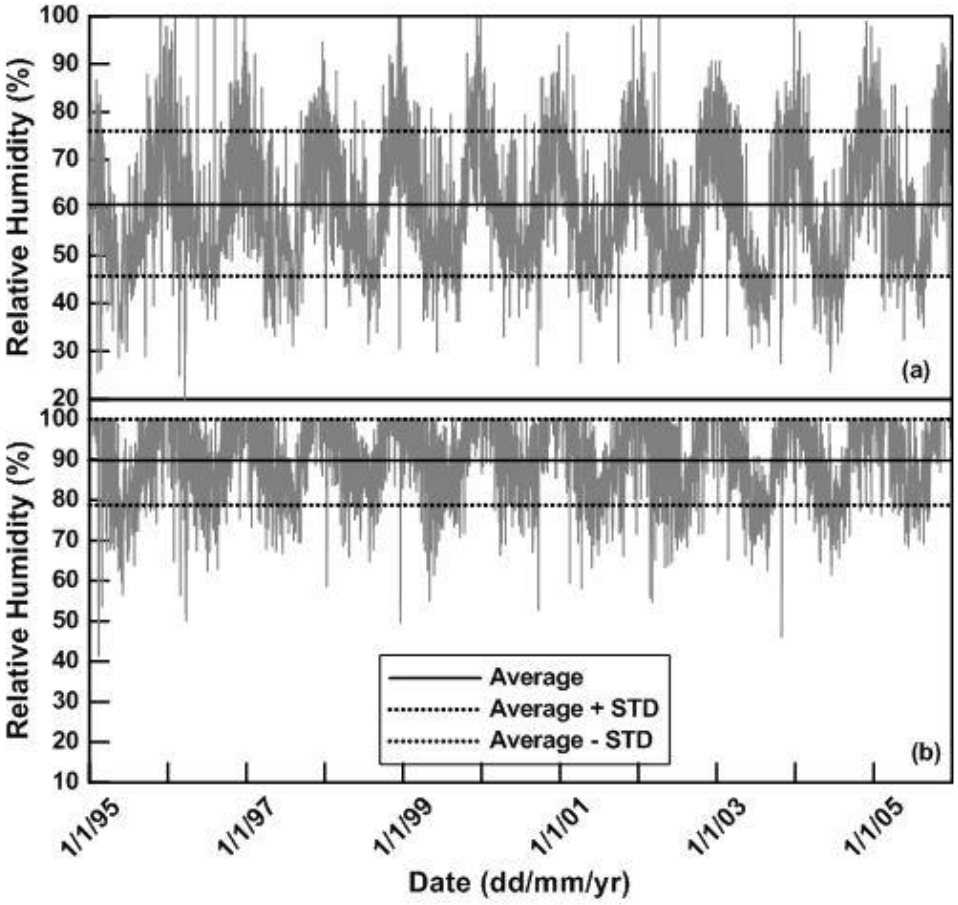

Figure. A.6.3: Relative humidity data for Vancouver (a) minimum (b) maximum

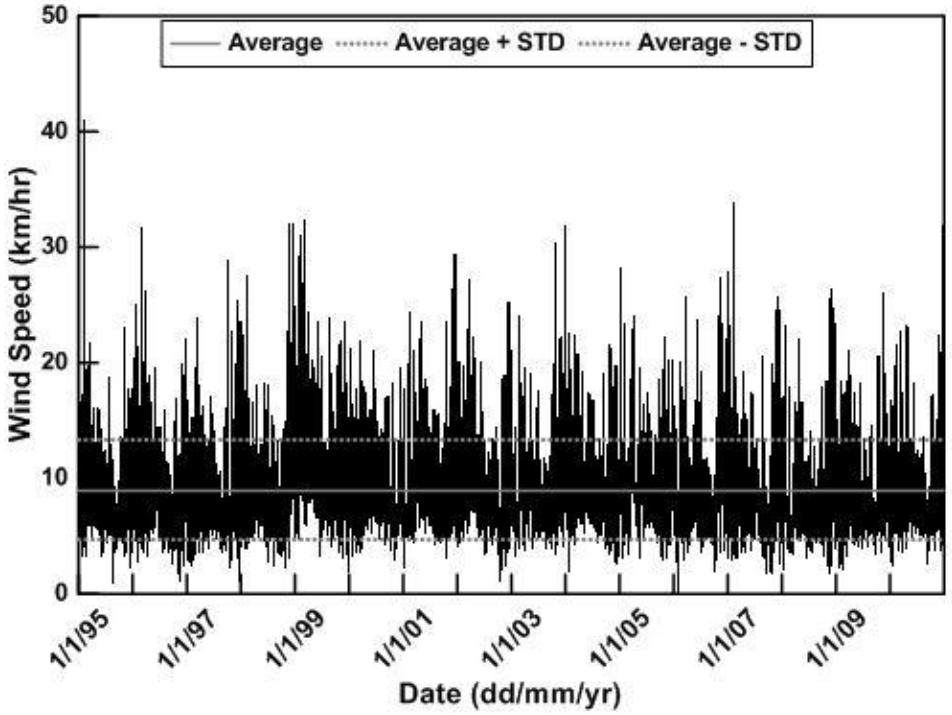

Figure. A.6.4: Average daily wind speed data city of Vancouver (1995-2010)

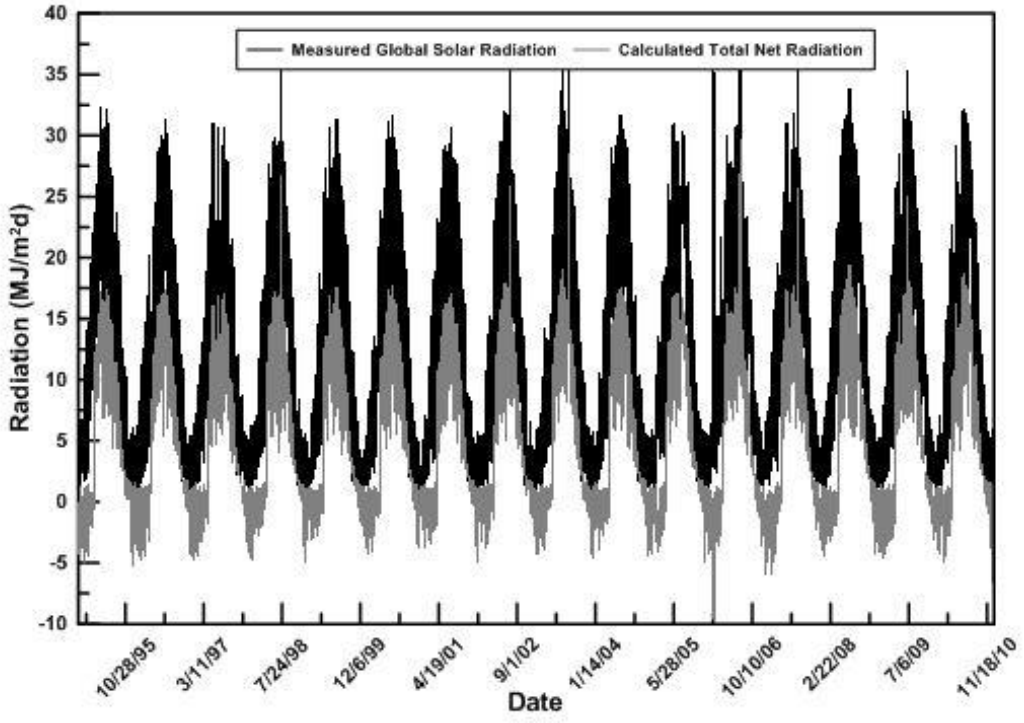

Figure. A.6.5: Average daily solar and net radiation data Vancouver (1995-2010)

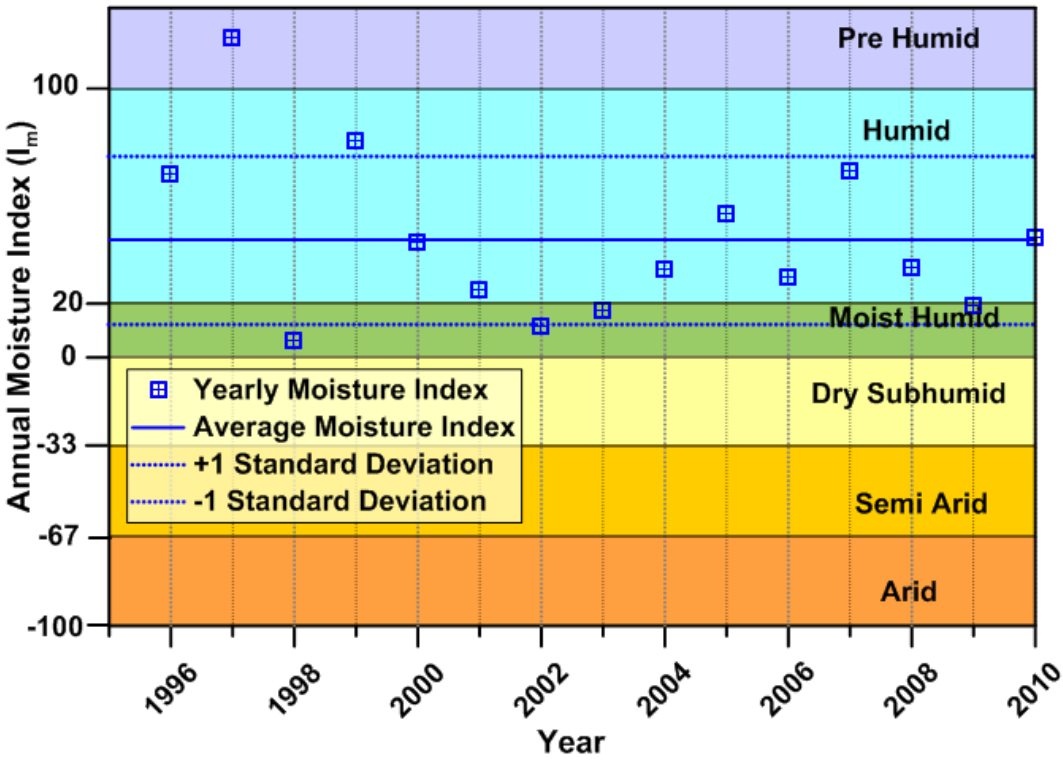

Figure. A.6.6: Climate classification city of Vancouver

Appendix A.7 - Compiled climate data – Barriere

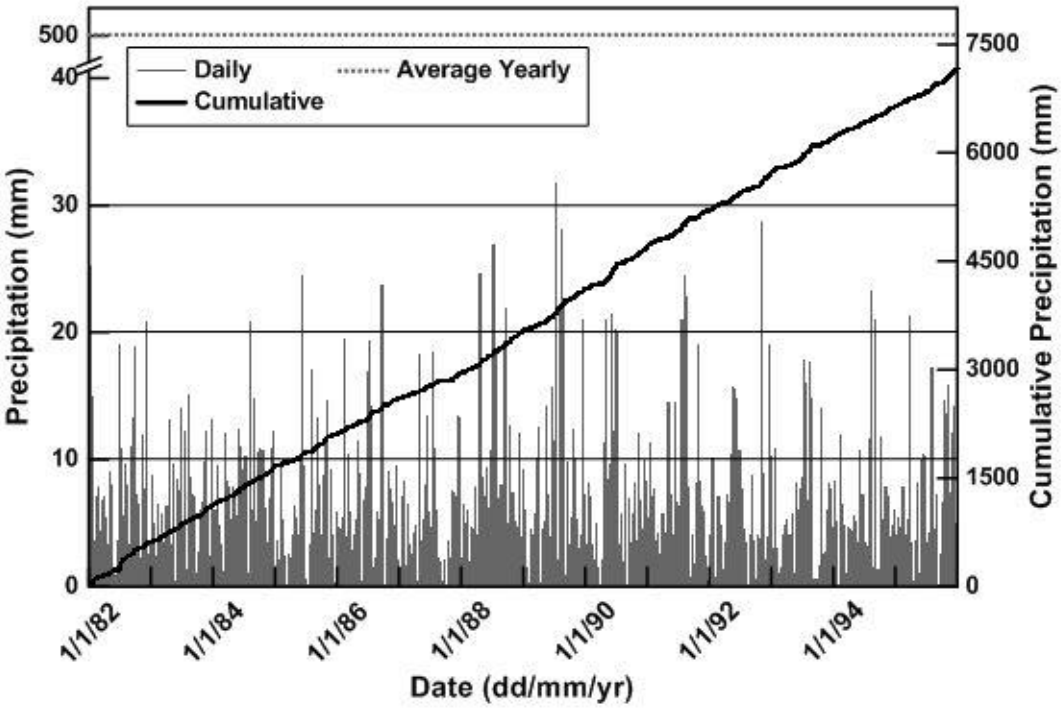

Figure. A.7.1: Precipitation data for the city of Barriere (1982-1995)

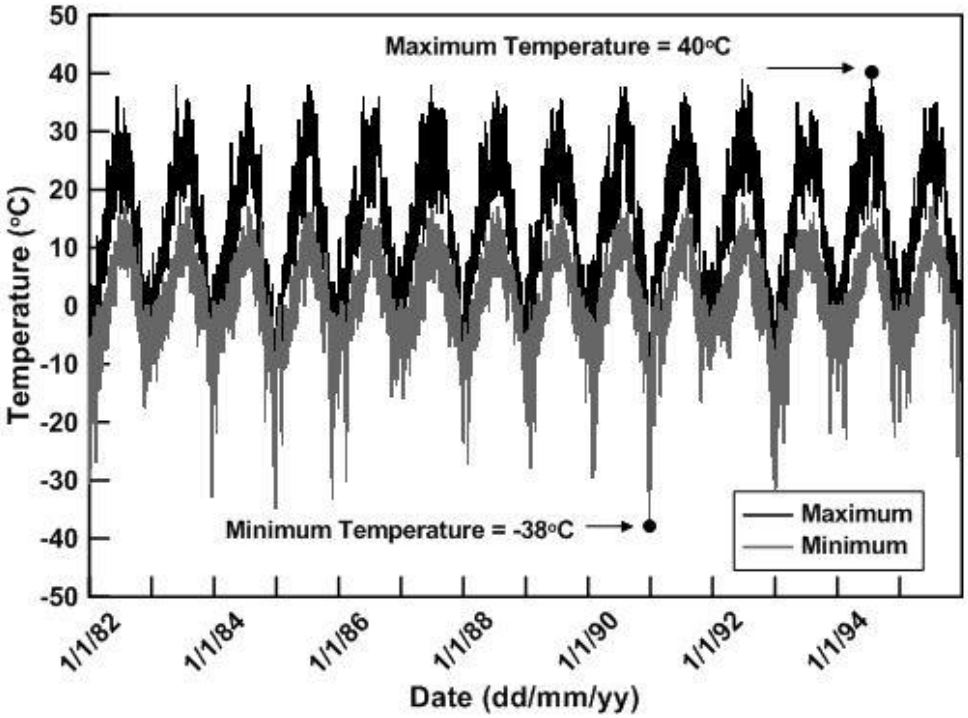

Figure. A.7.2: Temperature data for the city of Barriere (1982-1995)

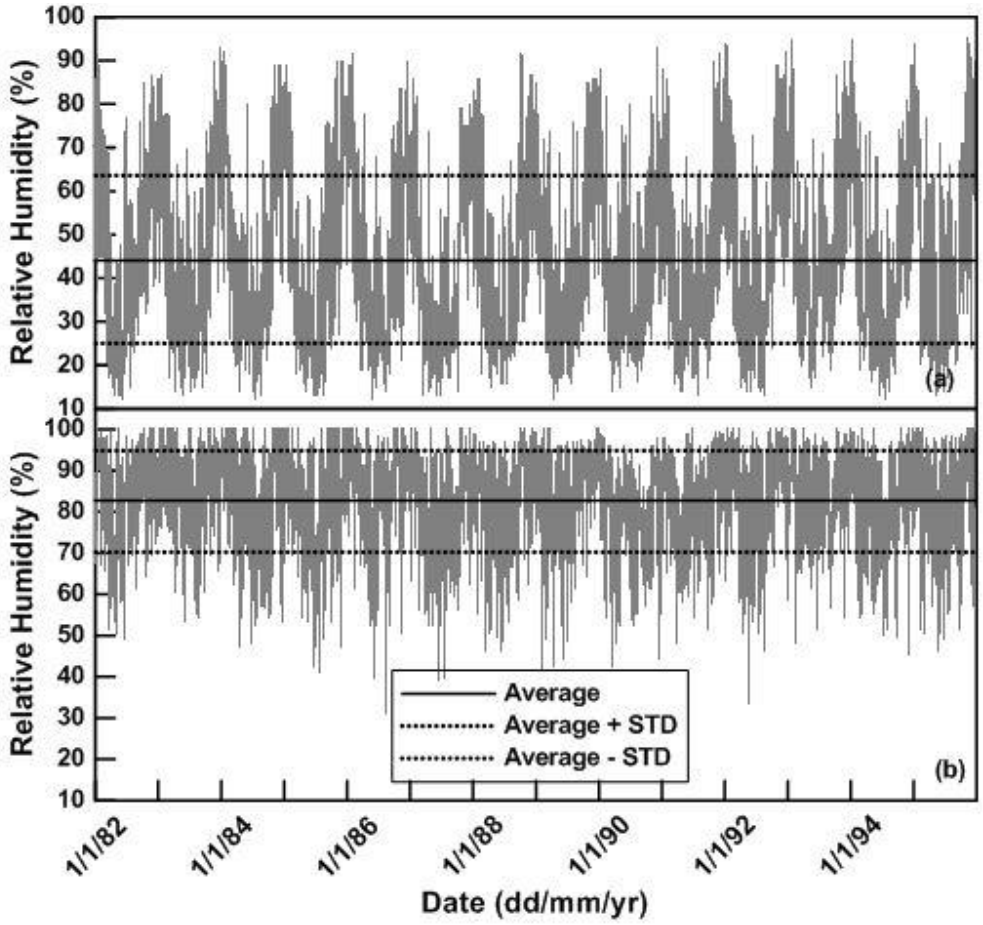

Figure. A.7.3: Relative humidity data for Barriere (a) minimum (b) maximum

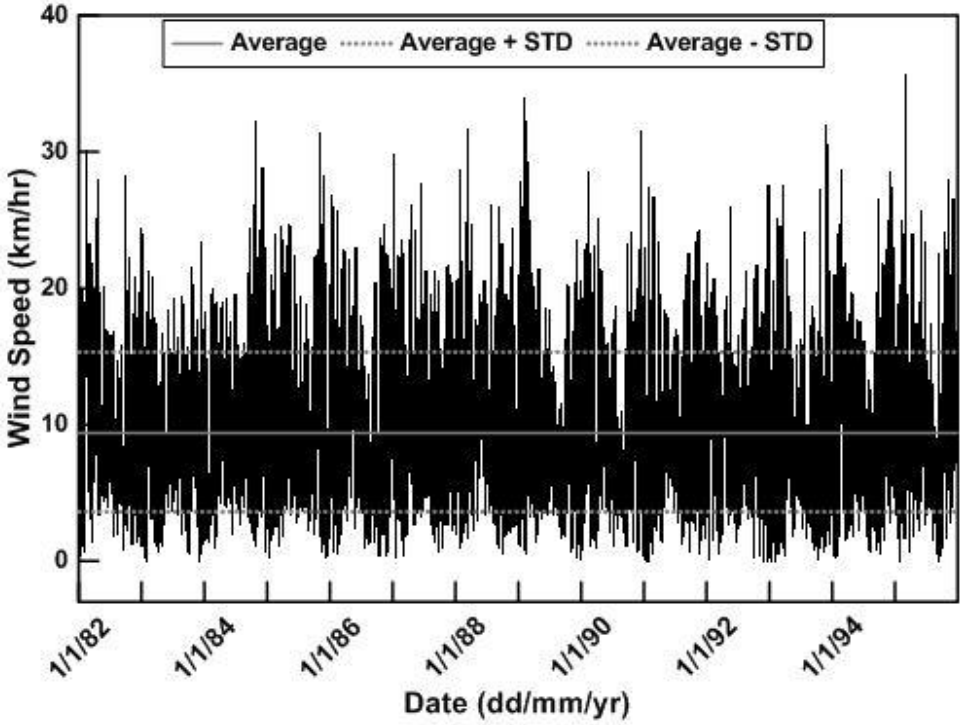

Figure. A.7.4: Average daily wind speed data city of Barriere (1982-1995)

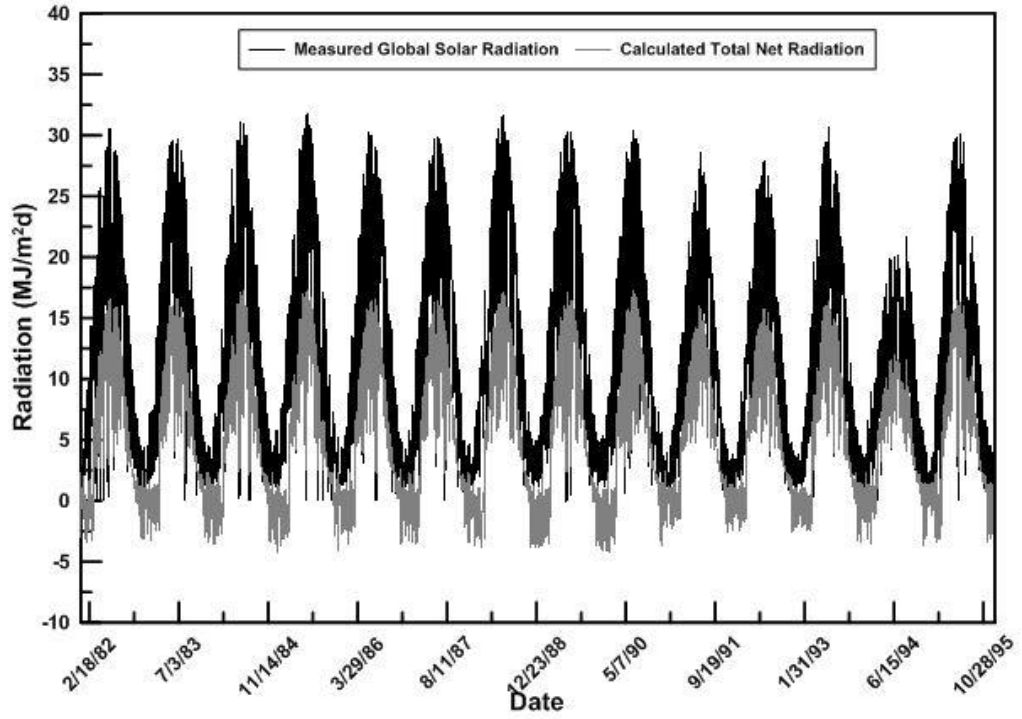

Figure. A.7.5: Average daily solar and net radiation data Barriere (1982-1995)

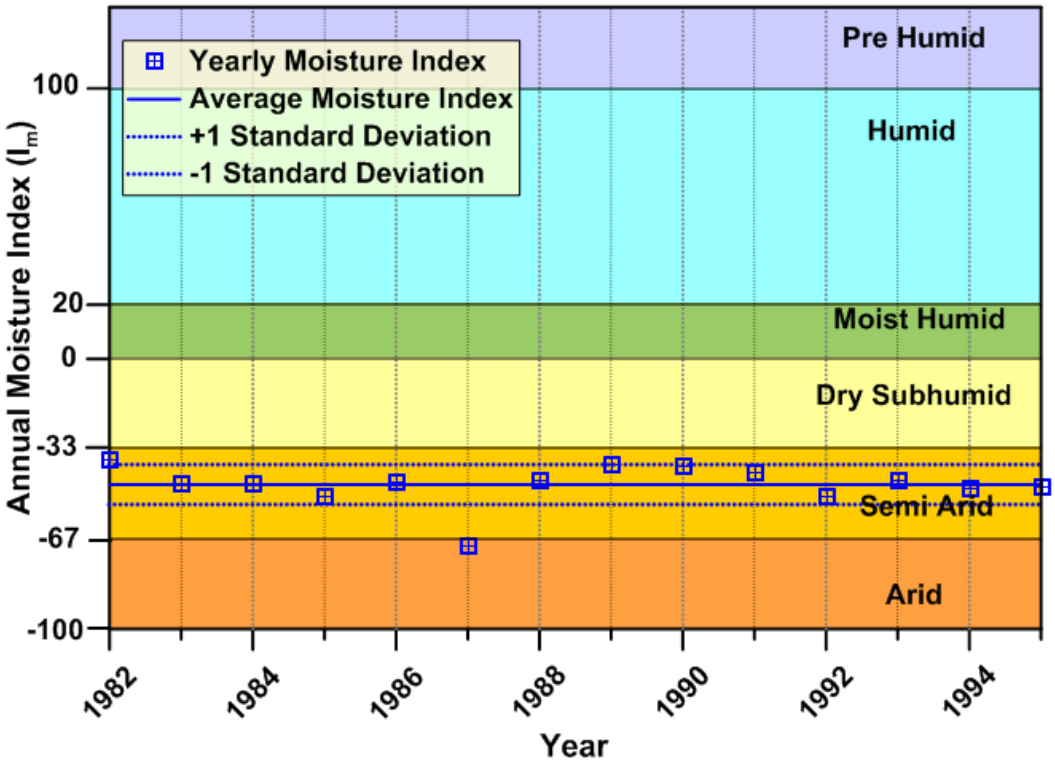

Figure. A.7.6: Climate classification city of Barriere

Appendix B.1 – Comparison of climate data – Toronto

Table. B.1.1: Comparison statistics for measured and simulated data

Variable	R^2	RMSD	MAD
Solar Radiation	0.96	1.62	1.25
Maximum Temperature	0.98	1.34	1.03
Minimum Temperature	0.98	1.12	0.88
Wind Speed	0.72	0.34	0.26
Dew Point Temperature	0.98	1.22	0.98
Relative Humidity	0.35	4.66	3.71

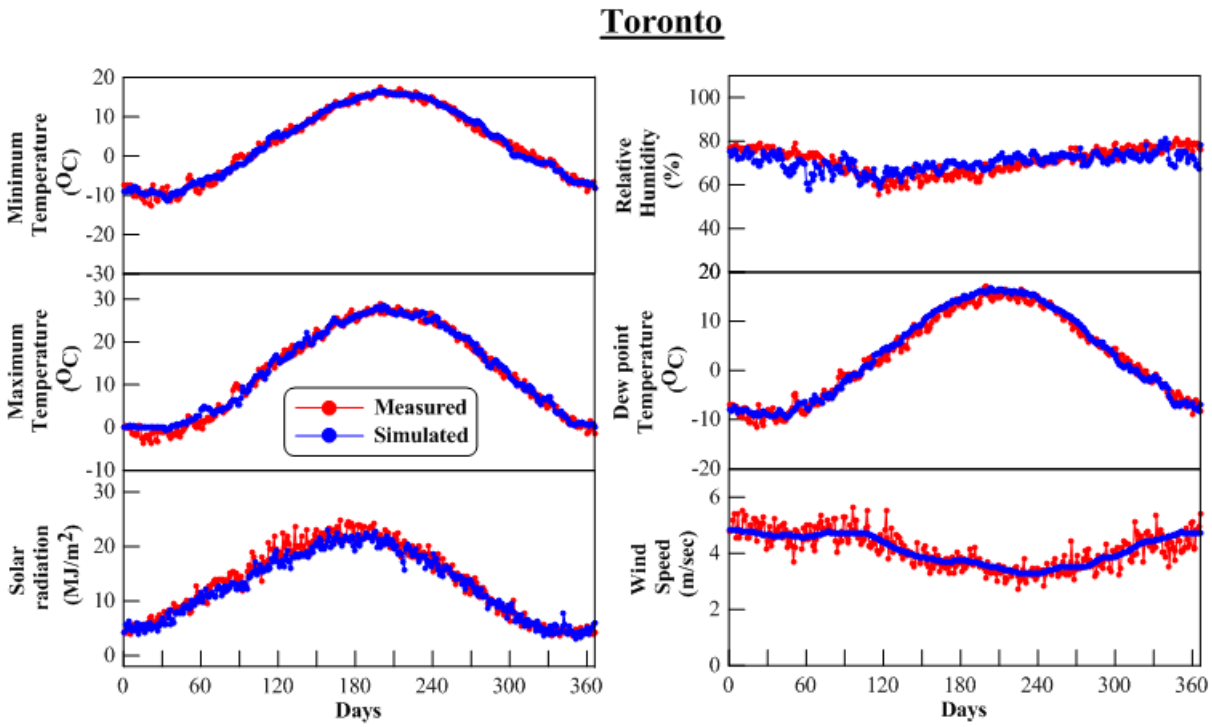

Figure. B.1.2: Comparison of measured and simulated data

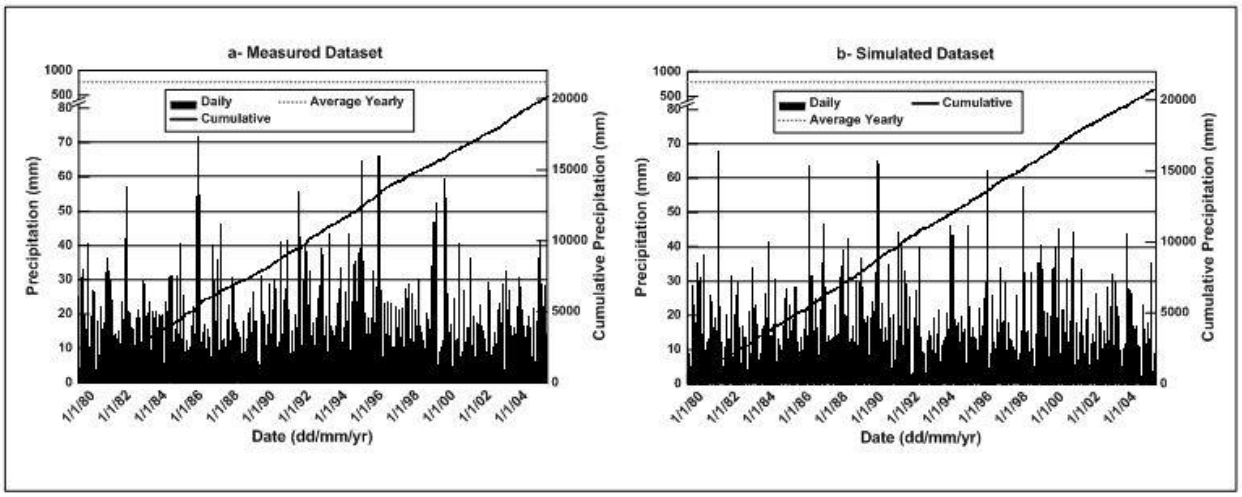

Figure. B.1.3: Comparison of measured and simulated precipitation

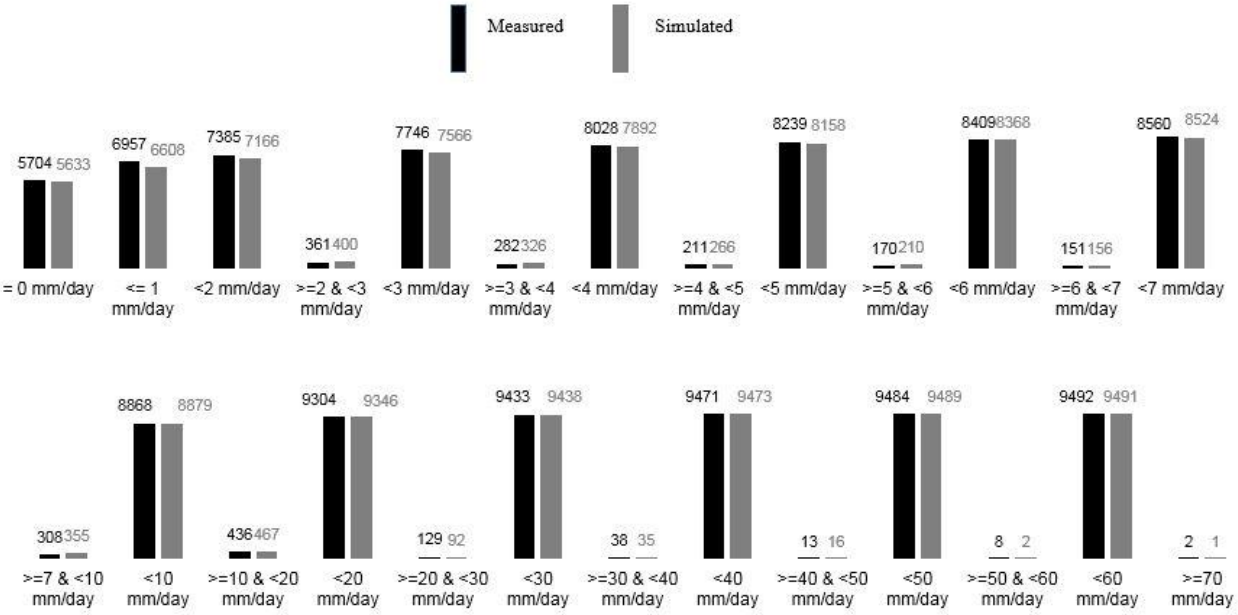

Figure. B.1.4: Comparison of measured and simulated precipitation occurrences

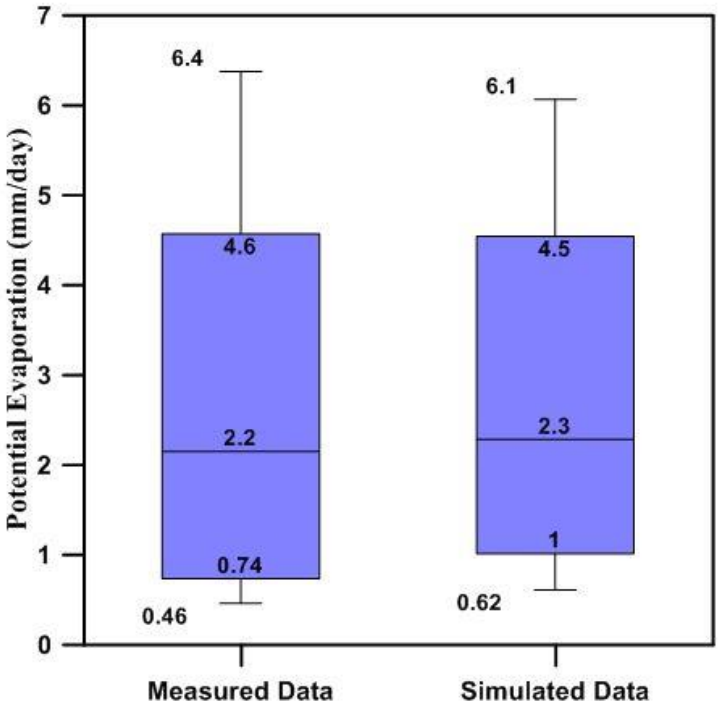

Figure. B.1.5: Comparison of measured and simulated potential evaporation

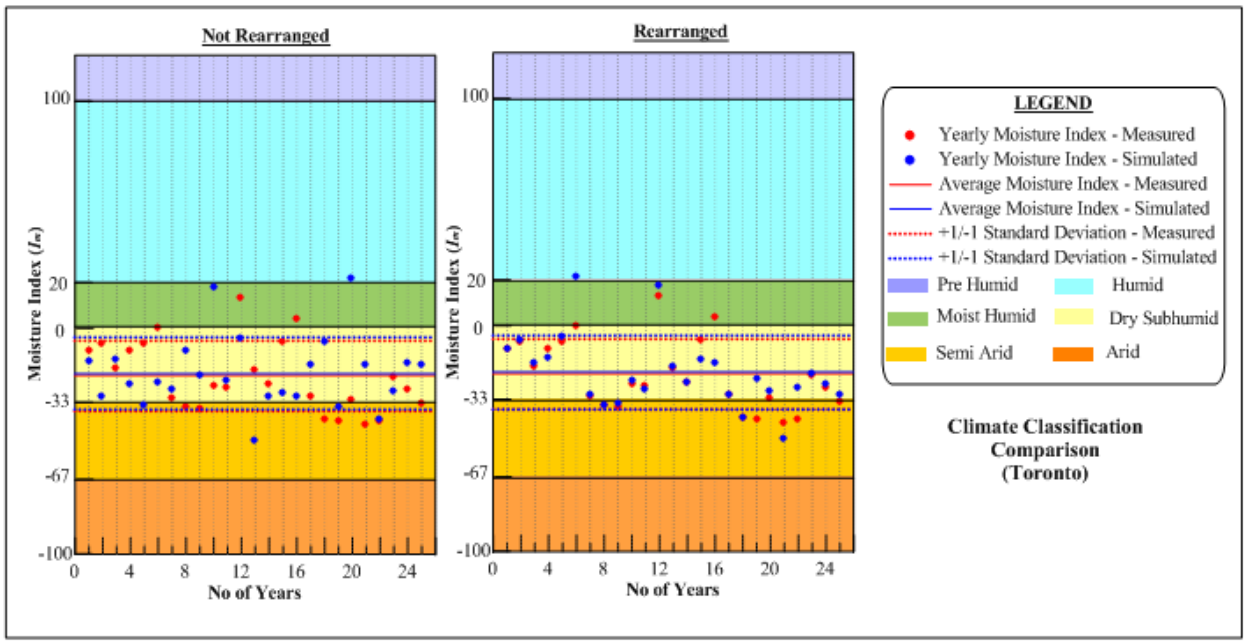

Figure. B.1.6: Comparison of measured and simulated climate classification

Appendix B.2 – Comparison of climate data – Timmins

Table. B.2.1: Comparison statistics for measured and simulated data

Variable	R^2	RMSD	MAD
Solar Radiation	0.96	1.25	0.96
Maximum Temperature	0.99	1.36	1.02
Minimum Temperature	0.98	1.81	1.35
Wind Speed	0.43	0.32	0.25
Dew Point Temperature	0.99	1.33	1.02
Relative Humidity	0.75	5.78	4.46

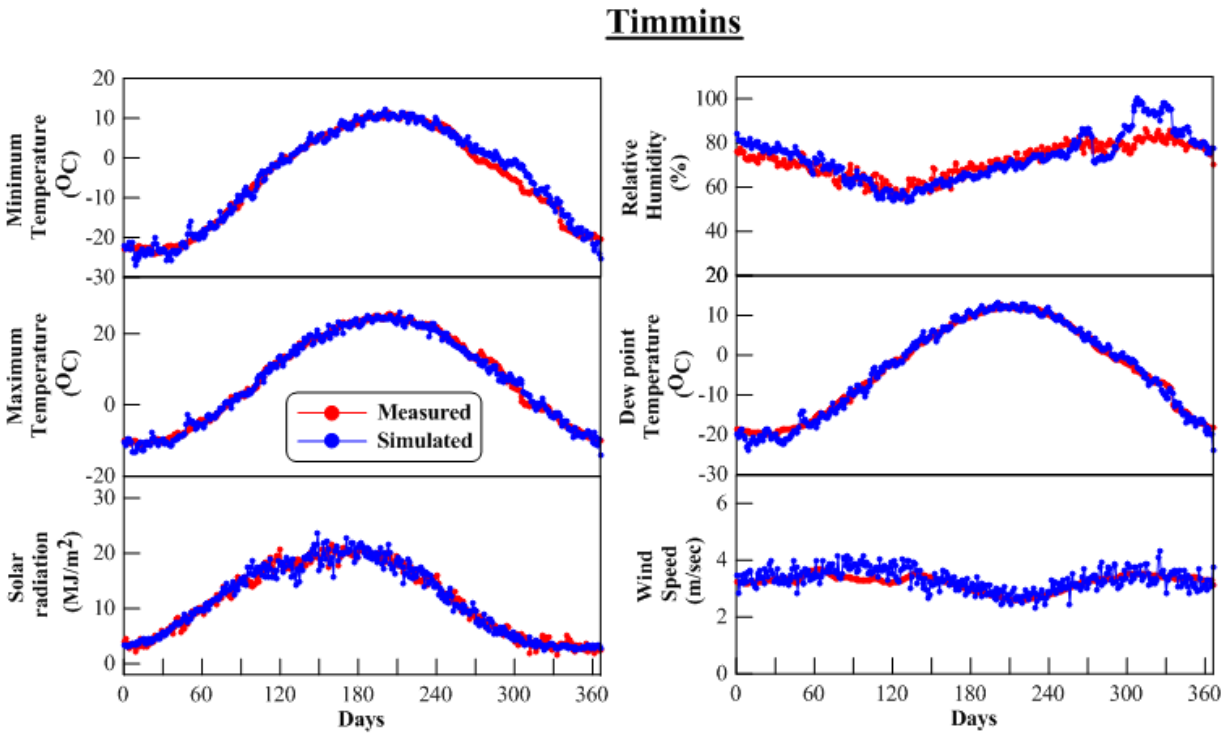

Figure. B.2.2: Comparison of measured and simulated data

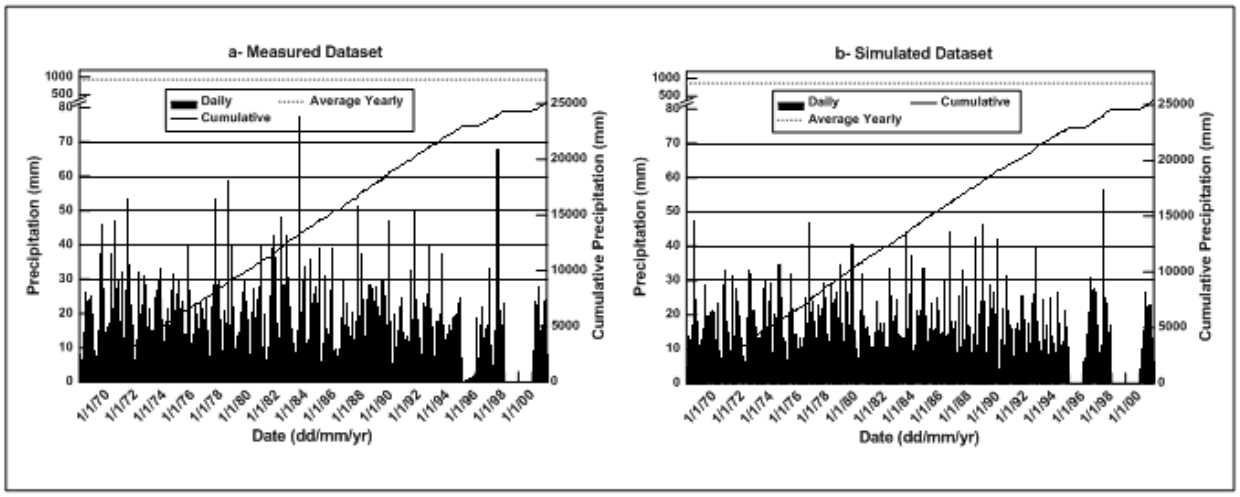

Figure. B.2.3: Comparison of measured and simulated precipitation

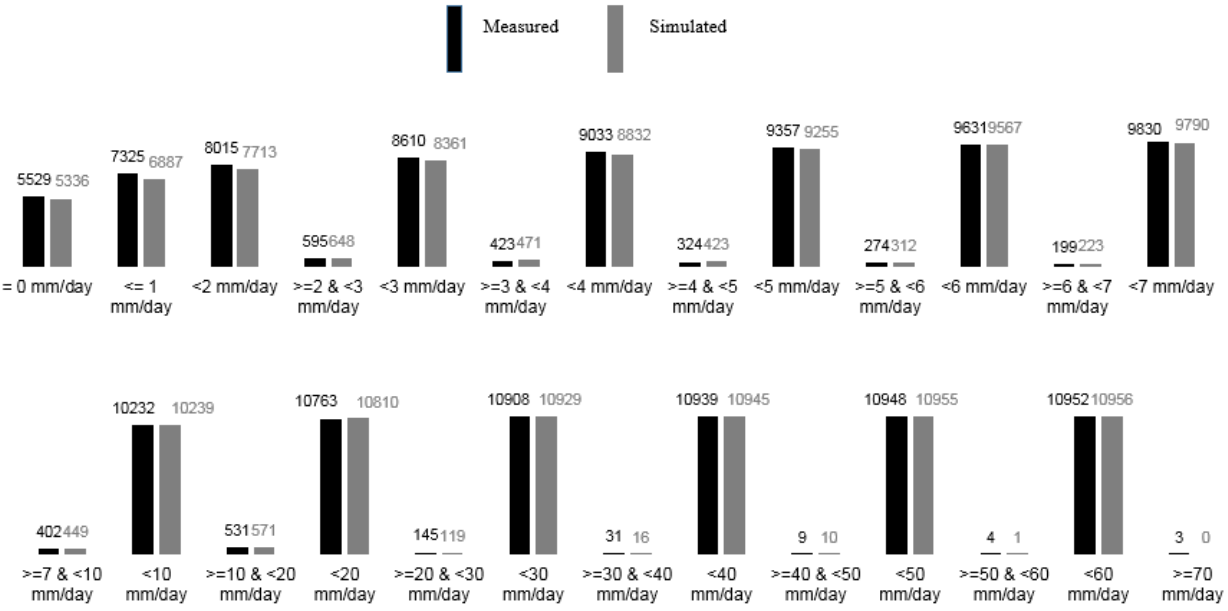

Figure. B.2.4: Comparison of measured and simulated precipitation occurrences

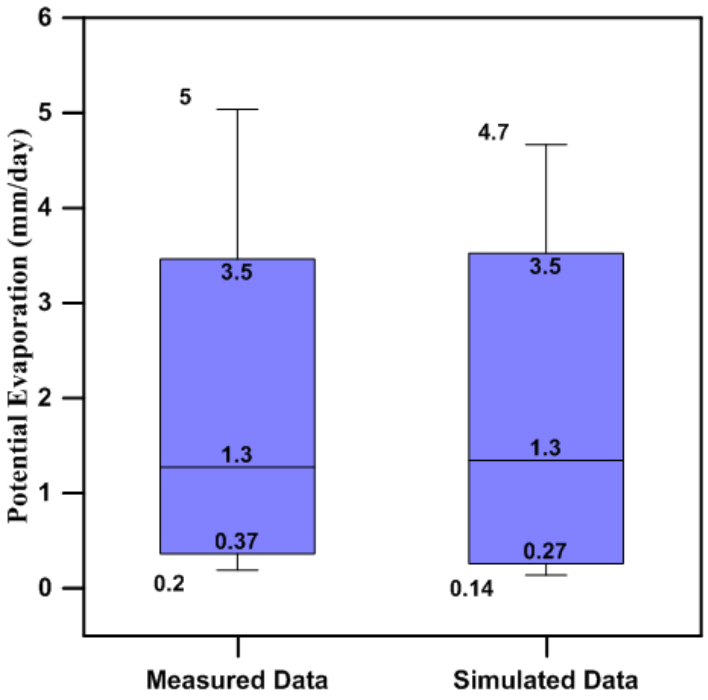

Figure. B.2.5: Comparison of measured and simulated potential evaporation

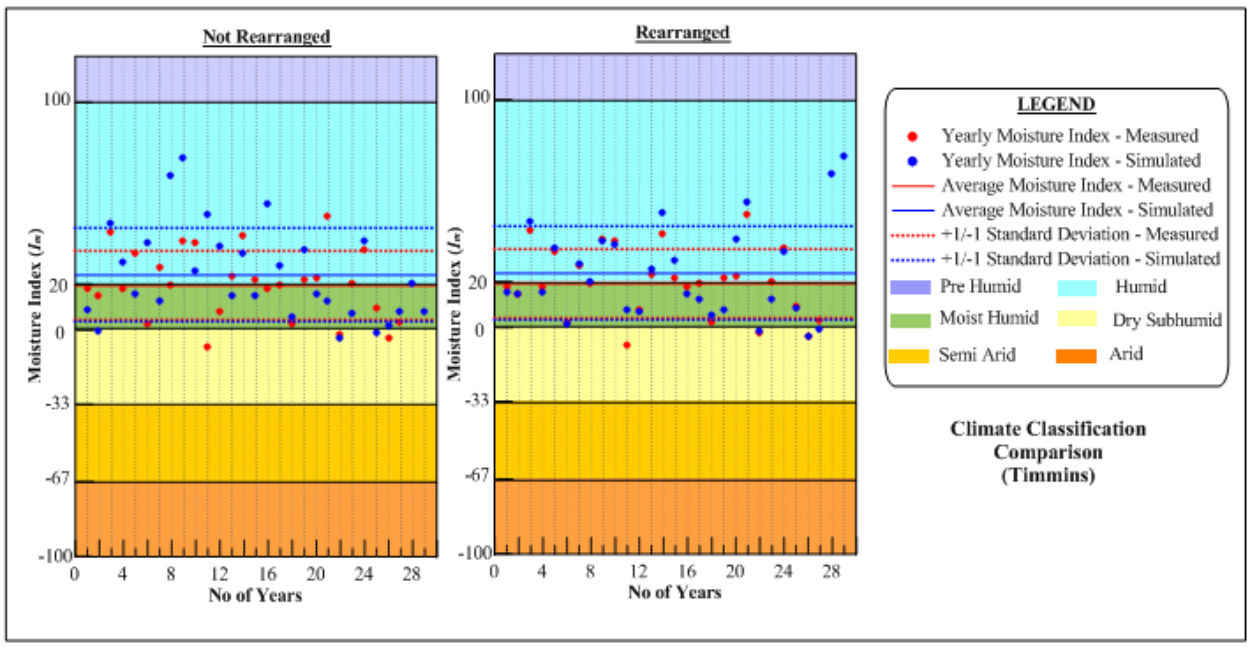

Figure. B.2.6: Comparison of measured and simulated climate classification

Appendix B.3 – Comparison of climate data – Whitecourt

Table. B.3.1: Comparison statistics for measured and simulated data

Variable	R^2	RMSD	MAD
Solar Radiation	0.96	1.60	1.28
Maximum Temperature	0.96	2.29	1.76
Minimum Temperature	0.97	1.54	1.17
Wind Speed	0.38	0.59	0.54
Dew Point Temperature	0.97	2.03	1.48
Relative Humidity	0.14	10.26	7.78

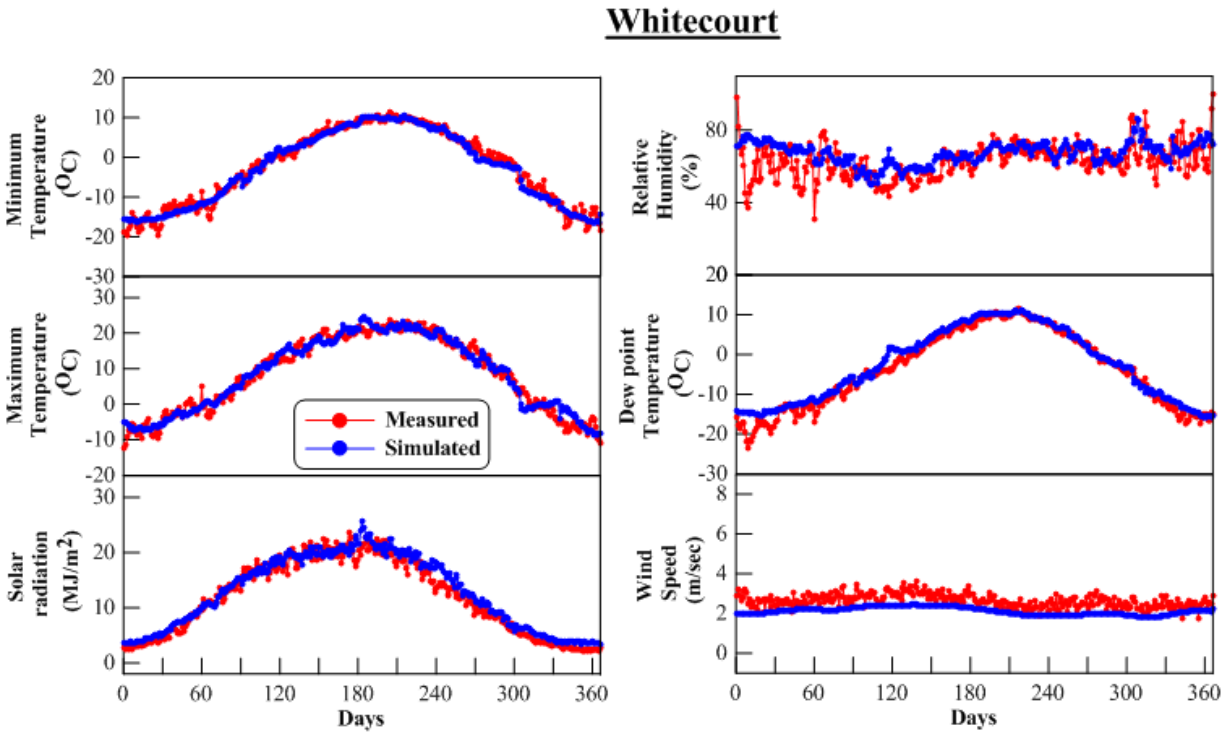

Figure. B.3.2: Comparison of measured and simulated data

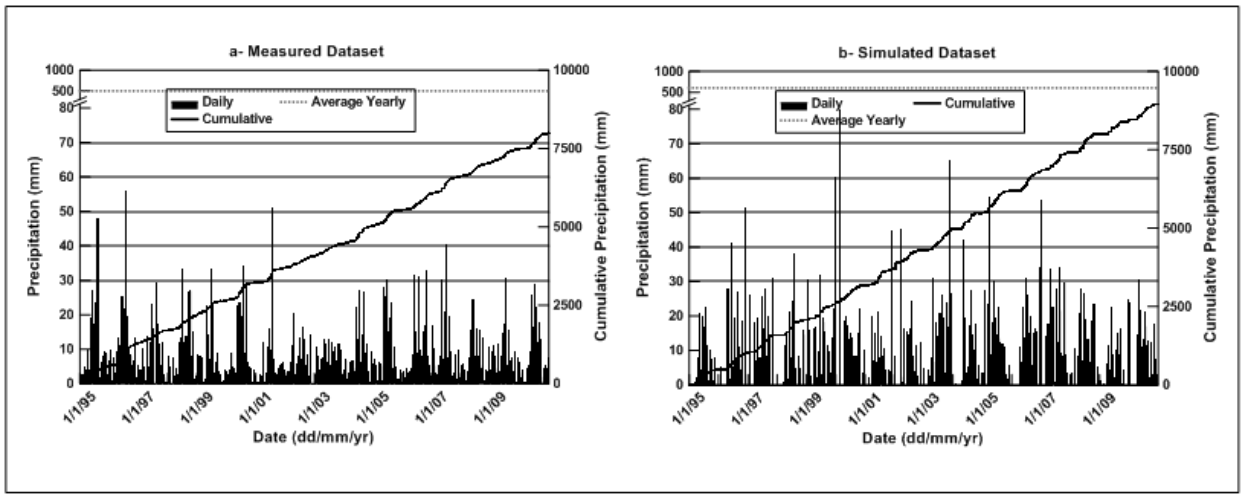

Figure. B.3.3: Comparison of measured and simulated precipitation

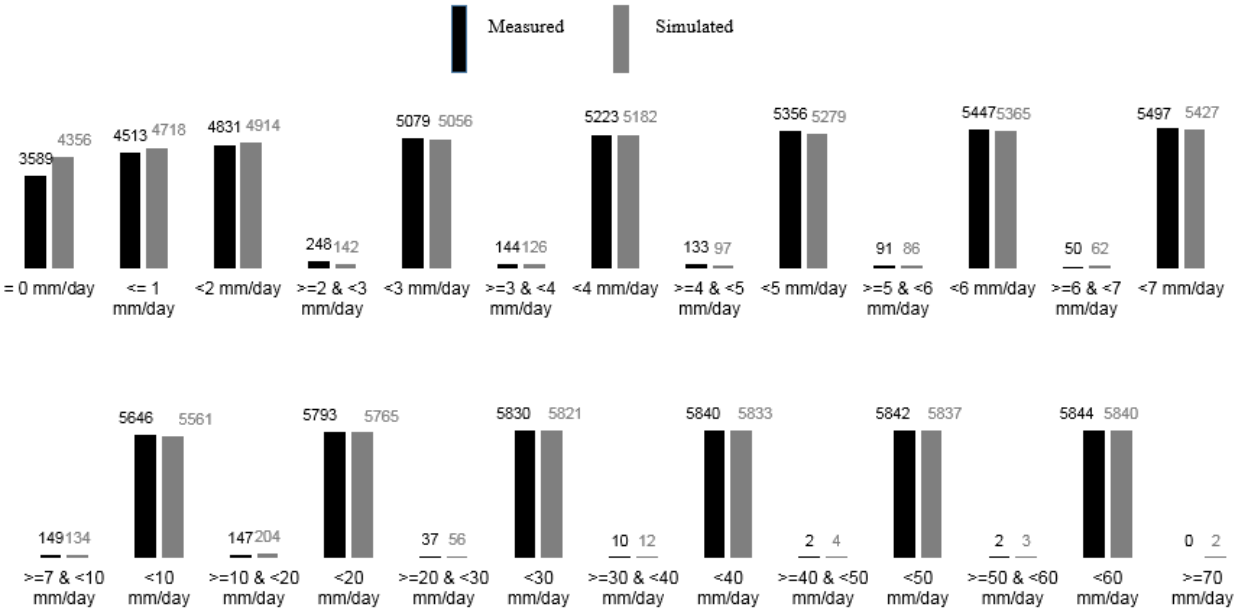

Figure. B.3.4: Comparison of measured and simulated precipitation occurrences

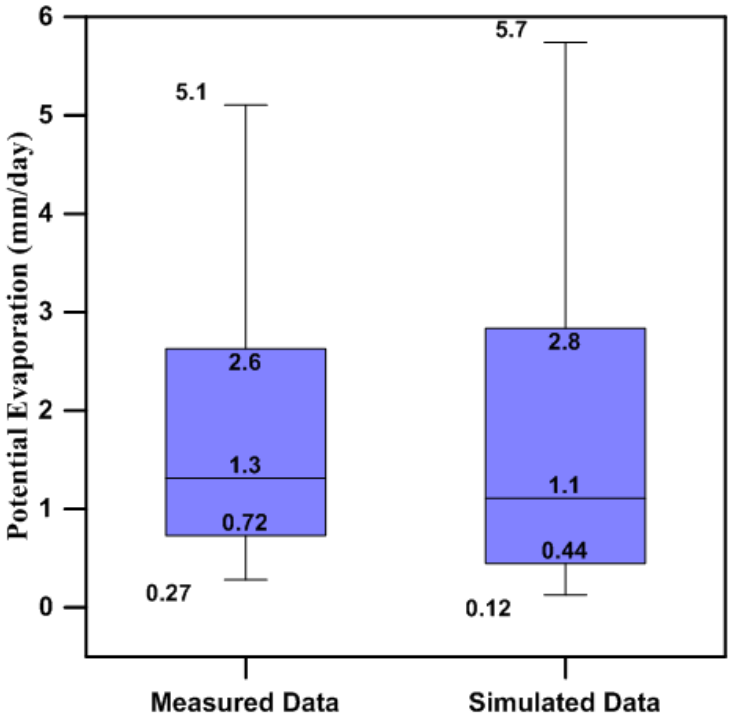

Figure. B.3.5: Comparison of measured and simulated potential evaporation

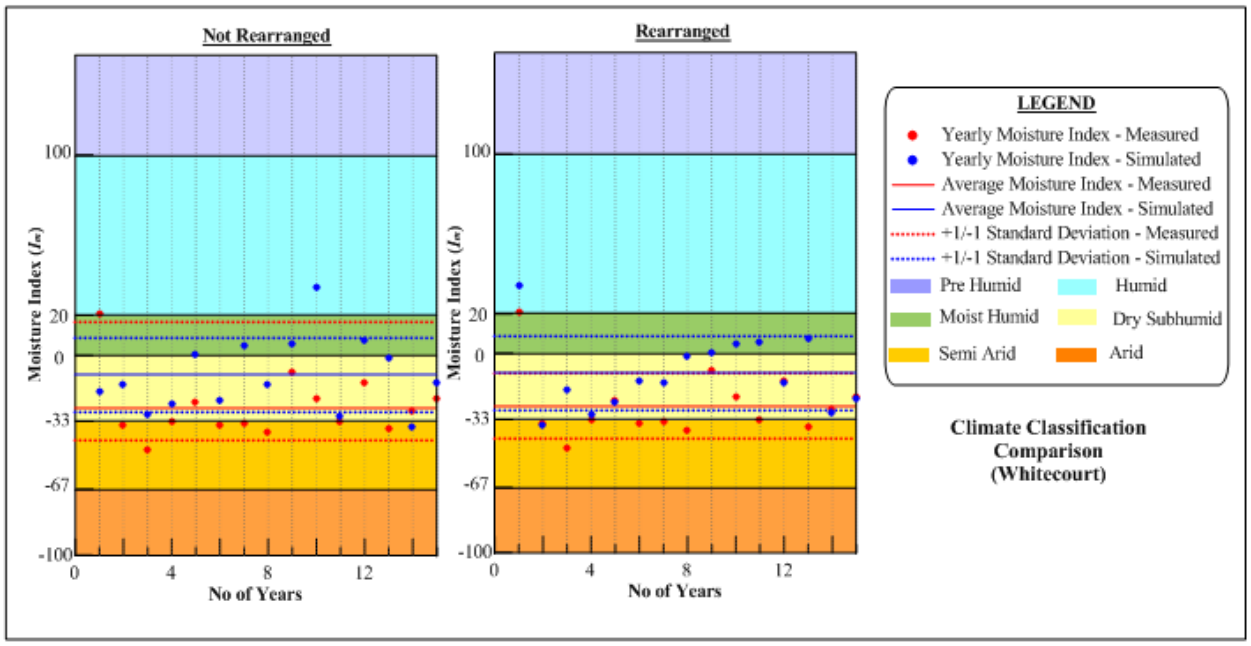

Figure. B.3.6: Comparison of measured and simulated climate classification

Appendix B.4 – Comparison of climate data – Regina

Table. B.4.1: Comparison statistics for measured and simulated data

Variable	R^2	RMSD	MAD
Solar Radiation	0.96	1.43	1.08
Maximum Temperature	0.98	1.65	1.35
Minimum Temperature	0.98	1.56	1.16
Wind Speed	0.21	0.57	0.44
Dew Point Temperature	0.98	1.39	1.04
Relative Humidity	0.74	3.86	3.00

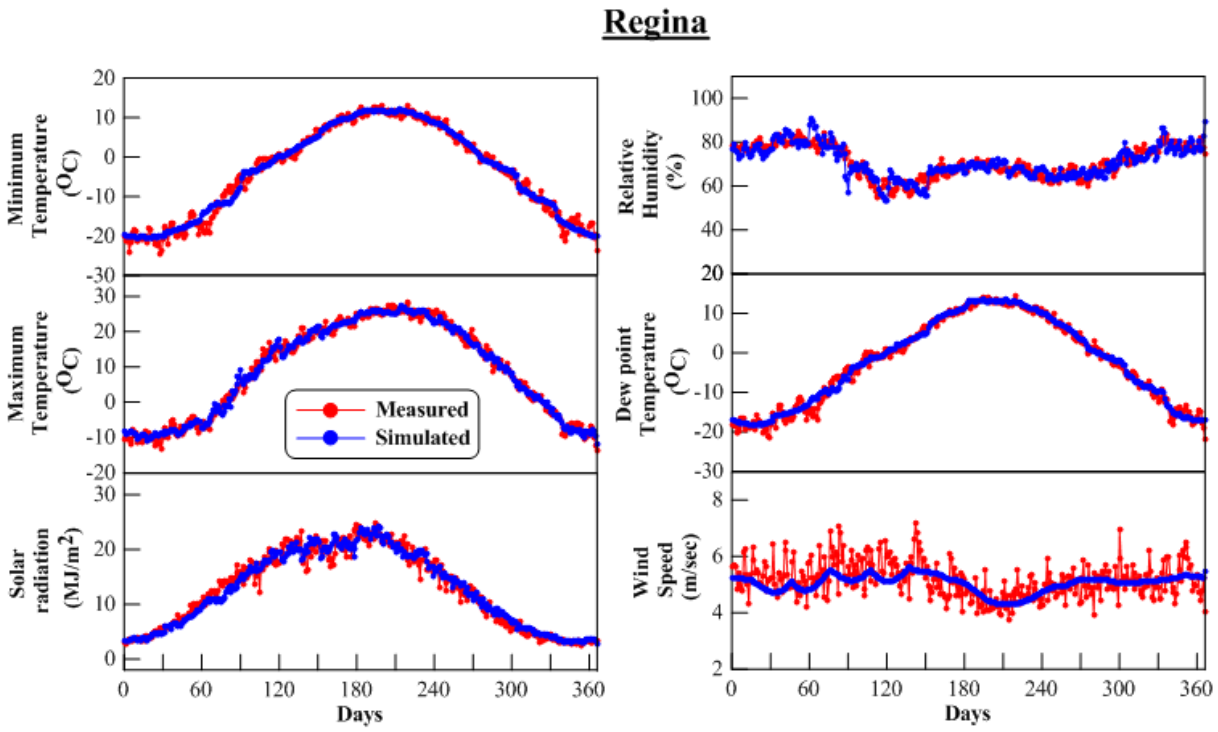

Figure. B.4.2: Comparison of measured and simulated data

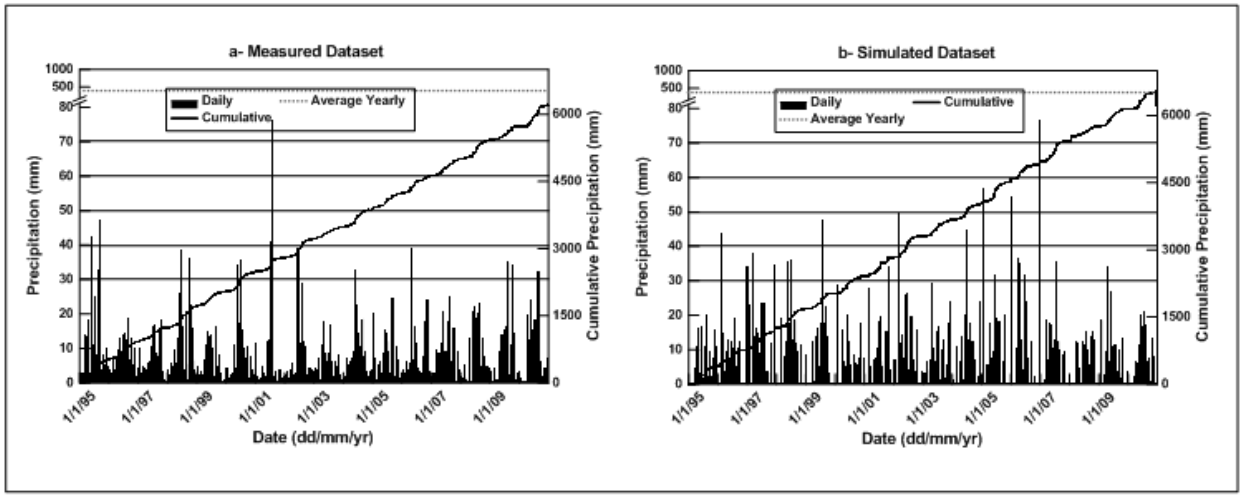

Figure. B.4.3: Comparison of measured and simulated precipitation

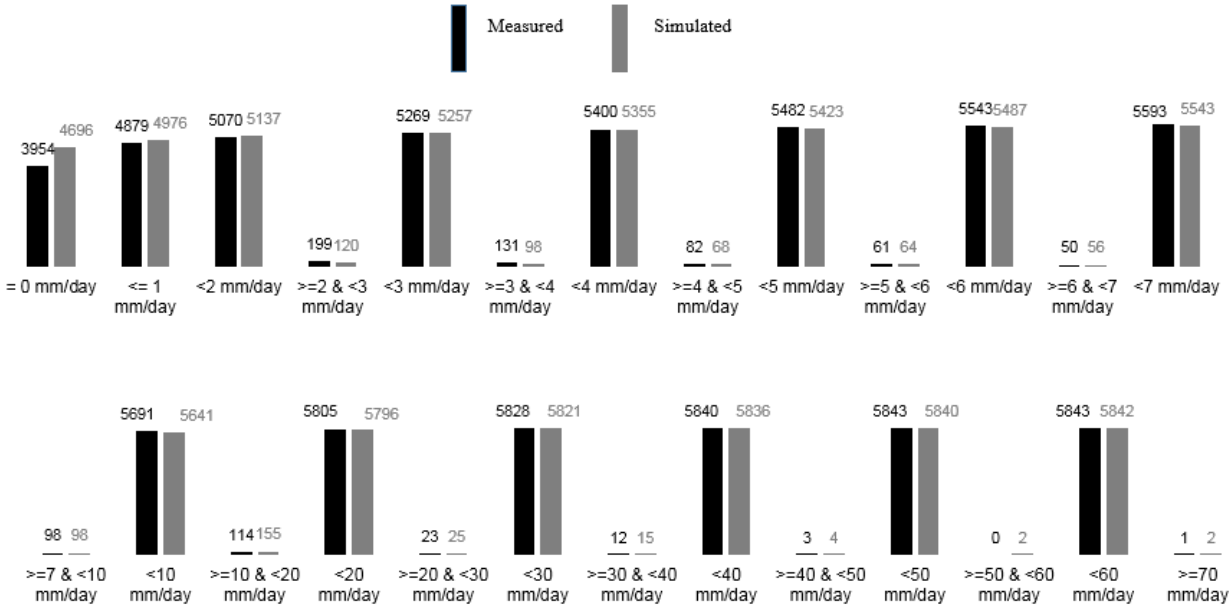

Figure. B.4.4: Comparison of measured and simulated precipitation occurrences

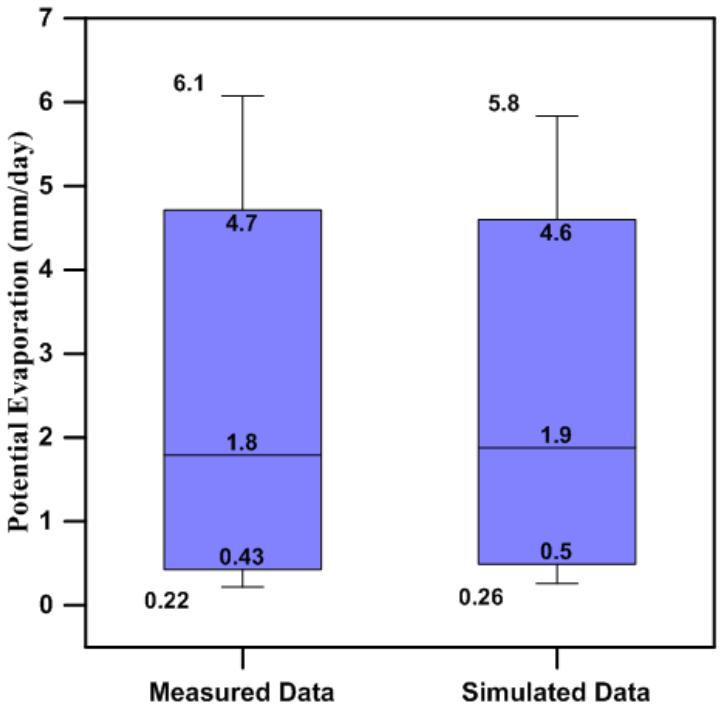

Figure. B.4.5: Comparison of measured and simulated potential evaporation

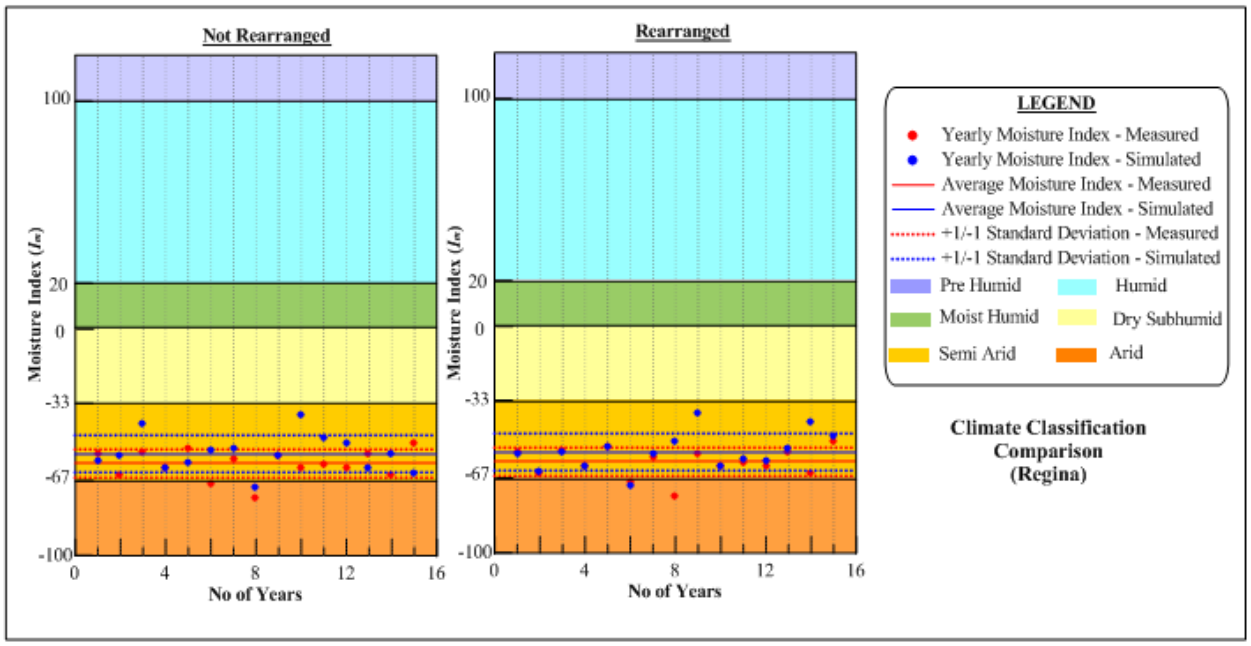

Figure. B.4.6: Comparison of measured and simulated climate classification

Appendix B.5 – Comparison of climate data – St. John's

Table. B.5.1: Comparison statistics for measured and simulated data

Variable	R^2	RMSD	MAD
Solar Radiation	0.95	1.96	1.41
Maximum Temperature	0.98	1.25	0.99
Minimum Temperature	0.99	0.83	0.66
Wind Speed	0.22	0.96	0.72
Dew Point Temperature	0.98	1.01	0.79
Relative Humidity	0.04	4.49	3.64

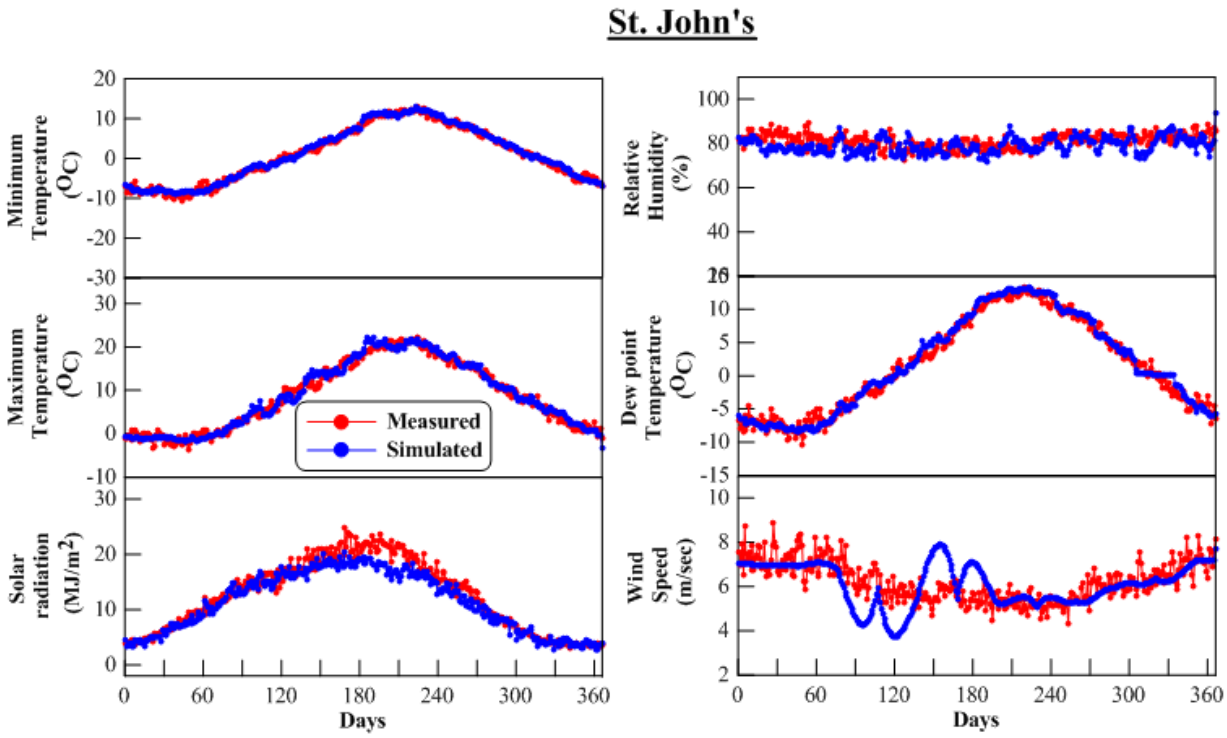

Figure. B.5.2: Comparison of measured and simulated data

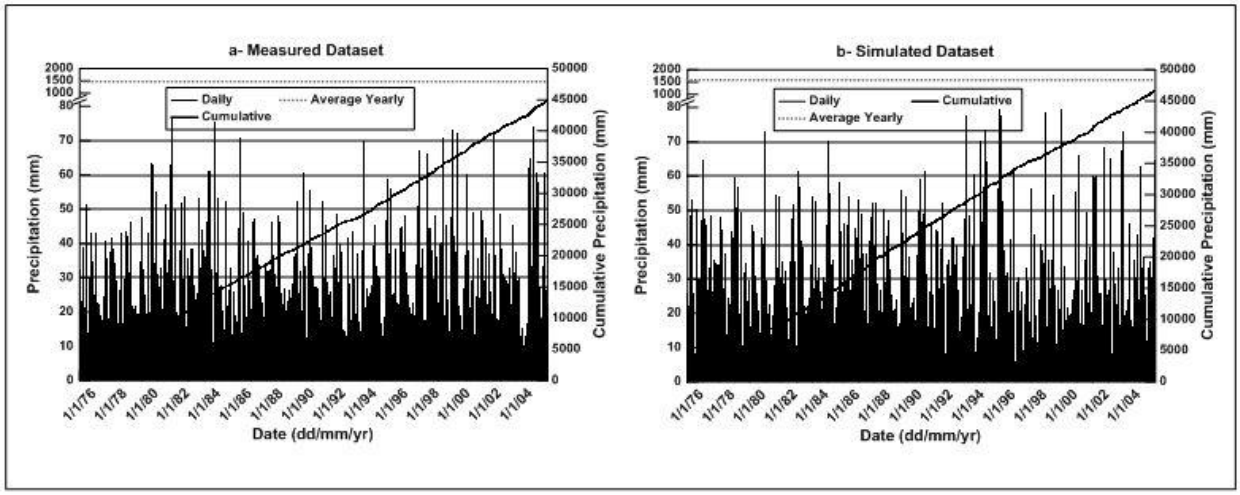

Figure. B.5.3: Comparison of measured and simulated precipitation

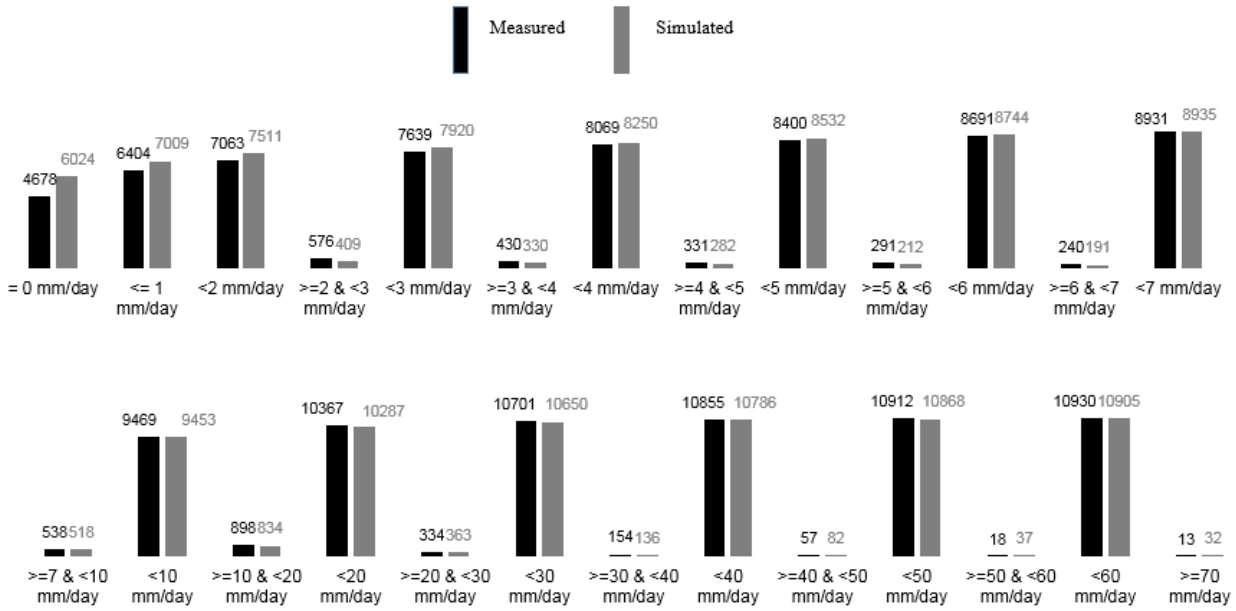

Figure. B.5.4: Comparison of measured and simulated precipitation occurrences

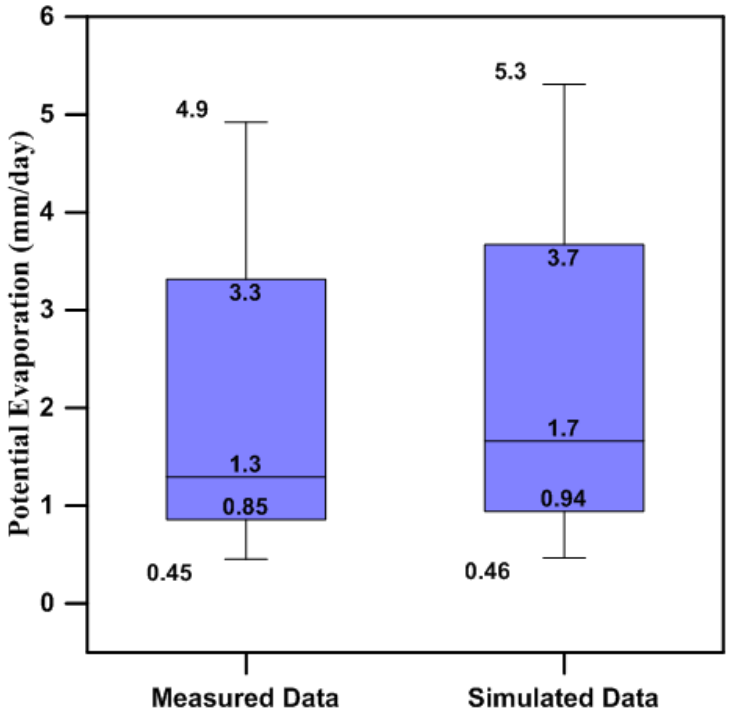

Figure. B.5.5: Comparison of measured and simulated potential evaporation

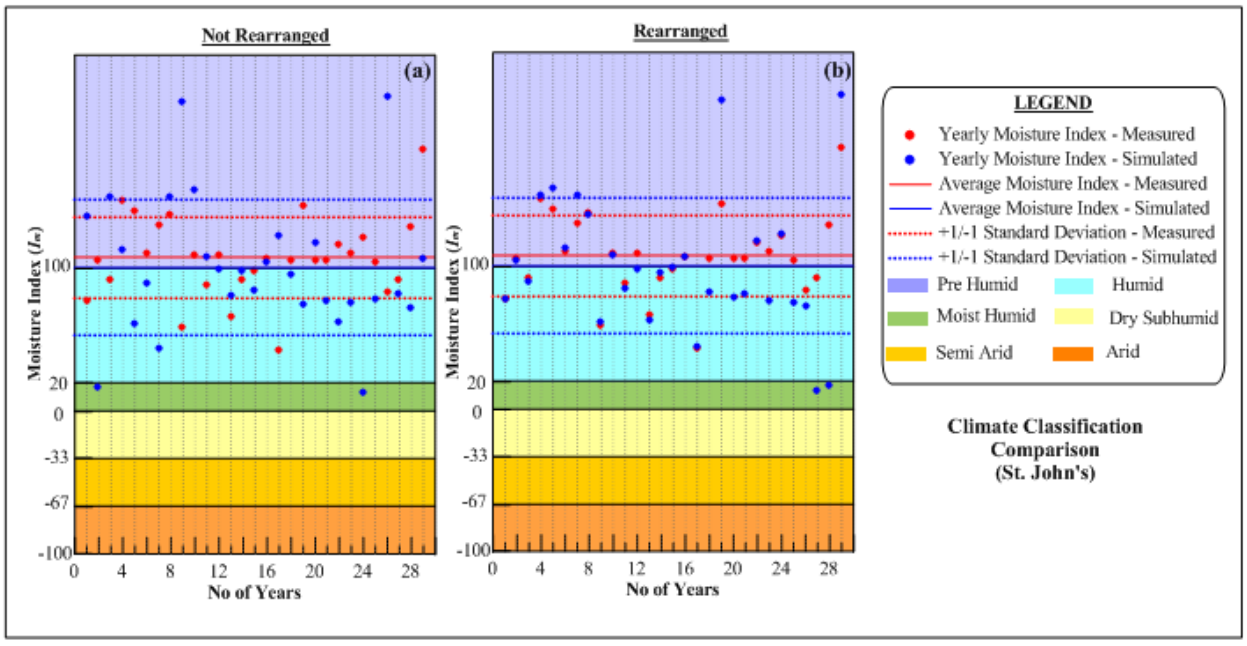

Figure. B.5.6: Comparison of measured and simulated climate classification

Appendix B.6 – Comparison of climate data – Vancouver

Table. B.6.1: Comparison statistics for measured and simulated data

Variable	R^2	RMSD	MAD
Solar Radiation	0.97	1.43	1.09
Maximum Temperature	0.96	1.21	0.96
Minimum Temperature	0.96	1.13	0.89
Wind Speed	0.66	0.41	0.37
Dew Point Temperature	0.96	1.41	1.19
Relative Humidity	0.24	8.38	7.07

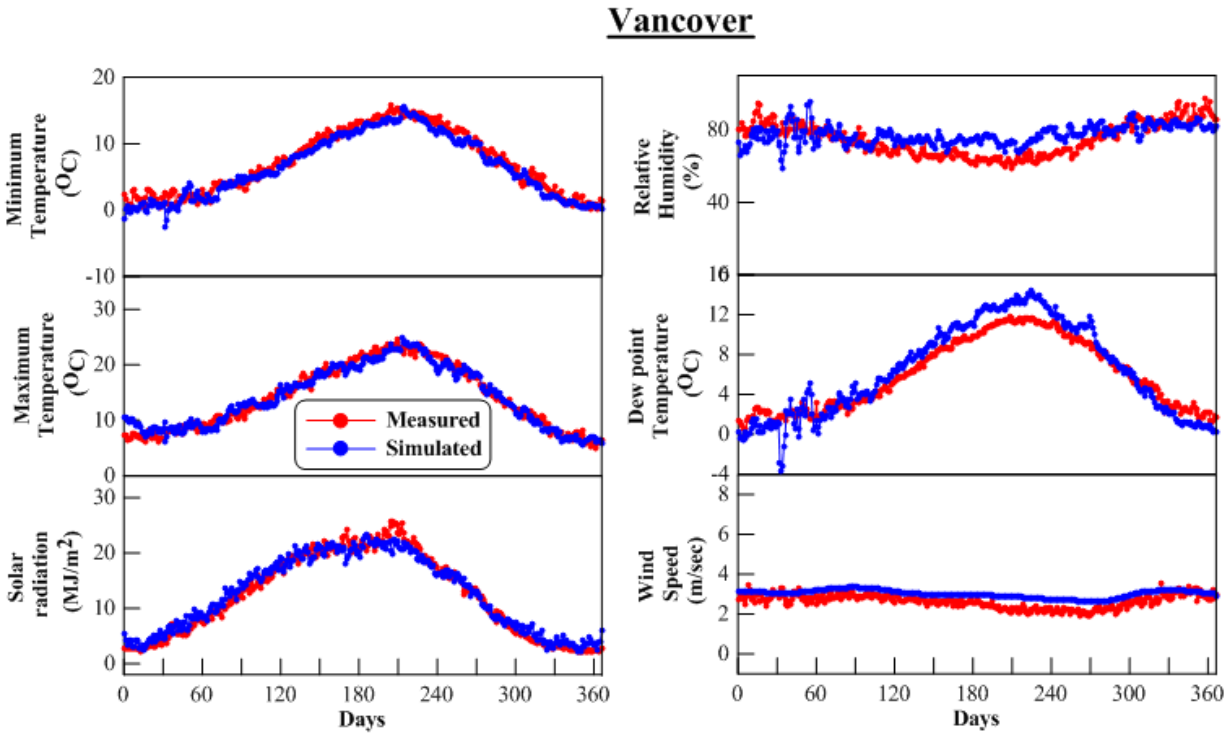

Figure. B.6.2: Comparison of measured and simulated data

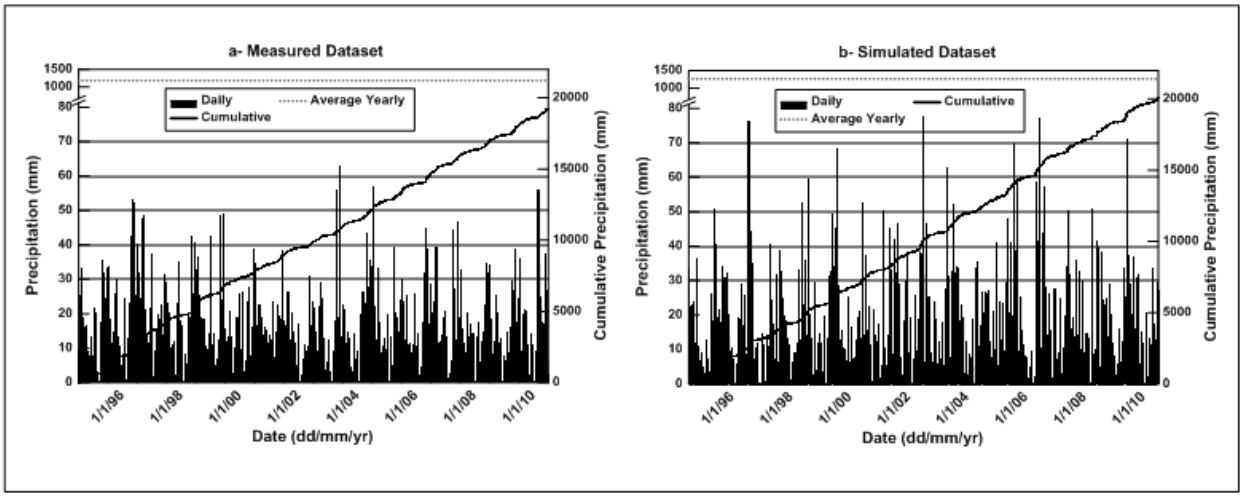

Figure. B.6.3: Comparison of measured and simulated precipitation

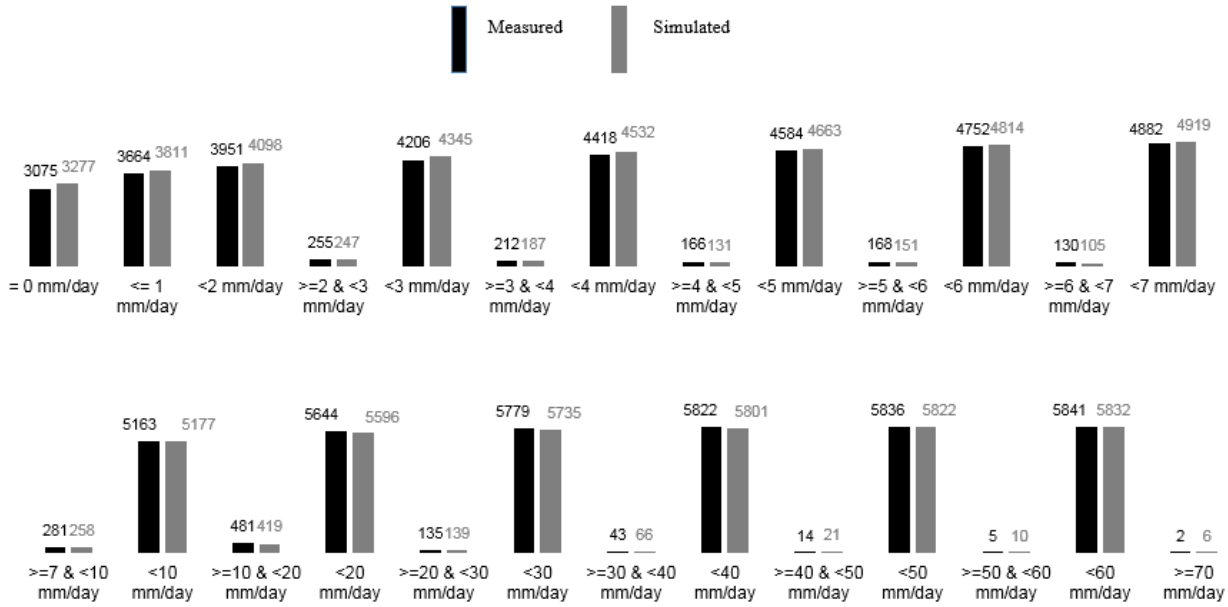

Figure. B.6.4: Comparison of measured and simulated precipitation occurrences

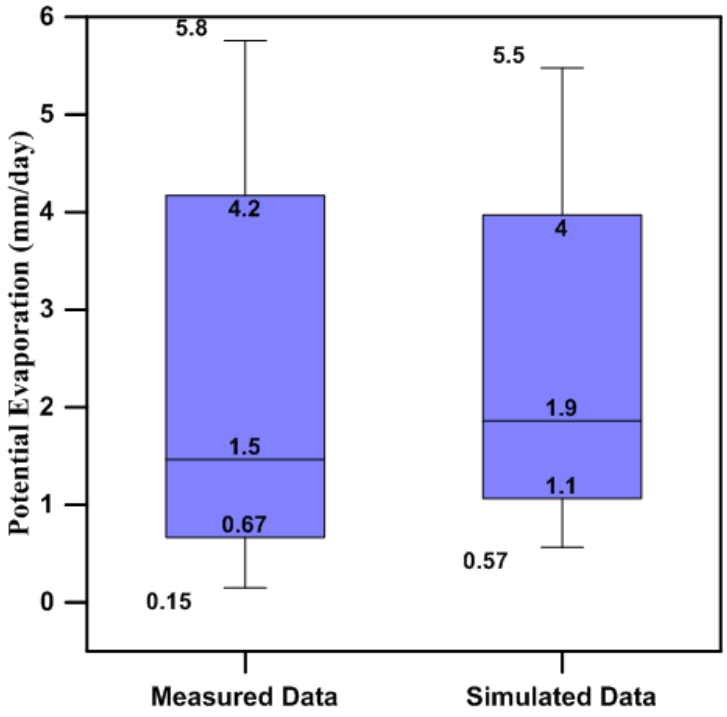

Figure. B.6.5: Comparison of measured and simulated potential evaporation

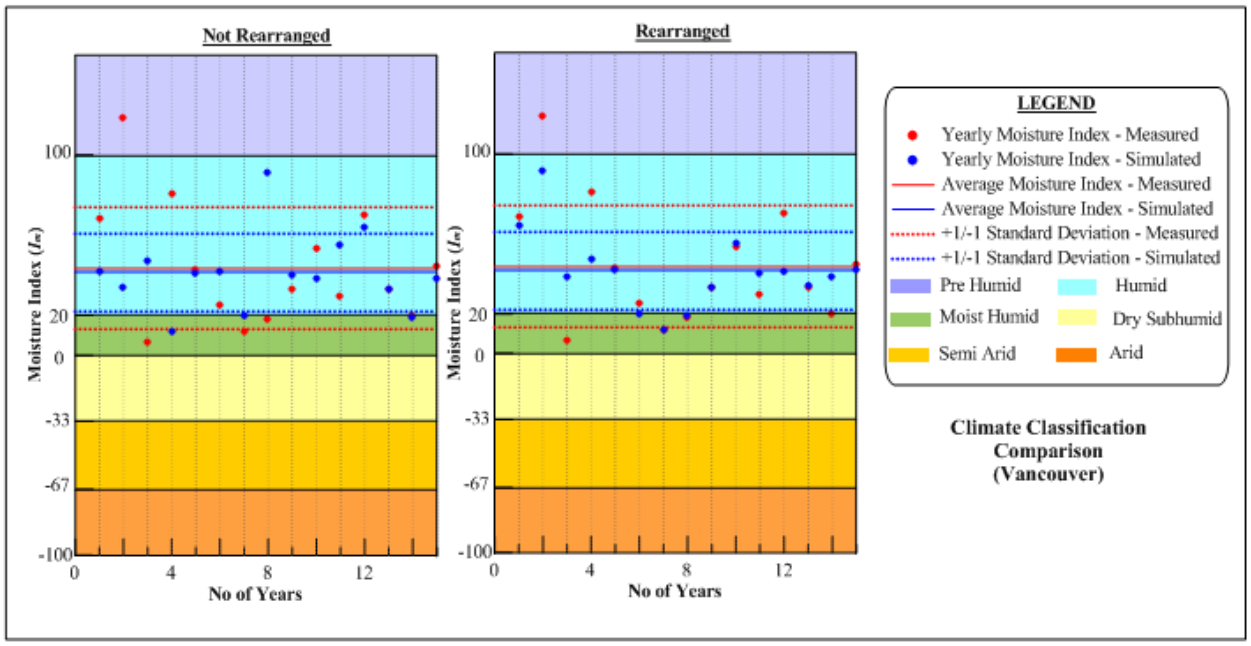

Figure. B.6.6: Comparison of measured and simulated climate classification

Appendix B.7 – Comparison of climate data – Barriere

Table. B.7.1: Comparison statistics for measured and simulated data

Variable	R^2	RMSD	MAD
Solar Radiation	0.94	1.92	1.49
Maximum Temperature	0.97	2.10	1.69
Minimum Temperature	0.95	1.91	1.51
Wind Speed	0.08	0.65	0.52
Dew Point Temperature	0.94	2.27	1.86
Relative Humidity	0.76	8.72	7.16

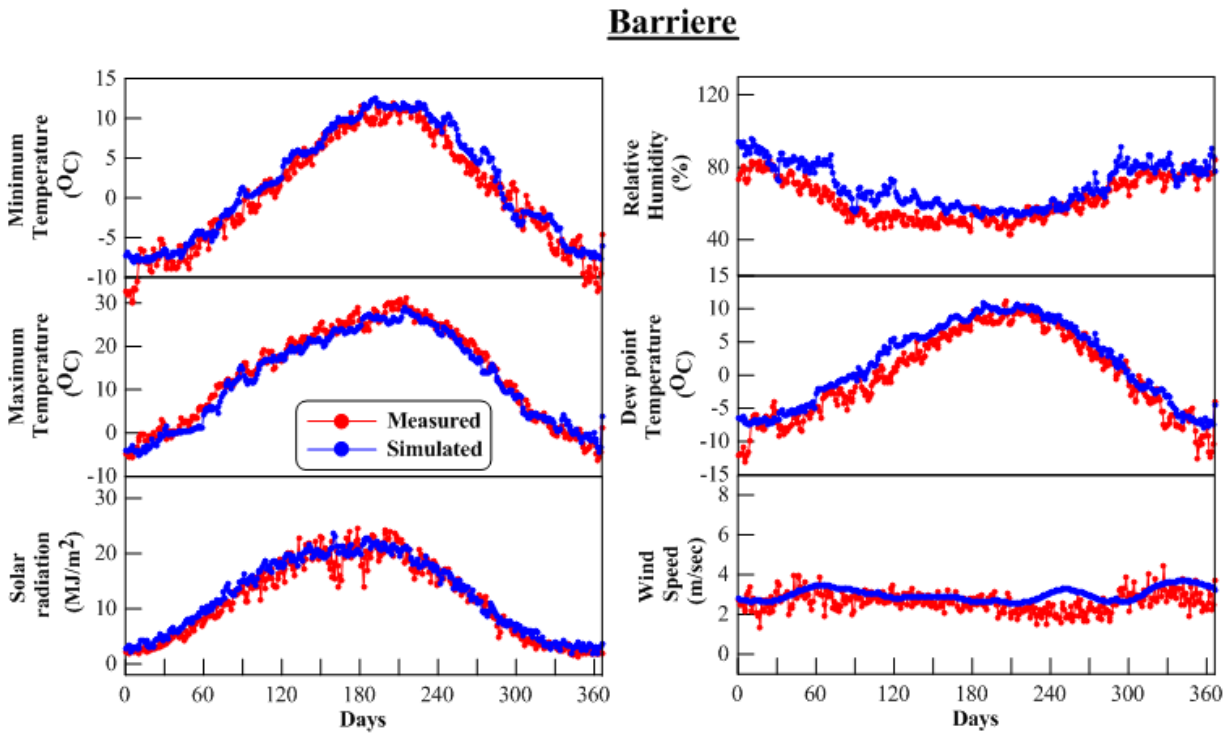

Figure. B.7.2: Comparison of measured and simulated data

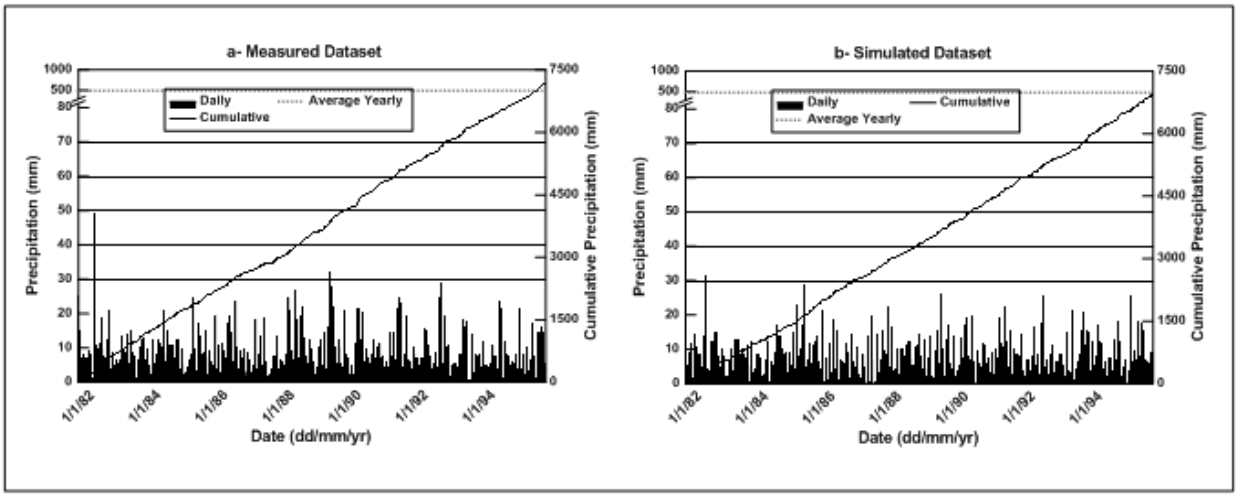

Figure. B.7.3: Comparison of measured and simulated precipitation

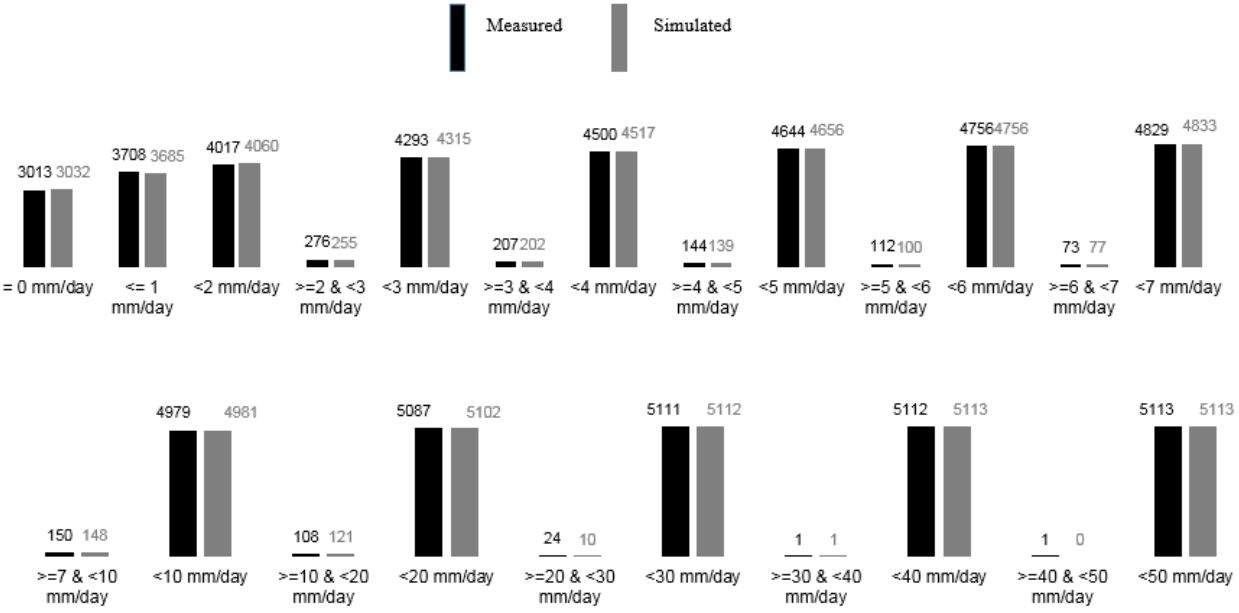

Figure. B.7.4: Comparison of measured and simulated precipitation occurrences

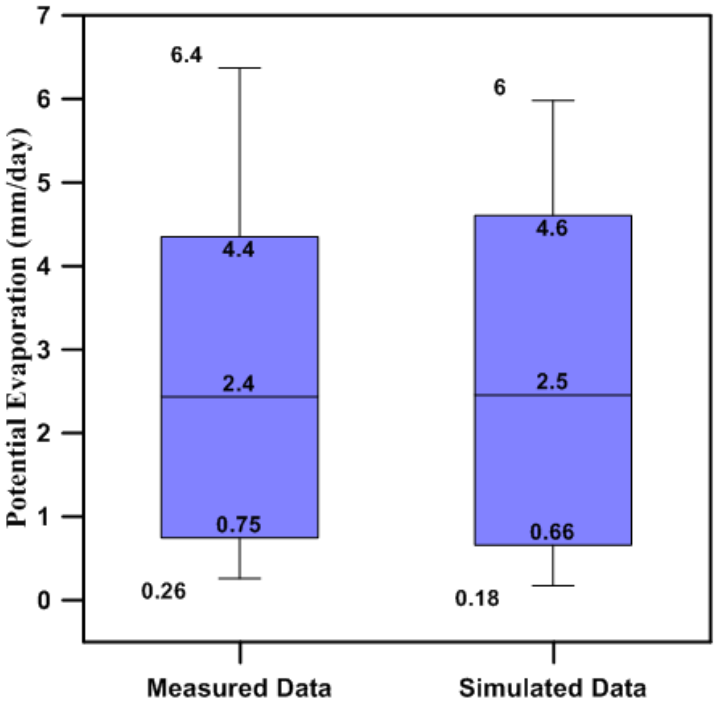

Figure. B.7.5: Comparison of measured and simulated potential evaporation

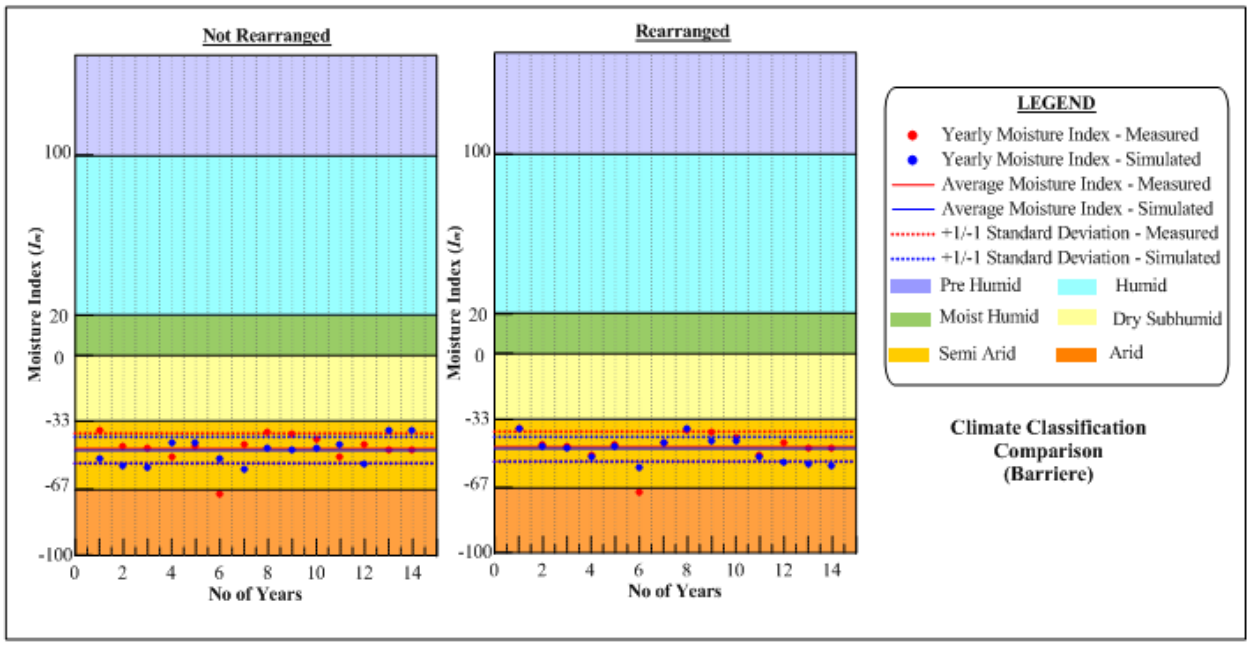

Figure. B.7.6: Comparison of measured and simulated climate classification

Appendix C.1 – *SIMETAW* – User Manual

TITLE PAGE

SIMETAW contains menu bars and toolbar buttons at the top of the title page, which allow for data input, output, and statistical analysis. Pulls down menus are available at the top of the title page. Alternatively, there are toolbar buttons just below the pull down menus. The headings and subheadings in the menu bar correspond to toolbar buttons that are listed immediately below. The operations are identical. An explanation of the pull down headings and subheadings are given on the next page.

Figure 1. Either the pull down menus or the toolbar buttons can be used to manage the SIMETAW program.

MENU BARS TO MANAGE SIMETAW

Choose pull down menu bars to tell *SIMETAW* what to do. *SIMETAW* contains eight menu bar headings. The menu bar headings are “Create Data Files,” “Apply Data Files,” “Output Files,” “Statistics,” “Help,” “About *SIMETAW*,” “Disclaimer,” and “Help About”. Each menu bar heading contains subheadings, which are briefly described below.

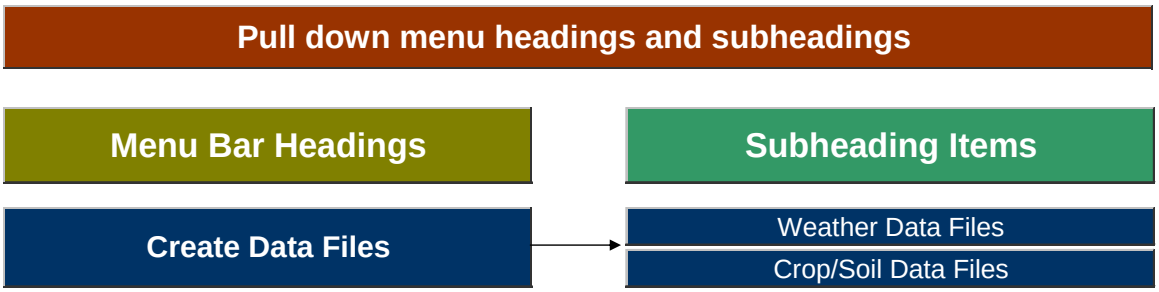

“Create Data Files” Menu Bar - used to create weather and crop/soil data files for managing SIMETAW.

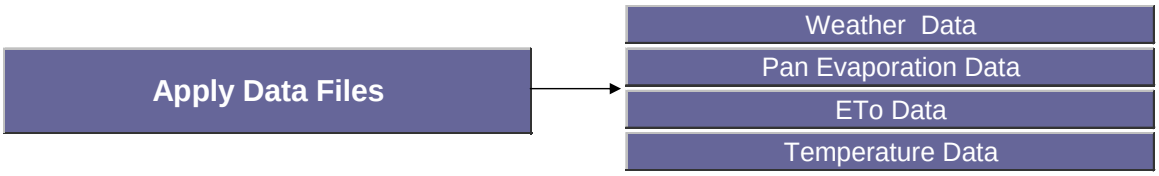

“Apply Data Files” Menu Bar - used to select weather, pan evaporation, reference evapotranspiration (ET_o), and temperature data to run *SIMETAW* for water balance calculations for the period of record.

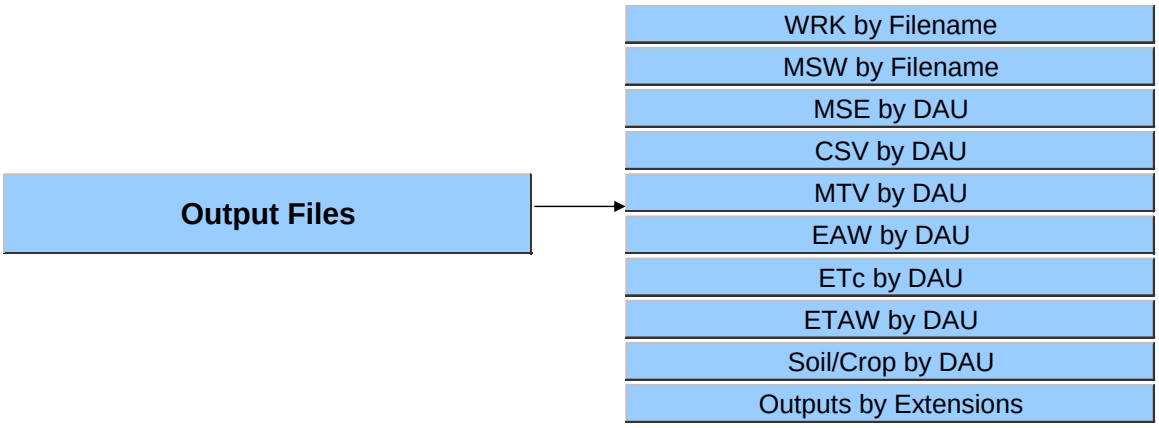

"Output Files" Menu Bar - used to view files created by *SIMETAW* on the computer screen.

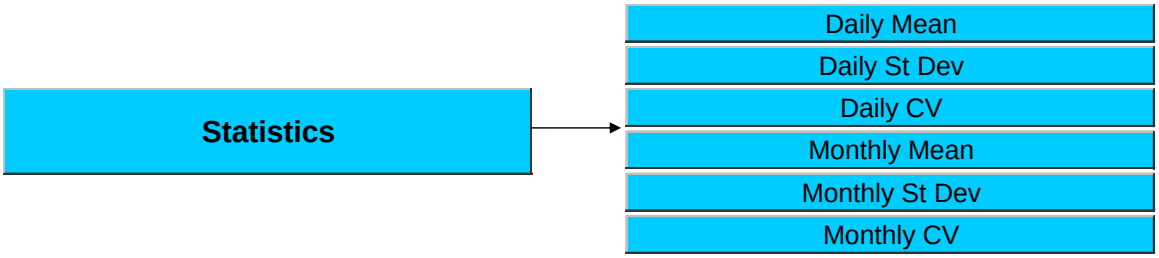

"Statistics" Menu Bar - used to show daily and monthly water balance statistics (mean, standard deviation and coefficient of variability) over the years of record.

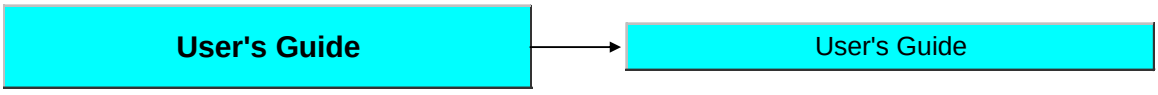

"User's Guide" Menu Bar - explains how to manage the *SIMETAW* program for making water balance calculations.

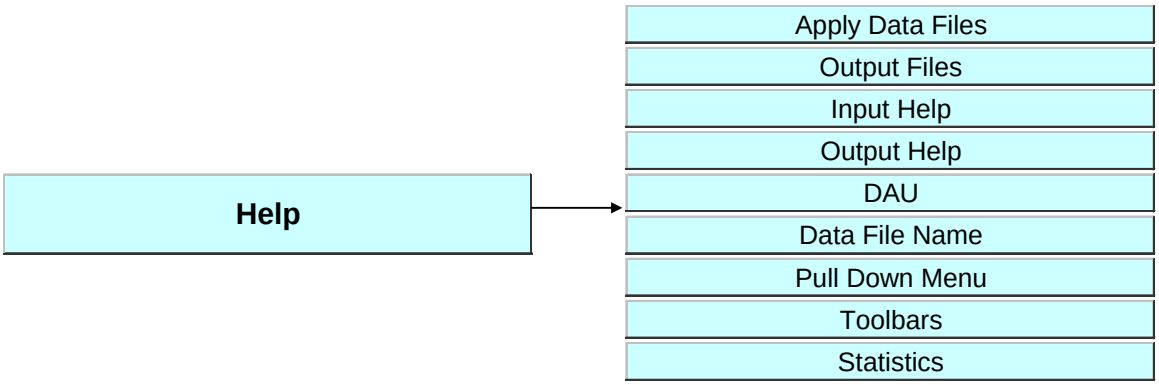

"Help" Menu Bar - provides step-by-step instructions on how to select the type input data files for water balance calculations and display files created by *SIMETAW*. In addition, it gives examples of the data format used in the input and output files.

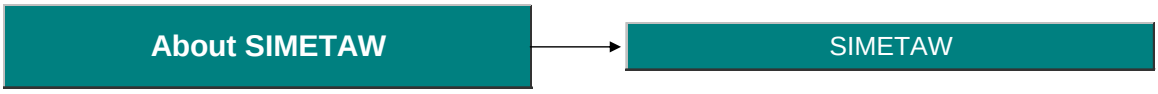

"About SIMETAW" Menu Bar - explains the *SIMETAW* program.

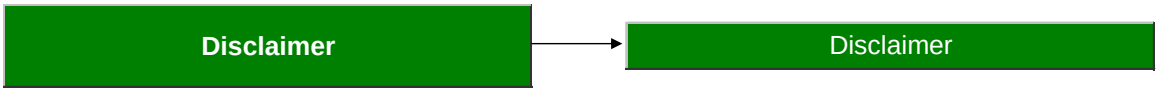

"Disclaimer" Menu Bar - explains that the California Department of Water Resources is not responsible for the accuracy, completeness, and quality of the data coming from the program.

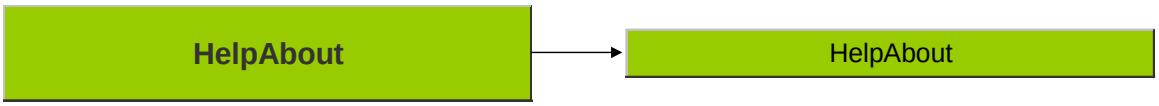

"HelpAbout" Menu Bar - Provides information about the program.

When you start the *SIMETAW* program, the title page opens. To begin working, you need to select menu bars or tool bars to tell SIMETAW what to do. The "Create Data Files" menu bar allows you to select a file extension and to create weather and soil/crop data base files in Microsoft Excel for managing *SIMETAW*. When you select the "Create Data Files" menu bar, the program will display a list of subheadings that you can use to create weather and soil/crop data bases in *SIMETAW* for making water balance calculations. As you can see in Figure 2, the "Create Data Files" menu

bar contains “Weather Data Files” and “Crop/Soil Data Files” subheadings. The formats for data bases are explained in chapter 2.

When you select the “Apply Data Files” menu bar, *SIMETAW* will display a list of subheadings that you can use to select the type of data for the water balance calculations.

The “Apply Data Files” menu bar allows you to select weather, pan evaporation, ET_o, and temperature data to run the *SIMETAW* application to make water balance calculations within a study area (*SA*) over the period of record. For example, to use weather data to make water balance calculations within a *SA* over the period of record, select the “Apply Data Files” menu bar at the top of the title page and then choose the “Weather Data” subheading. As seen in Figure 3, the “Apply Data Files” menu bar contains “Weather Data,” “Pan Evaporation Data,” “ETo Data,” and “Temperature Data” subheadings. You can also choose the toolbar buttons from the title page to select input data files for running the application. As described below, there are ten possible ways to use input data files in SIMETAW to make water balance calculations.

Figure 2. Window showing a list of subheadings of the “Create Data Filers” menu bar.

Figure 3. Window showing a list of subheadings of the "Apply Data Filers" menu bar

CREATING WEATHER DATA FILES

The "Create Data Files" Menu Bar

Selecting the "Weather Data Files" Subheading

This subheading from the "Create Data Files" menu bar allows you to select a file extension and to create a data base file in Microsoft Excel for analysis by *SIMETAW*. The formats for data bases are explained below. Creating a data base file is the first step to make the program work for you. In the *SIMETAW* model, all weather data files have a five-character filename with a three-character extension. In this user's guide, we use the generic filename "nnnnn" for discussion. The three-character extensions and the format for data files depend on the types of data, which are explained below. You can easily create a database for weather by using this menu bar. There are ten possible input data files for the *SIMETAW* program. The data base formats for the file extensions are explained later. The extensions corresponding to input data base types are:

nnnnn.day - This file name is used when daily raw weather data are used directly to make water balance calculations for the period of record. Weather data include, solar radiation, maximum and minimum temperature, dew point temperature, wind speed, and precipitation. Data in nnnnn.day must be in the proper order with the correct units [i.e., solar radiation ($MJm^{-2}\ d^{-1}$), maximum temperature (^oC), minimum temperature (^oC), wind speed ($m\ ^{-1}s$), dew point temperature (^oC), and precipitation (*mm*)].

nnnnn.dmn - This file name is used when daily weather data are first converted to mean daily climate data by month, which are used to simulate daily weather data over a specified number of years.

nnnnn.mon - This file name is used when mean daily weather data, total precipitation and number of rainy days by month are used in *SIMETAW* to simulate daily weather data for a specified number of years to calculate ET_o using the Penman-Monteith equation.

nnnnn.rtm - This file name is used when daily raw temperature and precipitation data are used to estimate ET_o (reference evapotranspiration) and water balance calculations for the period of record.

nnnnn.dtm - This file name is used when daily temperature data are first converted to mean daily temperature data by month, which are used to simulate daily temperature data over a specified number of years.

nnnnn.mtm - This file name is used when only daily mean temperature, total precipitation and number of rainy days by month are used to simulate many years of daily ET_o data using the Hargreaves-Samani equation.

nnnnn.det - If daily or monthly weather data are not available, daily ET_o can also be used. This file name contains daily raw ET_o and precipitation data for direct water balance calculations for the period of record.

nnnnn.etm - This file name is used when daily mean ET_o and temperature, total rainfall and number of rainy days by month are used in SIMETAW to simulate many years of daily ET_o data from direct input of monthly ET_o.

nnnnn.dpn - This file name is used when daily raw pan evaporation and precipitation data are used to estimate ET_o (reference evapotranspiration) and water balance calculations for the period of record.

nnnnn.mpn - This file name is used when daily mean pan evaporation, total precipitation and number of rainy days by month are used to simulate daily ET_o data over a specific number of years.

When you select the “Weather Data Files” subheading from the “Create Data Files” menu bar, SIMETAW will display a list of the file extensions in a dialog box that you can select to create a weather data base for water balance calculations.

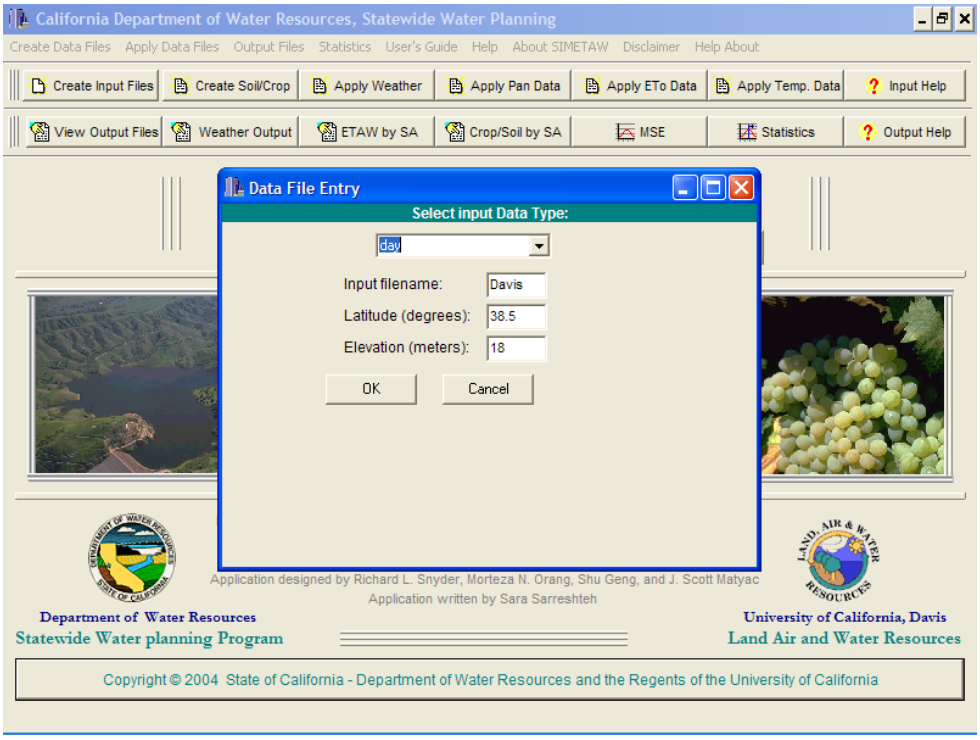

Figure 4. Window showing the dialog box for selecting a file extension for creating a weather data base.

After selecting an extension file and entering the corresponding weather site information in the dialog box, SIMETAW displays a file with Excel for entering input data requirements.

Davis.mon	38.5	18						
Mo	Solar	TMax	TMin	Wind	Td	Pcp	NRD	Pan
#	MJ/m^2	oC	oC	m/s	oC	mm	#	mm
1								-999
2								-999
3								-999
4								-999
5								-999
6								-999
7								-999
8								-999
9								-999
10								-999
11								-999
12								-999

The first row contains the file name, latitude, and elevation. The second row indicates the variables, and the third row has the units. Rows 4-12 contain the mean daily values by month for R_s, T_{max}, T_{min}, Wind, and T_d. It also has the monthly total precipitation and the mean number of rainy days per month. The right-hand column contains pan evaporation data. For 'nnnnn.mon', the pan column contains -999 to indicate missing data. When finished entering the weather data for a weather station, the "name.mon" file can be saved as a comma delimited in the directory where the *SIMETAW* program exists.

Note:

Before you begin to run the application, make sure that you close the Excel files you have just created, but do not exit from the Excel program until you are finished using SIMETAW. Otherwise, you cannot open other Excel files without exiting from SIMETAW.

Note:

When the file is displayed with Excel, all of the headings will initially show in column A of the worksheet. To separate variables into columns, click on the drop-down heading 'Data' and then the subheading 'Text to Column'. Then choose delimited and comma (,) as the delimiter to display the data in columns. An exaple of a "nnnnn.mon" file format is shown in Table 1.

Table 1. A sample of a "name.mon" file format.

CREATING CROP AND SOIL DATA FILES

Selecting the “Crop/Soil Data Files” Subheading

This feature helps you to create a database for particular soil and crop combinations for the water balance calculations. When you select the “Crop/Soil Data Files” subheading from the “Apply Data Files” menu bar or select the “Crop/Soil Data” toolbar, a window for data input is displayed (Figure 5).

You input soil and crop characteristics and the area planted (acreage) within a SA or study area, which is a region with a similar ET_o rate. These are used to determine effective rainfall and ET of applied water (ET_{aw}). After completing the form, save the input values as a row of data in the file ‘SAnnnnn.csv’ where ‘nnnnn’ is a 5-digit number 1-99999, which identifies the SA. For entries to be accepted, the SA number, crop name and acreage planted must be entered. If there are no entries for other variables, defaults are automatically included. To save the SAnnnnn.csv file, click ‘Save’ at the bottom of the window and enter the same path as where the SIMETAW program resides. If you decide not to save the entries, click on “Exit” rather than “Save”.

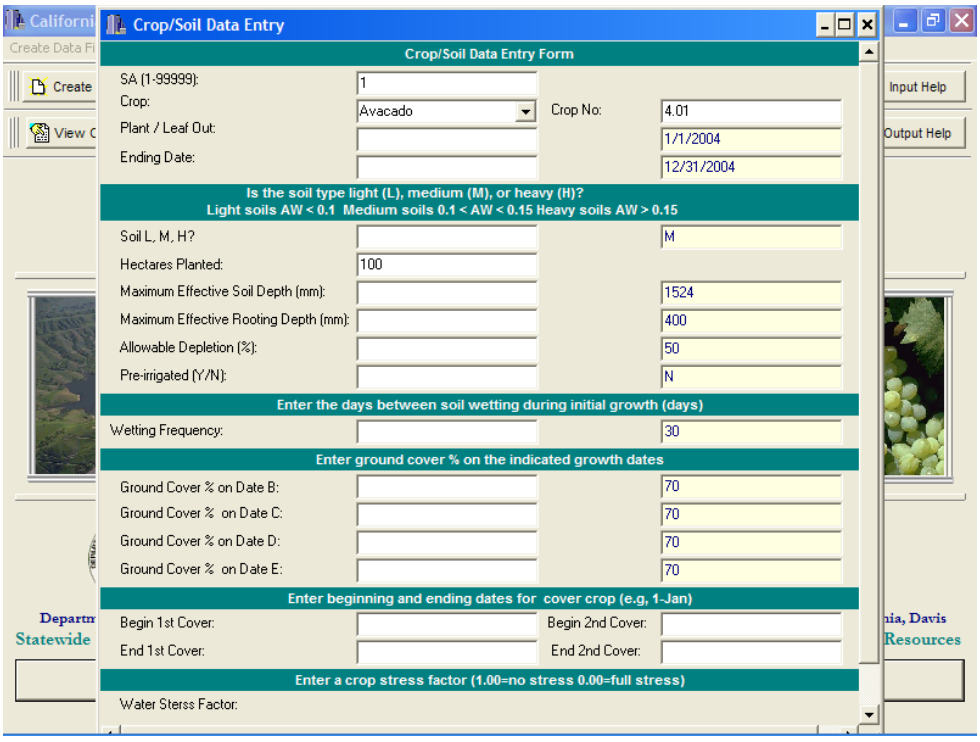

Figure 5. Window showing the form for entering crop and soil information for determining ET_{aw}.

Data are saved in a row of the SAnnnnn.csv file. After saving one can go onto the next crop and soil combination entry. When finished entering all of the crop and soil combinations for a particular SA, save the SAnnnnn.csv file.

SA (Study Area)

The study area (SA) is a number used to identify regions of similar reference evapotranspiration (ET_o) in California. For users outside of California, it is simply a method to identify a region. Any number from 1 through 99999 can be used. The crop number identifies a particular crop that will be used in the ET_{aw} analysis. Clicking the arrow on the right side of the input cell will display crop choices. When a crop is selected, a default planting or leaf out date and an ending date for the crop are displayed. These are only sample dates that are typical within the main growing region California and they can be changed to appropriate values for other regions.

Entering Crop and Soil Information

To run the application to determine ET_{aw} within a SA, you are also required to enter the crop and soil information into a data file specific to that SA. The input data include as following:

- A 5-digit SA number (1-99999)
- Crop name
- Planting date
- Ending date

1. Soil type

   If the input soil type is light, then enter ‘L’. Alternatively, use the characters ‘M’ and ‘H’ for medium and heavy textured soils).

- Acreage planted
- Maximum soil depth in inches (depth to hard pan or rock)
- Maximum effective rooting depth during growing season (in)
- Allowable depletion (%)

1. Pre-irrigation (Y/N)

   If there is a pre-irrigation, enter 'Y'. The character 'Y' means that there is pre-irrigation. The character 'N' indicates that there is no pre-irrigation)

1. Initial growth wetting frequency

   Irrigation frequency is the number of days between irrigation events during the initial growth period. (30 days is the default value). If a value more frequent than 30 days is input, the input irrigation frequency will be used.

- Ground cover percentage on date B, C, D, and E, which are used to account for immaturity effect on K_c values for tree and vine crops. Values of '70%' or greater indicate that the tree or vine crop is mature.

1. Cover crop dates

   If there is a cover crop for tree and vine crops, enter the beginning and ending dates. There can be two periods of cover crops during a year.

- Stress factor, (K_s)

  When K_s = 1, then it is assumed that there is no water stress. Lower values of K_s will reduce the crop evapotranspiration below the unstressed ET_c. Note that the default K_c values in SIMETAW are for unstressed crops.

Using data from each row of the SAnnnnn.csv file, SIMETAW determines a hypothetical irrigation schedule to calculate seasonal and annual ET_{aw} data.

Table 12 describes the variables contained in each row of the SAnnnnn.csv file.

Table 12. An example of 6 rows of a SAnnn.csv file.

Code	crop	Date	Date	Area	Dept	R.Dep
		DOY	DOY	acres	inches	inches
D001C2.01305151MNMks1.00IF30N	AlfaAlfa(annual)	305	151	0	60	78.74
D001C1.04305151MNMks1.00IF30N	Barely	305	151	0	60	59.06
D001C3.0191319MNMks1.00IF30N	Almonds	91	319	0	60	78.74
D001C1.34121273MNHks1.00IF30N	Rice	121	273	0	60	39.37
D001C1.34121273MNMks1.00IF30N	Rice	121	273	0	60	39.37
D001C1.34121273MNMks1.00IF30N	Rice	121	273	0	60	39.37

Crop Allowable	Available Water	Plant Available	Yeild Threshold	initial Growth	Date B	Date C	Date D
Depl	H.C	Water	Depl	W. Freq	G.C	G.Co	G.C
fraction	in/in	inches	fraction	day	%	%	%
50	0.12	7.5	3.75	30	0	0	0
50	0.12	7.38	3.69	30	0	0	0
50	0.12	7.5	3.75	30	0	70	70
50	0.17	6.89	3.44	30	0	0	0
50	0.12	4.92	2.46	30	0	0	0
50	0.12	4.92	2.46	30	0	0	0

Date E	#1 Begin	#1 End	#2 Begin	#2 End	% to	% to	% to					
G.C	C.C	C.C	C.C	C.C	Date B	Date C	Date D	Kc1	Kc2	Kc3	Ks	Pre-Irr
%	DOY	DOY	DOY	DOY				()	()	()	()	()
0	0	0	0	0	25	50	75	1	1	1	1	N
0	0	0	0	0	20	45	75	1.05	0.15	1.5	1	N
0	0	0	0	0	0	50	90	0.55	1.05	0.65	1	N
0	0	0	0	0	1	30	80	1.4	1.03	0.8	1	N
0	0	0	0	0	1	30	80	1.4	1.03	0.8	1	N
0	0	0	0	0	1	30	80	1.4	1.03	0.8	1	N

READING CLIMATE DATA FILES

It is possible to enter weather data from other sites within or outside of California as long as the data files have the proper format. You can use either daily mean weather data by month or raw weather data in SIMETAW for the calculations of ET_o. Weather data include, solar radiation, maximum and minimum temperature, dew point temperature and wind speed.

Using monthly data, daily data are simulated first and then ET_o calculations are made from the generated data. The monthly mean weather and ET_o data averaged over the period of record from CIMIS are available from the California Climate Data program on your CD.

The program allows for input of daily mean of ET_o and rainfall data by month or daily mean evaporation pan and rainfall data by month. If pan data are input, then the program automatically estimates daily ET_o rates using a fetch value (i.e. upwind distance of grass around the pan) without the need for wind speed and relative humidity data. If daily raw weather data are used, then SIMETAW calculates ET_o directly from the raw data.

USING WEATHER DATA TO DETERMINE ET_{aw}

Selecting the “Weather Data” Subheading

This allows you to select the weather data to make water balance calculations within a SA for a specified number of years. If the “Weather Data” subheading from the “Apply Data File” menu bar is selected, SIMETAW will display a window with a dialog box that you can use to choose the type of data to analyze. The selections include simulated and non-simulated (Figure 6).

Figure 6. Dialog box allows for simulated-weather and non-simulated data selection.

Selecting Simulated-Weather Path

After selecting Simulated-Weather from the dialog box, *SIMETAW* asks you to choose daily or monthly average data (Figure 7).

Figure 7. Dialog box allows for daily or monthly data selection.

Then the application asks you to enter the site information including the filename, latitude, elevation, SA number, and years to simulate. Entry of site information is described in the Weather Site Information section. For simulated raw data, the file extension is ‘dmn’. For simulated monthly mean data, the file extension is ‘mon’.

Selecting Non-Simulated Path

If non-simulated is selected, SIMETAW then will ask for the site information including, latitude, elevation, and SA number, as shown in Fig. 8.

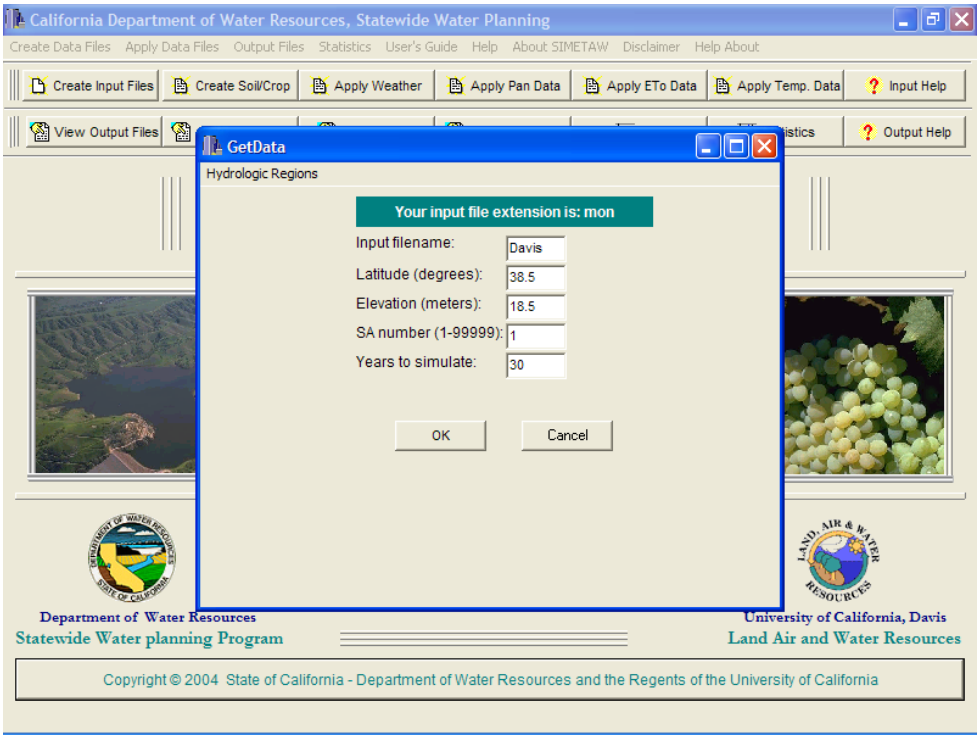

Figure 8. Dialog box allows for raw or CIMIS data selection.

For non- simulated raw data, the file extension is “day”.

A Flow Diagram of the “Weather Data” Subheading Selection

The flow diagram below shows the simulated and non-simulated paths for the “Weather Data” selection.

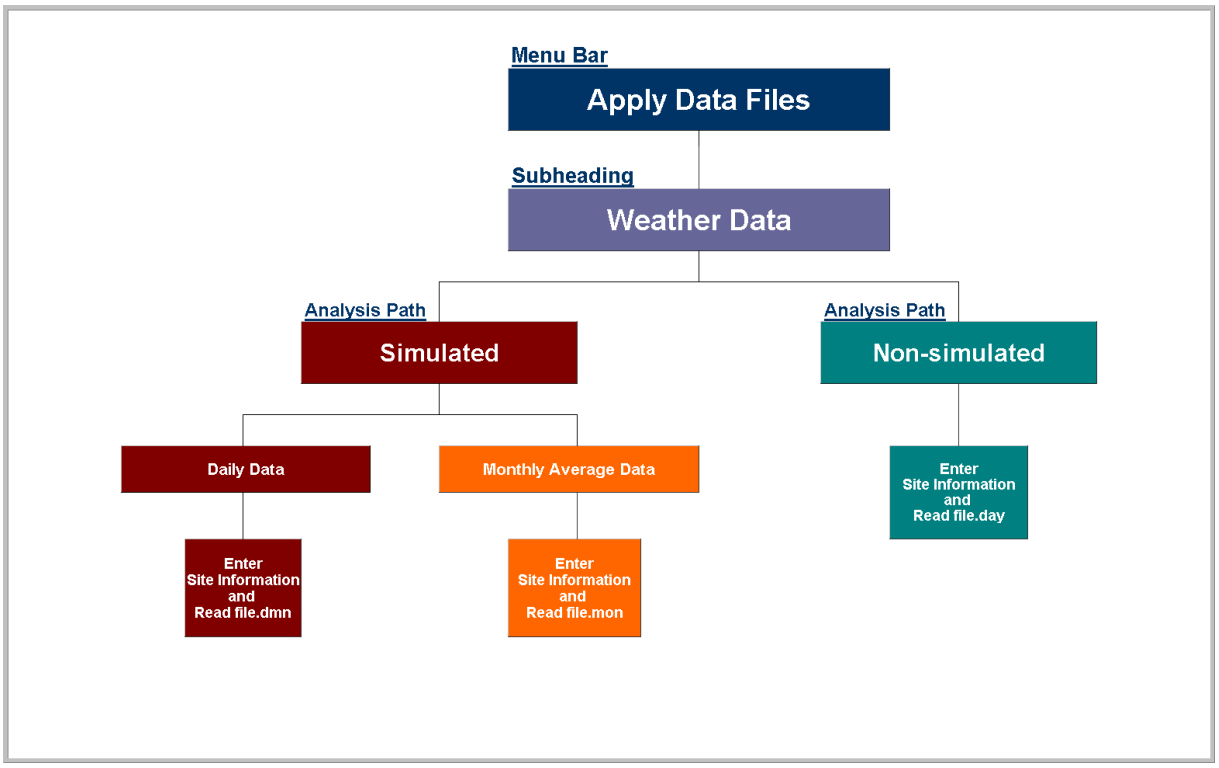

Figure 9. Flow chart for the drop down weather data selection.

ENTERING WEATHER SITE INFORMATION

After selecting the type of weather data and type of analysis, *SIMETAW* displays your input file extension (e.g., mon, day) and then asks for the weather site information. When you select a CIMIS station from the "Hydrologic Regions" menu bar in the dialog box, *SIMETAW* will automatically display the corresponding stored site information and 30 years to simulate in the program.

If the site information is different from *SIMETAW* defaults, you can change them by making entries into the dialog box. For example, shown in the above figure, the "Hydrologic Region" bar menu in the dialog box was used to select the Davis monthly data to run the simulation program and generate 30 years of data.

After clicking the "OK" button, the program simulates the selected number of years of daily weather data from climatic records and to estimate reference evapotranspiration (ET_o). Then soil and crop information are used to generate ET_c and hypothetical irrigation schedules to estimate the seasonal and annual evapotranspiration of applied water (ET_{aw}) for each crop for the specified number of years.

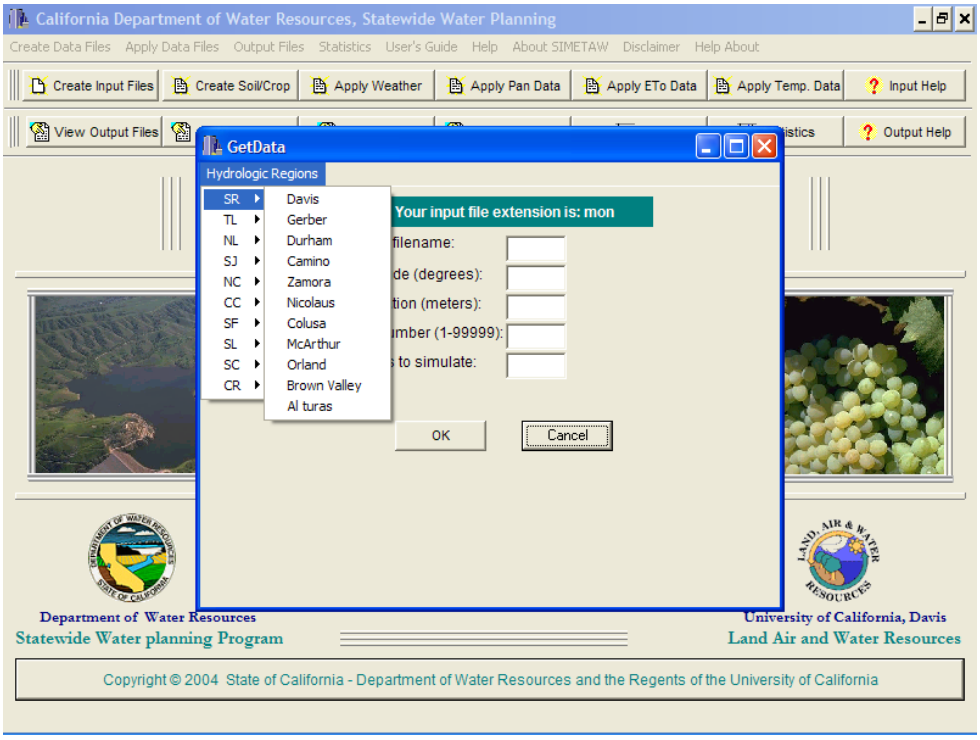

Figue 10. Dialog box allows for CIMIS weather station selection for including the site information.

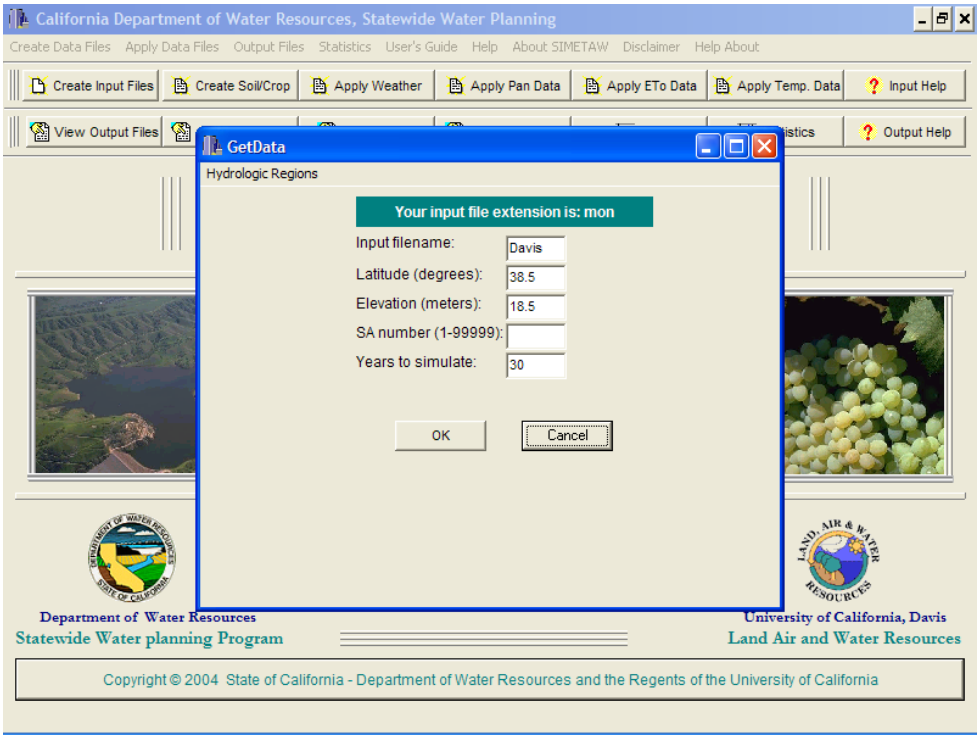

Figure 11. Window showing a dialog box with a filename, latitude, elevation, SA number, and 30 years to simulate daily weather data.

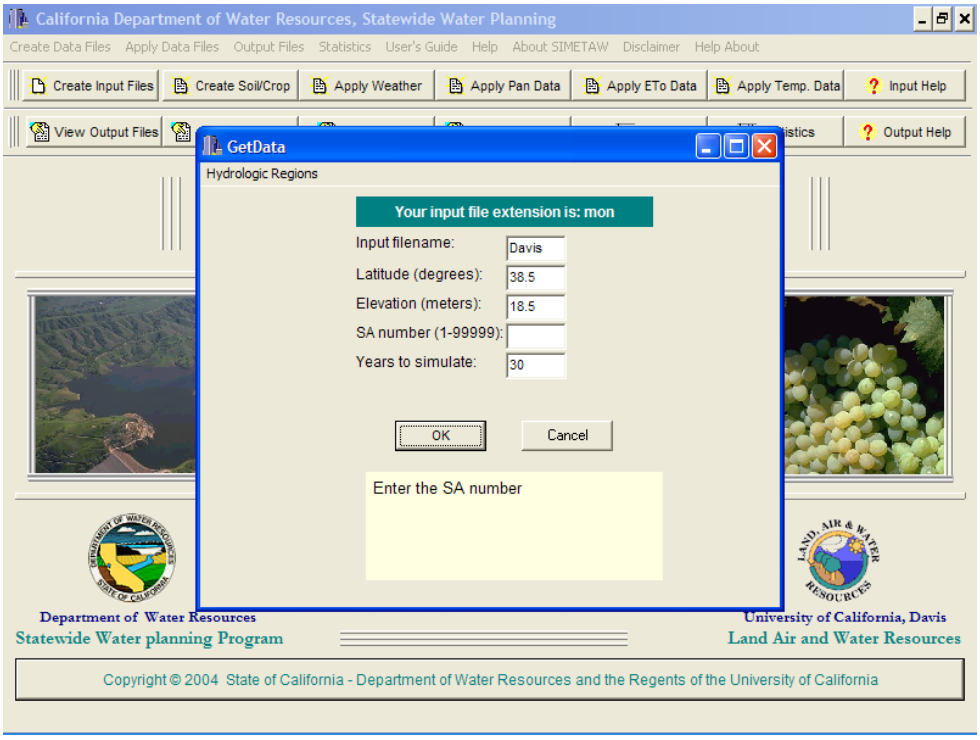

Figure 12. SIMETAW displaying an error message for missing SA number.

Note:

You are still required to enter SA number to run the application. If you do not provide SA number in the dialog box, the SIMETAW program will display an error message with a tip.

After the water balance calculations are completed, *SIMETAW* will give the user an opportunity to view or browse the output files created by *SIMETAW* (Figure 13).

Click the “View” button to view the output files on the computer screen, otherwise click the “Exit” button to exit. After you click the “View” button, a window appears and then you can select the file extension corresponding to the desired file type to display. The extensions include ‘wrk’, ‘msw’, ‘mse’, ‘csv’, ‘mtv’, and ‘eaw’. When you select the ‘wrk’ or ‘msw’ file type, then the program asks for the input file name. The input file name refers to weather station name (e.g., Davis) (Figure 14).

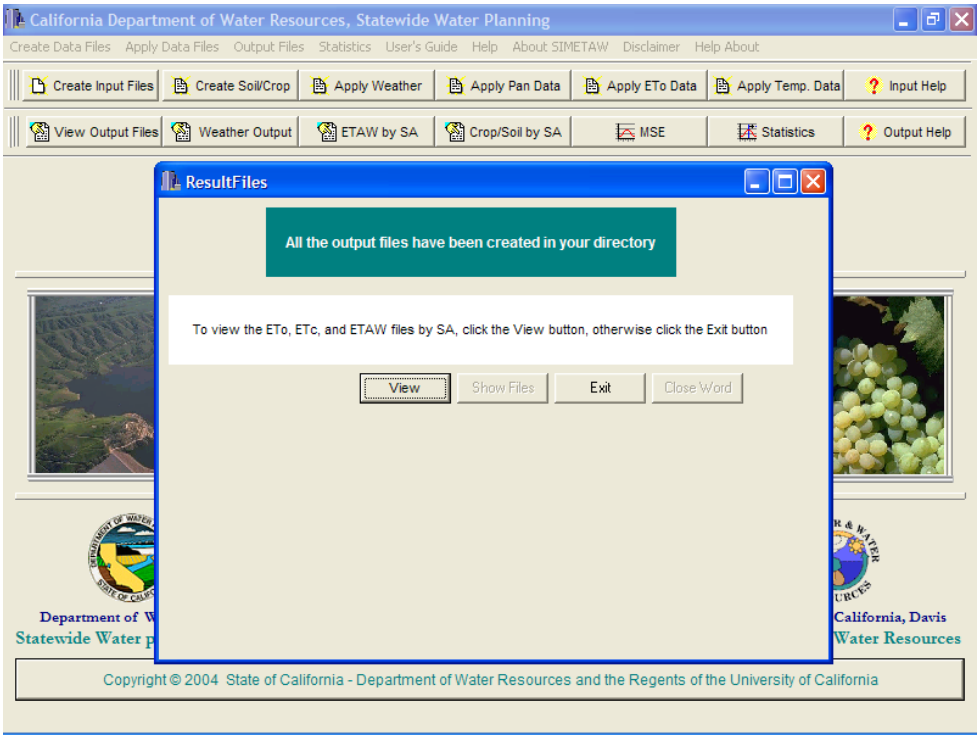

Figure 13. Window showing a dialog box for displaying the output files created by SIMETAW.

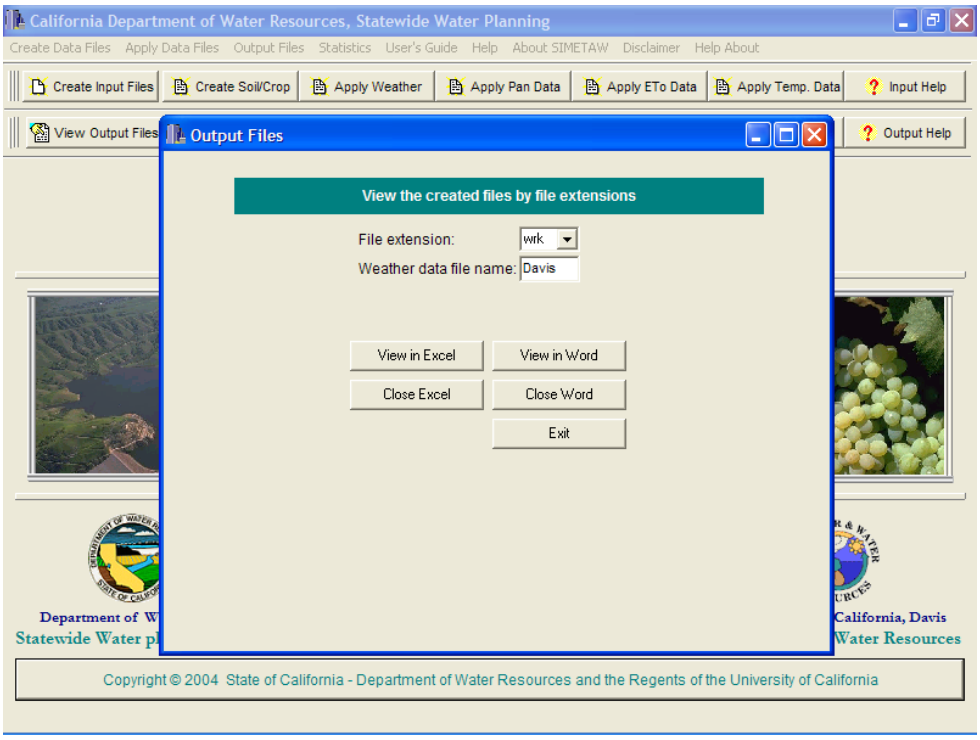

Figure 14. Window showing a dialog box for selecting the output files created by SIMETAW.

The ‘wrk’ file type is a large file and it can only be displayed by word software. The ‘msw’ file can be displayed by either Word or Excel software.

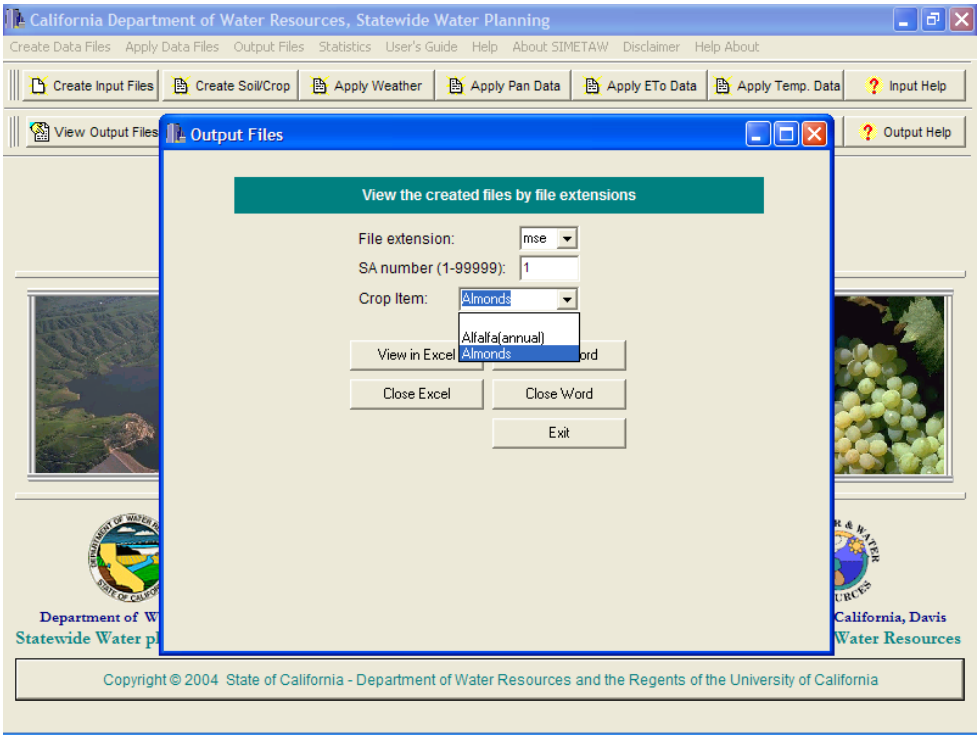

Figure 15. Window showing a dialog box for selecting the output files created by SIMETAW.

If the ‘csv’, ‘mse’, ‘mtv’, or ‘eaw’ file type is selected, the program will ask you to enter the SA number (e.g., 1). After entering the SA number, then *SIMETAW* asks you to choose the desired crop from the pull down menu (Figure 15). The output files can be displayed by either Word or Excel software.